A STUDY OF CHARGED PARTICLE TRACKS IN CELLULOSE NITRATE

Eugene V. Benton

Naval Radiological Defense Laboratory
San Francisco, California

January 1968

31

USMRDL-TR-68-14
22 January 1968

A STUDY OF CHARGED PARTICLE TRACKS IN CELLULOSE NITRATE

By

E. V. Benton

U.S. NAVAL RADIOLOGICAL DEFENSE LABORATORY

SAN FRANCISCO · CALIFORNIA · 94135

RADIOLOGICAL PHYSICS BRANCH
E. Tochilin, Head

PHYSICAL SCIENCES DIVISION
W. E. Kreger, Head

ADMINISTRATIVE INFORMATION

This report covers a portion of the independent exploratory development (6.2) program which is authorized and funded by the Director of Laboratory Programs, Office of Naval Material under Subproject SF 011 01 01. Segments of the work and closely related effort were sponsored and funded by the National Aeronautics and Space Administration, Ames Research Center under NASA-Defense Purchase Request Number A-69315 and Manned Spacecraft Center, Houston, Request Number T-68062-G.

ACKNOWLEDGMENT

The author feels deeply indebted to those who have contributed to this research. It is a pleasure to acknowledge and to thank the following individuals: Eugene Tochilin for his valuable advice and for reading and correcting the manuscript; Richard B. Menke for his contributions to the development of the range-energy program, the work connected with particle identification, and for the useful suggestions during the preparation of the manuscript; Michael M. Colliver for his valuable assistance with the various experimental phases of the research; Drs. Harry K. Heckman and John Lyman of the University of California Lawrence Radiation Laboratory for making the Bevatron irradiations possible; James C. Hodgen for his expert advice on microscope optics and equipment; Carole Haggmark for typing the manuscript.

DDC AVAILABILITY NOTICE

This document has been approved for public release and sale; its distribution is unlimited.

Eugene P. Cooper
Eugene P. Cooper
Technical Director

D. C. Campbell, CAPT USN
Commanding Officer and Director

ABSTRACT

Both experimental and theoretical contributions are presented on the topic of dielectric charged particle track detectors. Cellulose nitrate was the principal track recording material. The study covers four areas:

1. The Chemical Etch Development of Tracks.

There have been no previous systematic studies of the chemical etch development of particle tracks in dielectric track detectors. Part of the research reported here is an investigation of the effects of the different constituents of cellulose nitrate plastic on the chemical etch development of tracks. The dependence of track etching on certain etching solution parameters is discussed.

It has been found that the degree of preferential etching of the particle damage trails can be significantly increased by reducing the chemical attack rate, r_B, of the undamaged bulk material. The quantity r_B is lower for the more highly nitrated (12.4% vs. 10.9% N_2) and higher degree of polymerization (1000 vs. 50) nitrocellulose. The presence of plasticizers greatly reduces r_B, and the presence of residual solvents in concentrations of a few percent also has a similar, but smaller effect. Preferential etching can also be increased by etching at lower temperatures. The thermal stability of tracks is discussed. The geometry of tracks is examined. Useful relationships between track parameters are derived. Experimental observations of etched tracks in several types of cellulose nitrate plastic are reported.

2. Track Registration Criteria.

The knowledge of which particles produce latent (etchable) tracks in a given polymer is basic to the understanding of the track etch phenomena. It is also essential to the practical utilization of these detectors in quantitative measurements.

A new track registration criterion is presented. The criterion is based upon the restricted energy loss rate of charged particles. In order to produce an etchable track, a charged particle must possess a restricted energy loss rate above some critical value that is characteristic of the material. This criterion, as well as the two previously proposed criteria, are critically examined.

3. Range-Energy Calculations and Comparisons with the Etched Tracks Lengths.

The knowledge of range-energy relations is essential in the study and use of any charged particle detector. Most of the dielectric track detector materials require comprehensive range-energy data. The relationship between the ranges of particles, and the etched track lengths also needed to be established.

The calculations were carried out using the basic method of Barkas and Berger which has been modified and extended to include lower energies. Range-energy and energy loss data are given in the form of tables for a wide variety of particles and a broad energy spectrum in a wide variety of stopping materials. The range calculations have been checked experimentally with the use of lithium drifted solid state detectors. It is shown that the length of the etched tracks, when etched until the tips of the tracks become round, agrees closely with the calculated range and, therefore, is a good measure of the particle energy.

4. Charged Particle Detection.

The use of the dielectric track detectors for quantitative measurements of multicharged particles is examined. Measurements of the dependence of the track etch rate on the restricted energy loss rate of charged particles are presented. The information content of tracks is examined. A simple, direct and accurate method for charge determination of multicharged cosmic ray particles is presented. The method is based on the measurement of the portion of the particle range over which a latent track is produced by a charged particle penetrating layers of plastic.

SUMMARY

The Problem

In recent years a new class of charged particle detectors called dielectric track detectors has been discovered. The detecting principle is based on the delineation of individual paths of heavily ionizing charged particles in a number of dielectric solids, including minerals, glasses, and polymers. The most important features of these detectors are their capability to discriminate between light and heavy particles and a sharp threshold of sensitivity. The detectors appeared well suited for numerous applications involving measurements of heavily ionizing charged particles. The chief shortcoming of these detectors has been the lack of quantitative information about their behavior. Since such information is essential for the utilization of these detectors, some fundamental studies were undertaken. At the same time, it was hoped that such information would provide criteria for the future design of better detecting materials. Cellulose nitrate was chosen because it represents the most sensitive material presently available.

The Findings

Particle track development by means of the chemical etching technique was studied. The criterion for the design of better track recording cellulose nitrate plastics was found. A track registration

criterion for polymeric materials has been established. In order to produce a latent track, a charged particle must have a restricted energy loss rate greater than a critical value that is a function of the detecting material. Extensive range-energy tables for a wide variety of particles and a broad energy spectrum in a wide variety of materials were calculated. The calculated ranges agree closely with experimentally measured etched track lengths. Simple, direct and accurate methods for charge and mass determination of heavy charged particles were devised.

Numerous applications of these detectors to present and future needs of both Navy and NASA have become apparent.

1. The high chemical stability and mechanical ruggedness of these detectors makes them suitable for measurement of radioactive species in solutions. This may include monitoring the concentrations of alpha emitters in deep-ocean environments, measurement of alpha emitters released during undersea accidents, and measurement of alpha and fission fragment emitters in the presence of high backgrounds of gamma and beta radiation.

2. The Navy is currently involved in the Manned Orbiting Laboratory program. There will be Navy personnel aboard the satellite. NASA is contemplating 18 month, manned Mars missions. It is estimated that up to about 40% of the total dose received will result from heavy particle interactions. Also, high fluxes of alpha particles together with protons emitted during solar flares pose imminent danger to the astronauts if a large flare occurs during flight. Conventional passive dosimeters presently in use for the proton component of dose

are inadequate for the measurement of the multicharged component. A heavy particle dosimetry system capable of discriminating between different linear energy transfer (LET) multicharged particles can be achieved through the utilization of threshold type dielectric track detectors. The small size of the system would permit its inclusion into the radiation badge of the astronaut.

3. In several years Navy combat planes as well as the civilian supersonic transport planes will be flying at 60,000 - 65,000 foot altitudes. At the present time, the radiation environment at these altitudes is imperfectly known. This is particularly true in the case of the highly ionizing stopping primaries. Dielectric track detectors can be effectively utilized in mapping this radiation environment.

4. It now appears feasible to measure the fluxes of the ultra-high charge particles ($z > 26$) whose knowledge is currently of great interest to cosmic ray physicists. It is possible that the detectors could be refined, in the future, to the point where the measurement of the isotopic abundance of all of the elements present in cosmic rays could be achieved. The unique properties of these detectors make them also well suited to the measurement of the cosmic ray spectra outside of the earth's magnetosphere.

5. Bulk etch rate measurements of some of the dielectric track detectors can be utilized for measurement of dose in the range of about 10^6 to 10^9 rad. An application of particular interest would be measuring massive doses of low penetrating power, soft x or gamma radiations that accompany weapons tests. By successively etching,

each time removing only a few microns of the dosimeter surface, a depth-dose profile may be measured.

6. Individual fallout particles may be analyzed for their content of alpha emitters and, with neutron irradiation, for heavy, fissionable isotopes. The alpha particle energies may be determined by accurate measurement of etched track lengths.

7. The nature and extent of the cosmic dust in the vicinity of the earth has a practical bearing upon erosion of optical surfaces in satellites. Also, the physics of high velocity impact is currently of great interest to investigators in several fields of science and technology. It has been found that cellulose nitrate together with the chemical etch principle can be effectively utilized in these studies. In space exposures, simultaneous flux measurement of the heavy particle cosmic ray component, and of micrometeorites are feasible. The etching technique can be used to study the ionization and the healing phenomena in certain solids after passage of high velocity microparticles.

TABLE OF CONTENTS

APPENDICES

LIST OF TABLES

LIST OF ILLUSTRATIONS

CHAPTER 1

INTRODUCTION

A. Background Information

A new class of charged particle detectors called dielectric track detectors has recently been discovered. The detecting principle is based on the delineation of individual paths of heavily ionizing charged particles in a number of dielectric solids, including minerals, glasses, and polymers. Delineation is accomplished through the selective etching of the radiation damaged material along the particle's trajectory. This results in an etch pit, or in some cases a narrow channel, referred to as a track. Further etching enlarges tracks to a convenient size for direct viewing with an ordinary optical microscope.[1]

Dielectric track detectors have already found numerous applications in several different scientific fields including physics, geophysics and medicine. The physics applications include such studies as nuclear fission and spallation reactions,[2] lifetimes of heavy unstable nuclear particles,[3-7] ternary fission,[8-9] and neutron dosimetry.[10-14] In geophysics[15] these detectors have been used in geochronology[16-21] and studies associated with space erosion and atmospheric ablation of meteorites.[22,23] In medicine selectively

etched tracks in thin layers of plastic have been used as fine sieves for the filtration of cancer blood cells.[24]

It was early recognized that certain polymers, which represent the most sensitive materials in this class of detectors currently available, could be profitably utilized in measurements of the heavy particle component of cosmic radiation.[25] The characteristics which make these detectors particularly well suited for space applications include: small weight, simplicity, mechanical ruggedness, high latent track stability, freedom from distortion, and simple and direct processing. Their chief merit, however, lies in their ability to discriminate between light and heavy particles, making possible the registration and measurement of the highly ionizing charged particles while at the same time being insensitive to the high backgrounds of electrons, protons, neutrons and gamma radiation.

The chief shortcoming of these detectors has been the lack of quantitative information about their behavior. In 1965 at the commencement of this research, accurate range-energy and energy loss relations for heavy ions in the track detecting materials were not available. A reliable track registration criterion was needed to determine which particles will produce etchable tracks in a given polymer. It was not known how the sensitivity of a given polymer was affected by its composition parameters (molecular weight, plasticizers, residual solvents) or by the etching conditions (temperature, hydroxide concentration). Although it was recognized early that particle damage trails of very heavily ionizing particles (such as fission fragments) etch-out faster than tracks of lighter

particles (such as alpha particles) and also result in narrower tracks, no investigations were yet made on how this information could be utilized for particle identification. Since such information is essential for the utilization of these detectors, some fundamental studies of this nature were undertaken in this program.

The aim of this program has been to investigate several broad aspects of the dielectric track phenomena. It was hoped that such an investigation would provide the necessary background information and generate the understanding that is required if these detectors are to be used in quantitative measurements. At the same time, such information would provide criteria for the future design of better track detecting materials. Since a number of polymeric systems exhibit track recording properties, a comprehensive study of all systems was clearly beyond the scope of this work. Cellulose nitrate was chosen because it represents the most sensitive track recording material presently available and one which appears the most likely to be utilized in future applications. However, many of the concepts and techniques to be presented are not restricted to cellulose nitrate, but apply to other polymers and other track recording materials as well.

B. Previous Work on Dielectric Track Detectors:

In this section, the short history of the development of the dielectric track detectors will be reviewed. Attention will be focused on the fundamental developments rather than on the numerous reported applications. The original discovery of the chemical

etching of tracks and much of the subsequent development is due to Fleischer, Price, and Walker. A recent review of the subject is found in their reference.[1]

In 1958 Young first utilized the chemical etching technique by observing fission fragment etch pits in thick samples of lithium fluoride.[26] He reasoned that with respect to the chemical properties, the damage trail of a fission fragment is similar to that of a dislocation. He argued that the free energy of the particle damage region is higher than the surrounding undamaged material, and that this region should be preferentially attacked by a suitable chemical reagent. Accordingly, he found that by using a mixture of concentrated hydrofluoric acid, glacial acetic acid and ferric fluoride, surface etch pits could be produced at the sites where fission fragments entered the crystal.

In 1962 Price and Walker reported that fission fragment tracks in mica could be revealed by etching with hydrofluoric acid. They subsequently showed that this was a general phenomenon; tracks were observed in many other dielectric materials, including other minerals, glasses, and polymers.[27-30] Of all the track recording materials, polymers were found to be the most sensitive; tracks of low energy alpha particles were observed in cellulose nitrate.

1. The Chemical Etching Process - General Considerations

Although it is possible, under some circumstances, to directly observe tracks of charged particles with the electron microscope (see, for example, Figures I-1,2), this technique has a number of severe limitations: extremely thin (≤ 3000Å) samples are

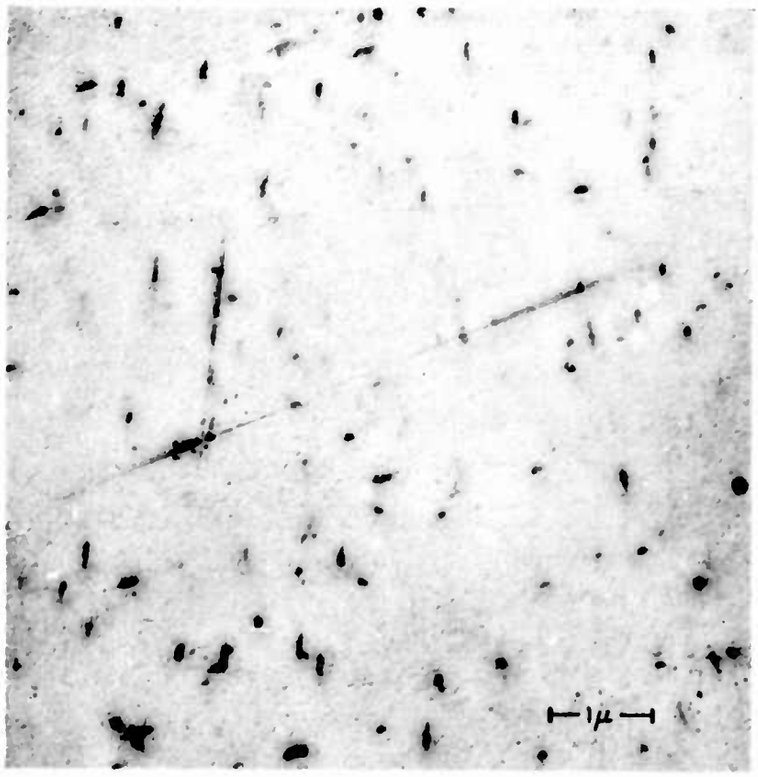

FIGURE I-1. Electron photomicrograph of unetched fission fragment tracks in a thin (< 3000A), shadowed specimen of NRDL-1 cellulose nitrate plastic. The specimen, containing atoms of ^{235}U was subjected to a high flux of thermal neutrons.

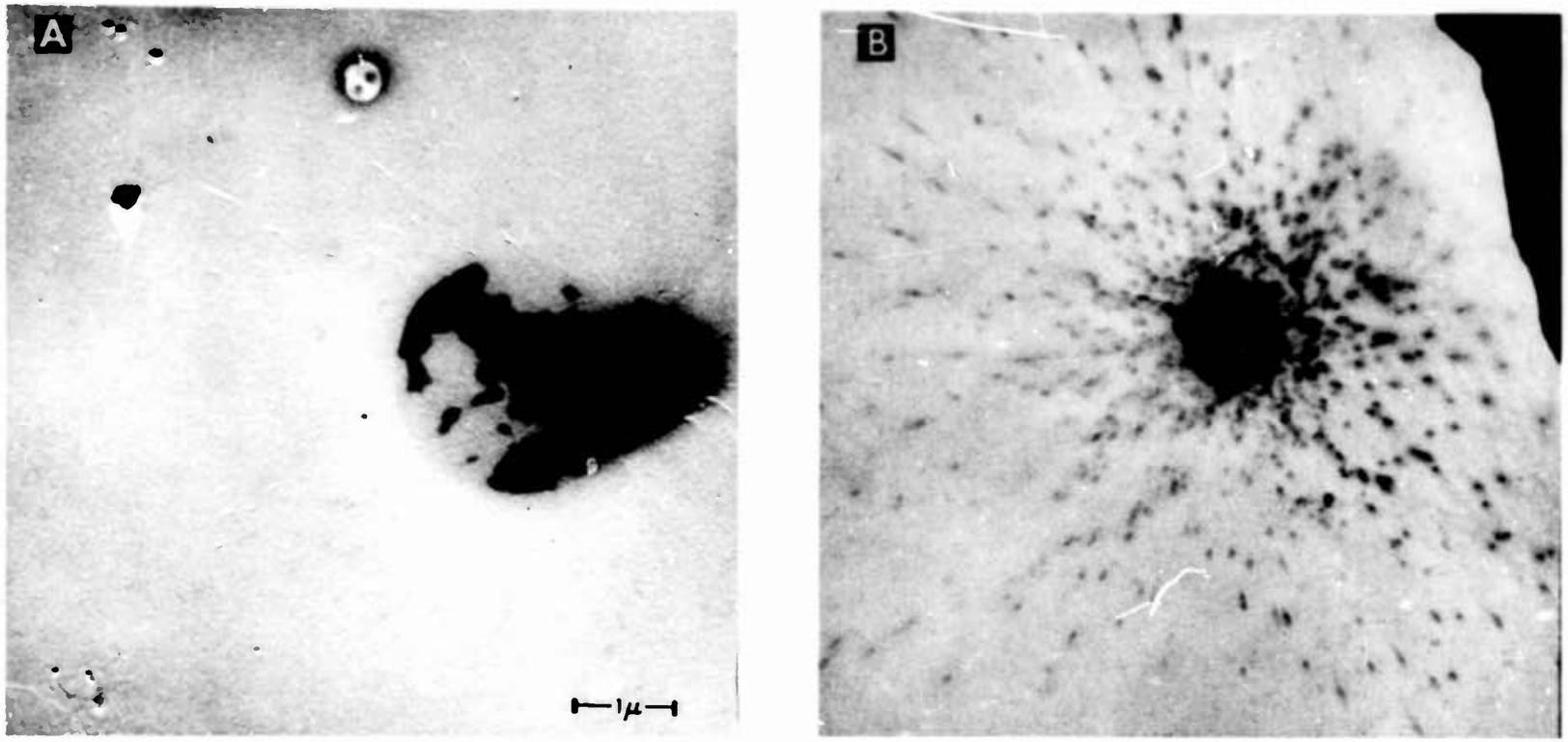

FIGURE I-2. Unetched fission fragment tracks are shown radiating away from micron size particles of ^{235}U that have been imbeded in a thin film of cellulose nitrate plastic. Specimen (A), shadowed at a grazing angle of 15^{o}, reveals the trough-like structure of tracks. Specimen (B) was shadowed at a steeper angle.

required, large densities of tracks are needed, only small track lengths can be examined, and measurements are limited to observations of tracks of very heavy particles.

A much more versatile and sensitive technique is now available for track delineation. The method consists of immersing the irradiated samples in a suitable chemical reagent. The reagent must be capable of slightly etching the bulk material, while at the same time preferentially attacking the particle damage trails. In the case of cellulose nitrate, a strong hydroxide, such as sodium hydroxide, is normally used. Bulk etching enlarges the track region to the point where it becomes visible under an ordinary light microscope. This makes possible the observation of relatively light particles over large track ranges. Large track densities are not needed, and observations can be made in virtually any sample thickness.

In their review artile[1] of dielectric track detectors, Fleischer et al. have noted that the chemical etch development of particle tracks in dielectric solids is as much of an art as a science. The etching process can be affected in a complex way by a large number of variables including the exact composition and history of the sample and the type, concentration, and the temperature of the etchant. Orientation of the surface, agitation of the etchant, as well as the presence of impurities in trace quantities may alter the etching behavior.

Development of charged particle tracks by means of chemical etching is, in principle, similar to that of the chemical etching of dislocations in crystals (see, for example, Amelinckx[31]). Tracks are

linear imperfections with a diameter less than about 100Å.[1] For track development the rate of chemical attack of the particle damage trail, r_T, must be greater than that of the bulk material, r_B, i.e., $r_T/r_B > 1$. We shall call the quantity r_T/r_B the etch rate ratio. It is an important parameter which is used to denote the degree of the preferential etching.

Under ideal etching conditions (absence of diffusion effects, homogeneous track recording material) the etched tracks are conical in shape, with sharp terminal ends. The quantity θ, one-half of the cone angle, is given by[1]

$$\theta = \sin^{-1} r_B/r_T. \qquad (1.1)$$

As etching proceeds, the vertex of the cone remains sharp until it reaches the point where the particle came to rest; further etching causes the apex to become rounded (see Figure I-3). In the case where the particle penetrates the entire thickness of plastic, etching can proceed from both sides, resulting in two collinear cones (see Figure I-4). If etching is allowed to proceed long enough, the two cones merge and produce a hole penetrating the thickness of the plastic.

Not all of the particle damage trails (latent tracks) which intersect the sample surface can be developed through the chemical etching technique. In order to produce a latent, etchable track, a charged particle must have a rate of ionization above a certain critical value, characteristic of that material (see Chapter V). The quantity r_T/r_B is a function of the rate of ionization of the charged particle, increasing as the rate of ionization rises. For

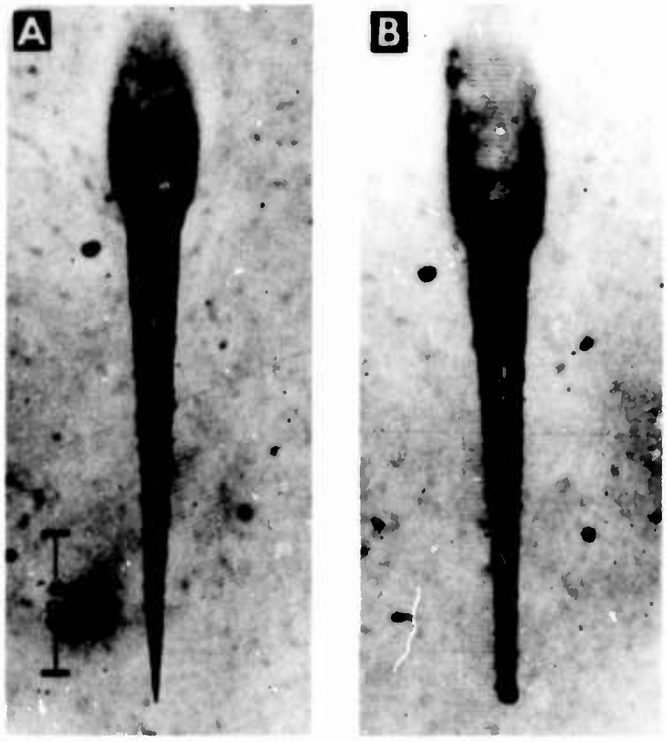

FIGURE I-3. Tracks of stopping heavy cosmic ray particles. (a) The etching has not reached the end of the particle range; (b) the etching has continued beyond the point where the particle came to rest.

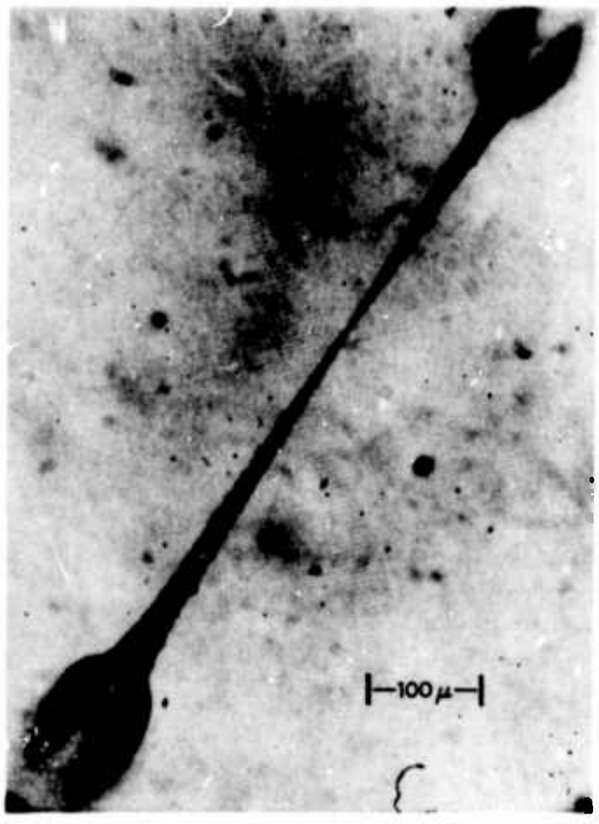

FIGURE I-4. Track segments of a slow heavy cosmic ray particle that traversed the entire thickness of the plastic layer. The etching which proceeded from both sides was terminated as the two tracks were about to merge.

lighter ionizing particles $r_T/r_B \rightarrow 1$, and tracks are not observed (see Chapter VII). There is also a geometrical restriction: latent tracks making an angle less than $\delta_c = \sin^{-1} r_B/r_T$ with the surface will not be seen because the surface dissolves more rapidly than the tracks can deepen.[1] Thus it is desirable to have the etch rate ratio as large as possible.

The bulk etch rate, r_B, is sensitive to a large number of variables such as the exact composition of the cellulose nitrate, the manner of sample preparation, the exact history of the sample, the type of etchant and the etching conditions. At the same time, the track etch rate, r_T, is also a function of the type and the velocity of the charged particle that produced the damage trail. Thus, the quantity, r_B, provides information with regard to the chemistry of the sample and of the etching process, while r_T also provides information about the charged particle. In order to understand the track etching process, it becomes necessary to study the effects of various parameters on r_B and r_T individually as well as on r_T/r_B.

2. The Critical Rate of Energy Loss Track Registration Criterion

The knowledge of which particles produce etchable tracks in a given polymer is basic to the understanding of the track etch phenomenon. It also allows the practical utilization of these detectors in various quantitative measurements.

Fleischer, Price, and Walker reported the first track registration criterion in 1964.[32] In order to produce a latent (etchable) track it was considered necessary for the charged particle to have a

rate of energy loss above some critical value, $(dE/dx)_{crit}$, characteristic of that particular detecting material. Data supporting this hypothesis for muscovite mica, Lexan polycarbonate resin, and cellulose nitrate plastic were given for heavy ions of energies of up to 10 MeV/nucleon. The $(dE/dx)_{crit}$ criterion predicted that the cellulose nitrate plastic used in these experiments should record tracks of relativistic ^{56}Fe nuclei. Subsequent cosmic ray experiments showed this prediction to be incorrect.[33]

The dE/dx of a charged particle is a measure of the total ionization produced by that particle. At high velocities of the incident heavy particle a large fraction of its total dE/dx results from high energy transfer electron collissions. These high energy electrons generate ionization trails of their own, which occur at a considerable distance away from the path of the primary particle and hence contribute little to track formation. For this reason the $(dE/dx)_{crit}$ criterion cannot adequately describe the spacial distribution of energy loss resulting from these secondary and tertiary energy transfer processes.

3. The Ion Explosion Spike Model of Track Formation

In 1965 Fleischer et al. reported a model for the formation of tracks in solids based on the Ion Explosion Spike Mechanism.[34] They reasoned that a cylindrical region of net positive charge is produced along the path of the incident heavy particle as a result of the ejection of electrons from this region by the primary particle. The mutual repulsion of the positive ions, if greater than the cohesive forces within the solid, result in lattice displacements;

these displacements, in turn, result in a region having a large number of imperfections, and thus a high chemical reactivity. This semiquantitative model satisfactorily accounted for the gross observations regarding the track phenomena. It predicts correctly the absence of etched tracks in conductive and good semiconductive materials. It also arranged the minerals in the correct order of sensitivity. When applied to polymers, predictions based on this model did not agree with experiments. The authors conclude that in the case of the high polymers, additional damage mechanisms exist.

4. The Primary Ionization Criterion for Track Registration

Recently Fleischer et al. introduced a new criterion for particle registration.[35] This criterion, which is an outgrowth of their "Ion Explosion Spike Model,"[34] is called the "primary ionization criterion". Specifically it states that an etchable track will be formed in a given polymer if the linear ion density produced by the primary particle along its trajectory is greater than a critical value required by the material. They postulate that the secondary ionization produced by the ejected electrons (δ-rays) is largely irrelevant to track formation. This is opposite to the view of Pfohl et al,[36] and that of the author, which is that the low energy δ-rays play a vital role in the mechanism of track formation in polymers.

The ion explosion spike mechanism predicts that a solid will record tracks if the rate of primary ionization, PI, exceeds a critical rate for that solid.[35] The PI criterion makes use of the expression of Bethe,[37]

$$\left(\frac{dJ}{dx}\right) = \frac{2\pi n(z^*)^2 r_o^2 m_o c^2}{\beta^2} \frac{r}{I_o} \left[\ln\frac{2m_o c^2 \beta^2 \gamma^2}{I_o} + S - \beta^2\right], \qquad (1.2)$$

giving the average number of collisions per g cm^{-2} that results in the ejection of an electron from an atom. Here, r and S are dimensionless constants of the stopping material equal to 0.285 and 3.04, respectively; I_o is the ionization potential of the outer shell of the atom, and the other symbols have the usual meaning (see Chapter V).[37] It should be noted that the above values of r and S are strictly true only for hydrogen (I_o = 13.5 eV). Thus, the absolute values of the primary ionization in plastics are not known; Fleischer et al. use relative values to explain track registration.

The primary ionization is a measure only of the ionization produced directly by the incident particle. In order to fit the experimental data Fleischer et al.[35] use a value of 2 eV for I_o. However, this value does not appear to be consistent with the ion explosion spike mechanism which requires electron ejection from the track region. The energy of 2 eV may suffice to break a chemical bond (raise the bonding electron to a higher energy state) but, in general, does not suffice to ionize the atom (remove the electron and thus alter the charge equilibrium). For ionization, a higher energy of 9-15 eV is required.[38]

5. Range-Energy and Energy Loss Relations for Multicharged Ions in Track Detecting Materials

The knowledge of range-energy relations and the associated derivative relations of (dE/dx) vs. energy is essential in the study of the properties of dielectric charged particle detectors since:

(1) the length of tracks is dependent upon the range of particles, and (2) the energy loss rate, (dE/dx), plays a role in particle registration. Extensive calculations and measurements of range-energy relations have been made for protons and alpha particles in many common materials. However, most of the dielectric track detector materials do not have comprehensive range-energy data available. The situation for heavy ions, $z > 2$, is considerably worse. Experimental data for particles of $z \leq 18$ and energies less than 10 MeV/nucleon are available for materials such as nuclear emulsion, aluminum, and some other common metals. For heavier ions with energies above 10 MeV/nucleon, very few theoretical or experimental data exist in the literature. The relationship between the ranges of particles, and the etched track lengths in dielectric track detectors also needs to be established.

C. Program of Investigation

From a review of the present state of knowledge of dielectric track detectors, it is clear that a great deal of research, both theoretical and experimental, remains to be accomplished. In this dissertation, contributions are presented in four areas: the chemical etch development of particle tracks, track registration criterion, comparison of etched track lengths with calculated range-energy relations, and techniques for identification of heavy, multicharged particles. The studies reported here were initiated early in 1965.

1. The Chemical Etch Development of Tracks

There have been no systematic studies of the chemical etch development of particle tracks in dielectric track detectors. In this

dissertation the geometry of tracks is examined. Useful relationships between track parameters are derived. Experimental observations are reported of etched tracks in several types of cellulose nitrate plastic.

The composition and a method for specimen preparation of a sensitive cellulose nitrate plastic is reported. The etching behavior in this plastic is examined in detail. This includes the investigation of the effect on the etch development of tracks of the parameters associated with the specimen composition, the etching solution, and the specimen preparation. The thermal stability of latent (unetched) tracks is examined.

2. Track Registration Criterion

A new track registration criterion is presented. The criterion is based upon the restricted energy loss rate of the charged particle. This criterion, together with the previously proposed criteria, is critically examined.

3. Range-Energy Calculations and Comparisons with the Etched Track Length

The purpose of these calculations was to provide range-energy relations for a wide variety of particles and a broad energy spectrum in a variety of stopping materials. The basic method is that of Barkas and Berger[39] which has been modified and extended to include lower energies. The range calculations have been checked experimentally with the use of lithium drifted solid state detectors. It is shown that the length of the etched tracks (etched until the track ends become round) agrees closely with the calculated range and, therefore, is a good measure of the particle energy.

4. Charged Particle Detection

The use of dielectric track detectors for quantitative measurements of multicharged particles is examined. Measurements are presented showing the dependence of the track etch rate on the restricted energy loss rate of charged particles. Different categories of tracks are examined to determine what types of information can be obtained from the measurements of the various track parameters. A new technique for identifying the charge and the mass of multicharged particles is presented.

CHAPTER II

CELLULOSE NITRATE

This chapter is included in order to provide a background and to familiarize the reader with the cellulose nitrate system. A brief description of the origin, the chemical composition, and the physical structure of this broad and very complex group of materials is presented. Also included is a short discussion of the effects of radiation on the atomic structure and the bulk properties of the material.

A. Cellulose

Cellulose is a naturally occurring carbohydrate which generally comes from either cotton linters or from wood pulp. The empirical formula can be written as $\left[C_6H_7O_2(OH)_3\right]_n$. The structural formula is shown in Figure II-1. Cellulose is thus composed of a large number of anhydroglucose units joined together by ether linkages. The molecular weight of the anhydroglucose unit is taken as 162, with end groups and trace substituents in the cellulose assumed to be negligible. The average number of anhydroglucose units in the molecule is several thousands for most native celluloses; and ranges from 500 to 2,500 for chemically purified celluloses.[40] Cellulose is considered to be a long, linear polymer of united rings as shown in Figure II-1. It occurs in a fibrous form having a specific gravity of about 1.50 - 1.55, and an

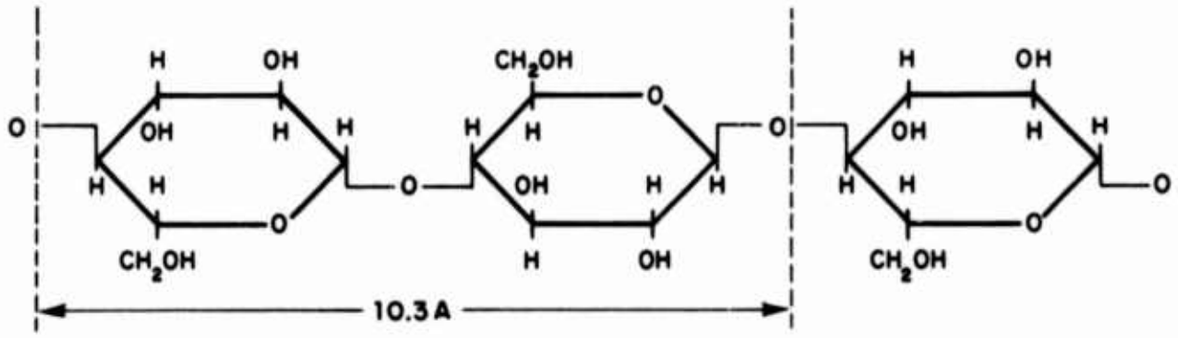

FIGURE II-1. The structural formula for cellulose. Three hydroxyl groups are shown in each of the anhydroglucose units, the latter being joined by ether linkages. The long chain molecule may be composed of as many as 3000 anhydroglucose units.

index of refraction of 1.599 along the fiber and 1.532 perpendicular to it. It is thought that the cellulosic fibers are built up of bundles of long molecules, held together in a more or less parallel alignment by intermolecular secondary valence forces due to the highly polar hydroxyl groups. The electric field configuration between neighboring chains is conducive to their parallel orientation. The crystallities are called micelles. The minimum dimensions of the micelle is thought to be 60 - 70Å wide and 600Å long. Individual chain molecules may traverse many micelles, resulting in an interlocking assembly of parallel miceles or submicroscopic crystallites. According to x-ray measurements, cellulose is about 70 percent crystalline. Cellulose is insoluble in all organic solvents, has no melting point, and is fairly resistent to thermal degradation.

B. Cellulose Nitrate

1. Chemical Composition

Cellulose nitrate is a condensation polymer produced by the esterification of cellulose with nitric acid in the presence of a catalyst, usually sulfuric acid. The hydroxyl ions are replaced by the nitrate ions, according to the following formula for complete nitration:

$$C_6H_7O_2(OH)_3 + 3HNO_3 \xrightarrow{H_2SO_4} C_6H_7O_2(NO_3)_3 + 3H_2O. \qquad (2.1)$$

The most important function of sulfuric acid is its role as a dehydrating agent for the additional undesirable water formed in the nitration reaction. Sulfuric acid also functions as a swelling agent allowing initial entry of the nitrate groups and influences the degree of substitution or nitrogen content.[40-43]

The structural formula of cellulose nitrate is shown in Figure II-2. The degree of substitution is defined as the average number of hydroxyl groups replaced per anhydroglucose unit and varies between 0 and 3. In principle it should be possible to replace all three hydroxyl groups in each anhydroglucose unit with nitrate groups to give cellulose trinitrate. Such a product, having a degree of substitution of 3, would contain 14.14% nitrogen. In practice, the practical upper limit for substitution is about 2.9, corresponding to a nitrogen content of 13.8%. To provide properties most valuable for industrial uses, the nitrogen content is maintained between 10.9 and 13.6%. Cellulose nitrate with a nitrogen content of about 11% is used in plastics, 12% in lacquers, and 13% in explosives. Cellulose nitrate with nitrogen cont[illegible]ess than about 10% is quite insoluble and hence not useful.

2. Physical Structure

The physical state of cellulose nitrate is intimately related to the forces between molecules and to the molecular length, shape, and symmetry. The covalent atomic bonds confer electrical and thermal resistance, rigidity, and hardness. The length of the polymer chain is specified by the number of repeat units in the chain. This is called the degree of polymerization (DP). The degree of polymerization, in turn, is related to the viscosity of the solution formed when cellulose nitrate is dissolved at a given concentration in a particular solvent. The viscosity of commercial cellulose nitrate is generally expressed in terms of either centipoises (cps) or in the time, expressed in seconds, required for a metal ball of

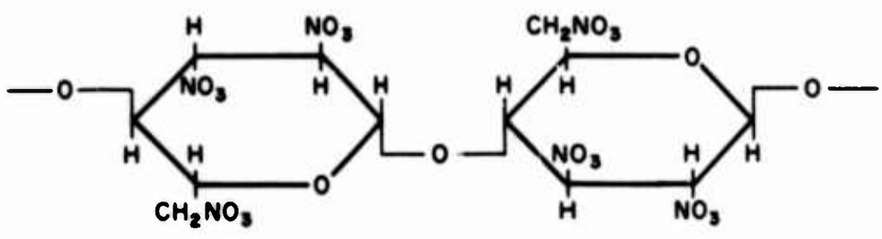

FIGURE II-2. The structural formula for cellulose trinitrate.

specified size and density to fall through a measured distance in a solution of specific formulation at 25°C. A viscosity of 1 second is equal to about 370 cps. Commercially available cellulose nitrate varies in viscosity from 18 cps to about 200,000 seconds. The approximate relation between viscosity, molecular weight, and the degree of polymerization is given in Table II-1.[42]

TABLE II-1 Approximate Relation Between the Viscosity, Molecular Weight, and the Degree of Polymerization of Cellulose Nitrate.

Viscosity	Molecular Weight	Degree of Polymerization
1/4 sec	22,000	74
30 - 40 sec	68,000	229
600-1000 sec	140,000	471

Although considerably less crystalline than the parent cellulose, cellulose nitrate possesses, in general, short range order. X-ray and electron diffraction studies amply support this view. In Figure II-3 is shown an electron diffraction pattern of a cellulose nitrate film used in this study. The ring pattern is characteristic of material having a short range order extending to about 20 to 30Å. The extent of crystallinity depends on many factors, such as, the degree of nitration and the exact conditions and manner of sample preparation. Cellulose nitrate is more naturally crystalline in the trinitrate state than in the less nitrated states. However, as the degree of nitration is decreased toward the pure cellulose form, the

FIGURE II-3. An electron diffraction pattern of a thin film of cellulose nitrate of the type used in this study (NRDL-1). This pattern is characteristic of a material having a short range order extending to about 20 to 30A.

polymer becomes more crystalline again. The extent of crystallinity has a definite influence on the mechanical properties of the material. As is the case with many polymers, this material has a viscoelastic response to an applied stress.

C. Cellulose Nitrate Plastic

Cellulose nitrate is only one of the constituents of cellulose nitrate plastics. In order to improve or otherwise alter the properties of the basic material, various modifier are added. These consist of plasticizers, resins, and pigments. Small amounts of solvent, left over from sample preparation, are also generally present. The presence of these substances affect both the chemical and the physical behavior of the plastic.

The function of plasticizers is based on the fact that it contains groups capable of solvating particular polymer groups. The polar bond from the plasticizer is believed capable of neutralizing or sufficiently weakening the Van der Waals forces that exist between the polymer chains. The addition of a plasticizer also produces swelling; the secondary valence forces are relaxed, permitting flexing of the long linear polymer chains. The addition of these lower molecular weight materials (generally organics) to high polymers changes a hard, brittle, glass-like solid to a softer, more flexible material. A plasticizer capable of becoming incorporated as a permanent component of the finished plastic product is called a primary plasticizer.

There are basically four different types of plasticizers used to plasticize cellulose nitrate; they are classified as solvent,

non-solvent, monomeric, or polymeric types. Solvent type plasticizers are defined as those which exhibit complete miscibility with cellulose nitrate in all proportions. They act as nonvolatile solvents which remain in the dried film. Dibutyl phthalate (DBP) is a typical example. Nonsolvent type plasticizers neither dissolve nor form a colloid with nitrocellulose, but are compatible with cellulose nitrate in the dry film. They also contribute flexibility to the film; castor oil is a typical example. Monomeric plasticizers such as dioctyl phthalate are generally of low molecular weight. The polymeric types of plasticizers have a relatively high molecular weight (1000 - 8000). These plasticizers show very low volatility, and do not leave the film even at high temperatures; Paraplex G-41 is a typical example.

Cellulose nitrate is soluble in ketones, esters, amides, nitroparaffins, and ethyl ether-ethyl alcohol mixtures.[41] These liquids are usually referred to as true, active, or primary solvents. Another group of liquids such as ethyl, isopropyl, or butyl alcohols, and others, are not true solvents in that they alone do not dissolve cellulose nitrate. However, when used in combination with a primary solvent, they improve the dissolving power of the primary solvent, resulting in solutions with appreciably lower viscosities. These liquids are called cosolvents or secondary solvents. Often several primary and secondary solvents, each having a specific desirable characteristic, are used in the preparation of films. A proper combination of primary and secondary solvents is needed in order to achieve a uniform evaporation, and thus a uniform plastic film. Some

of the physical properties of plasticized cellulose nitrate film[44] are listed in Table II-2.

TABLE II-2 Mechanical, Physical and Electrical Properties of Plasticized Cellulose Nitrate Films

Specific Gravity	1.35 - 1.60
Refractive index	1.5
Thermal conductivity (cal/sec cm ^{o}C)	$(3.1\text{-}5.1) \times 10^{-4}$
Electrical resistivity (volume) at 30^{o}C, ohm-cm	$(0.106\text{-}0.32) \times 10^{10}$
Specific heat, cal/^{o}C gram	0.34 - 0.38
Softening point	70^{o} - 90^{o}C
Effect of heat	Decomposition at 100-150^{o}C
Burning rate	Very high
Effects of ultra-violet light	Discoloration and embrittlement
Effect of water	Very slight swelling

D. Effects of Radiation

The interaction of radiation with a polymer and the subsequent events that occur can be chronologically divided into three distinct periods of time (see Alger[45]). The first period, lasting less than 10^{-15} sec, is that of energy dissipation by the incident radiation, and the absorption of this energy by matter. There are three ways to absorb energy in a solid: (a) electron displacement (both ionization and excitation are included under this heading), (b) atomic

displacement, and (c) generation of an impurity atom as a result of a nuclear reaction. The second period, lasting anywhere from 10^{-12} to 10^{-9} sec, involves the transport and disposition of absorbed energy by the molecular motion as the thermal equilibrium within the solid is established. Again, there are three alternatives: (a) energy can be emitted as luminescence, (b) it can be dissipated as heat, or (c) energy can be stored as potential energy in the form of chemically reactive species. The path followed depends strongly on the structure of the molecule and the environmental conditions. The third and final period is that of the establishment of chemical equilibrium. Here, the potential energy stored in the form of chemically reactive species is dissipated. Diffusion processes and reaction rates extend the duration from a minimum of about 10^{-8} sec up to months or years. To recapitulate, from the absorber point of view it is convenient to think of three distinct phases: (a) energy absorption, (b) establishment of a thermal equilibrium, and (c) the establishment of a chemical equilibrium.

The primary mechanism for the absorption of the energy deposited by charged particles is electronic and atomic displacements. The probability of a nuclear reaction is generally low, and the energy transfer resulting from this process can generally be neglected. Except at very low velocities of the incident particle, the predominant mechanism of energy absorption is through electron displacement, i.e., through ionization and excitation of electrons of the absorbing medium. Since cellulose nitrate does not readily luminesce, the bulk of the absorbed energy goes either into heat or is stored as

potential energy of reactive species. The manner in which the energy is divided between ionization and excitation depends upon the type of particle, its velocity and the state of the absorbing medium. Very little is known of the number, types, or distribution of the chemically reactive species that are formed. Even less is known of the manner in which these species react with each other or with substances present in the matrix of the bulk material (such as oxygen or water). It is in this area, the approach to chemical equilibrium, that our knowledge of this subject is least satisfactory.

In the studies of irradiated polymers it has been reported that in general the major reactions in polymers depend primarily on the total absorbed energy (dose) rather than on dose rate, the type of radiation, or its sources.[46-48] Fast electrons, x-rays, gamma rays, or mixed radiation from a reactor, including neutrons, all produce approximately the same effect for a given dose. However, the resultant changes in the chemical and physical structure of the polymer are very strongly dependent on the chemical structure of the original material, the physical state of the material during irradiation, as well as the environmental conditions of the irradiation.

In general, the irradiation of polymers produces either cross linking or scission.[46-48] It is reported that cellulose nitrate undergoes scission at a relatively high rate. The scission reaction breaks the molecule into smaller fragments, decreasing the molecular weight, increasing the solubility, and lowering the softening point. Scission is often accompanied by gas evolution. This is

particularly so for cellulose nitrate, where over 95% of evolved gas is hydrogen. The mechanical properties of cellulose nitrate are also changed by scission. The shortened chains and the larger number of chain ends lead to a weakening and embrittlement. Free oxygen present in matrix of the polymer is thought to play an important role in the process of scission. Instead of recombining with each other or some other portion of the polymer chain, the broken chain's ends now combine with oxygen to produce scission. Some of the known effects of radiation on cellulose nitrate are summarized in Table II-3.

TABLE II-3 Some Effects of High Energy Radiation on Cellulose Nitrate Plastic

1. Exitation
2. Production of unsaturation and bond rupture
3. Ionization
4. Hydrogen gas evolution
5. Scission of polymeric chains
6. Production of free radicals.

Polymers containing a high percentage of aromatic rings have been found to be resistant to radiation (for example the polycarbonate resins); those with highly aliphatic structure are the least resistant.[48] There is also a general trend for polymers with the largest molecular size to be more susceptible to radiation damage. This arises from the fact that a small number of chain scissions or cross links can change a large percentage of the molecules. In agreement with these observations, cellulose nitrate is found to be one of the most sensitive of all polymers to high energy radiation.

CHAPTER III

DESCRIPTION OF INSTRUMENTS AND EXPERIMENTAL TECHNIQUES

In this chapter the instruments and the experimental techniques used in these investigations are discussed. Emphasis is placed mainly on the unusual, new, or unique aspects of the experimental portion of the research. Four broad subject areas are considered: the instruments and the experimental techniques for specimen preparation, radiation exposure of specimens, etching of specimens, and the measurement of various track parameters.

A. Specimen Preparation

At the present time most investigators using dielectric track detectors use commercially available plastics. There are two good reasons for this. First, the preparation of uniform, thin films of large areas is a complicated and a time consuming procedure, which at times requires large presses and other industrial equipment. Secondly, the exact composition as well as the details of preparation of certain plastics are generally regarded by the manufacturer as trade secrets and, therefore, are not available to the public.

Although there are commercially available cellulose nitrate plastics suitable for track recording (see Table III-1), there are certain difficulties associated with their use. For example, since the

exact composition is generally unknown, it is not possible to calculate accurate range-energy relations or to study the effects of the various constituents of the plastic on track registration. Different batches of plastic, different plastics within a batch, and even the two surfaces of a given sheet of plastic, usually vary in their track recording characteristics. The plastics are generally available in only a few thicknesses. The aging plastics tend to pick up background tracks from the natural alpha particle emitting reactions such as $^{222}Rn(\alpha)^{218}Po$.

TABLE III-1 Cellulose Nitrate Plastics

Type	Highest Energy Alpha Particle Recorded*	Background Etch Pit Density
NRDL-1	4.0 MeV	low
Daicel, Japan (250μ, red)	~ 5.0 MeV	fairly high
Dynamit Nobel, Germany (250μ, clear)	~ 3 MeV	very high
Nixon-Baldwin, U. S. (500μ, organge, clear)	4.0 MeV	low
Rowland, U. S.	~ 3 MeV	high

*For the most sensitive surface of the plastic, etching was performed in 10M NaOH solution at 23°C.

1. NRDL-1 Cellulose Nitrate Plastic

During these investigations, a mixture of ingredients was found which when properly processed resulted in a superior type of cellulose nitrate film well suited for the registration of tracks.

This material is referred to as NRDL-1 Cellulose Nitrate Plastic. Many of the investigations reported here, and particularly the investigations described in Chapter IV, were carried out using this material.

The composition of the nitrocellulose solution from which the NRDL-1 cellulose nitrate plastic is prepared is given in Table III-2. A detailed description of the possible role played by each constituent is further discussed in Section B of Chapter IV. The nitrocellulose used is RS (11.8-12.2% N_2), 5-6 sec viscosity commercial grade and is manufactured by the Hercules Powder Company, of Wilmington, Delaware.[41] The plasticizers and solvents are also of commercial grade.

TABLE III-2 Composition of the Nitrocellulose Solution for Preparation of NRDL-1 Plastics

Constituent	Quantity (% by Weight)	
5-6 sec RS nitrocellulose	17.0	(primary constituent)
Dioctyl phthalate	4.0	(monomeric plasticizer)
Isopropyl alcohol	5.1	(secondary solvents)
Butyl alcohol	4.0	
Cellosolve acetate	8.0	(primary solvents)
Ethyl acetate	61.9	

The preparation of the specimen films proceeded as follows. Commercial nitrocellulose, which contains 30% by weight isopropyl alcohol, is dissolved in a solvent composed of butyl alcohol, cellosolve acetate, and ethyl acetate. Dioctyl phthalate plasticizer

is added, and the mixture is stirred vigorously for several hours. The solution is then aged at room temperature for about 4 days before sample preparation begins. This time is required for the solution to come to equilibrium, and for the trapped air (in the form of bubbles) to come to the surface. Plastic films are cast by pouring the liquid on a polished glass surface and allowing the solvents to gradually evaporate. The evaporation rate of the solvents can be controlled by placing a glass container over the drying liquid. It is important to keep the solvent evaporation rate low so as to achieve a smooth surface. A drying period of about 24 hours was found to give satisfactory results. A film of about 50 microns in thickness is formed in this manner; thicker films are prepared by pouring multiple layers. The dry film is then annealed at 70°C for about 12 hours. This is an important step as the solvent content of the film needs to be reduced to a few percent to achieve good track recording characteristics. The film is separated from the glass surface by briefly soaking in warm water, after which it is dried, and is ready for use. Sometimes, particularly with thicker samples which have a tendency to buckle, it is desirable to anneal a second time. In this case the plastic is placed between two polished glass plates, held together by spring type clamps, and heated for several hours at a softening temperature of about 100°C. This procedure generally results in flatter samples and surfaces which are more highly polished.

It is important to minimize the number of surface imperfections such as scratches, bubbles, and imbedded dust particles. These imperfections tend to etch out preferentially, resulting in a badly

pitted surface. Electron photomicrographs of shadowed carbon replicas of the surfaces of NRDL-1 and No. 1025 Daicel plastics are shown in Figures III-1 and III-2, respectively. The numerous surface inclusions and striations are characteristic of the commercial plastics. The striations are generally still observed even after an etch treatment that may remove several tens of microns of the bulk material. Some inclusions may have dimensions of several hundred microns. In Figure III-3 is shown a portion of a specimen that has a linear inclusion which etched more slowly than the adjoining bulk material. This remarkably repeating structure, with the repeat distance of about 20μ, may possibly be a remnant of a cellulose fiber.

Samples prepared from NRDL-1 solution were observed to show differences in the times necessary to etch out tracks. Samples prepared from freshly mixed solutions required less time than those from older solutions. This effect is shown in Figure III-4. Samples poured at 0, 1, 2, 3, 4, and 8 days after solution preparation were dried and heat treated in the standard way, and exposed to 3.2 MeV alpha particles. The samples were progressively etched in a 10M NaOH solution at 40°C, until all tracks were fully etched out. The time necessary to fully etch out tracks versus elapsed time in days before sample preparation is shown in Figure III-4. It is clear that about four days are needed for the solution to stabilize. There are other indications of the non-equilibrium state of the freshly prepared solution: the viscosity of the solution is observed to drop slightly during this time interval.

FIGURE III-1. Shadowed carbon replica of the surface of NRDL-1 plastic.

FIGURE III-2. Shadowed carbon replica of the surface of type No. 1025 Daicel plastic. The numerous surface inclusions and striations are characteristic of the commercial plastics.

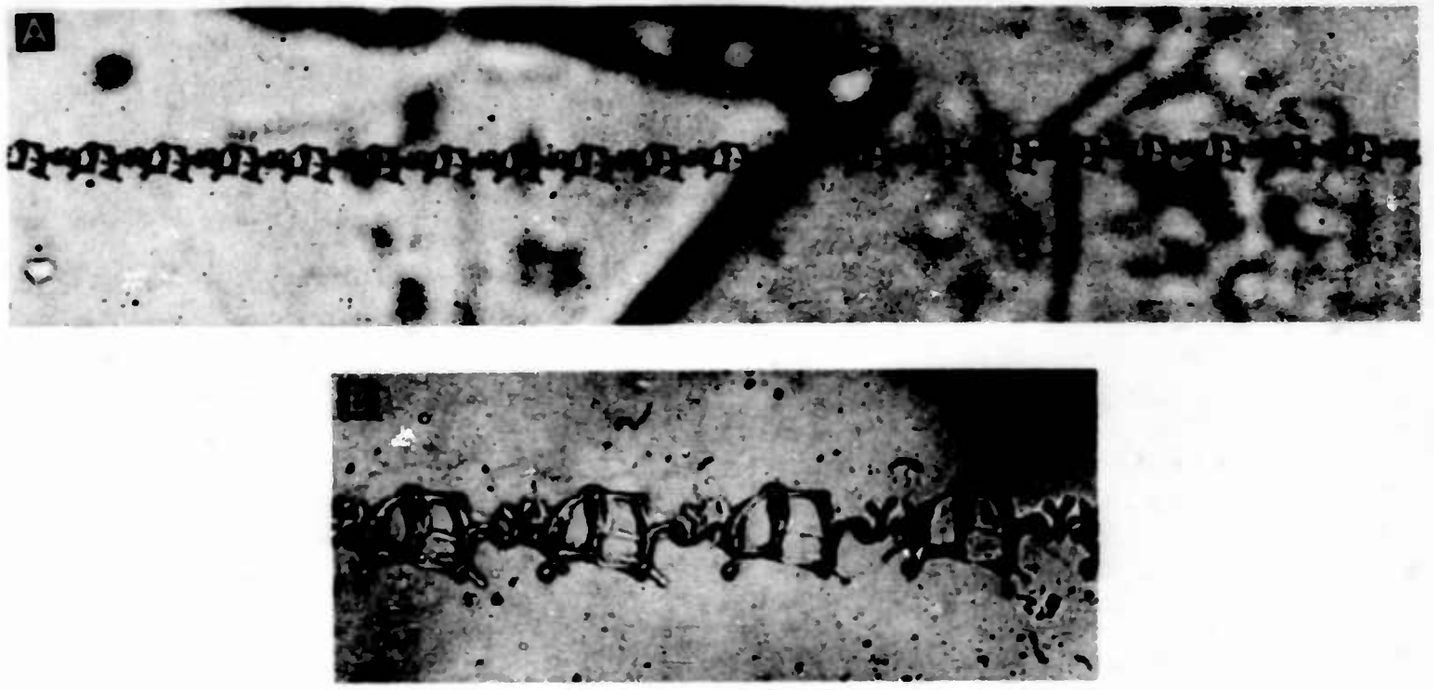

FIGURE III-3. Photomicrograph of an etched surface of cellulose nitrate plastic showing an inclusion. The material of the imperfection etched more slowly than the adjoining material.

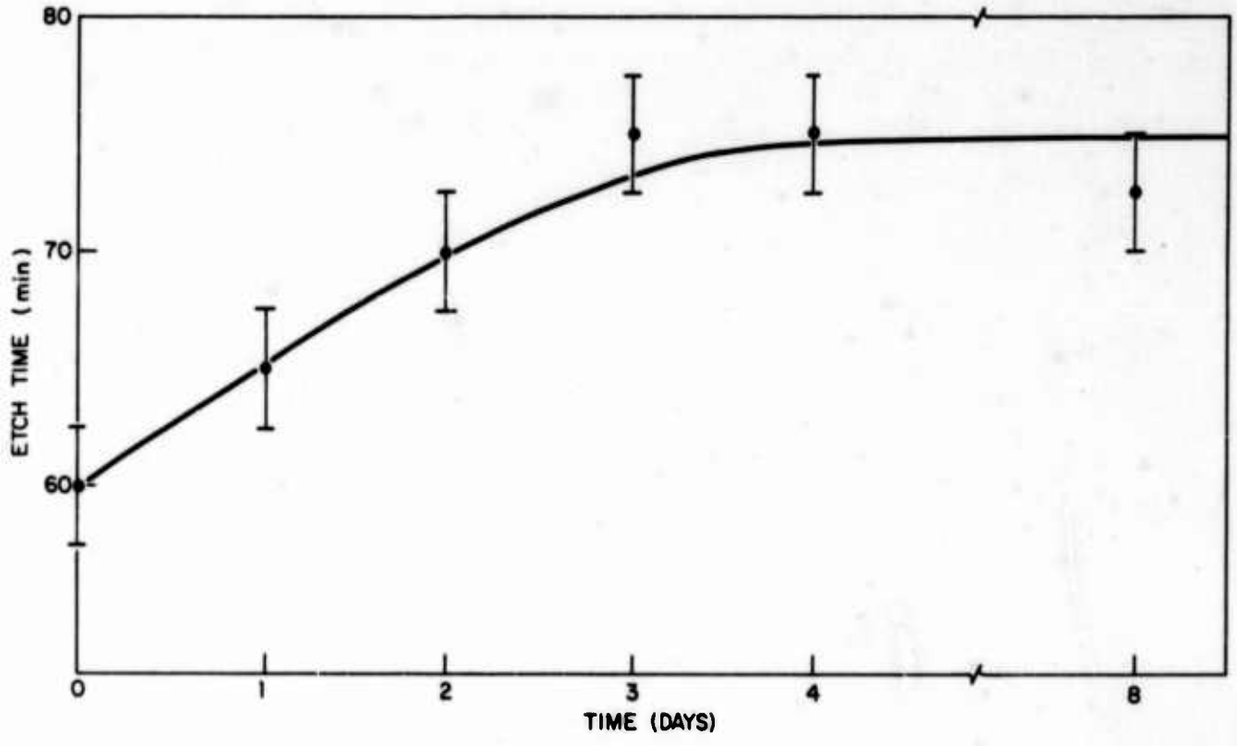

FIGURE III-4. The time (minutes) necessary to fully etch out 3.2 MeV alpha particle tracks as a function of the age, in days, of the nitrocellulose solution.

The chemical reactivity of cellulose and of cellulose nitrate has been reported to be highly dependent upon the impurities present.[49] During these studies it was not possible to determine the purity of either the nitrocellulose or the other constituents used in the specimen preparation. As an example of the types and concentration of metal ions present, a spectroscopic analysis of three different types of nitrocellulose is shown in Table III-3.*

TABLE III-3 Spectroscopic Analysis of Three Types of Nitrocellulose (ppm)

Ion	Degree of Nitration		
	12% (RS)	11.5% (AS)	11% (SS)
Pb	3	0.8	5
Zn	20	< 2.0	100
Cu	2	0.8	2
Mg	10	15	10
Mn	0.2	0.2	0.2
Ni	0.5	0.5	0.5
Fe	3	3	3
Al	10	5	10
Ca	30	30	15
Ti	2	0.2	< 0.2

2. Commercial Cellulose Nitrate Plastics

The cellulose nitrate plastics used in these studies are tabulated in Table III-1. The Daicel material, recording alpha particles of energies up to about 5 MeV (determined from track length measurements), is the most sensitive plastic tested. The Dynamit Nobel and the Rowland plastics are considerably less sensitive and also have poor surface etching characteristics. The Nixon-Baldwin material, although somewhat less sensitive than the Daicel plastic,

* The spectroscopic analysis data were obtained through the courtesy of Mr. C. Gilbert, Hercules Inc., Parlin, New Jersey.

nevertheless is a satisfactory track recording material. Unfortunately this material is no longer manufactured.

In general, the two surfaces of a single sheet of a commercial plastic will differ in sensitivity. The difference may be considerable. For example, while one surface may record alpha particles of up to 4 MeV, the other surface may register alpha particles only to about 1 or 2 MeV. A further difficulty with using commercial plastics is that the manufacturer generally insists on a rather large minimum order (160 pounds in the case of the Daicel Ltd.).

B. Radiation Exposure

The study called for exposures of cellulose nitrate plastic to a broad spectrum of heavy ion particle types and energies; in Table III-4 are listed the natural and artificial sources used.

TABLE III-4 Heavy Ions Used in this Study

Source	Particle	Energy (MeV/nucleon)
^{241}Am	^{4}He	1.37
^{252}Cf	fission fragments $1 < z < 4$, long range ^{4}He	~ 1 $\gtrsim 1$ 1.52
Hilac, Berkeley	^{12}C, ^{16}O, ^{40}Ar	1-10
High altitude balloon flights, Ft. Churchill, ~ 3.7 g/cm^2	^{16}O ^{56}Fe	$\gtrsim 140$ $\gtrsim 270$
Satellite exposures, (Gemini), > 1 g/cm^2	^{56}Fe	$\gtrsim 5 \times 10^3$

1. Alpha Particles

The principal source of alpha particles was a 2.87 μc ^{241}Am source in a form of a thin deposit on a 1 inch in diameter platinum disk. The isotope was electrodeposited on the central area of about 3 mm in diameter. The half life of this isotope is 458 years. The two modes of alpha decay have similar energies of 5.48 and 5.31 - 5.54 MeV. Calibration with nuclear emulsions revealed a negligible amount of self-absorption in the source, thus the alpha particles were considered to be monoenergetic.

Exposures were usually performed in a partially evacuated chamber with a standard source-to-sample distance. By varying the air pressure alpha particles of any energy from 5.5 to about 0.40 MeV could be readily obtained.

2. Fission Fragments

A 6 x 10^5 dpm spontaneously fissionable isotope of ^{252}Cf electrodeposited onto a thin platinum disk was used as a source of fission fragments. This isotope also emits alpha particles (6.12 and 6.08 MeV) and spontaneous neutrons. For approximately 1 out of every 10^6 fissions of ^{252}Cf, a long range, light ($1 \leq z \leq 4$) particle may also be emitted.[50,51] In Figure III-5 are shown photomicrographs of tracks of the three types of charged particles. The short, wide tracks are the overetched tracks of fission fragments. The short narrow track in B is that of an alpha particle; the long track in A is that due to a rare, long range, low z particle. The half life of the isotope is 2.55 years. The mass and kinetic energy distributions of fission fragments emitted from ^{252}Cf have been studied by Fraser et al.[52]

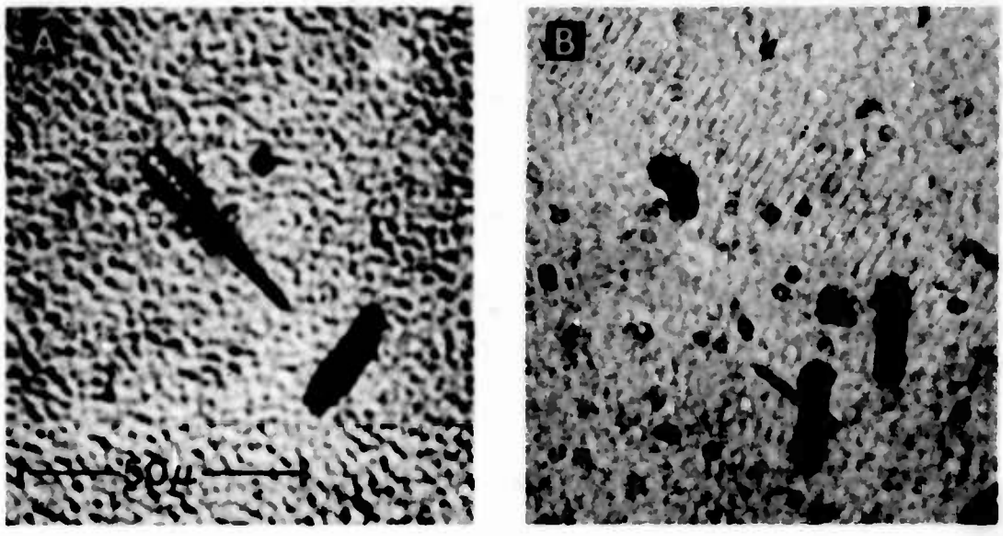

FIGURE III-5. Tracks of particles emitted from ^{252}Cf: the short, wide tracks are the overetched tracks of fission fragments; the short, narrow track in B is that of an alpha particle; the long track in A is that of a rare, long range, $z > 2$ particle.

3. Heavy Ions of Energy < 10 MeV/nucleon

Heavy ions, ^{12}C, ^{16}O, and ^{40}Ar with energies up to 10 MeV/nucleon, were obtained from the Heavy Ion Linear Accelerator (HILAC) at Berkeley.[53] Lower energies were obtained by degrading the full energy of the beam with predetermined thicknesses of aluminum. In this manner useful energies in the interval of from 1.0 to 10 MeV/nucleon were obtained. In order to make precise and independent energy determination possible, nuclear photographic emulsions were included with all irradiations.

4. Heavy Ions of Energy > 10 MeV/nucleon

The heaviest ion currently available at the HILAC is ^{40}Ar. Since there are presently no techniques available for artificially accelerating heavy ions to energies in excess of 10 MeV/nucleon, natural sources of these particles found in cosmic rays must be utilized. Specimens were flown on a variety of high altitude balloon and satellite flights for this purpose (see Table III-4, page 41).

C. Etching Techniques

Irradiated specimens were usually etched in an aqueous solution of 10M NaOH which was maintained at a constant temperature by means of a water bath.* Etching was usually performed at either 23, 40 or 60°C, although temperatures as low as 0°C and as high as 98°C were occasionally used. Since the etch products tend to settle to the bottom of the etching container, stirring of the solution is necessary; ultrasonic stirring has proved most effective.

* In this dissertation the symbol M is used to denote the molality of the etching solution.

When measuring track etch rates, it is desirable to view the tracks during the actual etching process. The removal of the specimens from the etching solution for this purpose causes some difficulties. There is evidence that a freshly etched surface reacts with the atmosphere to produce a thin layer of material whose etching properties are different from that of the bulk material. Also, extended rinsing in water of partially etched tracks may result in a large increase in both r_T and r_B for the remainder of the track. An example of this phenomenon is shown in Figure III-6. Here, a 10 MeV/nucleon ^{16}O ion track was first etched for 8 hours at 23°C in a 10M NaOH solution. This resulted in the observable track length ℓ_1. The specimen was then allowed to soak in distilled water overnight. The specimen was then etched again under the same etch conditions for 0.5 hours. This resulted in the observable track length, ℓ_2. An increase in the average track etch rate from 18 μ/hr for ℓ_1 to 200 μ/hr for ℓ_2 was observed. At the same time, the unusual appearance of the track indicates that the water soaking treatment also resulted in the increase in r_B for the previously unetched portion of the track. This type of behavior was not observed for the previously unetched tracks. Presoaking in water of previously unetched specimens resulted in an increase in the etch time needed to develop tracks.

A technique was devised for the observation of tracks during the actual etching process. If etching is carried out in a shallow container with a glass bottom for illuminating the specimen, tracks can be observed directly through the etching solution with the use of a very long working distance objective. The Leitz UMK 50X objective,

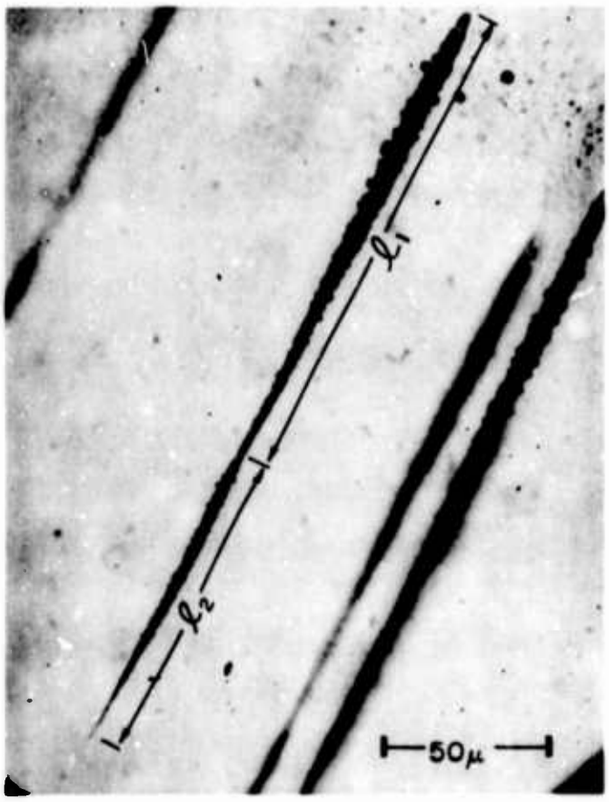

FIGURE III-6. Track of a 10 MeV/nucleon ^{16}O ion in NRDL-1 plastic etched in a 10M NaOH solution at 23°C. Specimen was first etched for 8 hrs (ℓ_1), then soaked in distilled water overnight, then etched again for 0.5 hr (ℓ_2).

described later in this chapter, was found to work satisfactorily. Tracks viewed in this manner are not very distinct; the resolution is only fair. The difficulty comes about because the track cavities are filled with the etchant which has an index of refraction similar to that of the plastic. This technique was used for etching at room temperatures only; however, it can readily be extended to etching at higher temperatures.

D. Optical Techniques for the Observation and Measurement of Tracks*

The chemical etch development of the particle damage trails produces permanent, three dimensional cavities or tracks. The dimensions of tracks may vary from a fraction of a micron to several hundred microns. The observation and measurement of tracks requires the use of an optical microscope. The precision with which track parameters of interest, such as track lengths, cone angles, or surface openings, may be measured depends upon the optical resolution attainable as well as the ability to perform the actual measurements.

The microscopy of etched tracks has a number of unusual aspects that are generally not encountered in ordinary microscopy. The problem centers on the fact that usually the etched tracks are in the form of transparent cavities rather than opaque objects such as silver grains in the processed nuclear photographic emulsions. Some of the major difficulties encountered are as follows:

1. The difference in the index of refraction of the track cavity and the bulk material is small.

*The actual microscope equipment for track analysis is described in Appendix VI.

2. Inhomogeneities and inclusions present in most commercial plastics cause a variation in the index of refraction of the bulk material.

3. The heavily pitted surfaces of the etched plastics degrade the optical image.

4. Thick specimens may require objectives and condencers with larger working distances than available.

5. Track cavities tend to fill up with liquids when immersion objectives are used, thus reducing track image contrast.

6. Track dimensions may be small, requiring the use of high numerical aperture (N.A.) objective-condencer combinations.

Most of these difficulties, in general, can be overcome by the use of either one or a combination of optical techniques that are described below.

1. Bright-Field, Transmitted Light Illumination

a. Dry Objectives:

For many measurements, track observations, and rapid scanning of the specimens at low magnifications, dry objectives are easy and convenient to use. A few dry lenses, even of moderate magnifying power, have long working distances. This permits the observation of steeply dipping, long tracks when tilting of the specimen is required. The Leitz, UMK 50X, N.A. 0.60 objective having a working distance of 5 mm is an excellent example of this type of lens. The photomicrographs of tracks shown in Figure III-7 were obtained using this objective. The gaps and the apparently missing terminal ends of tracks are the result of trapped liquids (in this case water from the

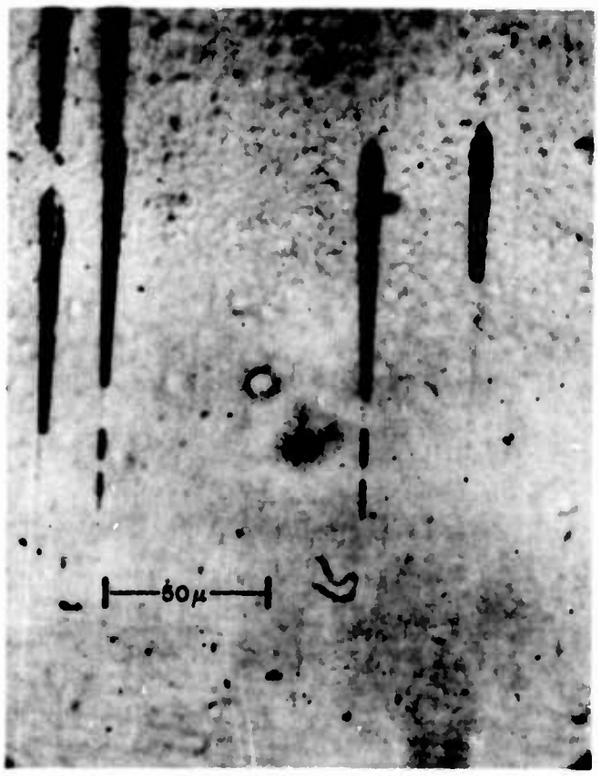

FIGURE III-7. The gaps and the apparent missing terminal ends of tracks are the result of trapped liquids.

washing process). The photomicrographs shown in Figure III-8A and B were also taken using this lens. In Figure III-8A is shown the usual appearance of a dry track; Figure III-8B shows the same track when the specimen is covered with a thin layer of ethyl alcohol. This technique can be used for viewing and photomicrography of tracks in specimens with badly pitted surfaces.

The main limitation of the dry objectives is the lack of high resolution. While dry objectives are available with N.A.'s of up to 0.95, most of the lenses with N.A.'s over about 0.60 require the use of an exact thickness coverglass. This requirement decreases considerably their utility. An exception to this rule is an objective such as the Tiyoda 60X, N.A. 0.85, which does not require a coverglass. This objective was found to be useful in the observation of relatively small size tracks, such as fission fragments (see Figure III-9). As is generally the case with the high N.A. dry lenses, the working distance of this objective is only 170 microns.

b. Immersion Objectives

These are generally of two types, oil or water. The immersion objectives are characteristically of higher N.A. (up to about 1.40) than the dry lenses. Consequently, they are capable of higher resolution. The use of these objectives requires procedures that are considerably more exacting than those necessary with the dry lenses. To achieve the full resolution of the objectives with N.A.'s of over 1.00 requires the use of an oil immersion condencer. However, the use of an oil immersion objective, without oiling the condencer, will still give greater resolution than that possible with the dry lenses. It is

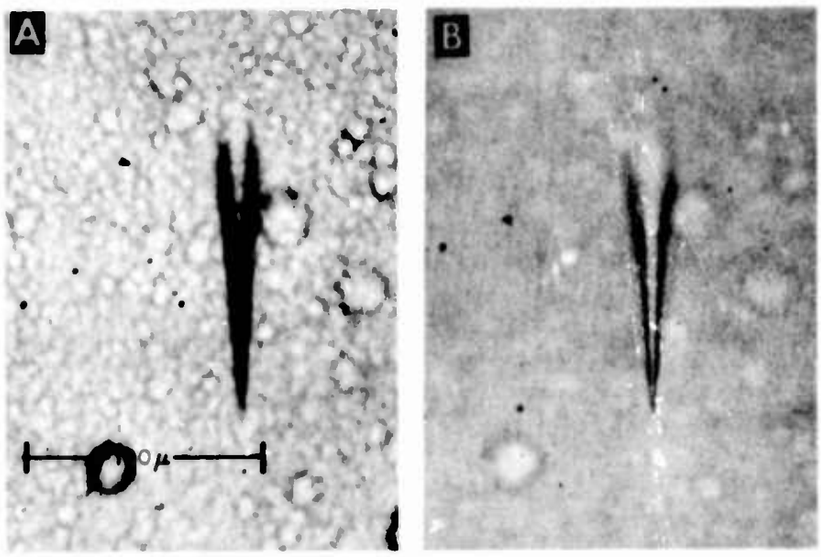

FIGURE III-8. In (A) is shown a typical, short track in a specimen with a moderately pitted surface. In (B) is shown the same track when the specimen is covered with a thin layer of ethyl alcohol. The terminal end of the track in (A) is not observable; it is distinct in (B).

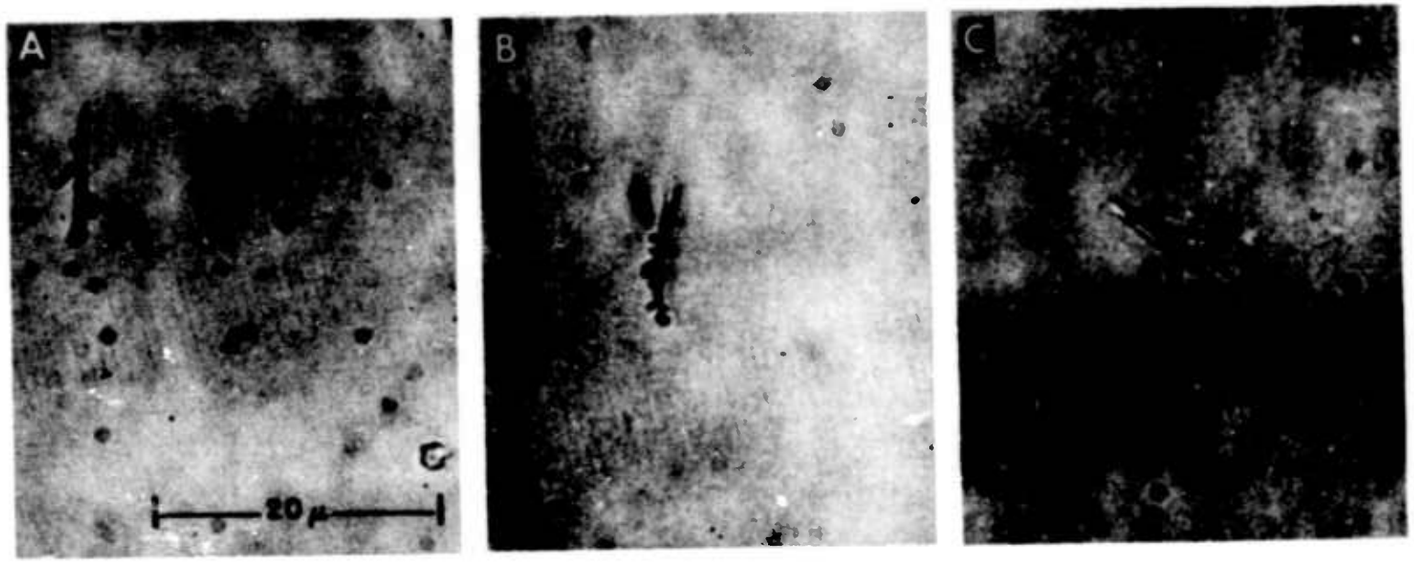

FIGURE III-9. Photomicrographs, taken with a Tiyoda 60X, N.A. 0.85 objective, of fission fragment tracks in NRDL-1 cellulose nitrate plastic. Note the numerous dots and spurs which are the secondary tracks produced by the recoiling nuclei.

possible to overcome the problem of oil seepage into track cavities by covering the specimen with a transparent film such as a glass coverslip or a thin plastic film. However, it is essential to eliminate the air gap between the coverslip and the specimen. Otherwise the numerical aperture greater than 1.00 cannot be achieved.

A decided advantage of these objectives over the dry lenses with high magnification is the generally longer working distance. In fact, one 100X objective (Leitz), developed for use with nuclear emulsions, has a working distance of up to 650 microns at a N.A. of 1.32. The depth of field of the high N.A. objectives is very small. This feature makes the oil immersion objectives less desirable for general scanning than the dry objectives. However, the immersion objectives are extremely valuable for precise measurements, particularly the measurements of the vertical (z) dimensions. In Figure III-10 is shown a photomicrograph of fission fragment tracks. The photograph was made using Leitz Plano 100X N.A. 1.32 oil immersion objective in combination with an oiled condencer.

2. Dark-Field Illumination

For track observation using bright field, oil immersion optics, the lower practical limit for track diameters was found to be about 0.4 microns. It is possible to observe tracks as small as 0.1 microns in diameters with the use of oil immersion, dark field illumination. Although this type of dark field illumination requires a careful and a time consuming optical alignment, it is one of the only techniques available for the observation of very small tracks, such as those of low energy recoiling particles. In Figure III-11 is

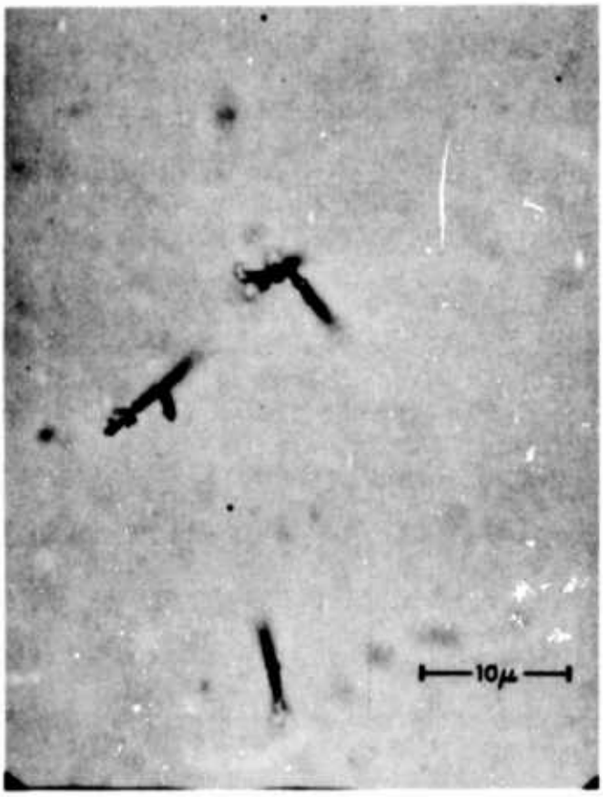

FIGURE III-10. Photomicrograph of fission fragment tracks taken with a Leitz Plano 100X N. A. 1.32 oil immersion objective in combination with an oiled condenser.

FIGURE III-11. Photomicrograph of tracks with diameters less than 0.2 microns taken using Leitz Apo 100X/1.32 oil immersion objective and an oiled condenser in dark field illumination (ultramicroscopy).

shown a photomicrograph of fission fragment tracks whose diameters are less than 0.2 microns.

The lower power, dry, dark field techniques are very useful in the general scanning work. The depth of field is considerably greater than with bright field illumination, permitting the observation of larger track segments. The considerable image contrast of track to background is also quite helpful. For accurate measurements, dark field is not particularly useful since track dimensions tend to be somewhat exagerated.

3. Phase Contrast Microscopy

For observation of small, low contrast tracks, such as shallow etch pits and recoil particle tracks, phase contrast microscopy can be effectively utilized (see Figures III-12A and B). It is particularly useful for the observation of long narrow tracks where the retention of liquids has rendered the terminal ends of tracks invisible under bright field illumination. However, if the track contrast is adequate for the standard bright field optics, the phase contrast image is less satisfactory. For the larger tracks with appreciable dip angles, a "halo" surrounds the image (see Figure III-12B).

Phase contrast is available in the normal, or the positive, and the negative types. For track observation the negative type was found to be more useful. In this case, the track image is delineated by a sharp black border. This unique feature distinguishes the image obtained with the negative phase contrast techniques from that of the positive phase, or the standard dark field illumination.

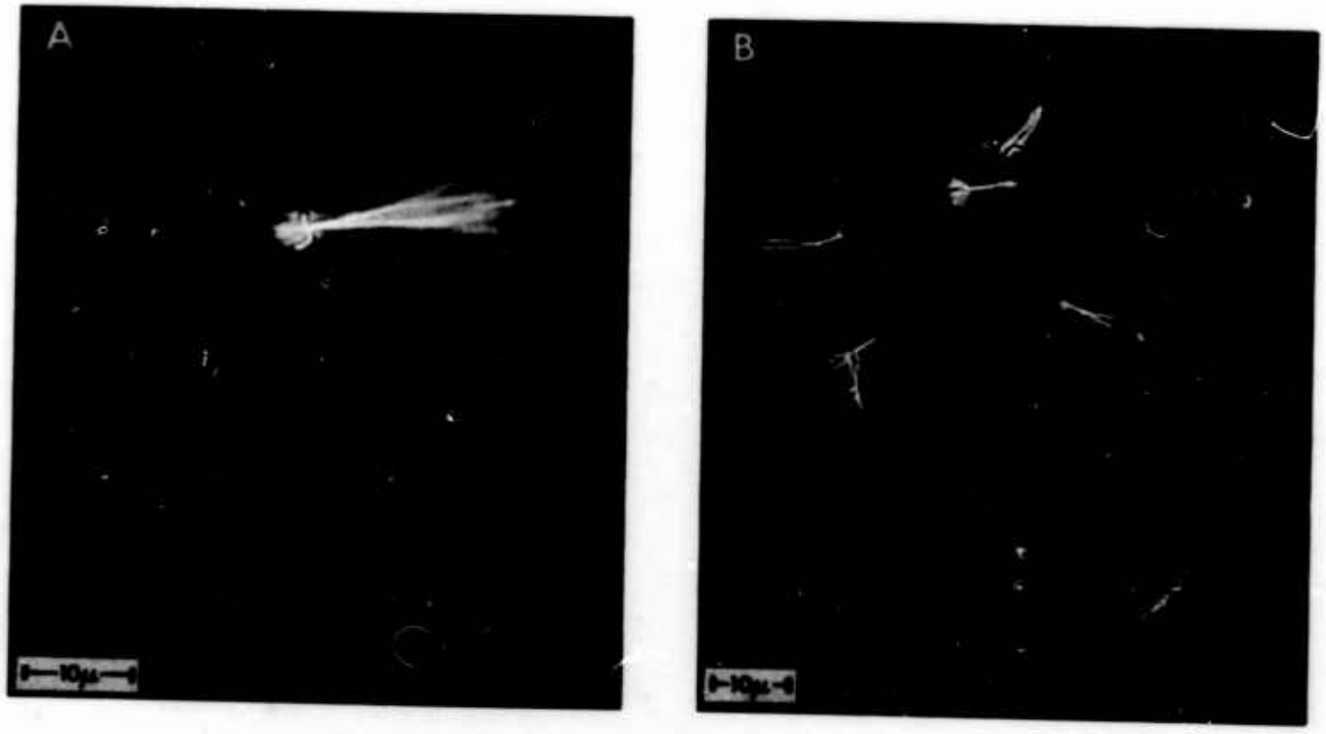

FIGURE III-12. (A) Negative phase contrast, using Reichert 100X/1.20 Anoptrol objective and a Polyphos oiled condenser. Note the black border around the small, secondary track. (B) Normal (positive) phase contrast, using Zeiss 40X/0.75 dry objective.

4. Incident Light Illumination

For track observation in specimens that are very thick (> 2 mm), or specimens containing inhomogeneities or inclusions, the use of the incident light optics was found to be useful. The Leitz Ultrapac and the Zeiss EPI-Condencer systems were both found to work satisfactorily. Usually the resolution is somewhat inferior to the transmitted light systems. Because of image degradation, observations are restricted to depths of less than about 50 microns into the volume of the specimen. With long working distances and dip cones available, incident light techniques can be used for observation of tracks in specimens that are still immersed in the etching solution contained in opaque etching tanks.

CHAPTER IV

TRACK DEVELOPMENT BY MEANS OF CHEMICAL ETCHING

The studies reported in this chapter were motivated by the need to better understand the variables that control the track etch process. It was hoped that criteria could be established for the design of plastics that are more sensitive and are better suited for track registration than the present materials.

The parameters that affect the chemical etch development of tracks can be conveniently divided into three broad categories: the specimen composition parameters, the etching solution parameters, and the parameters associated with the charged particle. The effects of the first two sets of parameters on the chemical etch development of tracks are discussed in this chapter, and the effects of the charged particle parameters are discussed in Chapter VII. The major part of this study centers around NRDL-1, cellulose nitrate plastic, which was chosen for this study because it is the most sensitive plastic whose composition is presently known. However, before proceeding further, it is instructive to examine the geometry of tracks.

A. Track Geometry

1. Theoretical Considerations

In Figures IV-1, (a) through (e), are shown a set of photomicrographs of etched tracks of 10.4 MeV/nucleon ^{40}Ar ions in NRDL-1 cellulose nitrate, incident on the plastic with dip angles of 5, 10, 20, 30 and 90 degrees, respectively. The dip angle, δ, is the angle between the particle trajectory and the surface. The plastic specimens were given only a partial etch so that the observed track length is less than the total range of the particles. From Figures I-3, I-4, and IV-1, one sees that tracks may be approximated as etch pits in the form of hollow cones which intersect the sample surface at various dip angles. The intersection of a dipping track with the surface results in an elliptical opening.

In practice, deviations of track shape from perfect cones are sometimes observed. This may occur for several reasons: the bulk material may etch anisotropically, the original surface of the plastic may have a different etch rate than the bulk material, the charged particle may experience a rapid change of ionization along its trajectory, for long tracks etchant diffusion effects may become significant, and the copious number of low energy δ-rays produced by a slow multicharged particle may alter the bulk etch rate in the vicinity of the particle's trajectory. These factors may combine to produce a track shape considerably different from a perfect cone. In the following derivation these complicating factors will be neglected. It will also be assumed that the preferential etch rate is restricted to a very narrow region along the particle's trajectory, much smaller than the final dimensions of the etched track.

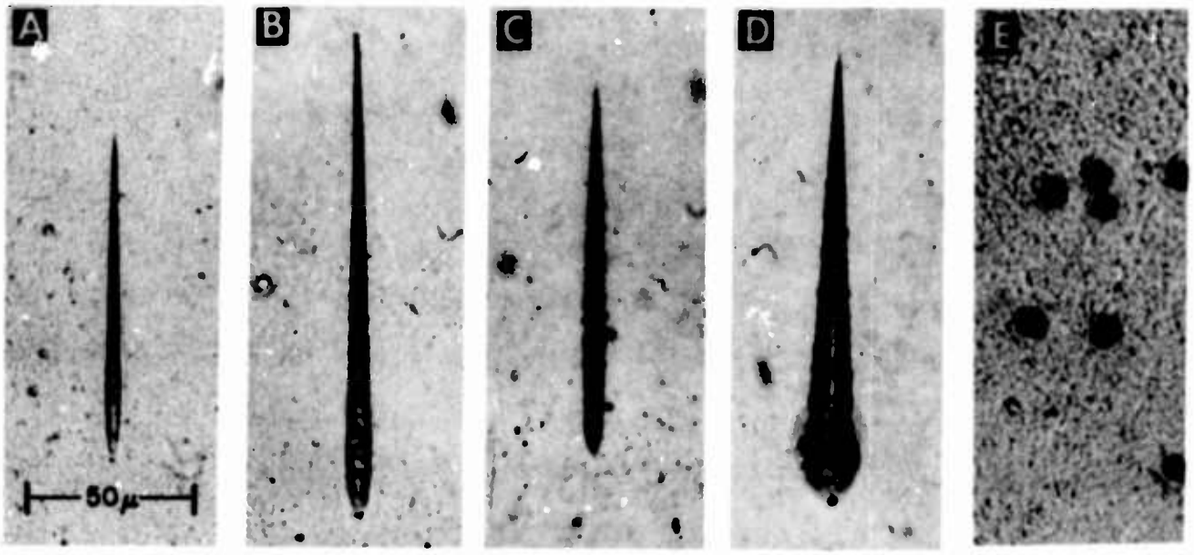

FIGURE IV-1. Tracks of the initial portions of 10.4 MeV/nucleon ^{40}Ar ions in NRDL-1 plastic. The tracks have dip angles of 5, 10, 20, 30 and 90 degrees, respectively.

The track quantities of the greatest interest are those that provide information with regard to the charged particle: the track length, ℓ, and the track cone angle, θ. It will be shown in Chapter VII that these quantities and the variation of these quantities as a function of range, can be used to determine the particle charge, mass, and velocity. Also of interest is the particle's range, R, in the plastic. This quantity, which is related to the particle's kinetic energy, E, is measured from the point of entry into the original surface before etch, to the point where the particle came to rest.

In the measurement of track length, ℓ, it is necessary to know which point in the ellipse, formed as a result of the intersection of the track cavity with the plastic's surface, represents the point on the incident charged particle trajectory. Also, since the observation and measurement of tracks is performed with a microscope, measurements are made of the projected track quantities such as ℓ_p and θ_p rather than ℓ and θ. Thus we seek relationships between the projected and the real parameters as well as other useful relations between the readily measurable track quantities and the track parameters of interest.

The equation describing a cone may be written as

$$(x')^2 + (y')^2 = (z' + \ell)^2 \tan^2\theta, \qquad (4.1)$$

where x', y', z' are points on the surface of the cone in a primed coordinate system which is rigidly fixed to the cone. In order to find the equation of a cone with an arbitrary dip angle, δ, with respect to the fixed laboratory coordinate system, (x, y, z), the unprimed system is rotated through an angle (δ-90) degrees about the

y axis (see Figure IV-2). The equations of transformation are

$$x' = x \sin\delta + z \cos\delta$$
$$y' = y, \quad \text{and} \tag{4.2}$$
$$z' = -x \cos\delta + z \sin\delta .$$

Substituting Equations (4.2) into Equation (4.1) gives the equation of the cone in the fixed laboratory frame (see Figure IV-2),

$$(x \sin\delta + z \cos\delta)^2 + y^2 = (-x \cos\delta + z \sin\delta + \ell)^2 \tan^2\theta. \tag{4.3}$$

The vertex position of the cone is at

$$x = \ell \cos\delta,$$
$$y = 0, \quad \text{and} \tag{4.4}$$
$$z = -\ell \sin\delta.$$

Setting $z = 0$ and transforming Equation (4.3) into the form

$$\left(\frac{x - x_o}{a}\right)^2 + \left(\frac{y}{b}\right)^2 = 1, \tag{4.5}$$

gives the equation of the ellipse with

$$a = \frac{\ell \tan\theta \sin\delta}{(1-\cos^2\delta \sec^2\theta)}, \tag{4.6}$$

$$b = \frac{\ell \tan\theta \sin\delta}{(1-\cos^2\delta \sec^2\theta)^{1/2}}, \quad \text{and} \tag{4.7}$$

$$x_o = \frac{-\ell \cos\delta \tan^2\theta}{(1-\cos^2\delta \sec^2\theta)}, \quad \text{(see Figure IV-3).} \tag{4.8}$$

It can be seen that the center of the ellipse is at $x_o < 0$ and is not at the particle trajectory, (0,0), for $z = 0$. From Equations (4.6) - (4.8) it is observed that the quantities a, b, and x_o become

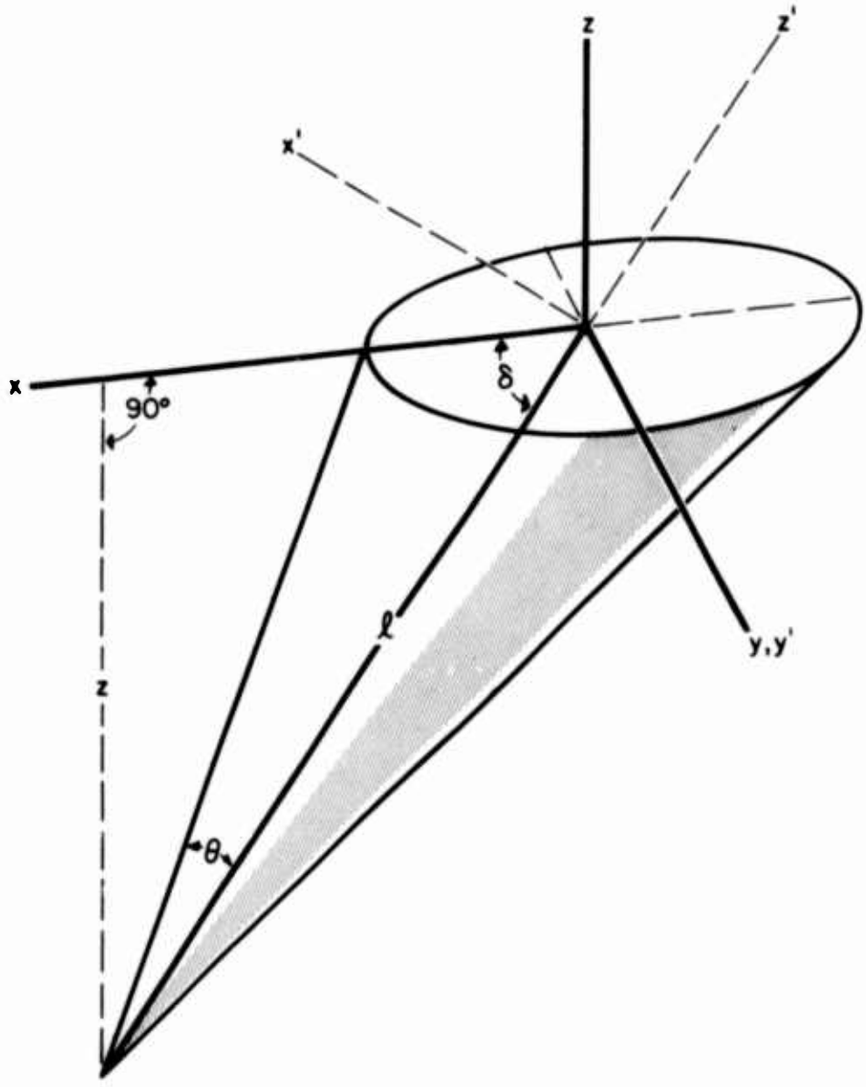

FIGURE IV-2. The surface of a cone when the primed coordinate system is rotated through an angle of (δ-90) degrees about the y axis.

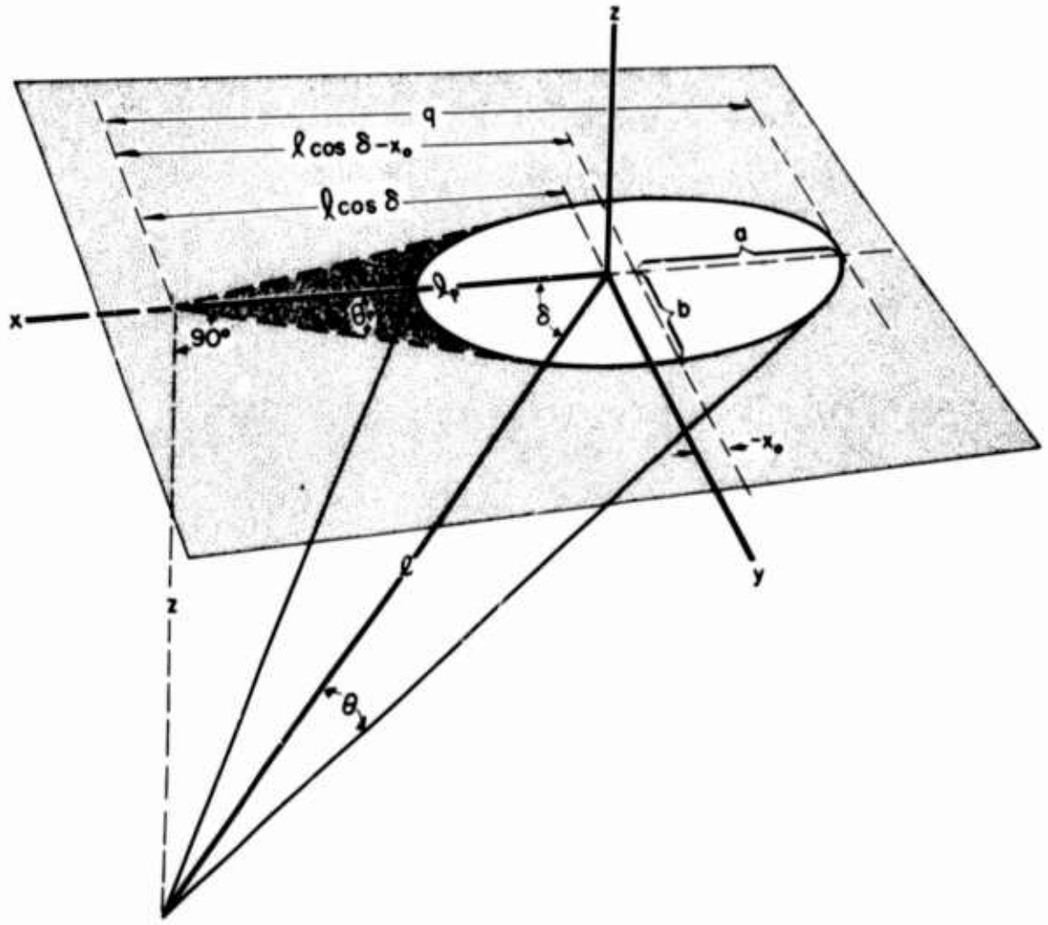

FIGURE IV-3. A general case of a cone which intersects the xy plane at an angle δ.

very large as θ approaches δ; when θ equals δ then a, b, and x_o become infinite.

The point in the ellipse which represents the point on the incident charged particle trajectory, x_o, is found from Equations (4.6) and (4.8) to be conveniently given by

$$x_o = -a \frac{\tan\theta}{\tan\delta} \quad . \tag{4.9}$$

Or, since the semiminor axis, b, can usually be measured more accurately than the semimajor axis, a, x_o can be expressed as,

$$x_o = -b \frac{\tan\theta}{\tan\delta \ (1-\cos^2\delta \ \sec^2\theta)^{1/2}} \quad . \tag{4.10}$$

The ratio of Equations (4.6) and (4.7) yield,

$$\frac{a}{b} = \frac{1}{(1-\cos^2\delta \ \sec^2\theta)^{1/2}} \quad . \tag{4.11}$$

If δ is known, then Equation (4.11) can be used to find θ. An example of a track with $\theta \simeq \delta$ is shown in Figure IV-4. Here δ is known to be 20°; measurements of a/b together with Equation (4.11) yield $\theta = 18 \pm 2$ degrees.

In Figure IV-3 is shown a general case of an ideal track and its projection onto the xy plane. The parameters of interest are ℓ, θ, and δ. However, the readily measurable parameters are θ_p, q, a, b, and z. The relationship between the projected cone angle, θ_p, and the actual cone angle, θ, can be shown to be,

$$\sin\theta = \cos\delta \ \sin\theta_p \quad . \tag{4.12}$$

This relation is required when measurements of θ are made using an eyepiece-gonimeter combination. The track length, ℓ, may be found

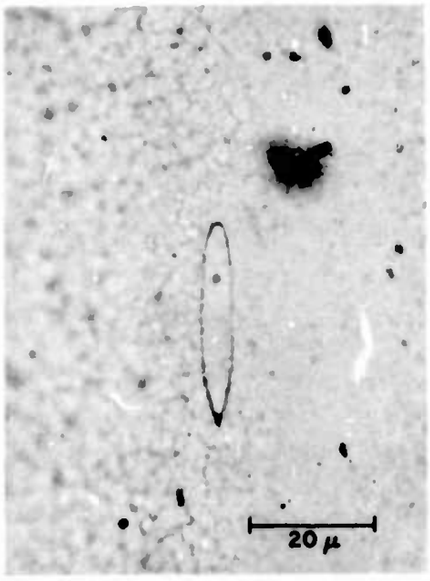

FIGURE IV-4. An example of a track with $\theta \sim \delta$. Here δ is known to be 20°; the measurement of a/b together with Equation (4.11) yield $\theta = 18 \pm 2^{\circ}$. The photomicrograph has been slightly retouched in order to delineate the track boundary more distinctly.

from the measurements of the projected track length, ℓ_p, by

$$\ell_p = \ell \cos\delta . \tag{4.13}$$

The dip angle, δ, can be found from the measurements of a, b, and θ_p from,

$$\cos\delta = \left[\frac{1 - (\frac{b}{a})^2}{1 + \sin^2\theta_p [1-(\frac{b}{a})^2]} \right]^{1/2}, \tag{4.14a}$$

or if z is known, from

$$\tan\delta = \frac{q(z^2+b^2) + b[(z^2+b^2)\,(z^2+q^2)]^{1/2}}{z(q^2 - b^2)} . \tag{4.14b}$$

The observed track length, ℓ, for a track incident at an angle δ to the surface is given by

$$\ell = \int_o^t \left[r_T - r_B(\csc\delta) \right] dt' , \tag{4.15}$$

where t is the etch time. The bulk etch rate, r_B, can generally be assumed to be a constant. The second term in Equation (4.15) represents the length of the track lost as a result of the loss of $(r_B t)$ thickness of the surface. If $r_T/(r_B \csc\delta) > 1$, ℓ will increase with etch time until the etchant reaches the end of the particle damage trail, where $r_T = r_B$. With continued etching the terminus of the etched track will become round. If the plastic etches isotropically, further etching results in the track opening becoming larger while the ratio a/b remains constant. The rate of change of the length of overetched tracks (those with rounded ends) with time is given by,

$$\frac{d\ell}{dt} = r_B(1-\csc\delta) \ . \tag{4.16}$$

Thus, for $\delta < 90^\circ$, the tracks decrease in length; the decrease is most rapid at small values of δ.

The true track length (the length from the original surface to the terminal end of the track),

$$L \equiv \ell + r_B t \csc\delta \ , \tag{4.17}$$

can be conveniently found from,

$$L = \frac{z}{(\sin\delta - \sin\theta)} \ , \tag{4.18}$$

where z is the vertical distance to the terminal end of the track measured from the etched surface. The amount of surface removed, $r_B t$, during an etch interval t is given by

$$r_B t = \frac{z \sin\theta}{(\sin\delta - \sin\theta)} \ . \tag{4.19}$$

It is sometimes more convenient to determine $r_B t$ from the measurement of b rather than z. In this case $r_B t$ is given by

$$r_B t = b\left[\frac{\tan\frac{1}{2}(\delta+\theta)}{\tan\frac{1}{2}(\delta-\theta)}\right]^{1/2} . \tag{4.20}$$

Meaningful information can be obtained even from grossly over-etched tracks. Since the ratio of the major to minor axis of the elliptical track opening remains approximately constant, and since the dip angle can generally be estimated, the track cone angle, θ, can be deduced with the help of previously developed equations.

2. Experimental Observations

The geometry of tracks may differ considerably from the ideal case, that of a perfect cone. For example, the track shape was found to depend on the type of cellulose nitrate plastic used, as well as on the etching conditions. There is also dependence on the dE/dx of the incident charged particle and the manner in which the ionization changes along the trajectory. Etching performed at the higher temperatures ($\sim 60^{\circ}C$) was found to result in tracks closely approximating the ideal track shape irrespective of the particle types or the sources of cellulose nitrate plastic (see Figures I-1, I-2, IV-1). However, at room temperature and below, the etch process is different from that at high temperatures. Here, diffusion effects retarding the removal of reaction products from the track cavities become evident. Etching performed at $0^{\circ}C$ results in tracks that are no longer hollow cones, but rather cavities which are filled with the etch reaction products.

At the lower temperatures, the difference in track shape between plastics obtained from the various sources becomes apparent. Photomicrographs of tracks from four different sources are shown in Figure IV-5, all etched in 10M NaOH at $23^{\circ}C$. Those labeled (A), (B), and (C) are tracks of 10 MeV/nucleon ^{40}Ar ions (a single exposure at the Hilac) in NRDL-1, Nixon-Baldwin, and Rowland cellulose nitrate plastics, etched together for 4.5 hr. Those labeled (D) and (E) are tracks of 5 MeV/nucleon ^{12}C ions (again a single exposure) in Daicel and NRDL-1 cellulose nitrate plastics etched together for 5.0 hr. The etching behavior in commercial plastics has been observed to be distinctly different from that in NRDL-1 material. The commercial

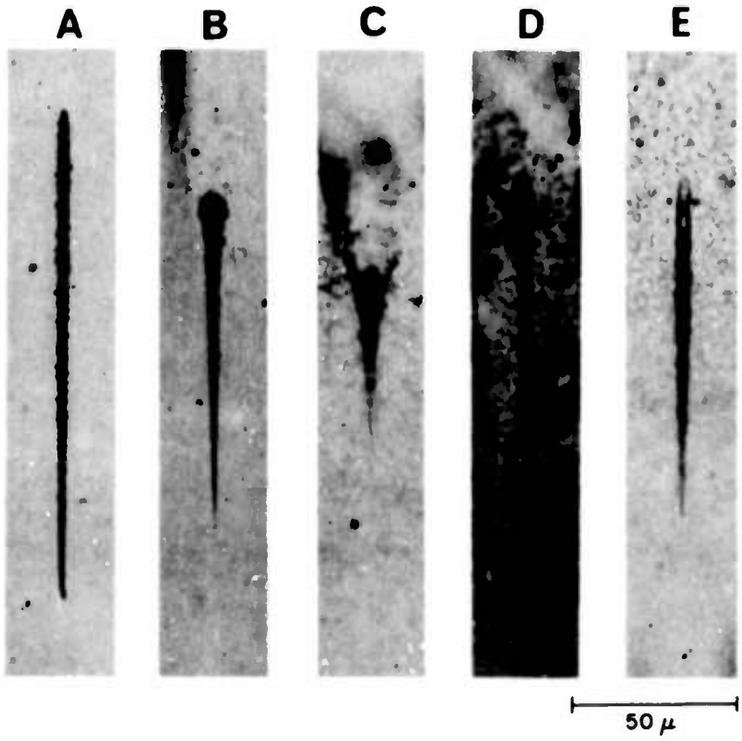

FIGURE IV-5. Tracks in four different types of cellulose nitrate plastic etched at 23°C. Tracks in (A), (B) and (C) are due to 10 MeV/nucleon ^{40}Ar ions in NRDL-1, Nixon-Baldwin, and Rowland plastics. Tracks in (D) and (E) are due to 5 MeV/nucleon ^{12}C ions in Daicel and NRDL-1 plastics.

plastics exhibit a characteristically large track opening at the surface and a cone angle which noticeably decreases over the initial portion of the track. This implies a larger r_B near the surface than in the interior of the specimen. The background density of surface imperfection etch pits differs considerably, being lowest for the Nixon-Baldwin and highest for the Rowland materials. Tracks in NRDL-1 plastic exhibit a characteristically small surface opening and a cone angle that at first increases, resulting in a cigar-like track shape (this behavior is not observed at the higher etching temperatures, $T \gtrsim 40^{\circ}C$). The surface etch pit density of NRDL-1 plastic is low and is comparable to that of the Nixon-Baldwin material.

One may wonder why it is necessary to be concerned with effects that can be minimized or almost totally eliminated by etching at higher temperatures. It will be shown (section C of this chapter) that etching at the lower temperatures considerably increases the etch rate ratio, r_T/r_B. Although deviations from the ideal track shape are bothersome and increase the difficulties of measurement and interpretation, this price is well worth the increased r_T/r_B achieved.

B. Effects of the Specimen Composition Parameters

The etching reaction is a heterogeneous process involving a solid-liquid interface. The driving force for the reaction is the reduction in the free energy of the system. It is a two step process, the steps being in series. Step 1 is associated with the diffusion of the OH^-

ions to the interface and the diffusion of the products away from the interface; step 2 is the interface reaction. If K_D is the rate of the diffusion, and K_I is the rate of the interface reaction, then the over-all etch rate, K_T, is given by

$$1/K_T = 1/K_D + 1/K_I. \tag{4.21}$$

For short tracks with large cone angles and with etching performed at a high temperature, the diffusion effects are small and the etch rate is determined primarily by the rate of the interface reaction.

The chemical reaction between a strong hydroxide and cellulose nitrate is quite complex. It cannot be throught of as a reaction reverse to that of nitration (see Equation (2.1)). There are complex changes in which oxidation products appear and the nitrate radical is converted into the nitrite ion. The list of products includes modified cellulose, inorganic nitrates and nitrites, ammonia, cyanides, carbon dioxide, oxalic, maleic, glycollic and malonic acids among others, some of which have not been identified.[40] Denitration in alkaline media is <u>always</u> accompanied by chain degradation. It is likely that the action of a hydroxide on radiation damaged cellulose nitrate plastic is even more varied and complex.

During the course of this investigation it was observed that the etching behavior of a cellulose nitrate plastic is a function of a large number of variables including the degree of polymerization, the degree of nitration of the nitrocellulose, what the other constituents of the plastic are (plasticizers, residual solvents, water, air), the exact details of specimen preparation, and the history of the specimens before the etching process. Commercial

plastics from different suppliers, different batches from the same supplier, and even the two surfaces of a single sheet are found to behave differently. Clearly it is important to investigate and, if possible, isolate the variables that control the etching behavior of a plastic.

1. Effect of the Degree of Polymerization

The irradiation of cellulose nitrate with high doses of gamma radiation results in scission of large molecules into smaller fragments (see Chapter II). It is reasonable to expect that similar effects are also produced along the trajectories of heavy charged particles. As a first approximation we may expect that a heavily ionizing charged particle will produce the same degree of damage irrespective of the degree of polymerization (DP) of the nitrocellulose, i.e., all bonds in the path of the charged particle are broken. This implies that r_T should be independent of the DP. However, the bulk etch rate, r_B, (and the solubility in solvents) has been observed to decrease with increasing DP (see Table IV-3). From these considerations, we expect that r_T/r_B should increase for the higher molecular weight nitrocellulose.

To investigate this effect, specimens of plastic were prepared from Hercules nitrocellulose of the following viscosities: 0.5, 5-6, 15-20, 60-80, 730, and 1500-2000 sec. The nitrocellulose contained (30% by weight) isopropyl alcohol; ethyl acetate was the primary solvent; no plasticizers were used. Specimens were prepared and heat treated in a standard manner (see Chapter III). Irradiations were performed with 5 MeV/nucleon ^{12}C ions, and 10.1 MeV/nucleon

^{40}Ar ions. Etching was done in a 10M NaOH solution at 23°C, and was terminated when easily measurable, short track segments appeared in all specimens. Measurements of θ were made using a goniometer eyepiece combination.

The results of the measurements are presented in Table IV-1. Here, the cone angle is given as a function of the viscosity of the nitrocellulose. Although a considerable scatter of points exists there is a definite trend, e.g., a decrease of the cone angle with increasing degree of polymerization. Additional data are given in Figure IV-6. Here are shown photomicrographs of the initial portions of 10.1 MeV/nucleon ^{40}Ar ions 18-25 cps and 0.5 sec viscosity unplasticized nitrocellulose. Again a definite decrease of the cone angle is observed. It was difficult to achieve high precision in the measurements of θ and r_B (see Tables IV-1 and IV-3). The etch rates are quite sensitive to small variations in the specimen composition and content of volatiles. Their dependence on the etching procedure is also quite strong (specimens prepared in an identical manner have shown a variation in r_B of up to a factor of two). However, the existence of a trend and its direction, decrease in r_B for the higher DP nitrocellulose, is clearly demonstrated in Tables IV-1 and IV-3.

To recapitulate, a decrease in θ is achieved when plastic specimens are prepared from the higher DP nitrocellulose. The decrease in θ results primarily from the decrease in r_B. The higher DP materials have a larger number per unit volume of strong, intra-chain type bonds. The inter-chain type bonds are relatively weak. The longer molecular chains undergo a much greater degree of entanglement

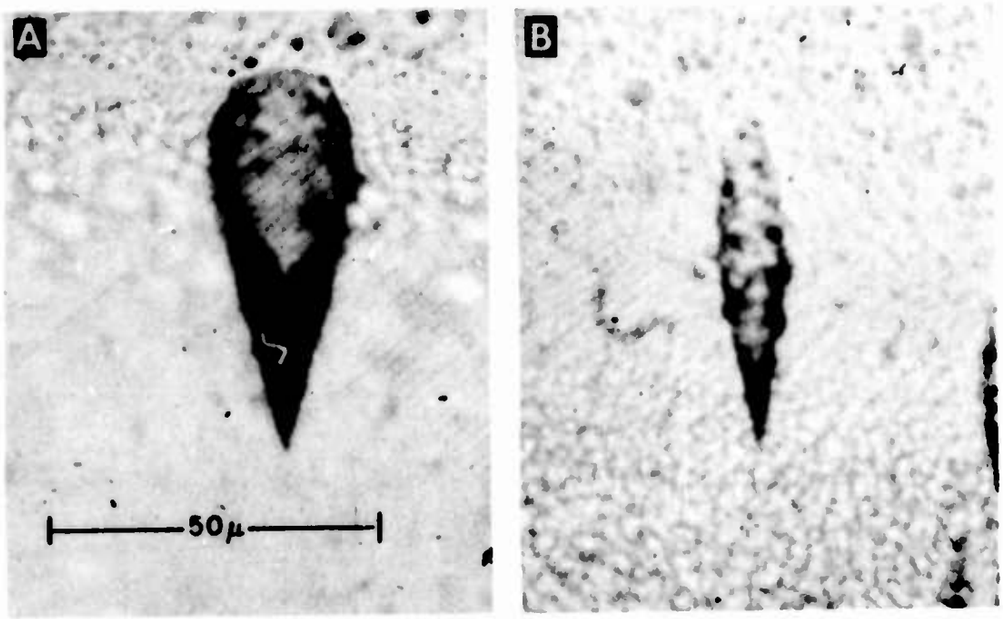

FIGURE IV-6. Initial portions of 10.1 MeV/nucleon ^{40}Ar ions in (A) 18-25 cps RS type, and (B) 0.5 sec RS type, unplasticized cellulose nitrate.

than the shorter chains. The decrease in r_B probably follows from the fact that in order to remove, through chemical etching, a given thickness of material from the specimen surface, a larger number of intra-chain type bonds must be broken by the etchant.

TABLE IV-1 Variation of θ with the Viscosity of RS Type, Unplasticized Nitrocellulose

Viscosity (sec)	θ (degrees)
0.5	44
5-6	34
15-20	15
60-80	23
730	12
1500-2000	15

2. Effects of the Degree of Nitration

The effects on the chemical etch development of tracks of the degree of nitration of the nitrocellulose were investigated. Specimens were prepared according to the NRDL-1 formula (see Chapter III), except for the omission of the cellosolve acetate. The nitrocellulose used was of the 5-6 second variety, nitrated to 10.9-12.2 (SS), 11.3-11.7 (AS), and 11.8-12.2 (RS) percent nitrogen. The etching was carried out in a 10M NaOH solution at 24°C. The measured values of the bulk etch rate are shown in Table IV-2. A factor of five decrease in r_B was observed for the RS as compared with SS type nitrocellulose. Measurements of tracks of 3.2 MeV alpha particles, and 10 MeV/nucleon ^{16}O ions also showed a decrease

in θ for the more highly nitrated specimens. This increase in θ is compatible with the observation that the increase in r_T/r_B is achieved primarily through the reduction of r_B because r_T remains essentially constant. Again, for a heavily ionizing charged particle the degree of radiation damage achieved along the trajectory appears to be independent of the degree of substitution of the NO_3^- for the OH^- ions in the nitrocellulose. Thus, the chemical reactivity of the latent track region, and hence of r_T remains approximately constant. However, r_B is found to decrease with increasing nitrogen content (measurements were made up to 12.6% N_2). The decrease in r_D may possibly result from the higher crystallinity of the higher nitrated specimens (see Chapter II).

TABLE IV-2 Bulk Etch Rate (Microns/Hour for a Single Surface) of Plasticized Cellulose Nitrate as a Function of the Degree of Nitration of the Nitrocellulose

Percent N_2	r_B (microns/hr)
10.9-11.2 (SS)	0.556
11.3-11.7 (AS)	0.309
11.8-12.2 (RS)	0.101

3. Effects of Plasticizers and Solvents

Initial attempts to prepare specimen films of cellulose nitrate plastic in the laboratory for the purpose of charged particle detection gave poor results when compared with some of the commercially available materials. Specimens prepared from various types of pure nitrocellulose, as well as samples prepared from recasting of

the commercial plastics showed both low values of r_T/r_B, as well as a high density of background surface etch pits. It quickly became apparent that the other constituents of the plastic (plasticizers, residual solvents, trace impurities, air, water) profoundly affected the etching behavior of the plastic. For example, in Figure IV-7 are shown photomicrographs of the initial portions of 5 MeV/nucleon ^{12}C ion tracks. Specimen (A) was prepared from RS, 5-6 second type nitrocellulose with the only other constituent being isopropyl alcohol (30% by weight). Specimen (B) was prepared from NRDL-1 solution. Both specimens were poured from an ethyl acetate solution and were etched in a 10M NaOH solution at 23°C, for 10 hours and 5 hours, respectively. Large differences in the cone angles are clearly evident. Cone angles in the unplasticized material are so large that plastic films prepared in this manner are not useful as charged particle detectors. Further investigation showed that the types of primary and secondary solvents used during specimen preparation, as well as the details of sample preparation (particularly the annealing treatment), all influenced the etching process. While a systematic examination of each of these variables was clearly beyond the scope of this effort, a series of experiments was performed in an attempt to answer some of the more fundamental questions such as: (1) What is the function of a plasticizer? (2) What is the optimum concentration? (3) What are the effects of the different types of plasticizers? (4) What are the effects of the different solvents and their concentration in the finished specimens?

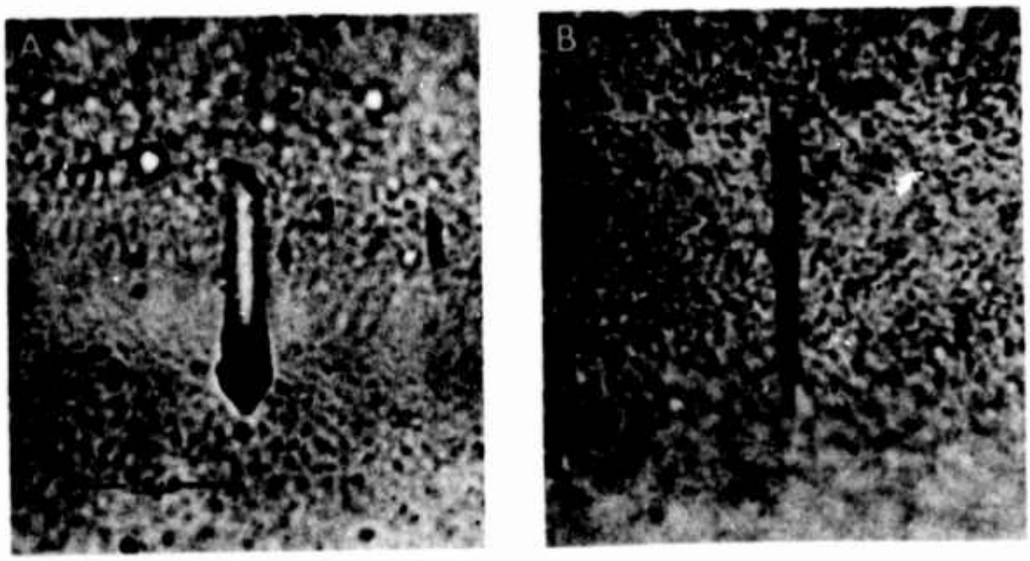

FIGURE IV-7. Initial portions of tracks of 5 MeV/nucleon ^{12}C ions in (A) unplasticized 5-6 sec RS type, and (B) plasticized 5-6 sec RS type cellulose nitrate.

The effects of the primary solvents were not investigated. All specimens prepared for this study were made using ethyl acetate exclusively. Plasticizers compatible with cellulose nitrate were chosen, at least one of each type (solvent, non-solvent, polymeric, and monomeric). The secondary solvents used were those most commonly employed in preparation of cellulose nitrate films. All of the specimens were prepared in the standard manner from RS 5-6 second type cellulose nitrate. The nitrocellulose was first dissolved in ethyl acetate and then the other constituents were added. The mixture was stirred vigorously for several hours and was allowed to age for a period of 4 days. Specimens were poured and heat-treated in the standard manner (see Chapter III). Exposures were made to 3.2 MeV alpha particles, fission fragments, and 10 MeV/nucleon ^{16}O ions. All etching was performed in a 10M NaOH solution at 40°C.

The results are shown in Figures IV-8 through IV-15. For Figures IV-8 - IV-11 the following data are tabulated for each specimen: specimen number, plasticizer type and content, secondary solvent type and content, photomicrographs (at magnification of 957X) of alpha and fission fragment tracks, the etch time, and in some cases, the measured cone angle. The following abreviations are used: DBP - dibutyl phthalate, DOP - dioctyl phthalate, CA - cellosolve acetate, BA - butyl alcohol. The number which appears after a plasticizer or a solvent is the concentration ratio of the amount by weight of the plasticizer or of the solvent to the dry nitrocellulose.

Sample Number	Plasticizers	Solvents	Alpha Particles	Fission Fragments	Remarks
1	None	None	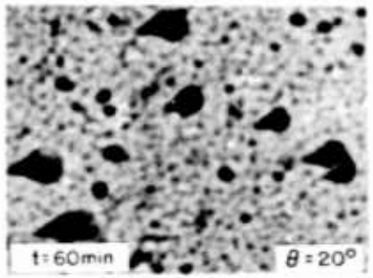	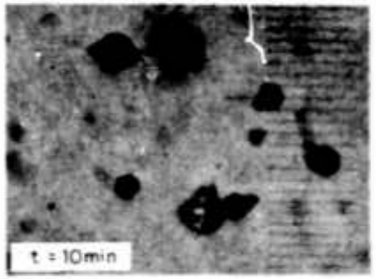	Largest θ's found; very large θ even for fission fragments, high background etch pit density. Compare with 2 and 3.
2	None	CA (0.45) BA (0.23)	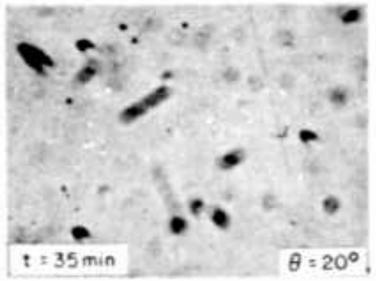	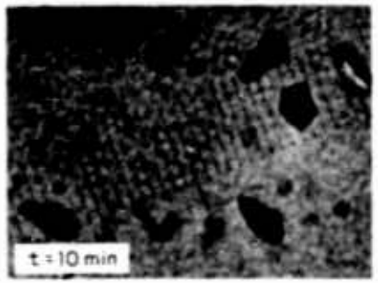	Slightly smaller θ's than specimen 1. Compare with 1, 3, 12, and 13.
3	DOP (0.22)	None	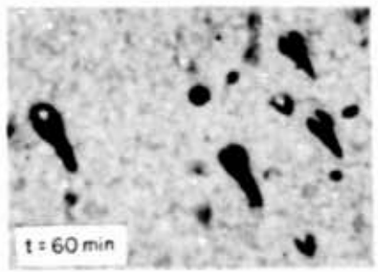	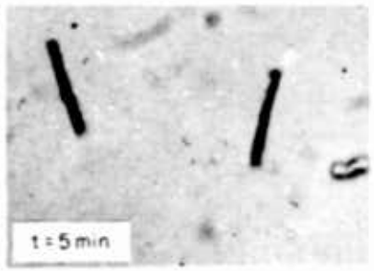	Smaller θ's than specimen 2.
4	DBP (0.22)	CA (0.45) BA (0.23)	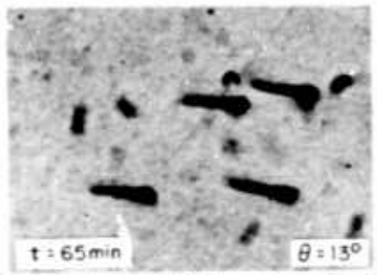	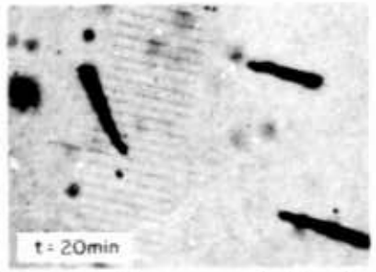	Compare with 5, 7, and 8.

FIGURE IV-8. Comparison of tracks of alpha particles and fission fragments in various cellulose nitrate plastics.

Sample Number	Plasticizers	Solvents	Alpha Particles	Fission Fragments	Remarks
5	Camphor (0.22)	CA (0.45) BA (0.23)	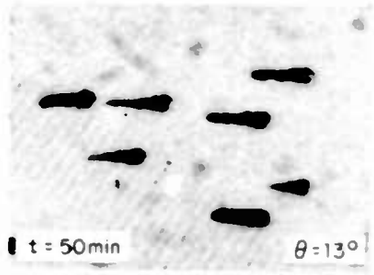	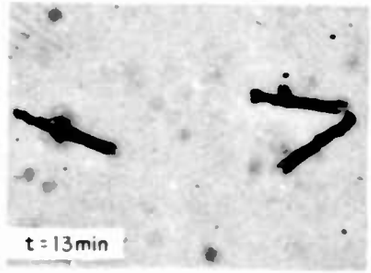	Compare with 4 and 8.
6	Castor Oil (0.02)	CA (0.45) BA (0.23)	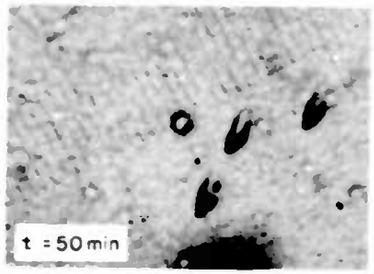	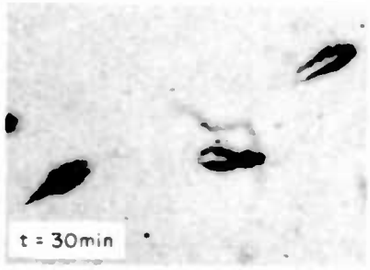	Smaller θ's than 2; comparable with 7.
7	Castor Oil (0.22)	CA (0.45) BA (0.23)	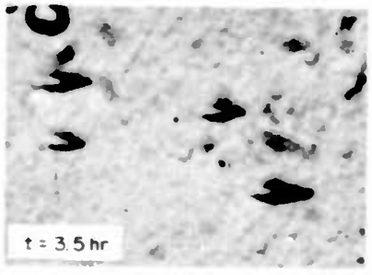	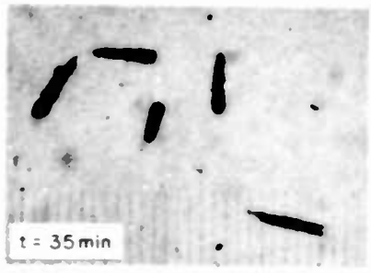	Larger θ's than 4, 5 and 8; compare with 6.
8	DOP (0.22)	CA (0.45) BA (0.23)	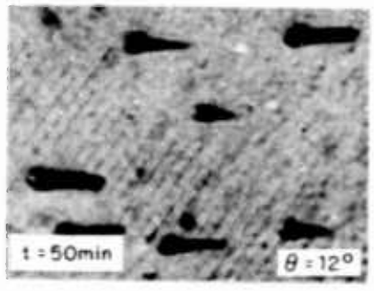	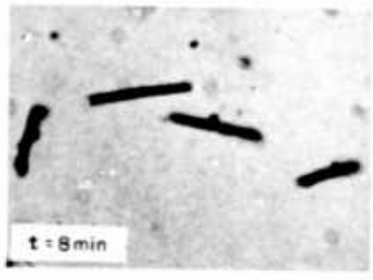	Comparable with 1, 2, 3, 4, 5 and 7.

FIGURE IV-9. Comparison of tracks of alpha particles and fission fragments in various cellulose nitrate plastics.

Sample Number	Plasticizers	Solvents	Alpha Particles	Fission Fragments	Remarks
9	DOP (0.50)	CA (0.45) BA (0.23)		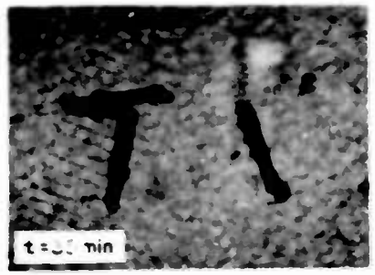	Long etch times; high surface etch pit density; compare with 8.
10	Paraplex G-41 (0.22)	CA (0.45) BA (0.23)	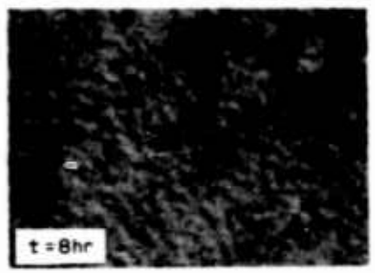		Slightly overetched; very long etch time; compare with 4, 5, 7, 8 and 11.
11	Paraplex RG-2 (0.22)	CA (0.45) BA (0.23)	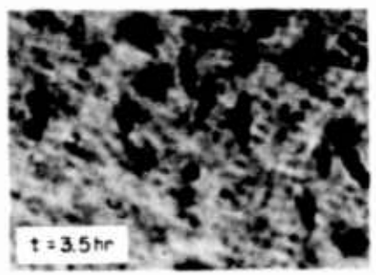		Specimen considerably overetched.
12	None	CA (0.45)	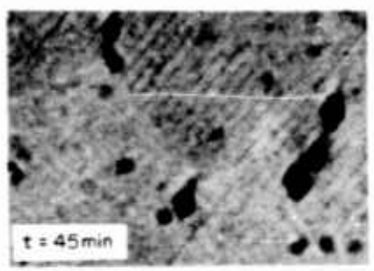	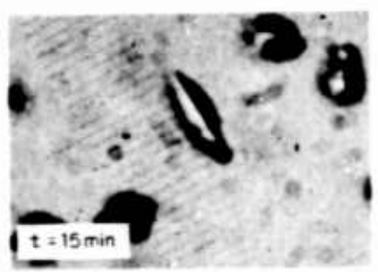	Larger θ's than 2; smaller θ's than 1; compare with 13.

FIGURE IV-10. Comparison of tracks of alpha particles and fission fragments in various cellulose nitrate plastics.

Sample Number	Plasticizers	Solvents	Alpha Particles	Fission Fragments	Remarks
13	None	BA (0.23)	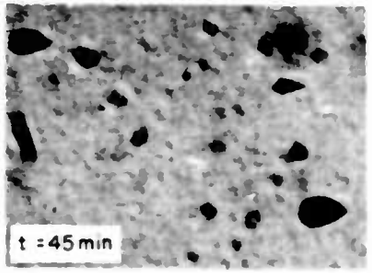	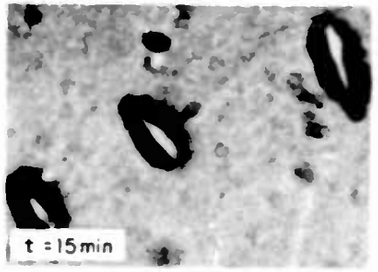	Comparable to 12.
14	DOP (0.22)	BA (0.23)	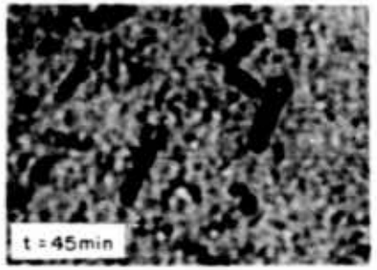		Compare with 15 and 16.
15	DOP (0.22)	CA (0.45)	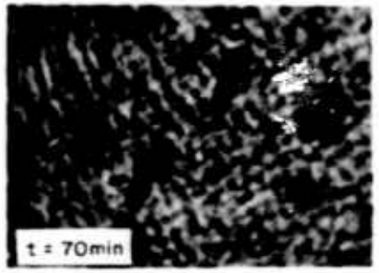		Overetched.
16	DOP (0.22)	CA (0.45) BA (0.23)	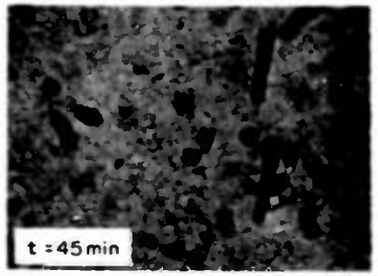		Fewer background etch pits than 14 and 15. Composition same as 8.

FIGURE IV-11. Comparison of tracks of alpha particles and fission fragments in various cellulose nitrate plastics.

In Figures IV-12 - IV-15 are shown photomicrographs and data for specimens bombarded with 10 MeV/nucleon ^{16}O ions. The specimen numbers for these figures correspond to the specimen numbers in Figures IV-8 - IV-11 and identify the specimen composition. The following data are tabulated for each specimen: specimen number, magnification of the photomicrograph, etch time, the initial specimen thickness, the specimen thickness after etch, and an arrow that designates the direction of motion of the charged particle. The ^{16}O ion irradiations were performed such that particles entered the specimens at a dip angle of 20^{o}. Most of the specimens used had a pre-etch thickness of less than 100 microns. These were not thick enough to stop the bombarding ions. Consequently, in a number of photomicrographs sets of two collinear tracks can be observed. The track registration characteristics of the various specimens vary considerably. In some instances etched tracks were observed only for the surfaces from which the particles emerged. The arrow serves to identify the entrance and the exit surfaces of the plastics.

The presence of plasticizers in the matrix of the cellulose nitrate plastic has a profound effect in reducing the bulk etch rate. This is demonstrated in Figures IV-8 through IV-15 through the observation of cone angles. In the non-plasticized specimens large cone angles are observed for both alpha particles and fission fragments. Also, ^{16}O ion tracks are observed only on the particle exit side of thin specimens. It can be seen that the inclusion of secondary solvents into the solution from which specimens are prepared also has the effect of reducing the cone angle. Generally, the secondary solvents are

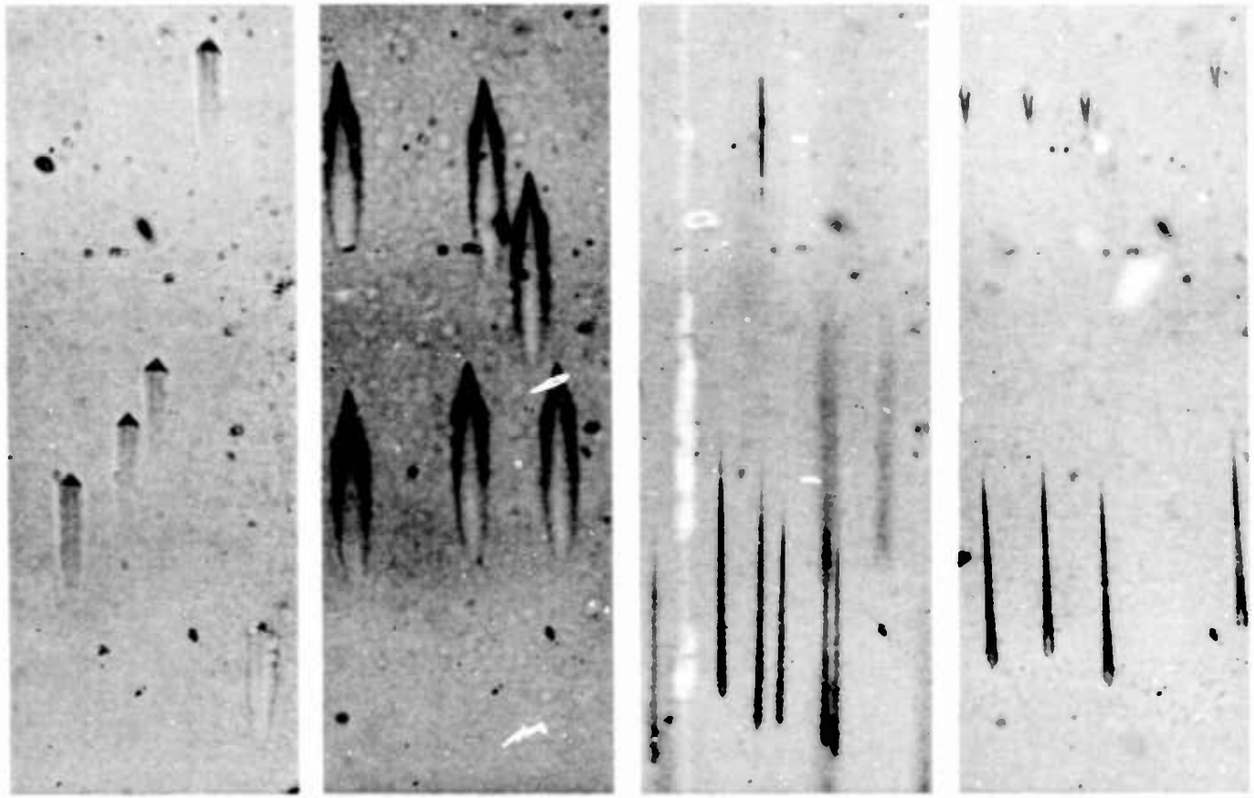

	1	2	3	4
Mag.;P.D.	900X ↓	900X ↓	460X ↓	460X ↓
Etch t(hr)	1.0	1.0	0.5	1.0
$(Thick)_{in}(\mu)$	37	41	66	62
$(Thick)_{f}(\mu)$	25	27	65	58

Remarks

Specimens 1 and 2: tracks on particle exit side only; large r_B.

Specimens 3 and 4: tracks on entrance and exit sides of specimens. Note:

$(r_T)_{exit} > (r_T)_{entr.}$

FIGURE IV-12. Comparison of tracks of ^{16}O ions in various cellulose nitrate plastics.

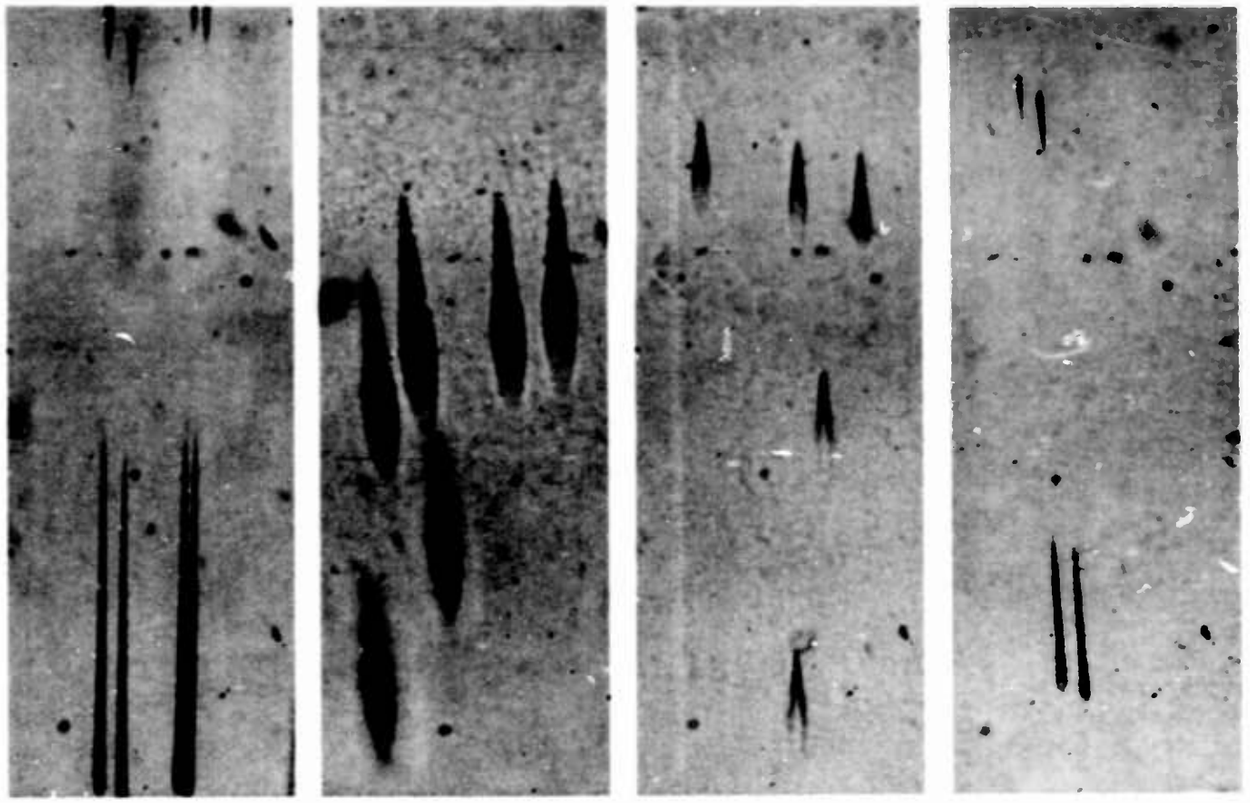

	5	6	7	8
Mag.;P.D.	460X ↓	900X ↓	900X ↓	460X ↓
Etch t(hr)	1.0	1.0	2.0	0.5
$(Thick)_{in}(\mu)$	88	76	69	63
$(Thick)_{f}(\mu)$	82	66	58	61

Remarks

Specimen 5: large r_T; uniform track lengths.

Specimens 6 and 7:

$(r_B)_6 > (r_B)_7$;

note:

$(r_T)_6 \simeq 2\,(r_T)_7$.

Composition of specimen 8 is the same as of 16. However, note the difference in r_B's.

FIGURE IV-13. Comparison of tracks of ^{16}O ions in various cellulose nitrate plastics.

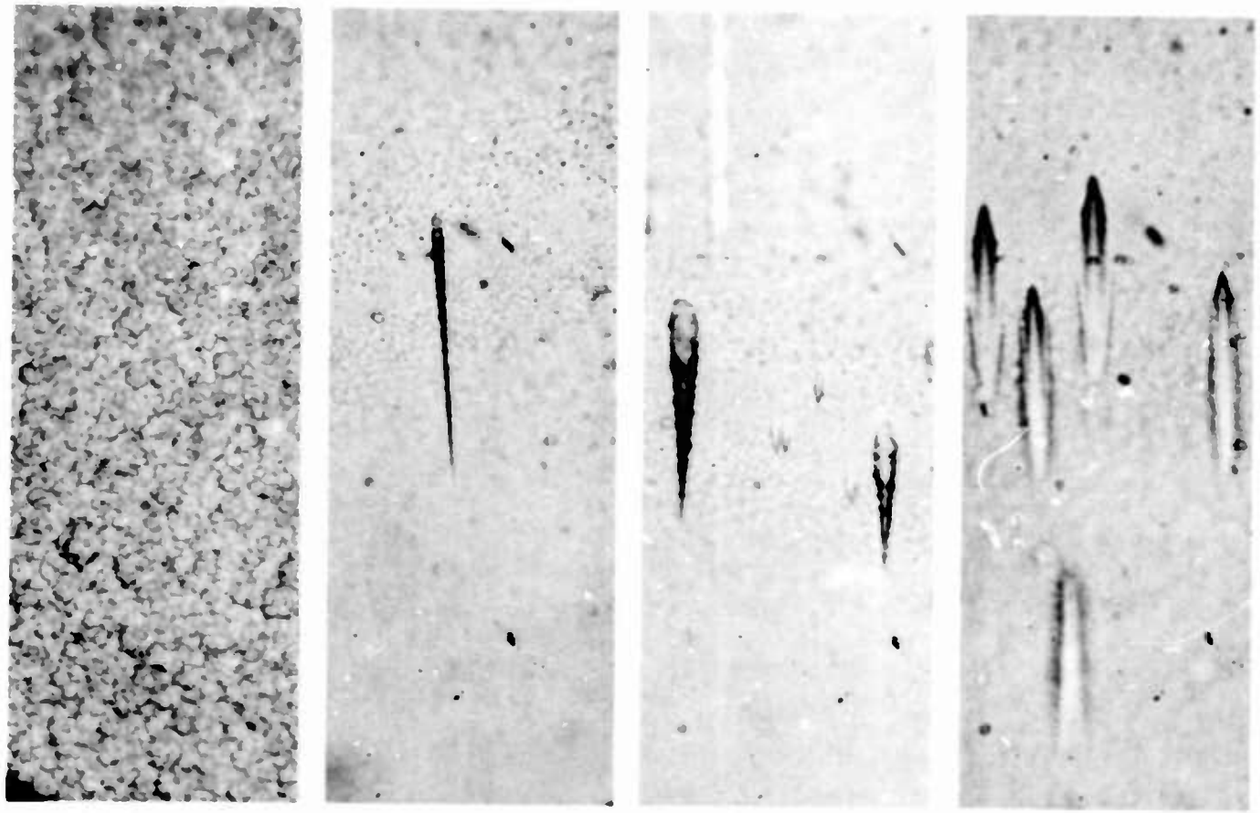

	9	10	11	12
Mag.;P.D.	460X ↓	460X ↓	460X ↓	900X ↓
Etch t(hr)	2.6	4.5	2.0	1.0
$(Thick)_{in}(\mu)$	110	154	179	59
$(Thick)_{f}(\mu)$	88	146	165	43

Remarks

Specimen 9: no tracks.

Specimen 10: very low r_B; relatively low r_T as compared with 3, 8, 14 and 16.

Specimen 11: broad track length distribution.

Specimen 12: smaller θ's than in 1, comparable to 2.

FIGURE IV-14. Comparison of tracks of ^{16}O ions in various cellulose nitrate plastics.

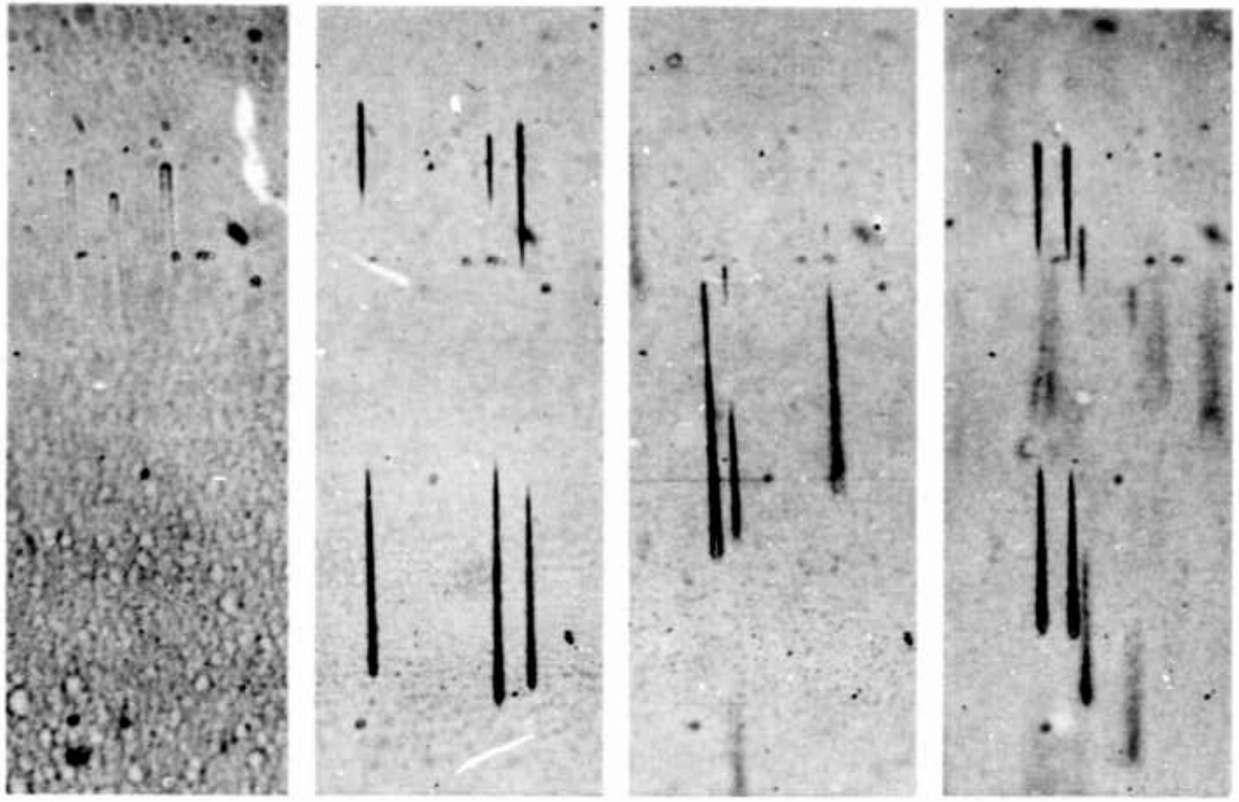

	13	14	15	16
Mag.;P.D.	900X ↓	460X ↓	460X ↓	460X ↓
Etch t(hr)	1.0	0.5	0.5	0.5
$(Thick)_{in}(\mu)$	37	61	34	58
$(Thick)_{f}(\mu)$	22	58	31	52

Remarks

Specimen 13: large θ's; thinner specimen than 12.

Specimens 14, 15 and 16. Note variations in track lengths, particularly in 15.

FIGURE IV-15. Comparison of tracks of ^{16}O ions in various cellulose nitrate plastics.

less volatile than ethyl acetate, and consequently are retained by the plastic in greater proportions. It should be noted that even after the specimens are annealed some of the solvents remain in concentrations of a few percent. It is well known that the unplasticized nitrocellulose has a high affinity for solvents, much greater than the plasticized materials. It is thought that the residual solvents in the specimen play a similar role to that of plasticizers. To a first approximation, they may be thought of as very volatile plasticizers.

The effect of plasticizers on reducing the bulk etch rate are presented in Table IV-3. Here the bulk etch rate (microns/hour for a single surface) is given as a function of the viscosity of the RS type nitrocellulose for both the unplasticized and for the plasticized specimens. The plasticized specimens were made according to the NRDL-1 formula. Etching was carried out in 10M NaOH solution at 23°C. Approximately a ten fold reduction in r_B is observed for the plasticized 5-6 sec RS nitrocellulose. The effect varies with viscosity, being greater for the higher viscosity materials. For the extra high viscosity, 200,000 sec, polymer a reduction of r_B by a factor of about 40 is observed. This material is of a slightly higher degree of nitration (12.2-12.4% N_2) than the RS type nitrocellulose. This may also contribute to the reduction of r_B.

The plasticizer type has a large influence on r_B and θ (see Figures IV-8 - IV-15). For example, the presence of castor oil results in tracks with smaller cone angles than that of non-plasticized specimens, but larger than for other plasticizers. The effect of the

TABLE IV-3 Bulk Etch Rate (Microns/Hour for a Single Surface) as a Function of the Nitrocellulose Viscosity for Unplasticized and Plasticized RS Type Cellulose Nitrate Plastics

Viscosity		r_B(Unplasticized)	r_B(Plasticized)	$(r_B)_{unp.}/(r_B)_{p.}$
18-25	cps	2.50	0.465	5.38
0.5	sec	2.28	0.271	8.42
5-6	sec	1.33	0.101	13.1
15-20	sec	2.15	--	--
30-40	sec	--	0.113	--
60-80	sec	1.56	0.077	20.2
125-175	sec	0.78	--	--
600-1000	sec	0.78	0.059	13.2
1500-2000	sec	1.05	--	--
~200,000	sec*	0.92	0.021	43.8

* This extra high viscosity nitrocellulose is nitrated to a somewhat higher degree (12.2 - 12.4% N_2) than the RS types.

different plasticizers on r_B is demonstrated in Table IV-4. Here is shown the variation in r_B for the 5-6 sec, RS type nitrocellulose prepared according to NRDL-1 formula as a function of the plasticizer type. The etching was carried out in 10M NaOH solution at 23°C. While the difference in r_B for some plasticizers is small (DOP, camphor, DBP), the use of a polymeric plasticizer, Paraplex G-41, results in considerable reduction in r_B. This reduction is reflected in the very long etch times that are required to develop tracks in specimens plasticized with this material (see Figures IV-8 - IV-15). The various plasticizers that are compatible with the nitrocellulose system have other important properties that merit attention. For example, castor oil, if used alone, tends to gradually migrate out

TABLE IV-4 Comparison of Bulk Etch Rates for 5-6 sec, RS Type Nitrocellulose Plasticized with Different Plasticizers

Plasticizer	r_B(μ/hr)
DOP	0.222
Camphor	0.200
DBP	0.154
Castor Oil	0.136
Paraplex G-41	0.081

of the film. Both camphor and DBP have a considerably higher volatility than DOP (DBP is about six times more volatile). In time, the volatile plasticizers tend to evaporate from the film, resulting in a gradual transition of the properties of the plastic back to the unplasticized state. This may be a problem under some circumstances such as prolonged exposures in a vacuum, such as prolonged space exposures. In these cases the use of either DOP or (preferably) a polymeric type of plasticizer would be the best choice.

The concentration of the plasticizers in a cellulose nitrate plastic specimen also has a considerable influence on the chemical etch process. For example, the secondary solvents plus a very small amount of castor oil (0.02, see Figures IV-8 - IV-15) are only slightly more effective in reducing θ than the secondary solvents alone (compare specimens no. 2 and 7). Also, in varying the concentration ratio of DOP (0, 0.22, 0.50, 1.47) it is found that the smallest cone angles are observed at a ratio of 0.22. At the

concentration ratio of 0.50, tracks of alpha particles and fission fragments have a cone angle only slightly smaller than those in specimens without a plasticizer. At this concentration ratio, tracks of ^{16}O ions were not observed. For a higher concentration ratio of 1.47 (not included in the figures) even tracks due to fission fragments were not observed. The optimum concentration of plasticizers appears to be less than about 0.25 the weight of the dry nitrocellulose. However, this ratio may vary for other types of plasticizers.

The presence of excess quantities of residual solvents in improperly annealed specimens has been observed to have unfavorable effects similar to those caused by the presence of excess quantities of plasticizers. The optimum concentration of residual solvents is of the order of a few percent.

So far, the discussion has been restricted to the effects of plasticizers on r_B. It was shown that the presence of plasticizers decreases r_B and increases the etch rate ratio r_T/r_B. It is now of interest to independently examine the effect of the presence of plasticizers on the track etch rate, r_T. Unfortunately, precise measurements of r_T are fairly difficult. Only a few measurements of r_T were made. Comparisons of r_T (etching was performed in a 10M NaOH solution at 40°C) for NRDL-1, and 6.2 sec RS unplasticized cellulose nitrate showed that for 5 MeV/nucleon ^{12}C ions, the presence of plasticizers has the effect of reducing r_T by about a factor of two. Hence, it appears that plasticizers reduce both r_B and r_T. However, since r_B is reduced to a much greater extent, the net effect is a substantial increase in r_T/r_B.

Observing the tracks in Figures IV-8 - IV-15 reveals a feature that merits particular attention because of its significance in the utilization of plastics as charged particle detectors. It can be seen that in a number of the specimens not all of the tracks are of the same length. Yet, all tracks appearing in a given specimen are the result of identical particles of nearly equal energies (for Hilac particles the spread in incident energies is about 0.2%). It was found that the track length is controlled not only by r_T, but also by how quickly a particular track starts to etch after the sample is immersed in the etching solution. For all of the plastics studied (including the commercial plastics) it was found that there exists a distribution in time for the inception of track etching which manifests itself in a distribution of etched track lengths. This phenomenon was observed under all etching conditions. From Figures IV-8 - IV-15 it is seen that in thin specimens the tracks which are associated with the particle exit surface of the specimen are considerably longer, and also exhibit track lengths that are more nearly equal than the corresponding tracks that are associated with the particle entrance surface of the specimen. Observations made in separate experiments confirm that the breadth of track length distributions is directly related to the rate of ionization of the particle at the surface of the specimen. For heavily ionizing particles, tight distributions are observed. For light particles, or for particles near the threshold of registration (see Chapter V) very broad distributions occur. The width of track length distribution is also dependent on the plastic specimen type. In

Figure IV-16 are shown two distributions for Daicel and NRDL-1 plastics bombarded with 5 MeV/nucleon ^{12}C ions and etched in 10M NaOH solution at 40°C for 35 and 60 minutes, respectively. The Daicel plastic shows a much narrower distribution, probably because it is more sensitive than NRDL-1 plastic. Tighter distributions can be obtained in NRDL-1 material by using more heavily ionizing particles. Conversely, broader distributions are observed in Daicel plastic if the bombarding ion is more lightly ionizing, such as 6 MeV alpha particles. A complete explanation of this phenomenon is not presently available. It is likely that at least part of the answer lies in the microscopic inhomogeneity of the plastics.

The composition of NRDL-1 cellulose nitrate plastic was given in Chapter III. A few words with regard to the function of its constituents are now appropriate. Isopropyl and butyl alcohols are secondary solvents, ethyl acetate and cellosolve acetate are primary solvents. In order to achieve a smooth, homogeneous, level film it is necessary to have a continuous, steady evaporation of solvents during the drying process. Ethyl acetate, being very volatile, evaporates rapidly from the film; cellosolve acetate, however, has a very low evaporation rate, and if used in excess, is difficult to remove from the film. The function of the butyl alcohol is to couple the evaporation rates of these two primary solvents in such a way that there is a fairly constant rate of solvent loss during the entire drying process. Butyl alcohol has yet another function. Although neither the isopropyl nor the butyl alcohol alone will dissolve nitrocellulose, when used in conjunction with primary solvents they

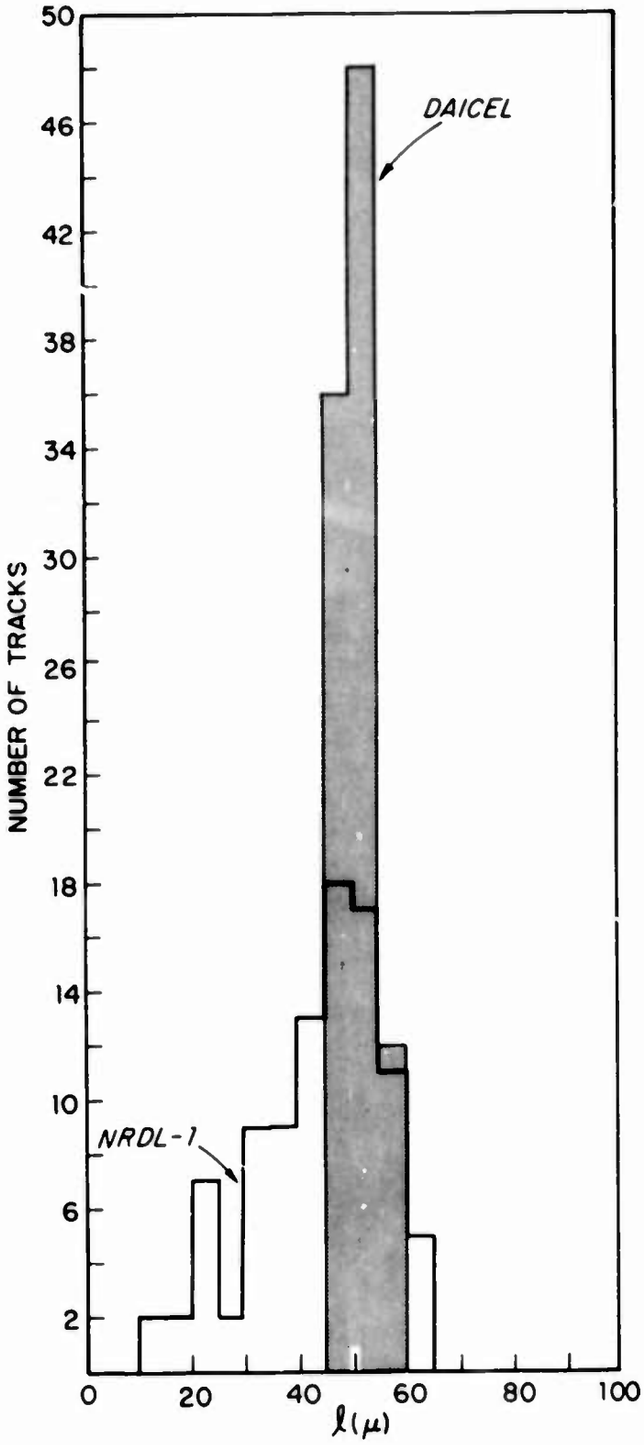

FIGURE IV-16. Track length distributions for 5 MeV/nucleon ^{12}C ions in Daicel and NRDL-1 plastics etched at 40°C in 10M NaOH for 35 and 60 minutes, respectively.

increase the solvency power of the primary solvent. This, in turn, has a favorable effect on the homogeneity of the film.

For numerous applications the NRDL-1 plastic is well suited to being used as a charged particle detector. However, it represents by no means the only combination of constituents that work. From the previous discussion it is clear that a large number of combinations of nitrocellulose types, plasticizers, and solvents will work as well or even better. Of course, the constituents must be used in the proper proportions and specimen preparation must include an adequate annealing treatment.

It is possible to achieve large r_T/r_B ratios by using either a high viscosity (large DP) nitrocellulose or a polymeric type of plasticizer. For example, it was found that the 200,000 sec nitrocellulose, used in combination with the other constituents of the NRDL-1 formula, yields values of $r_T/r_B > 1000$ for 8 MeV/nucleon ^{16}O ions etched in 10M NaOH solution at 23°C.

The sensitivity of the various laboratory-prepared plastics was found to be approximately the same, except for the 200,000 sec material which is somewhat less sensitive. Sensitivity, as the term is used here, refers to the maximum energy of alpha particles that a specimen is capable of recording when etching is performed in 10M NaOH solution at 23°C. The alpha particle energy is determined from track length measurements when a two micron thick layer has been removed from the surface of the specimen. Using this definition, NRDL-1 plastic is found to record 3.5 MeV alpha particles with a registration efficiency of 90%. Using the same criterion, the red, No. 1025, Daicel plastic is capable of recording alpha particles of

4.5 MeV. This value is for the most sensitive surface of the plastic; the opposite surface is considerably less sensitive. The specimens of the Daicel plastic which were studied showed considerable inhomogeneities. In fact, the subsurface material of this plastic was found to be less sensitive than the NRDL-1 plastic. In some manner, during the manufacturing process, one of the surfaces of each sheet of this plastic is sensitized.

The inclusion of plasticizers (and to a lesser extent of low concentrations of residual solvents) in the nitrocellulose matrix has a profound effect in reducing the bulk etch rate of the plastic. It is thought that this occurs as a result of reduction of the solubility of OH^- ions in the plasticized cellulose nitrate. The etchant is restricted in its penetration of the plastic. The etching process now more nearly resembles that of etching of an inorganic crystal, where each layer of atoms must be removed before the next layer is susceptible to chemical attack. Some plasticizers, such as camphor, have very strong affinity for nitrocellulose. The plasticizer molecules cluster around the polymeric chain of the nitrocellulose and thus offer a degree of protection. The etchant must degrade the plasticizer before gaining access to the nitrocellulose chain, further reducing the rate of the etching reaction. The use of high molecular weight, polymeric, non-hydrophyllic plasticizers can further reduce r_B. This reduction probably occurs for reasons similar to those effecting the reduction in r_B in the case of high DP nitrocellulose types. While plasticizers have a large effect on r_B, their effect on r_T is considerably smaller. A heavily ionizing charged particle traversing a specimen has the capability of breaking all bonds along

its trajectory. The nitrocellulose chains as well as the plasticizer molecules are affected. The nitrocellulose chains are degraded into smaller fragments. The solubility of the OH^- ions in this degraded region is probably quite high. From Table IV-3 it is seen that the effect of plasticizers in reducing r_B is considerably smaller for the low DP than in the high DP nitrocellulose types. In the case of lightly ionizing particles, or particles near the threshold of registration, the plasticizers may have a greater effect on r_T. Assuming for the moment that the surface of a plasticized plastic specimen consists (on the microscopic level) of regions of segregated plasticizer, and regions having a very small percentage of plasticizer (perhaps even of regions where the nitrocellulose chains are completely exposed). If a surface of this type is bombarded by a homogeneous beam of charged particles near the threshold of registration and then etched, not all tracks will start to etch at the same time. Rather, possibly tracks in regions of little or no plasticizer will start to etch out first. The last tracks to etch will be those where the particle had penetrated a thicker portion of plasticizer before reaching the nitrocellulose chains. A delay in etching will occur in these regions. In time, a distribution of track lengths will be observed. At present it is not known if the above picture is correct. If the model is correct, it may be possible to reduce this effect by the use of smaller quantities of plasticizers in order to reduce segregation. The use of plasticizers that have the tendency to segregate, such as castor oil, should be avoided. To obtain a uniform distribution of a plasticizer in the nitrocellulose matrix, a plasticizer such as camphor should be used. It may be possible to

obtain a more uniform specimen surface by subjecting the specimen to a high temperature for a short period of time. This should volatilize and remove a thin layer of plasticizer (such as camphor or DBP) thus creating a depletion layer near the specimen surface.

C. Effects of the Etching Solution Parameters

The etching conditions include the type, concentration, and temperature of the etchant, the types and concentrations of impurities, and the geometrical position of the sample in the etching solution.

1. Effects of Temperature on the Etch Rates

Of the above variables, the temperature is by far the most influential parameter. Measurements of r_B for NRDL-1 and 6.2 sec, RS, unplasticized plastics in 10M NaOH solutions at different temperatures are given in Table IV-5 and again in Figure IV-17. It is clear that the rate of chemical attack is highly temperature dependent. An increase in etch temperature of 20°C results in an order of magnitude increase in the etch rate. In Figure IV-17 the natural logarithm of r_B is plotted as a function of 1/T (°K). The slope of the curve gives the activation-free energy, for bulk etching, $\Delta F_B = 1.07$ eV for the NRDL-1 material. The activation energy for bulk etching of the unplasticized material is slightly lower. It is of interest to note that at higher etch temperatures the etch rates for both plasticized and unplasticized materials approach each other. The track etch rate, r_T, is also very temperature dependent. In quantitative measurements of the etch rates, it is important to maintain a constant etch temperature.

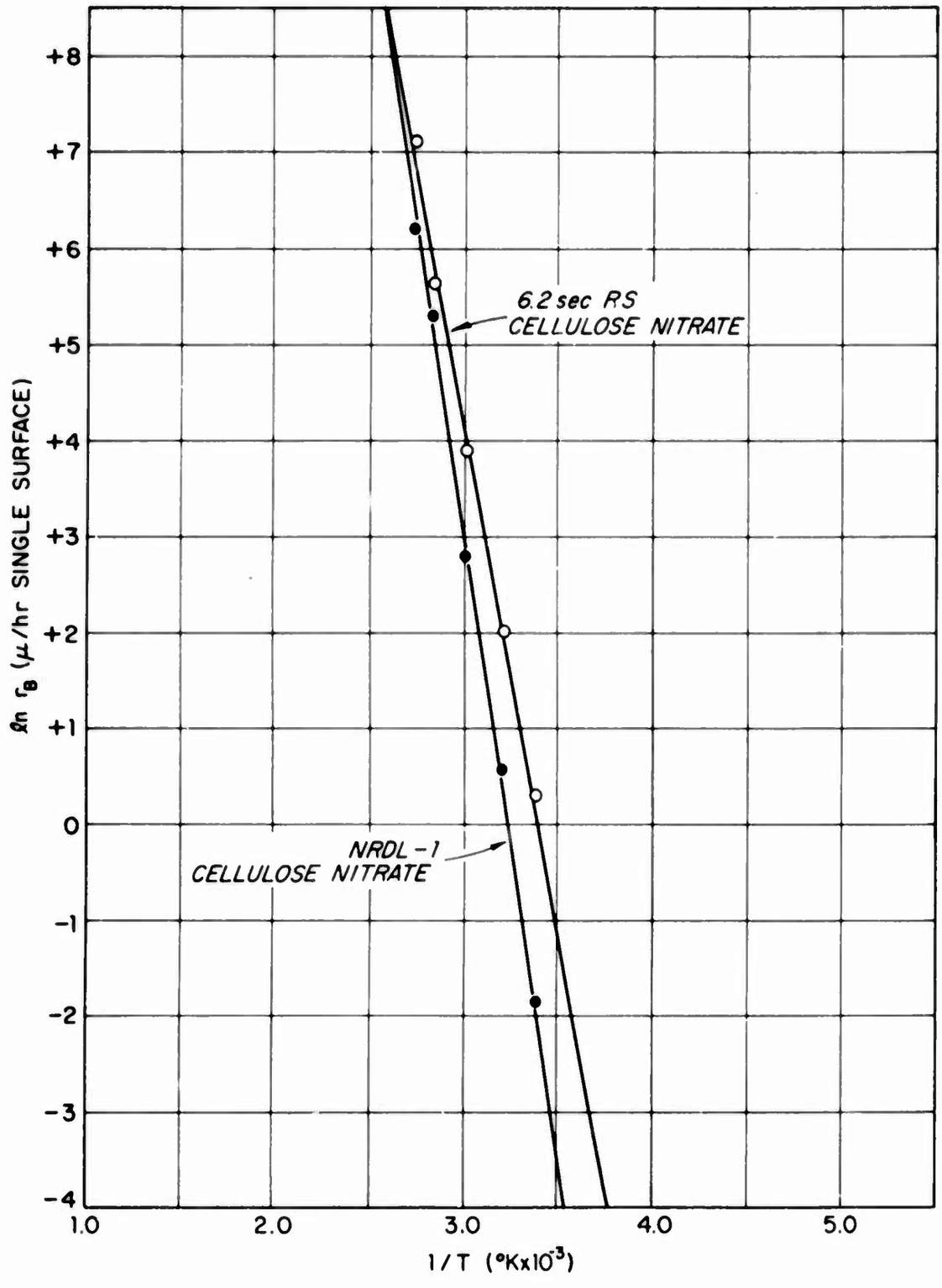

FIGURE IV-17. The bulk etch rate as a function of temperature for plasticized and unplasticized 5-6 sec, RS type cellulose nitrate.

TABLE IV-5 Bulk Etch Rate (microns/hour for a single surface) as a Function of Temperature for Plasticized and Unplasticized RS Type Cellulose Nitrate

T(°C)	(r_B) NRDL-1	(r_B) 6.2 sec RS
24	1.57×10^{-1}	1.38×10^{0}
40	1.73×10^{0}	7.5×10^{0}
60	1.62×10^{1}	4.80×10^{1}
80	1.96×10^{2}	2.79×10^{2}
95	4.95×10^{2}	1.26×10^{3}

2. Dependence of the Etch Rate Ratio on the Temperature

It was noted that as the etch temperature is decreased narrower track cone angles are observed, suggesting that the etch ratio r_T/r_B is increased (these observations were made in only one plastic -- NRDL-1 cellulose nitrate). It is possible to predict this dependence by considering a simple model. Adopting a diagram similar to that used in the Activation Complex Theory of chemical reaction rates, the free energies of the reactants and products are plotted in Figure IV-18. Here, F_B is the free energy associated with the bulk polymer and the etchant, F_T is the free energy of the track region and the etchant, F_A is the free energy of the activated complex, and F_P is the free energy of the products. The quantity ΔF_T^* is the activation energy for track etching, ΔF_B^* is the activation energy for bulk etching, and ΔF is the reaction free energy. The free energy associated with the region of the polymer traversed by a highly ionizing

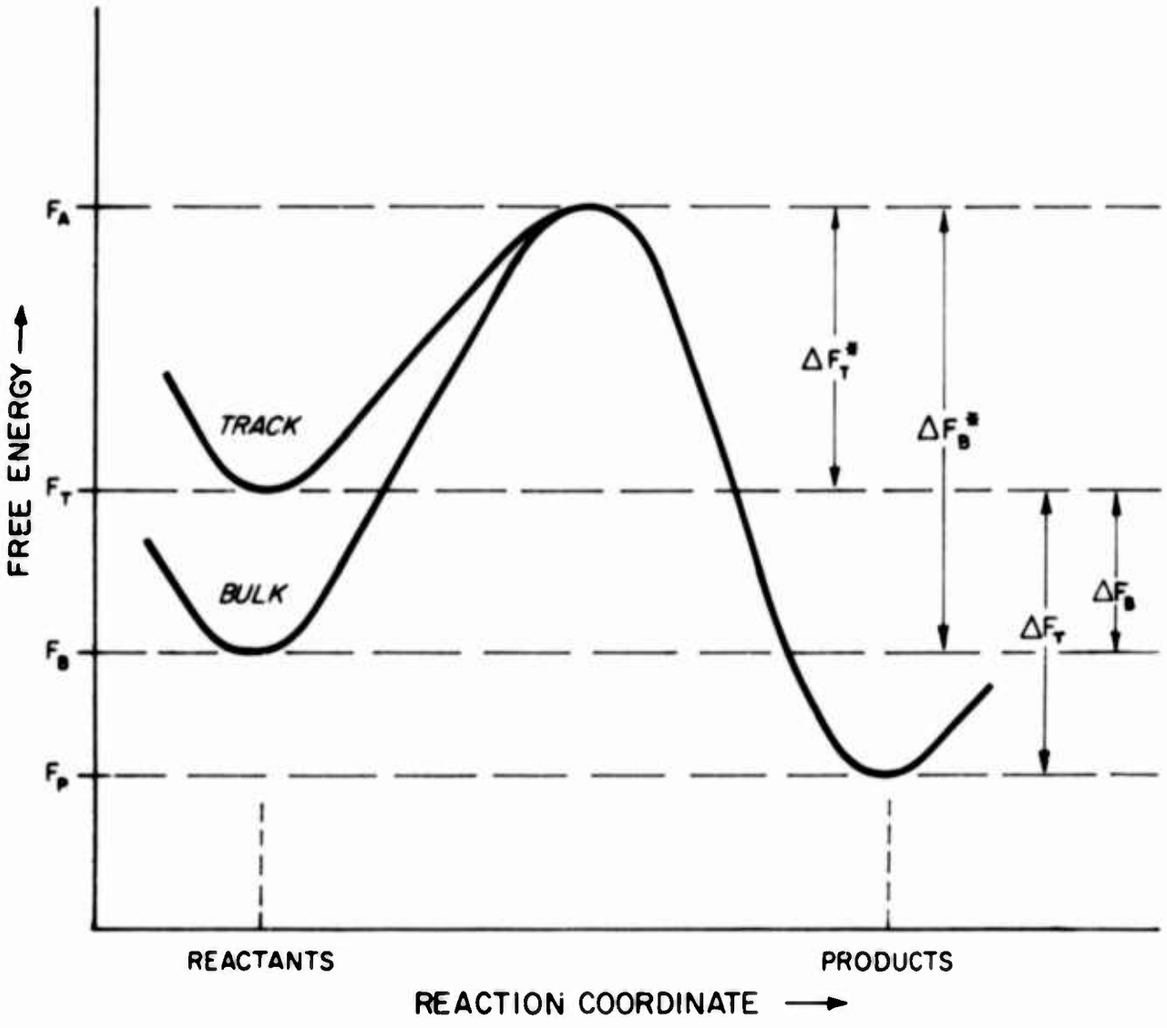

FIGURE IV-18. A free energy diagram of irradiated and unirradiated cellulose nitrate.

particle is greater than that of the bulk material, $F_T > F_B$. From statistical mechanics we know that the probability that an atom undergoing thermal vibration will have a value of free energy equal to or greater than any value ΔF^* above its ground state is given by $P = \exp(-\Delta F^*/kT)$. If in the chemical reaction in question, the rate controlling step has an activation free energy per atom of ΔF^*, the rate of this reaction will be proportional to $\exp(-\Delta F^*/kT)$. The overall rate of the reaction can simply be expressed as

$$K = B\, e^{-\Delta F^*/kT} , \tag{4.22}$$

where B is a proportionality constant. Apply this relationship to the chemical etching of tracks, the etch rate along the particle trajectory is given by

$$r_T = C\, e^{-(F_A - F_T)/kT} , \tag{4.23}$$

and the bulk etch rate is given by

$$r_B = B\, e^{-(F_A - F_B)/kT} . \tag{4.24}$$

Taking the ratios of Equations (4.22) and (4.23) we find

$$r_T/r_B = \frac{C}{D}\, e^{(F_T - F_B)/kT} . \tag{4.25}$$

Equation (4.25) predicts that as T is decreased r_T/r_B will increase; also, as the difference between F_T and F_B is increased r_T/r_B will increase, and if $F_T = F_B$ and $C = D$ then $r_T = r_B$. These predictions agree with experiment.

By noting that $\sin\theta = r_B/r_T$, Equation (4.25) can be transformed into the following useful form,

$$\ln(1/\sin\theta) = (F_T - F_B)/kT + \ln(C/D) . \tag{4.26}$$

The above equation shows a linear relationship between $\ell n(1/\sin\theta)$ and $1/T$, with a slope of $(F_T-F_B)/k$. This dependence was tested by etching tracks of 5 MeV/nucleon ^{12}C ions in NRDL-1 plastic in 10M NaOH at 0, 23, 40, 61, 88 and 96°C. The results are tabulated in Table IV-6, and plotted in Figure IV-19. The predicted linear dependence is indeed observed. The slope shows that $(F_T-F_B) = 0.11$ eV. Measurement of the slope of Figure IV-17 gives $\Delta F_B^* = 1.07$ eV, hence the activation free energy for track etching, ΔF_T^* is found to equal 0.96 eV. It would be interesting to repeat these measurements using a more heavily ionizing particle such as ^{40}Ar ions and see if ΔF_T^* is observed to decrease as predicted by Equation (4.26).

TABLE IV-6 Variation of the Cone Angle, θ, with the Temperature of Etch

T(°C)	θ(degrees)
0	2.0 ± 0.1
23	5.0 ± 0.2
41	6.9 ± 0.2
61	8.1 ± 0.3
88	14.0 ± 0.3
96	17.2 ± 1.0

The above phenomenon has an important practical significance, namely, by etching at low temperatures a considerable increase in r_T/r_B is achieved.

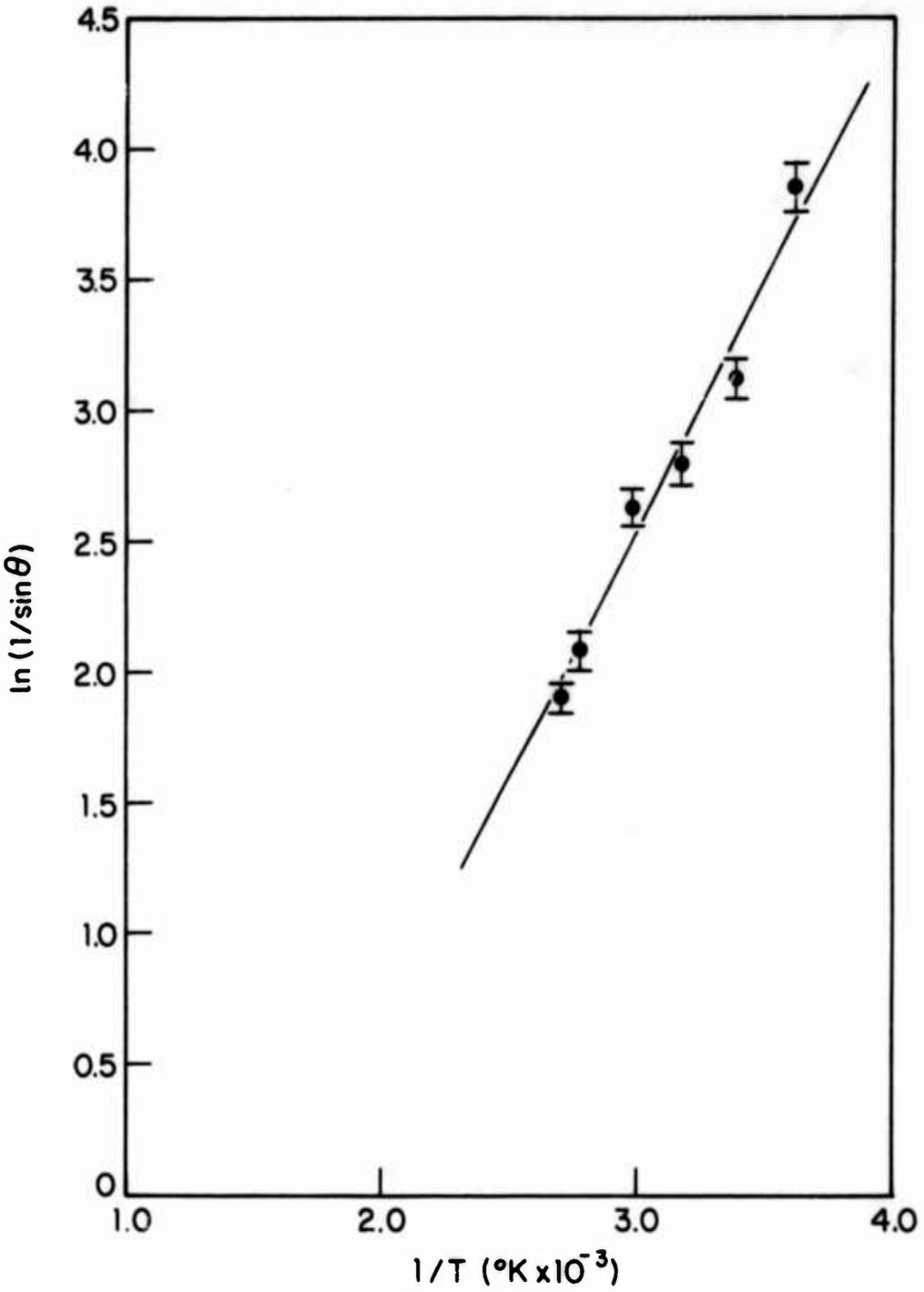

FIGURE IV-19. Dependence of the cone angle on the temperature of etch for NRDL-1 plastic.

3. Dependence of the Track Etch Rate on the Hydroxide Concentration

In these studies the etchant used was generally NaOH; however, any of the weak or strong hydroxides were found to work. Of the alkali hydroxides used, (Cs, Rb, K, Na and Li) all were found to give approximately the same results. The rate of attack was found to vary with the concentration of the OH^- ions. This is demonstrated in Figure IV-20 where the time in minutes needed to completely etch out fission fragment tracks in NRDL-1 plastic is given as a function of the concentration of NaOH. A temperature of 60^oC was used. Tracks etched in solutions as dilute as 10^{-3} moles were observed; for lower concentrations the etch times became prohibitively long (10^5 minutes). Considerable swelling of specimens also occurred in the dilute solutions. Over the entire range of concentration (10^4M) tracks of comparable appearance were observed. The addition of an anion surfactant, Benax 2A1*, was found to increase both r_T and r_B; however, r_T/r_B was found to remain essentially constant.

During the etching process, the etching products tend to settle near the bottom of the container. The color of the etch products is initially dark yellow (the color of cellulose nitrate); in time the color disappears and a white precipitate is observed. The color change may be caused by the further degradation and decomposition of cellulose nitrate by the hydroxide. Homogeneous etching is best achieved by the vigorous agitation of the solution such as with ultrasonic vibrations.

* A product of the Dow Chemical Company, Midland, Michigan.

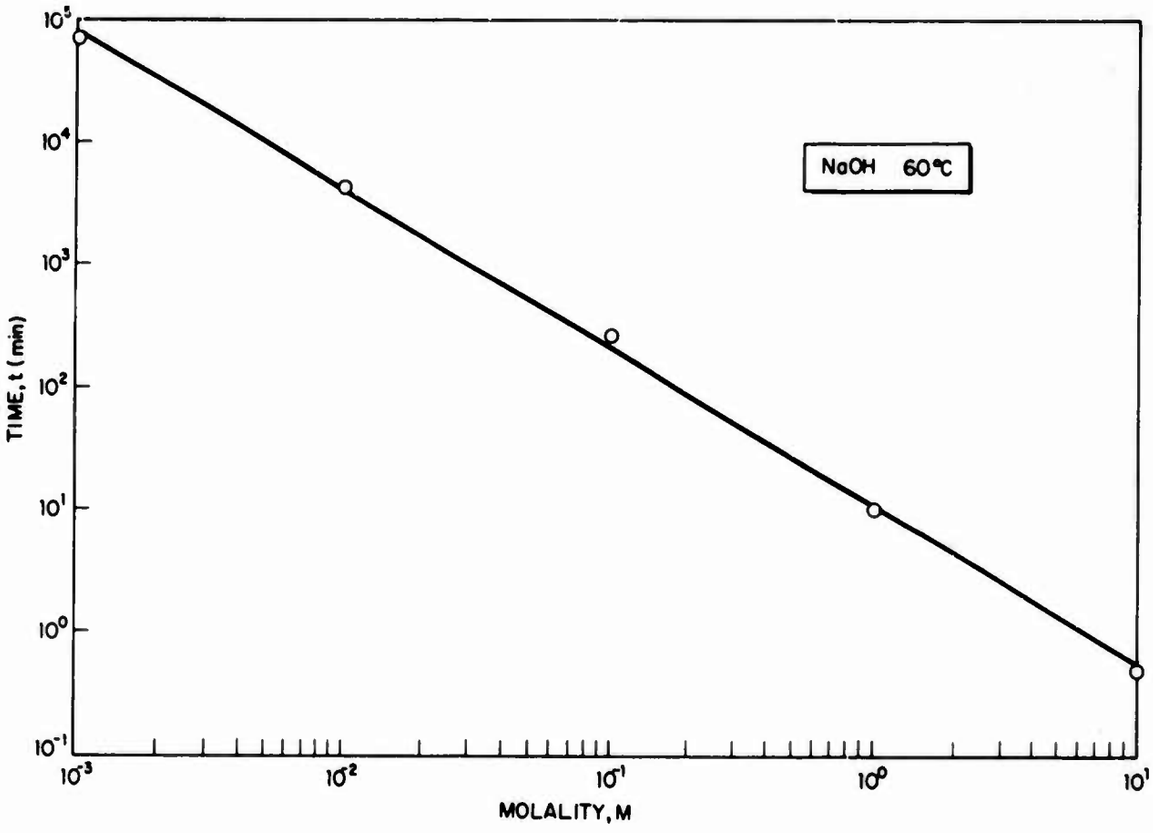

FIGURE IV-20. The time required to etch out fission fragment tracks in NRDL-1 plastic as a function of NaOH concentration.

D. Latent Track Fading

The latent (unetched) tracks are remarkably thermally stable. NRDL-1 cellulose nitrate exposed to 3.2 MeV alpha particles and processed after 18 months storage at room temperature showed no evidence of fading. A series of annealing experiments were carried out using 3.2 MeV alpha particles and fission fragments from ^{252}Cf in order to investigate the latent track fading phenomenon. The exposed specimens were annealed at various temperatures (50-102°C) for various times (2-8700 minutes) then etched for 15 minutes in a 10M NaOH solution at 60°C. The data are shown in Figure IV-21. Here, the rate of fading (reciprocal of the fading time) is plotted as a function of $1/T(^{\circ}K)$. The degree of fading is represented by the fraction of the circle that is filled. Closed points indicate a lack of fading, the open circles indicate essentially complete fading. It was observed that greater etch times revealed tracks in samples which failed to show tracks at 15 minute etch times. Latent tracks of fission fragments required an order of magnitude greater annealing times.

To summarize, annealing reduces the track etch rate r_T. How much r_T is reduced is a function of the dE/dx of the particle, the annealing temperature and the time. Since the activation free energy for the annealing process is of the order of 1 eV, the process involves atomic motion (in agreement with Fleischer et al.[1]).

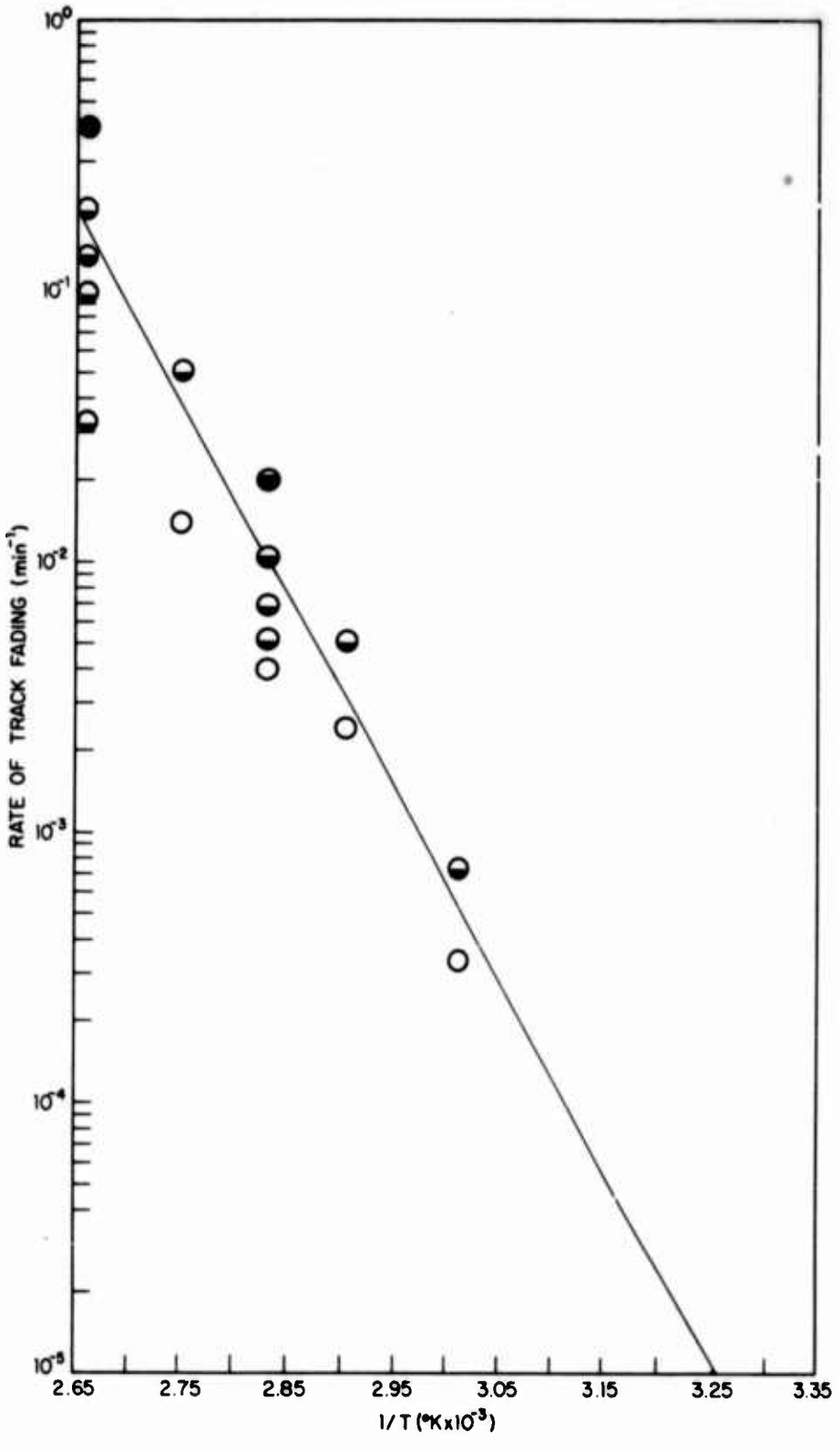

FIGURE IV-21. The temperature dependence of latent track fading for 3.2 MeV alpha particles in NRDL-1 plastic etched for 15 minutes in 10M NaOH solution at 60°C. The degree of fading is represented by the fraction of the circle that is filled.

CHAPTER V

TRACK REGISTRATION CRITERION

A. Introductory Remarks

The knowledge of and the ability to predict which particles will produce latent (etchable) tracks in a given polymer is a basic requirement to a better understanding of the chemical etch phenomenon. The formulation of a track registration criterion is also essential to the practical utilization of the dielectric track detectors in the various problems of nuclear physics and dosimetry.

In this Chapter a new track registration criterion is proposed. This criterion, called the Restricted Energy Loss Rate (REL) criterion, differs from the previously proposed Primary Ionization (PI) criterion[35] (see Chapter I) by taking into account the secondary ionizations and exitations produced by the low energy recoil electrons (low energy δ-rays). Since the value of such criterion is strongly dependent upon its general applicability, the criterion is also applied to the polycarbonate plastics as well as to cellulose nitrate, the two most important polymer track detecting materials for which experimental data are presently available.

B. The Restricted Energy Loss Rate Criterion

It is well known that the energy expended in forming one ion pair in a gas is approximately a constant and is reasonably independent of the type and energy of incident radiation (~ 35 eV in air). This concept is often extrapolated to solids. The energy deposited per unit volume of the detecting material can then be taken as an approximate measure of the density of such ion pairs. In this work the assumption is made that the total energy deposited per unit track volume (track dose) by the incident charged particle determines the chemical reactivity of the latent track region. At present, the diameters of the latent track regions are not known. The same can be said of distribution of deposited energy within these damage regions.

A heavy charged particle, upon traversing matter, loses its energy predominantly through collisons with atomic electrons. The rate of energy loss is a function of the particle charge, z, its velocity, β, and the nature of the stopping material. For a given particle, the distribution of the deposited energy as a function of distance from the particle trajectory is largely a function of the particle velocity. A low velocity particle loses its energy through many low energy collisions, this energy being confined to a small cylindrical volume about the particle trajectory. This contrasts sharply with fast particle interactions where a substantial fraction of the energy goes into the production of high energy recoil electrons (high energy δ-rays). Because of their considerable range, these electrons transfer and deposit the energy over a

much larger volume. A heavy charged particle with relativistic velocity (energy of GeV/nucleon)* can produce δ-rays with energy, ω, of several MeV. The maximum value of ω is given by:[54,55]

$$\omega_{max} = \frac{2\beta^2}{(1-\beta^2)} m_o c^2 \qquad (5.1)$$

where

$m_o c^2$ = 0.511 MeV, the rest energy of an electron, and

$\beta = \frac{v}{c}$, the velocity of the incident heavy particle.

These high energy electrons, which can have ranges of several millimeters, are produced collinearly with the incident particle trajectory but tend to be scattered and thereby deposit this energy a considerable distance from the path of the heavy ion. Since the polymer detectors used in practice are often in the form of thin, 100 micron thick sheets, the energetic δ-rays, and most of their accompanying energy, are lost from the detector. It is reasonable to assume that this energy does not play a deciding role in the processes of track formation. In this case the total rate of energy loss, dE/dx, of a charged particle clearly cannot be used as a criterion for track registration.

The energy per unit path length given to electrons by a charged particle penetrating matter can be conveniently separated into two parts according to the value of the impact parameter, namely the energy loss due to close and distant collisions:[56]

$$(dE/dx) = (dE/dx)_{\omega > \omega_o} + (dE/dx)_{\omega < \omega_o} . \qquad (5.2)$$

---

*A table of particle energy in MeV/nucleon as a function of the particle velocity, β, appears in Appendix I.

The distant collisions are defined as those resulting in the ejection of electrons of energy ω less than some predetermined value ω_o. The energy ω_o is chosen in the energy range such that, for close collisions, the atomic electrons can be considered as free particles, while for distant collisions the incident heavy particle is treated as a point charge.[56] The rate of energy loss due to close collisions is given by:[56,57]

$$(dE/dx)_{\omega > \omega_o} = \frac{2\pi n(z^*)^2 r_o^2 m_o c^2}{\beta^2}\left[\ln\frac{\omega_{max}}{\omega_o} - \beta^2\right], \qquad (5.3)$$

where

n = density of electrons in the stopping material,

z^* = effective charge of the ionizing particle, and

$r_o = e^2/m_o c^2$, the classical electron radius.

The rate of energy loss due to distant collisions is given by:[56,57]

$$(dE/dx)_{\omega < \omega_o} = \frac{2\pi n(z^*)^2 r_o^2 m_o c^2}{\beta^2}\left[\ln\left(\frac{2m_o c^2\beta^2\gamma^2\omega_o}{I_{adj}^2}\right) - \beta^2 - 2\frac{C}{Z} - \delta\right], \qquad (5.4)$$

where

$\gamma = (1-\beta^2)^{-1/2}$,

I_{adj} = mean excitation potential of the material (see Chapter VI),

C/Z = tight binding shell correction, and

δ = correction for the density effect.

The total rate of energy loss, (dE/dx), is then given by the sum of Equations (5.3) and (5.4), which is the Bethe-Bloch formula.[57-59]

$$(dE/dx) = \frac{2\pi n(z^*)^2 r_o^2 m_o c^2}{\beta^2}\left[\ell n \frac{2m_o c^2\beta^2\gamma^2\omega_{max}}{I_{adj}^2} - 2\beta^2 - 2\frac{C}{Z} - \delta\right]. \qquad (5.5)$$

The density effect correction, δ, was neglected in these calculations as it becomes important only when the particle velocity exceeds about 0.87c (~ 1 GeV/nucleon).[60] The energy removed from the vicinity of the track by the Cerenkov radiation was also neglected for it is small in condensed matter (about 10^{-3} $\frac{\text{MeV cm}^2}{\text{g}}$ for a singly charged particle).[57] The mean excitation potential of the material, I_{adj}, as well as the tight binding shell correction, C/Z, were calculated according to procedures outlined by the National Academy of Sciences, National Research Council Subcommittee on Penetration of Charged Particles in Matter.*[60] The effective charge of the ionizing particle, z*, was obtained from the empirical relation of Barkas[56] based upon the data of Heckman et al.[61], for nuclear emulsions:**

$$z^* = z\left[1-\exp(-125\,\beta/z^{2/3})\right]. \qquad (5.6)$$

Although strictly true only for nuclear emulsions, Equation (5.6) can be used for other solids, except for very heavy ions at low incident velocities.[61]

Equation (5.4) can be used to evaluate the energy deposited in the vicinity of the track from the distant collisions. This energy loss is often referred to as the restricted energy loss

---

* Numerical values of the tight binding shell correction, C/Z, for cellulose nitrate are given in Appendix II.

** Numerical listing of z* obtained from Equation (5.6) appear in Appendix III.

rate.[56-58] It should be pointed out that Equations (5.4) and (5.5) strictly hold only above about 8 MeV/nucleon.[60] However, Equation (5.5) is in a satisfactory agreement with the empirical calculations of (dE/dx), as described in Chapter VI, down to energies of about 3 MeV/nucleon for several polymeric materials investigated.

The parameter ω_o is an average energy of the recoil electron that deliniates the boundary between those electrons which contribute and those that do not contribute to the formation of the latent track region. In this work ω_o was treated as an adjustable parameter. It was found that a value of $\omega_o = (1.0 \pm 0.2)\ 10^3$ eV gave the best agreement with experimental data (for the polycarbonate plastic this is only an approximate value). In Figures V-1 and V-2 the restricted energy loss rate, $(dE/dx)_{\omega < 10^3}$, is plotted as a function of energy per nucleon for a number of heavy ions in NRDL-1 cellulose nitrate and polycarbonate resin plastics, respectively. The theoretical curves of Figures V-1 and V-2 are generated in the following way. In the energy interval from 0.1 to 0.5 MeV/nucleon the total (dE/dx) is used since $\omega_{max} \leq 10^3$ eV. Above 0.5 MeV/nucleon the values given by Equation (5.3) are subtracted from the total (dE/dx) calculated empirically. Above 3 MeV/nucleon, Equation (5.4) can also be used to evaluate the restricted energy loss rate. The experimental data on track registration in the two materials are superimposed on the theoretical curves in the form of closed and open circles and squares. Closed points indicate track registration, open points indicate a lack of registration. The circles correspond to data obtained by the author, the squares indicate data taken from

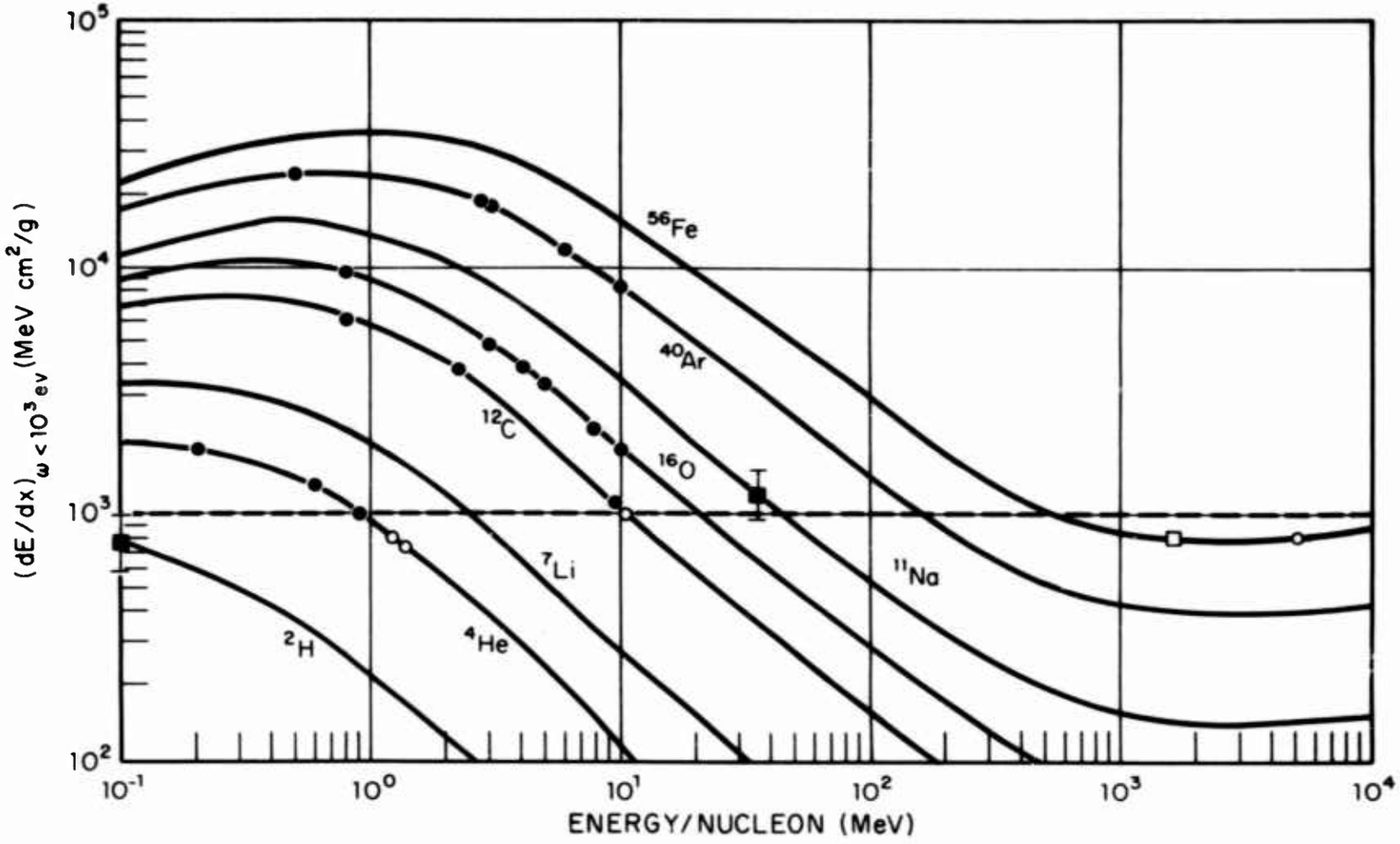

FIGURE V-1. Restricted energy loss rate, $(dE/dx)_{\omega < 10^3 eV}$, as a function of energy per nucleon for a number of heavy ions in cellulose nitrate (I = 81.1 eV). The experimental data on track registration is superimposed on the theoretical curves in the form of closed and open points, indicating track registration and lack of track registration, respectively. The threshold for track registration is about 1.1 x 10^3 MeV cm^2/g.

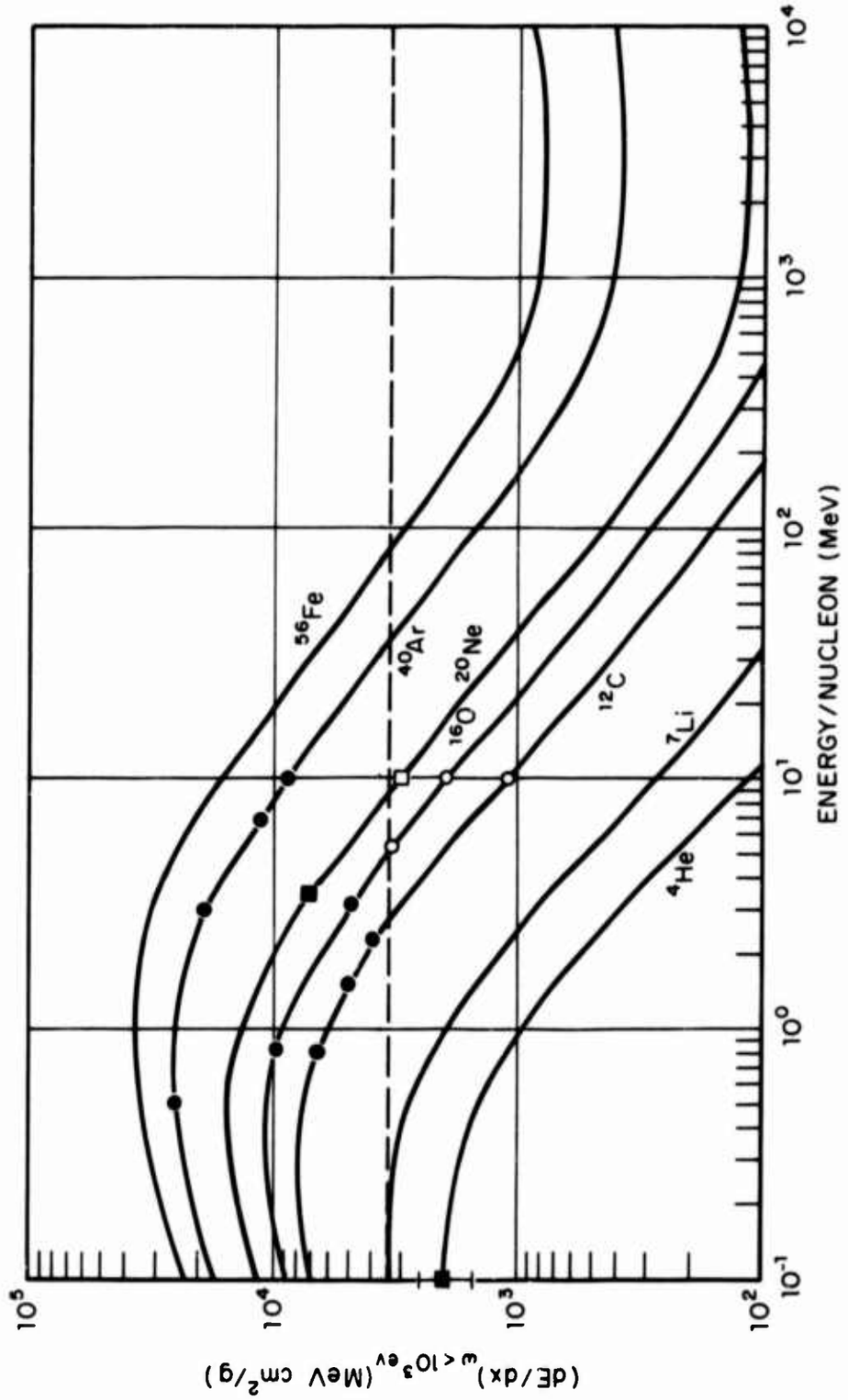

FIGURE V-2. Restricted energy loss rate, $(dE/dx)_{\omega < 10^3 eV}$, as a function of energy per nucleon for a number of heavy ions in Lexan polycarbonate resin (I = 69.5 eV). The experimental data on track registration is superimposed on the theoretical curves in the form of closed and open points, indicating track registration and lack of track registration, respectively. The threshold for track registration is about 3.3 x 10³ MeV cm²/g.

Fleischer et al.[35] The ^{4}He data were obtained with the use of a thin ^{241}Am alpha particle source; the remainder of data were obtained through the use of full and degraded energy beams obtained at the Hilac in Berkeley. The etching was carried out in 10M NaOH solutions at 23° and 60°C for cellulose nitrate and polycarbonate plastics, respectively. Although more measurements are clearly desirable (particularly for the polycarbonate plastic) the existing data suggests that a critical value of the restricted energy loss rate can be chosen for each of these materials. The thresholds for track formation in NRDL-1 cellulose nitrate and polycarbonate plastics are found to be 1.1×10^3 and 3.3×10^3 MeV cm^2/g, respectively.

The restricted energy loss rate of charged particles is a measure of the energy deposited in the vicinity of the particle trajectory and, consequently, is a measure of the ionization and exitation produced in the vicinity of a latent track. The quantity, REL is a measure not only of the primary ionization, but of higher orders as well.

C. Discussion

Let us briefly look at the manner in which the energy of a fast incident charged particle is distributed among the various possible types of electron collisions.

Equation (5.3) together with the total (dE/dx) can be used to evaluate the fraction of (dE/dx) deposited into δ-rays of energy greater than 10^3 eV for various heavy charged particles. In

Figure V-3 the fraction of (dE/dx) deposited into δ-rays of energy greater than ω is given as a function of the δ-ray energy for 0.8 MeV/nucleon ^{4}He, 9.5 MeV/nucleon ^{12}C, and 10^{3} MeV/nucleon ^{56}Fe particles in cellulose nitrate. The three ions have a (dE/dx) of 1.09×10^{3}, 1.60×10^{3}, and 1.35×10^{3} MeV cm^{2}/g, respectively. It is of interest to note that for all three of these widely different ions approximately half the (dE/dx) goes into energy transfer collisions of less than 10^{2} eV. However, the other half of the (dE/dx) is distributed very differently for the three particles. If it is assumed that only electron collisions with energy transfer of less than 10^{3} eV contribute to the formation of an etchable track, then it can be seen that for 0.8 MeV/nucleon ^{4}He ions about 90% of the (dE/dx) is effective in track formation and 10% is ineffective, while for 9.5 MeV/nucleon ^{12}C particles some 27% of the total (dE/dx) is ineffective. The above two particles have equal restricted energy loss rates,

$$\left[(dE/dx)_{\omega < 10^{3}} \simeq 1.1 \times 10^{3} \text{ MeV cm}^{2}/g\right],$$

and both produce etchable tracks in NRDL-1 cellulose nitrate. On the other hand, the 10^{3} MeV/nucleon Fe particle with a total (dE/dx) in excess of that of a 0.8 MeV/nucleon ^{4}He ion, loses about 42% of this energy in high energy δ-rays and, hence, does not register a track.

The above criterion for track registration implies that if a dose (energy per unit volume for the volume of the track) corresponding to that from a heavy ion is deposited in a track detecting polymeric material, a preferential etching of this region should

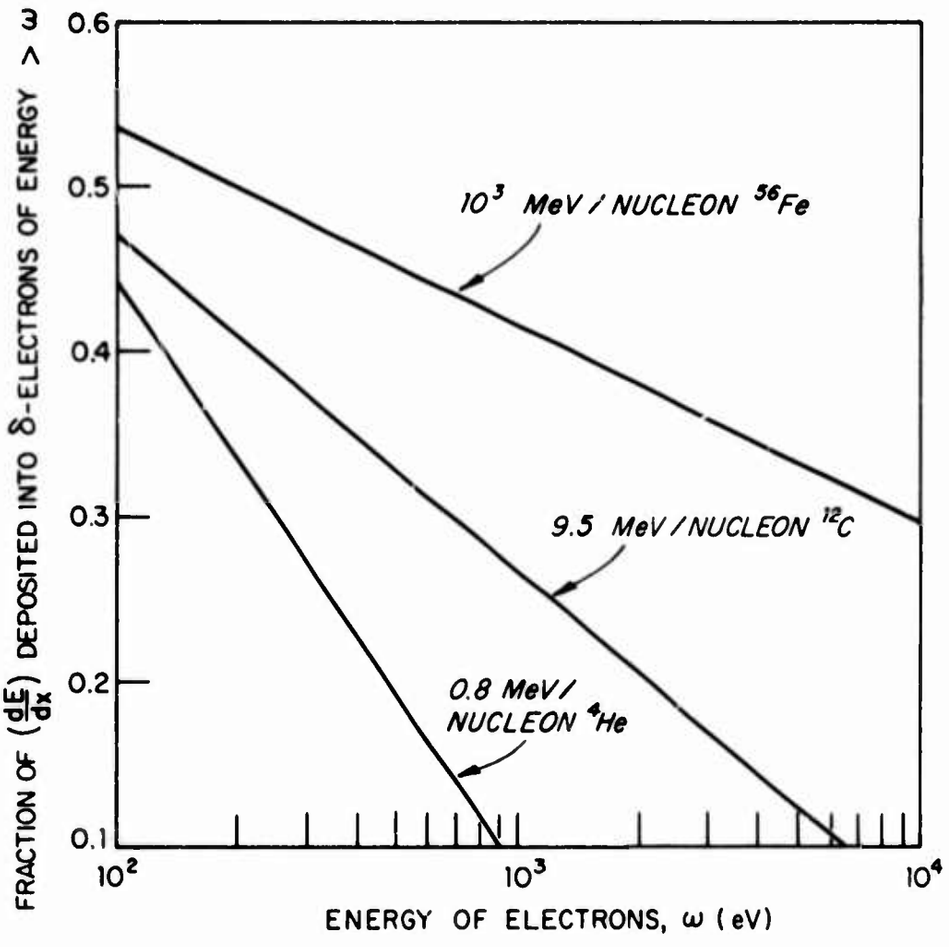

FIGURE V-3. The fraction of the total (dE/dx) lost in energy transfer collisions of energy greater than ω as a function of ω for 0.8 MeV/nucleon ^{4}He, 9.5 MeV/nucleon ^{12}C, and 10^3 MeV/nucleon ^{56}Fe.

occur. The exact dimension, or the distribution of energy within the latent track region is at present not known. It is thought that the diameters of unetched fission fragment tracks in a polycarbonate plastic are probably no greater than about 100Å.[1] If the threshold for charged particle track registration in cellulose nitrate, 1.1×10^3 MeV cm^2/g, is assumed to be deposited within this track volume, the average dose distributed over this cylindrical volume is found to be $\sim 2.5 \times 10^7$ rad. The track width of 100Å is for a particle well above the threshold; for particles at the threshold, the widths are probably narrower, resulting in a dose $> 2.5 \times 10^7$ rad.

This hypothesis was tested by irradiating cellulose nitrate with β-particles from a 2 curie ^{90}Sr source in such a manner that only a small area of the sample was exposed while the remainder was shielded by a lead mask. After irradiation, the specimens were etched at 23°C in a 10M NaOH solution for times comparable to that needed to develop tracks of heavy ions. A dose of about 4×10^7 rad resulted in a preferential etch rate comparable to that from heavy ions. Similar effects also have been observed with gamma rays. Bulk etch rates (microns/hour for a single surface) of gamma irradiated cellulose nitrate plastics appear in Table V-1. A ^{60}Co source was used; etching was carried out in a 10M NaOH solution at 25°C.

The Primary Ionization, PI, and the Restricted Energy Loss, REL, criteria give similar predictions as to track registration for the lighter ions ($2 < z \lesssim 18$). This similarity of predictions by the two criteria is attributed primarily to the fact that the functional

TABLE V-1 Bulk Etch Rate (microns/hour for a single surface) of Gamma Irradiated Cellulose Nitrate Plastics

Dose (rads)	NRDL-1	Daicel No. 1025 (red)	Nixon-Baldwin (Orange)
0	0.194	0.188	0.250
1.2×10^6	0.212	0.198	0.260
5×10^6	--	0.234	--
10^7	0.445	--	0.764
2×10^7	--	0.480	--
3.9×10^7	3.22	1.61	2.23
10^8	20.1	7.80	5.82
2×10^8	--	35.2	--

dependence of Equations (5.4) and (1.2) on β is very similar.[54,55] Also, each approach uses an adjustable parameter to fit the existing experimental data. For heavier ions ($z \gtrsim 18$) the REL criterion predicts registration up to higher energies of the incident particle (see Table V-2). However, these predictions are quite sensitive to the exact REL_{crit} value used. A 10% increase in the REL_{crit} value for NRDL-1 cellulose nitrate lowers the maximum predicted energy for ^{56}Fe registration from 485 to 400 MeV/nucleon. The latter value is predicted by the current PI criterion (I_o = 2 eV). Both criteria agree almost equally well with the presently available experimental data. The point for 0.1 MeV/nucleon deuterons in cellulose nitrate, and the point for 0.1 MeV/nucleon alpha particles in the polycarbonate plastic fall somewhat below the predicted region of track

TABLE V-2 Predicted Maximum Energy (MeV/nucleon) of Heavy Ions Producing Tracks in NRDL-1 Cellulose Nitrate

Ion	Primary Ionization Criterion	Restricted Energy Loss Rate Criterion
^{1}H	0.14	0.1
^{4}He	0.8	0.8
^{7}Li	2.1	2.3
^{9}Be	4.0	3.9
^{11}B	7.1	6.5
^{12}C	10.0	9.5
^{14}N	14.0	14.0
^{16}O	19.0	19.0
^{19}F	24.5	25.0
^{20}Ne	31.5	32.5
^{40}Ar	135	140
^{40}Ca	165	200
^{48}Ti	225	260
^{52}Cr	300	350
^{56}Fe	400	485

registration according to the REL criterion (see Figures V-1 and V-2). However, since the rates of energy loss for the two ions are quite uncertain at these energies, it is not known if this discrepancy is real. Experimental data for registration of heavy, high energy ions is required for an accurate determination of the parameters ω_o and REL_{crit}.

It is of interest to note that a number of charged particle detectors have a response that is considerably affected by the low energy δ-rays generated by the incident heavy particle, namely, photographic emulsions, bubble chambers, cloud chambers, and scintillation counters. The blob density along a high energy particle track in a photographic emulsion as well as the drop count in a cloud chamber have been found to parallel closely the restricted energy loss rate with ω_o of the order of a few keV. It is useful to compare the energies needed to produce a "signal" in a particle detector. An order of magnitude comparison is given in Table V-3.[60] It is evident that a rather large amount of energy is needed to produce a track in cellulose nitrate compared to other types of detectors. The merit of dielectric detectors lies in the fact that they are capable of selectively measuring the highly ionizing charged particles in the presence of high backgrounds of lightly ionizing radiation.

Some of the important aspects of the REL track registration criterion should be pointed out. Based on this model, a stopping particle will produce a latent track over the extent of its range where its $REL > REL_{crit}$ for that material. The length of this region of the particle trajectory we will call R_{reg}, the registration

TABLE V-3 Energy Necessary to Produce a Signal in Various Particle Detectors

Detector	Energy Necessary to Produce a Signal
Scintillator	10^2 eV/scintillation
Photographic emulsion	10^3 eV/blob
Bubble chamber	3-5 x 10^3 eV/bubble
NRDL-1 Cellulose nitrate	150 x 10^3 eV/micron of track

range. In Figure V-4 the predicted R_{reg} for NRDL-1 cellulose nitrate, and for the polycarbonate plastic (Lexan) is given as a function of z for the most abundant isotope of each element. It is observed that R_{reg} is a very sensitive function of z, thus suggesting a possible technique for particle charge determination (see Chapter VII).

Based on the above criterion, a z of 32 or greater would be required for a relativistic particle at minimum ionization ($\beta \simeq 0.96$) to preoduce an etchable track in NRDL-1 cellulose nitrate. Similarly, a z of 55 would be needed for track registration in the polycarbonate plastic.

It is now possible to assign a sensitivity in terms of a microscopic dose to each of the polymer detectors. The quantity of interest then becomes the restricted energy loss rate of the particle and not its total (dE/dx).

The β and γ irradiations have demonstrated that an "ion explosion" is not essential for track formation in polymers. What is required is the production of a sufficient number and density of chemically

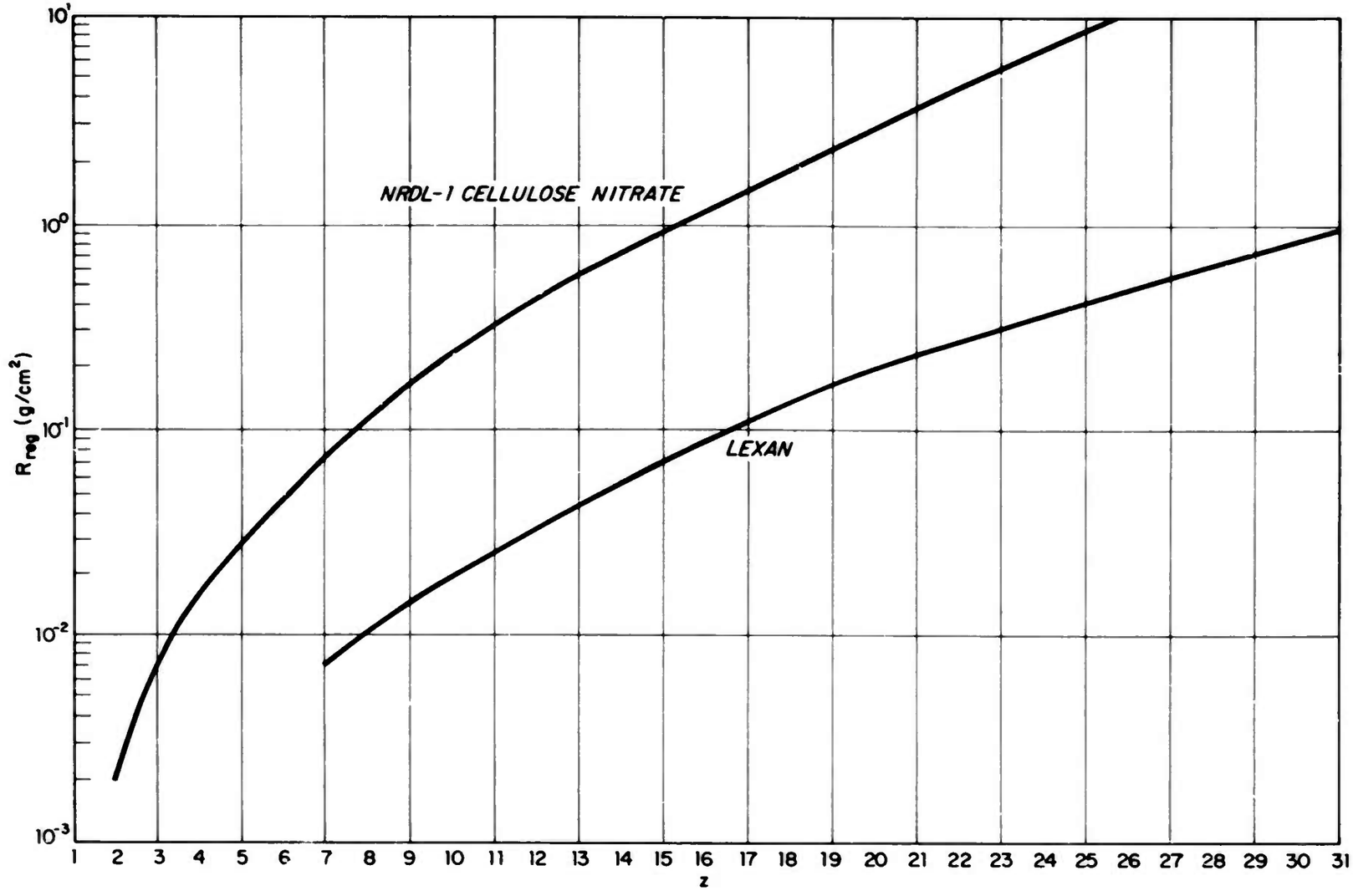

FIGURE V-4. The predicted maximum registration range, R_{reg}, in NRDL-1 cellulose nitrate and Lexan.

reactive species. These species are also apparently capable of being formed by low energy δ-rays. The distribution of these chemically reactive species near a particle trajectory is unknown. It is reasonable to assume that a minimum concentration of these centers is needed in order to be able to develop a track through the chemical etching technique.

In order to refine the REL criterion, more track registration data, particularly for the heavy ions at high energies, are required. It is possible that the different sensitivity polymers may require the use of different values of ω_o.

Since, at the present time, the phenomena of the chemical etch development of tracks is poorly understood, the exact role of the primary, secondary, and higher orders of ionization are not known. However, in the highly radiation sensitive polymers such as cellulose nitrate, it is reasonable to expect that the low energy electrons (low energy δ-rays) which have received a sufficient energy, ~9 - 12 eV, to free them from their parent atoms will contribute to the total dose of the latent track region. These low energy δ-rays are produced in copious numbers by the heavy ions. Having small kinetic energies and correspondingly small ranges, these electrons undergo multiple scattering throughout the latent track region, and deposit their energy in and near the region of the primary ionization. For particles at the threshold of registration, this may be an important contribution. For the particles that are well above the threshold for registration (such as fission fragments) the contribution of the higher orders of ionization will most likely have to be taken into consideration in theoretical predictions of the preferential

track etch rate, r_T, and in predictions of the geometry of the resulting etch cavities. This may be another area where the concept of the restricted energy loss rate will be useful.

CHAPTER VI

RANGE-ENERGY AND ENERGY LOSS RELATIONS FOR HEAVY PARTICLES; COMPARISON OF RANGE WITH THE ETCHED TRACK LENGTH

The knowledge of accurate range-energy and energy loss relations for charged particles is an essential requirement in the development and use of any charged particle detector. In this Chapter a general method for the calculation of range-energy and energy loss relations is described. The relations themselves are given in the form of tables (Appendix V) for a number of materials useful in the study of the dielectric track detectors. The accuracy of the relations is discussed. It is shown that the etched track length of the stopping particles in plastic is a good measure of the particle energy. The work involving the computational part of this chapter was performed jointly with R. P. Henke.

A. Calculations

1. Introductory Remarks

In these calculations the energy loss experienced by a charged particle traversing matter is assumed to result strictly from the interactions with electrons of the stopping medium; inelastic nuclear collisions are neglected. This is a good approximation for energies below 500 MeV/nucleon; for energies above this value the probability

for nuclear interaction becomes significant and the full range, given by this calculation, may not be achieved.[62] The distinction between the path length and range is also not made. Strictly speaking, this calculation gives the total path length of a charged particle, rather than its range; however, for heavy ions this difference is small. Also, the density effect correction, δ, is neglected as it becomes important only at velocities of about $\beta \simeq 0.87$ ($\sim$ 1.0 GeV/nucleon).[57,60]

2. Method of Calculation

a. General Expressions

In order to achieve a broad coverage of the spectrum of particles, energies, and stopping materials, the methods of Barkas and Berger[60] have been employed in these calculations. Their empirical representations of range-energy data have been modified and extended to lower energies.

The range of a charged particle in matter can be expressed by the general formula:

$$R(\beta) = \frac{M}{z^2}\left[\lambda(\beta) + B_z(\beta)\right], \qquad (6.1)$$

where

M = mass of the particle in units of the proton,

z = charge of the particle in units of the proton,

$\lambda(\beta)$ = range of an "ideal" proton with velocity βc, and

$B_z(\beta)$ = the range extension in the same material.

The units of $\lambda(\beta)$ and $B_z(\beta)$ are moles of electrons per cm^2, and the units of $R(\beta)$ are g/cm^2.

An "ideal" proton is a particle of protonic mass and charge which does not capture electrons or interact strongly with nuclei. The range extension, $B_z(\beta)$, is the extension of the range caused by the neutralization of the moving ion's charge by charge pick-up near the stopping end of the trajectory. The subscript, z, on $B_z(\beta)$ indicates that the range extension is dependent upon the atomic number of the moving ion.

Equation (6.1) permits the calculation of ranges in g/cm^2 as a function of five parameters: A/Z, I_{adj}, z, M, and E.[60] The ratio A/Z is the atomic mass per electron of the stopping material in amu/electron; I_{adj} is the mean value of the ionization potential in electron volts for the stopping material adjusted by assuming that the shell correction for relativistic particles is zero;[60] z, M, and E are the atomic number, mass, and energy of the incident ion, respectively.

The rate of energy loss, (dE/dx), is defined as $(dE/dx) \equiv + (dE/dR)$, and is obtained by differentiating Equation (6.1);

$$\frac{dR}{dE} = \frac{M}{z^2}\left[\lambda'(\beta) + B_z'(\beta)\right]\frac{d\beta}{dE} \quad , \tag{6.2}$$

where R is the residual range of the particle. It is convenient to express λ as a function of the proton kinetic energy τ, then $\lambda(\beta) \rightarrow \lambda(\tau)$, and

$$\frac{dR}{dE} = \frac{M}{z^2}\left[\lambda'(\tau)\frac{d\tau}{dE} + B_z'(\beta)\frac{d\beta}{dE}\right] . \tag{6.3}$$

The quantity τ is the energy of a proton with the same β as that of the particle, so that

$$E = \tau M , \tag{6.4}$$

and

$$\frac{d\tau}{dE} = \frac{1}{M} \cdot \tag{6.5}$$

Since the kinetic energy of the particle is given by

$$E = \left[\frac{Mm_p c^2}{(1-\beta^2)^{1/2}} - Mm_p c^2 \right] \tag{6.6}$$

then

$$dE/d\beta = \frac{Mm_p c^2}{(1-\beta^2)^{3/2}} = 1/\frac{d\beta}{dE} \ , \tag{6.7}$$

where m_p is the mass of the proton.

Using Equations (6.3), (6.5), and (6.7) we find,

$$\frac{dE}{dx} = 1/\frac{dR}{dE} = \frac{z^2}{\left[\lambda'(\tau) + \frac{B_z'(\beta)(1-\beta^2)^{3/2}}{Mm_p c^2 \beta}\right]} \cdot \tag{6.8}$$

The velocity β is given by the following relativistic expression,

$$\beta = \left[\frac{E}{Mm_p c^2}\left(2 + \frac{E}{Mm_p c^2}\right)\right]^{1/2} \Big/ \left[1 + \frac{E}{Mm_p c^2}\right] , \tag{6.9}$$

where

$$M = A/1.008, \text{ and}$$

$$Mm_p c^2 = 931.141\ A \text{ (MeV)}.$$

The quantity A is atomic weight of the ion, and E is the kinetic energy of the ion.

Equations (6.1) and (6.8) express the range, R, and the rate of energy loss, (dE/dx), of a charged particle as a function of $\lambda(\tau)$, $\lambda'(\tau)$, $B_z(\beta)$, $B_z'(\beta)$ and β.

b. The Adjusted Mean Ionization Potential - I_{adj}

Assuming Bragg's rule of the additivity of the stopping power effects of the various components, the value of I_{adj} for a given stopping material is computed from the I_{adj}'s of the individual constituents. For the i^{th} constituent[60],

$$\left(I_{adj}\right)_i = 12\ Z_i + 7 \text{ eV} \qquad \text{for } Z \leq 13$$

$$\left(I_{adj}\right)_i = 9.76\ Z_i + \frac{58.8}{Z_i^{0.19}} \text{ eV} \qquad \text{for } Z \geq 13\ . \tag{6.10}$$

These empirical expressions of the experimental results are only approximate for values of $Z \lesssim 13$. If a more reliable value of I_{adj} is available it is taken from Table VI-1, which was compiled from the National Academy of Sciences, National Research Council Publication-1133. The values given in Table VI-1 are only those that differ from values computed from Equation (6.10) and represent the median values given in Reference 60.

TABLE VI-1 Values of I_{adj} (Reference 60) which Differ from the Computed Values (Equation (6.10))

Ion	Z	I_{adj}
H	1	165*
He	2	42
Li	3	38
Be	4	60
N	7	85
O	8	96*
Ne	10	131
Mg	12	156

*For compounds

From the individual $\left(I_{adj}\right)_i$ the I_{adj} for a compound is given by[60]

$$\ell n\ I_{adj} = \langle A/Z\rangle \sum \frac{f_i Z_i}{A_i}\ \ell n \left(I_{adj}\right), \tag{6.11}$$

where

f_i = fraction by weight of the i^{th} component of the stopping material,

A_i = atomic weight of the i^{th} component, and

Z_i = atomic number of the i^{th} component.

For a molecular material,

$$f_i = \frac{\mu_i A_i}{\sum \mu_j A_j}\ , \tag{6.12}$$

where μ_j is the formula number of the i^{th} component.

It is assumed that

$$\langle A/Z\rangle = \frac{1}{\langle Z/A\rangle}\ , \tag{6.13}$$

where the quantity

$$\langle Z/A\rangle = \sum f_i \frac{Z_i}{A_i}\ . \tag{6.14}$$

c. The Ideal Proton Range and Its Derivative

The ideal proton range, $\lambda(\beta)$, and the actual proton range, $\lambda(\beta) + B_1$, are in practice hardly distinguishable.[60] Using the available range-energy data for protons, Barkas and Berger summarize the entire body of range data by a formula of the type:

$$\ell n\ \lambda = \ell n\ \langle A/Z\rangle + \sum_{n=0}^{N} \sum_{m=0}^{M} a_{mn} \left(\ell n\ I_{adj}\right)_1^m \left(\ell n\ \tau\right)_1^n , \tag{6.15}$$

where a_{mn} are the coefficients used to fit λ. In this fashion, λ is a smooth function of I_{adj}. The quantity $\langle A/Z \rangle$ is the total number of nucleons per electron in the stopping material and can be calculated for an arbitrary stopping material from Equation (6.14).

The quantity $\lambda'(\tau)$ is obtained by differentiation of Equation (6.15),

$$\lambda'(\tau) = \frac{\lambda}{10\tau} \sum_{n=0}^{N} \sum_{m=0}^{M} n\, a_{mn} \left(\ell n\, I_{adj}\right)_1^m \left(\ell n\, \tau\right)_1^{n-1}, \qquad (6.16)$$

where

$$\left(\ell n\, I_{adj}\right)_1 = \frac{\ell n\, I_{adj}}{10} \quad \text{and} \quad \left(\ell n\, \tau\right)_1 = \ell n\, \frac{\tau}{10} \ .$$

Three different sets of coefficients, a_{mn}, have been used to fit λ in three different energy regions:

Low energy region: up to about 1.0 MeV/nucleon

Medium energy region: 1 - 9 MeV/nucleon

High energy region: 7 - 1200 MeV/nucleon.

For the low energy region, a least square fit of the form above (Equation (6.15)) was made to all of the low energy experimental range-energy data given by Whaling[63] up to 0.95 MeV/nucleon. The ideal proton's range was calculated by subtracting the range extension from the real range. In order to ensure a smooth connection to the medium energy region, points were also included from the fit of Barkas and Berger at 1, 2, and 3 MeV/nucleon. The coefficients of Equations (6.15) and (6.16) for the low energy region are given in Table VI-2.

TABLE VI-2 Coefficients for $\lambda(\tau)$ in the Low Energy Region

N = 3 M = 3

m \ n	0	1	2	3
0	- 8.725	18.797	74.192	752.005
1	8.309	11.139	-528.805	-5558.937
2	-13.396	-64.808	1264.232	12843.119
3	12.625	54.043	-934.142	-9306.336

For the medium and the high energy regions the coefficients of Equations (6.15) and (6.16) are taken from Tables 3 and 9 of Barkas and Berger.[60] The fits in the different energy regions were connected at the appropriate points, functions of I_{adj}, which provide a minimum discontinuity in both λ and its derivative.

d. The Range Extension and Its Derivative

The range extension, $B_z(\beta)$, was computed using the range extension for emulsion,[61] $C_z\left(\frac{137\beta}{z}\right)$, scaled to an arbitrary material. The scaling is such that $B_z(\beta)$ has the same asymptotic value given by Barkas and Berger,[60]

$$(7.0 + 0.85\ I_{adj}^{5/8})\ \langle A/Z\rangle\ 10^{-6}\ z^{8/3}. \qquad (6.17)$$

Thus, the range extension, $B_z(\beta)$, is given by

$$B_z(\beta) = (31.8 + 3.86\ I_{adj}^{5/8})\ \langle A/Z\rangle\ 10^{-6}\ z^{8/3}\ C_z\left(\frac{137\beta}{z}\right), \qquad (6.18)$$

where $C_z\left(\frac{137\beta}{z}\right) \rightarrow C_z(X)$ is given in regions:

$$C_z(X) = -0.00006 + 0.05252X + 0.12857X^2 \qquad X \leq 0.2,$$

$$C_z(X) = -0.00185 + 0.07355X + 0.07172X^2 - 0.02723X^3 \qquad 0.2 \leq X \leq 2.0, \qquad (6.19)$$

$$C_z(X) = -0.0793 + 0.3323X - 0.1234X^2 + 0.0153X^3 \qquad 2.0 \leq X \leq 3.0, \text{ and}$$

$$C_z(X) = 0.220 \qquad X \geq 3.0.$$

For $X \leq 0.2$, $C_z(X)$ was obtained from the measurements of Henke and Benton (see Figure VI-1).[64] For $X > 0.2$ the fit was made to data of Heckman et al. (see Figure VI-2).[61]

The derivative of the range extension, $B_z'(\beta)$, is obtained by taking the derivative of Equation (6.18) with respect to β,

$$B_z'(\beta) = (4.357 + 0.5288\, I_{adj}^{5/8})\, \langle A/Z \rangle\, z^{5/3}\, 10^{-3}\, C_z'\left(\frac{137\beta}{z}\right), \qquad (6.20)$$

with corresponding $C_z'(\beta)$:

$$C_z'(X) = 0.05252 + 0.25714X \qquad X \leq 0.2,$$

$$C_z'(X) = 0.07355 + 0.14344X - 0.08169X^2 \qquad 0.2 \leq X \leq 2.0, \qquad (6.21)$$

$$C_z'(X) = 0.3323 - 0.2468X + 0.0459X^2 \qquad 2.0 \leq X \leq 3.0, \text{ and}$$

$$C_z'(X) = 0 \qquad X \geq 3.0.$$

The range, R, and the energy loss rate, (dE/dx), can now be evaluated from the fits to quantities $\lambda(\tau)$, $B_z(\beta)$ and their derivatives $\lambda'(\tau)$ and $B_z'(\beta)$.

3. Discussion of the Method

The range extension, $B_z(\beta)$, is functionally related to the effective charge of the ion by:[60]

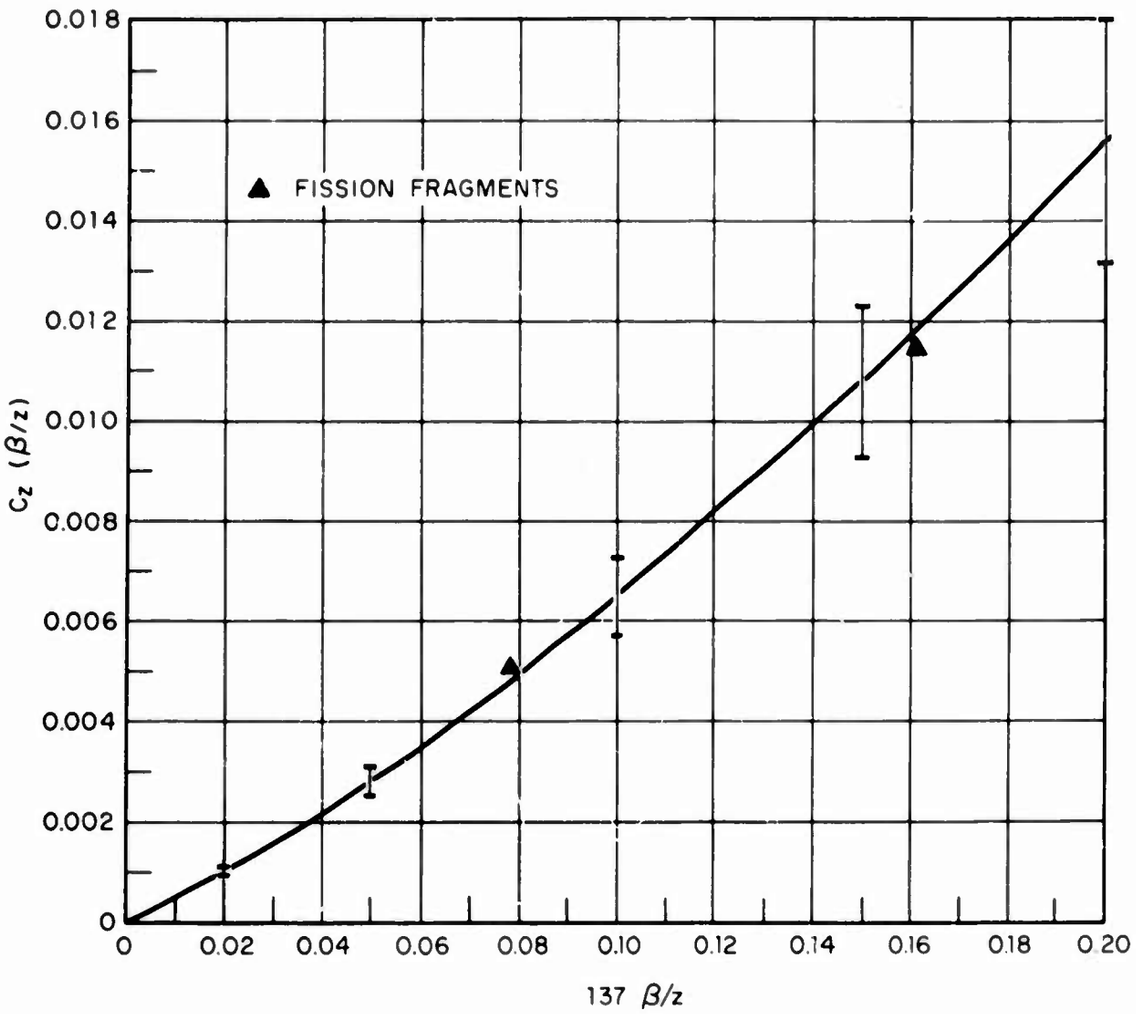

FIGURE VI-1. Empirically derived curve relating the range-extension term to the velocity of the ion in units of the K-electron velocity. (Reference 64)

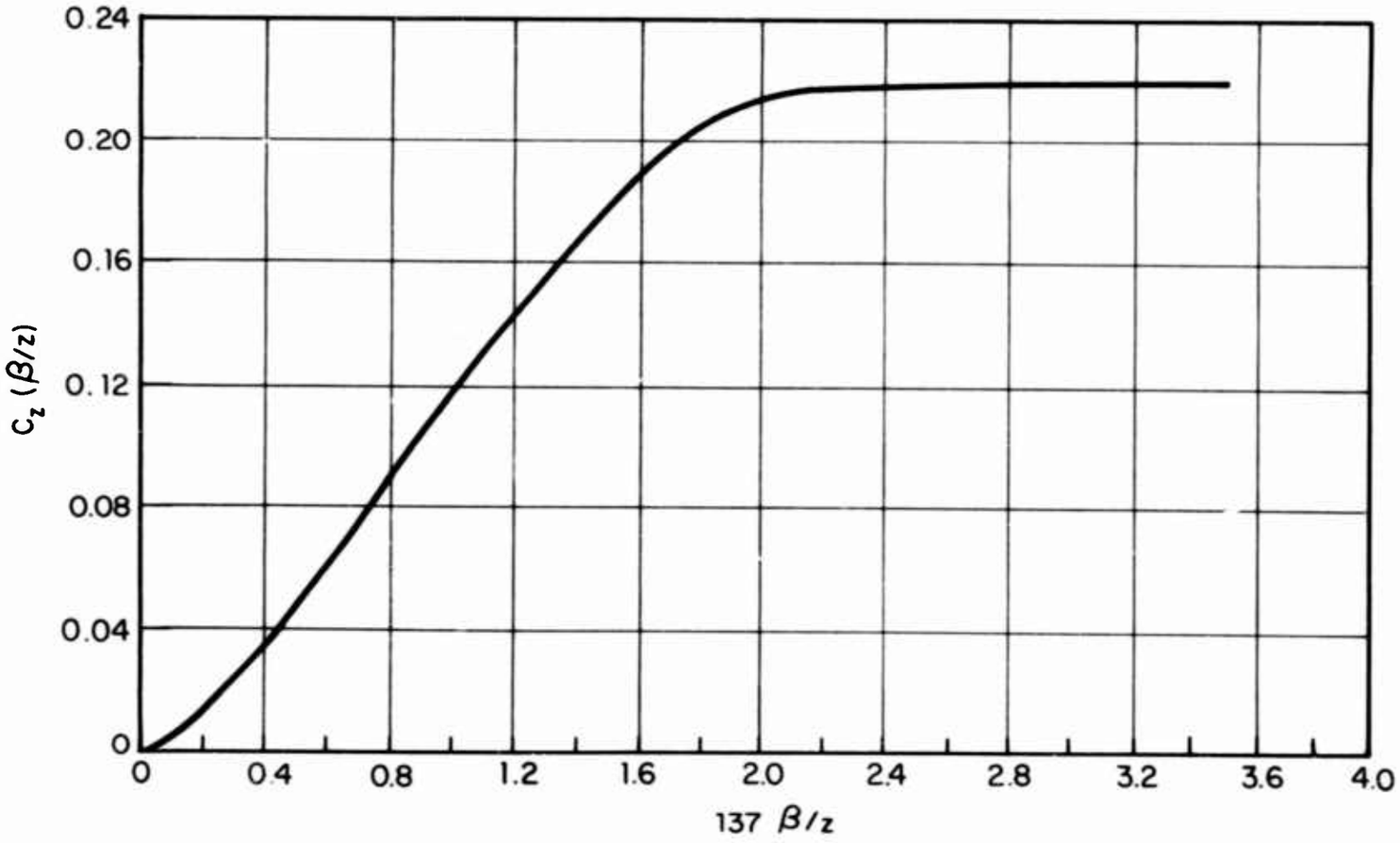

FIGURE VI-2. Empirically derived curve relating the quantity $C_z(\beta/z)$ to the velocity of the ion in units of K-electron velocity. (Redrawn from Reference 61)

$$B_z(\beta) = \int_0^{\beta} \left[(z/z^*)^2 - 1 \right] \frac{d\lambda}{d\beta'} \, d\beta' \, , \qquad (6.22)$$

where z*e is the effective charge of the moving ion with atomic number z. The quantity $B_z(\beta)$ is obtained by scaling the corresponding experimental expression for emulsion to other materials. It can be seen from Equation (6.22) that this procedure relies on two assumptions: (1) the effective charge, z*e, is only a function of β and z, not a function of the stopping materials, and (2) the proton range expression, $\lambda(\beta)$, can be scaled for different stopping materials.

The validity of the first assumption, that z*/z is independent of the stopping material, seems to be demonstrated experimentally except for very heavy ions at low incident particle energy and very low stopping material density.(61)

The second assumption is approximately true for small values of β. Barkas and Berger have used the expression,

$$\lambda = (11.1 + 1.34\, I_{adj}^{5/8}) \langle A/Z \rangle \beta^{10/3} \text{ g/cm}^2 \, . \qquad (6.23)$$

The $(1 + 0.121\, I_{adj}^{5/8})$ dependence of the range-energy relation and hence of B_z has been retained, but the experimental results for emulsion have been used to obtain the universal function that is to be scaled. Deriving B_z in this fashion is an improvement over the use of the simplified analytic expression obtained from Equations (6.22) and (6.23), but still does not take into account the slight dependence of the shape of the curve $\lambda(\beta)$ upon the stopping material. Thus, an error will be introduced when I_{adj} of the material deviates significantly from I_{adj} for emulsion if $B_z(\beta)/\lambda(\beta)$ is not small. This situation is encountered when β is small and z is large.

In Figure VI-3 is shown a comparison of C_z used in this calculation, (a), with the equivalent function used by Barkas and Berger, (b). While the two functions closely approximate each other in absolute values their slopes differ. Function (b) has a discontinuity at $(\beta/z) = 14.6$, thus resulting in a discontinuity in the (dE/dx). Also, while the function (b) can safely be used for calculating R and (dE/dx) of particles with $E > 1.0$ MeV/nucleon, it leads to serious errors at lower energies.

Range-energy and energy loss tables for nine heavy ions in several stopping materials are listed in Appendix V. The materials are arranged in the order of increasing I_{adj}. The various parameters for the stopping materials for which range-energy relations were calculated are given in Table VI-3. The chemical formulae, when available, are not representative of all the commercial materials available under a given name. The differences are due to such factors as the varying types and quantities of plasticizers used, and the varying methods of sample preparation (solvents used, amount of drying).

4. Evaluation of Results

The R.M.S. dispersions of the input range energy points about the computed points for the high (7 - 1200 MeV/nucleon) and medium (1 - 9 MeV/nucleon) energy regions are 0.6% and 2%, respectively.[60] For the high energy region the spread of the stopping power values is 1.3%. The R.M.S. spread of Whaling's data (for 16 stopping materials) about the computed values for the low energy region are given in Table VI-4 for several values of the proton energy.

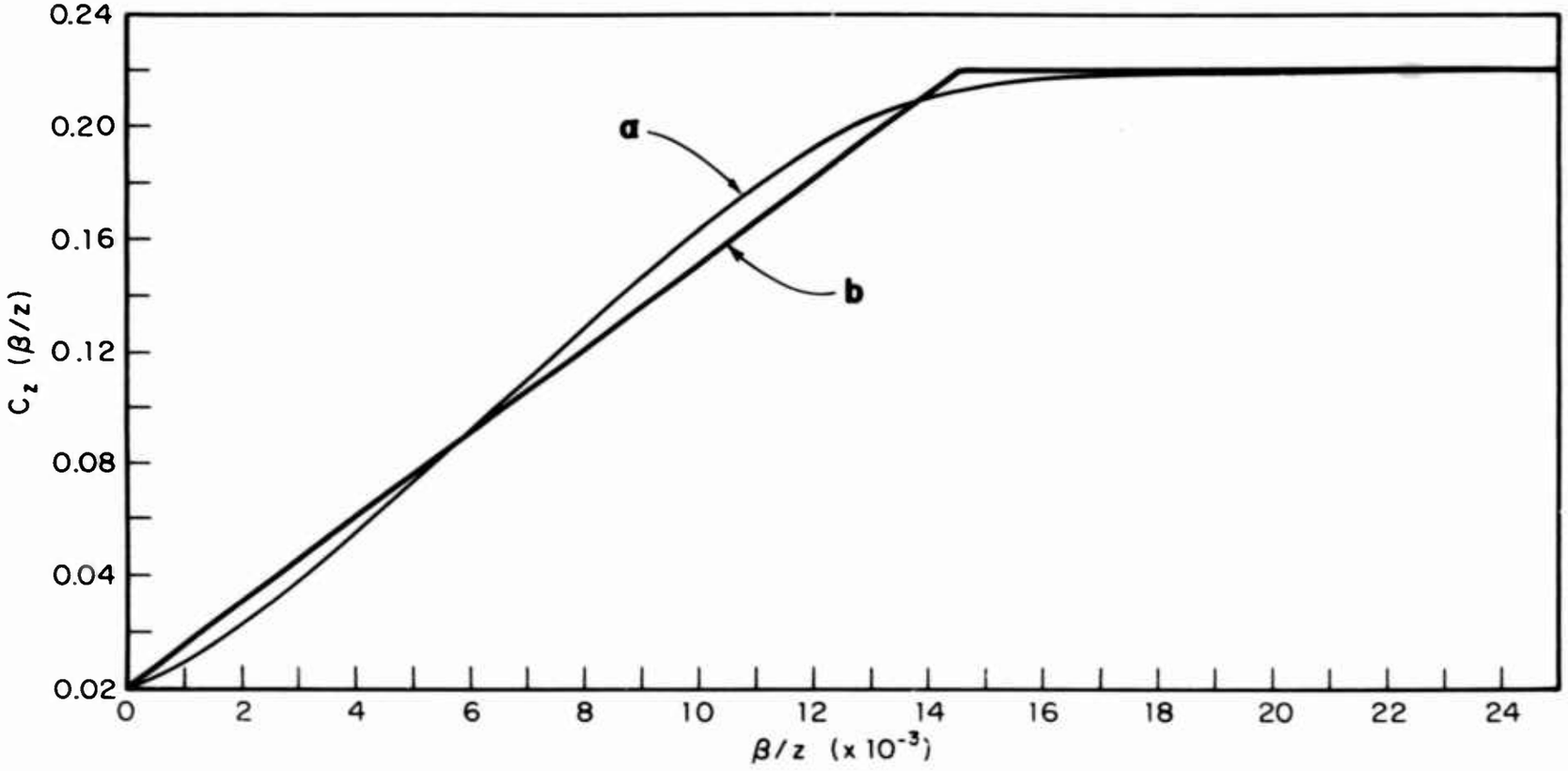

FIGURE VI-3. The range extension functions, $C_z(\beta/z)$, as a function of $(\beta/z) \times 10^{-3}$. Function (a) used in this calculation, function (b) is of the form used by Barkas and Berger.

TABLE VI-3 Parameters of the Stopping Materials

Material	Composition	I_{adj}	$\langle A/Z \rangle$
1. Bisphenol-A polycarbonate (Lexan)	$C_{16}H_{14}O_3$	69.5	1.896
2. Polyethylene terephthalate (Mylar)	$C_{19}H_{16}O_7$	73.2	1.915
3. NRDL-1 cellulose nitrate	--	77.2	1.918
4. Cellulose nitrate (unplasticized)	$C_6H_8O_9N_2$	81.1	1.939
5. Aluminum	Al	163.0	2.075
6. Silicon	Si	172.3	2.004
7. Nuclear photographic emulsion	--	303.4	2.204

TABLE VI-4 Smoothness of Low Energy Data

Energy (MeV)	R.M.S. Spread in Range (Percent)	R.M.S. Spread in Energy Loss Rate (Percent)
0.1	28.2	23.3
0.2	17.1	14.5
0.5	8.5	5.2
1.0	4.8	2.3
2.0	4.4	1.7

The error in the smoothed relations may be considerably smaller since the error quoted largely represents fluctuation of the data, not in the poorness of the fit. There are only 16 stopping materials involved, however; hence the error of the smoothed curve probably exceeds $1/\sqrt{16}$ of the quoted spreads. A large contributor to the extreme spread of the data about the smoothed relations seems to be the integration constants used by Whaling.[63] His range-energy curves were obtained by the integration of energy loss rate data. Another possible contributor is the questionable practice of using I_{adj} as the smoothing parameter for this low energy region.

It is known that for low energies, at a given β, the z^* differs for the solid and the gaseous stopping materials. In order to obtain a good fit for the very low (less than 1 MeV/nucleon) energy ideal proton range-energy relations, both the gaseous and the solid data of Whaling had to be used. Consequently, for low energies this calculation is a compromise between the two types of materials. However, since at the low energies the range is predominantly determined by the range extension (which was measured in a solid, nuclear emulsion), the heavy ion ranges tend to be more nearly correct for the solid stopping materials.

B. Measurement of Range-Energy Relations Using Lithium Drifted Silicon Detectors

In order to examine the accuracy of the range-energy calculations and to investigate their general applicability to different stopping materials, lithium drifted silicon detectors were used in

conjunction with the heavy ion beams from the Hilac. The method consisted of measuring the energy of the beam before and after it passed through a thin foil of a given stopping material of a predetermined thickness. The difference in the calculated residual range at the two energies was compared to the actual thickness of the foil. Using ^{12}C and ^{20}Ne ions with energies between 2-10 MeV/nucleon, measurements were made on the following stopping materials: Mylar, aluminum, and Muscovite mica.

The results of the measurements are tabulated in Table VI-5. The largest disagreement occurred generally for the heavier ions at the lowest energies.

TABLE VI-5 Accuracy of Range-Energy Calculations as Determined from Lithium Drifted Silicon Detector Measurements

Stopping Material	Bombarding Ion	Number of Measurements	Average Systematic Error (%)
Mylar	^{12}C	4	2.61
Mylar	^{20}Ne	5	3.36
Aluminum	^{12}C	1	0.96
Aluminum	^{20}Ne	1	1.61
Muscovite mica	^{12}C	1	2.27
Muscovite mica	^{20}Ne	1	3.89

C. Track Length Measurements - Comparison with Calculated Range

The relationship between the calculated range of stopping heavy ions and the etched track length was investigated. Heavy ions from

the Hilac, monitored by means of nuclear emulsions, were used. Nuclear emulsions, present during each irradiation, served as a means for precise determination of the energy of the accelerated ions. Ilford, 100 micron thick, glass backed, 1 x 3 in., K.5 and G.5 emulsions were used. The beams consisted of ^{12}C, ^{16}O, and ^{40}Ar ions. The beam energy was varied by allowing the beams to penetrate thin aluminum foils of predetermined thickness before striking the target. The samples and emulsions were placed in a holder at the end of an evacuated beam tube in such a way that the incoming ions entered with a dip angle of 20^{o} to the sample surface. Exposed in this manner, all ions recorded on a single plate had essentially the same energy. The emulsions were processed in a D-19 type developer.

Track length measurements of 50 tracks in each nuclear emulsion plate were made. In order to achieve maximum accuracy, a 100X oil immersion objective and a 25X eyepiece were used. The ion energies were obtained by relating the measured track lengths to the available range-energy tables for nuclear emulsions.(61)

The irradiated NRDL-1 cellulose nitrate samples were etched at room temperature in a 10M NaOH solution. The process was terminated when tracks developed rounded terminal ends. Measurements of track length were performed in the manner that took into account the geometry of tracks, as well as the loss of a portion of a track due to the bulk etching of the samples (see Section A, Chapter IV). In Figure VI-4 is shown the comparison between the calculated ranges for NRDL-1 cellulose nitrate and the measured track length for four ions. The horizontal error bars represent the uncertainty in energy of the ions as determined with the use of nuclear emulsions. The absence of error bars represents

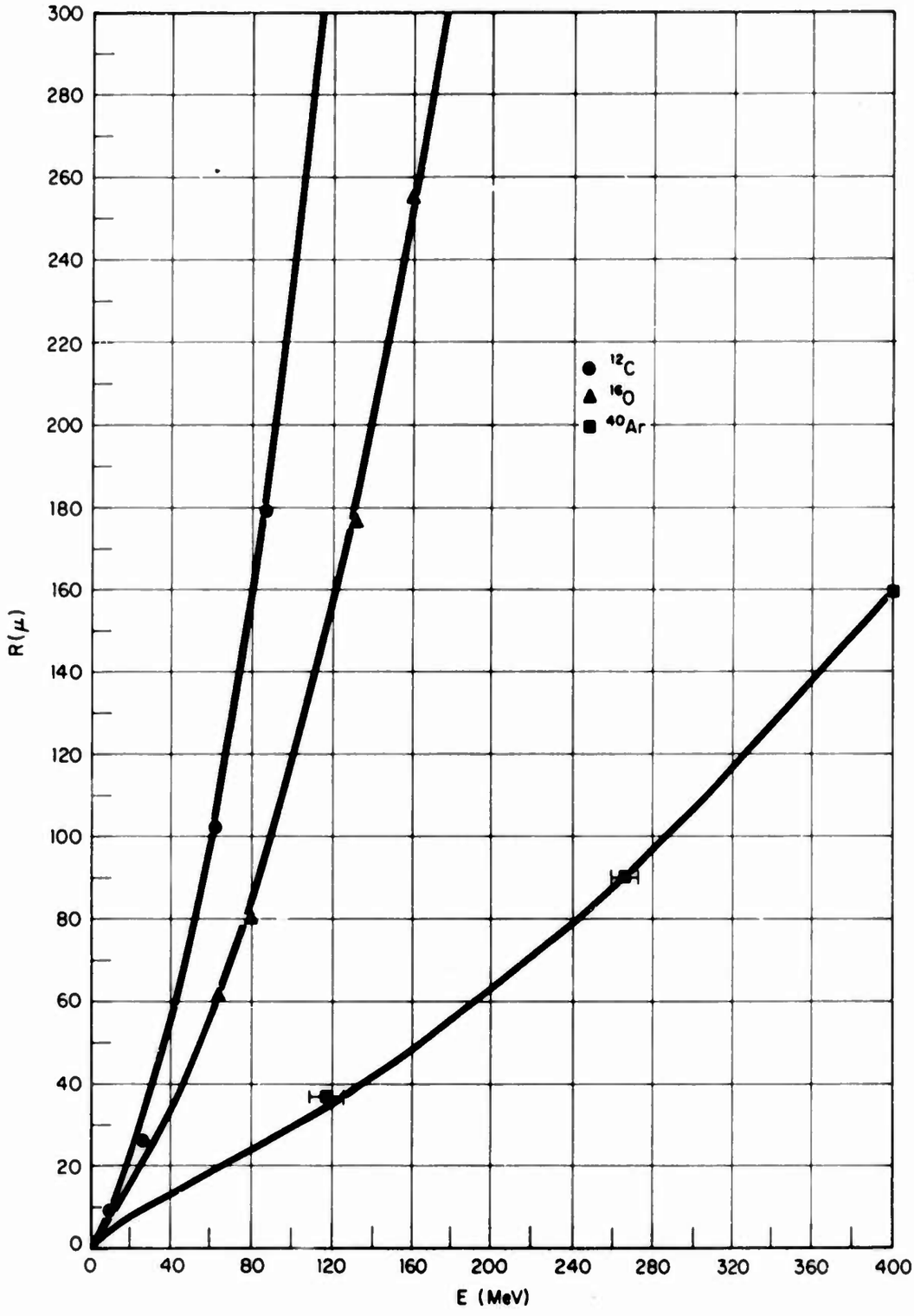

FIGURE VI-4. Comparison between the calculated range-energy relations (solid lines) for NRDL-1 cellulose nitrate and the experimentally measured etched track lengths (points) for ^{12}C, ^{16}O, and ^{40}Ar ions.

an uncertainty smaller than the dimensions of the points. Thus, for energies above 1 MeV/nucleon, excellent agreement between the calculated and the measured ranges was observed for all ions. In an independent set of measurements, Price[65] has reported agreement between the calculated range and the measured track length is better than 2 percent for the cellulose nitrate and the polycarbonate plastics.

The computer code for the generation of range-energy and energy loss tables, described in this chapter, is found in Reference 66.

CHAPTER VII

CHARGED PARTICLE DETECTION

In this chapter measurements of the dependence of the track etch rate on the particle REL rate are presented, the information content of tracks is discussed, and particle identification techniques are proposed and applied to measurements on tracks found in a stack of cellulose nitrate layers exposed to cosmic radiation. The REL criterion is used; however, other criteria (such as the Primary Ionization) can be easily substituted in place of REL in the methods and techniques described.

A. Dependence of the Track Etch Rate on the Particle Parameters

In etching tracks of light and heavy particles (such as alpha particles and fission fragments), it is immediately observed that tracks of heavy particles etch faster. The faster preferential etch rate results in the tracks having correspondingly smaller cone angles. For a given etch time, the tracks also have correspondingly longer track lengths. For example, in Figure VII-1 are shown tracks of (a) 2 MeV/nucleon ^{12}C ions, and (b) 10 MeV/nucleon ^{40}Ar ions in 18 - 25 cps, RS type, unplasticized cellulose nitrate plastic. This kind of behavior was observed in all plastics examined, irrespective of the source or type.

In Chapter V it was shown that the restricted energy loss rate, REL, of the charged particles can be used to predict whether a latent (etchable) track will be produced. In other words, the REL criterion

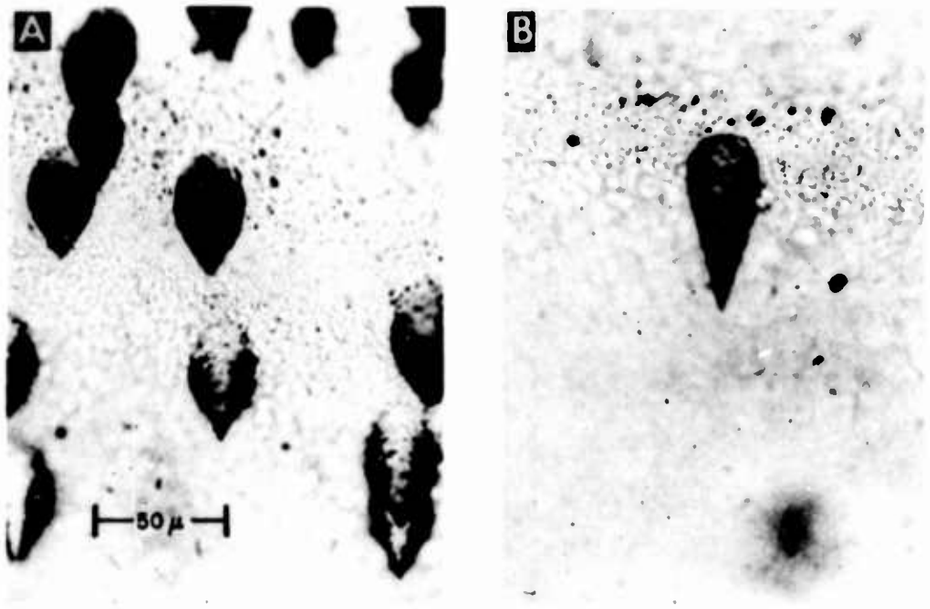

FIGURE VII-1. Tracks of (a) 2 MeV/nucleon ^{12}C ions, and (b) 10 MeV/nucleon ^{40}Ar ions in 18-25 cps RS type, unplasticized cellulose nitrate plastic.

predicts which portion of the particle trajectory in the plastic has $r_T > r_B$. It becomes important to investigate the behavior of r_T as a function of the particle REL.

Measurements of r_T as a function of the particle's REL are presented in Figure VII-2. The data were obtained by bombarding NRDL-1 cellulose nitrate with heavy ions from the Hilac. Full energy, 10 MeV/nucleon, and degraded ions were used. The bombarded specimens were etched in 10M NaOH solution at 60°C for one minute. It is observed that r_T rapidly approaches r_B for small values of REL; the point where $r_T = r_B$ defines the REL_{crit} point. This very rapid decrease in r_T is the key to the threshold characteristic of this detector (see the registration data for ^{12}C in Figure V-1). For large values of REL, the etch rate, r_T, approaches a constant value. Thus the detector appears to saturate at high values of REL. The variation of r_T between these extreme values gives a useful range where a measure of r_T is a measure of the particle's REL.

B. Information Content of Particle Tracks

The disturbed region along the trajectory of the particle in the dielectric track detector is that particle's signature. It contains information about the particle that produced it. The problem is twofold: to determine what information exists, and to find ways of extracting this information.

To date the only way to delineate a track (other than by means of electron miscroscopy) is by means of the chemical etching technique. In Chapter IV it was shown that the chemical etch development of tracks

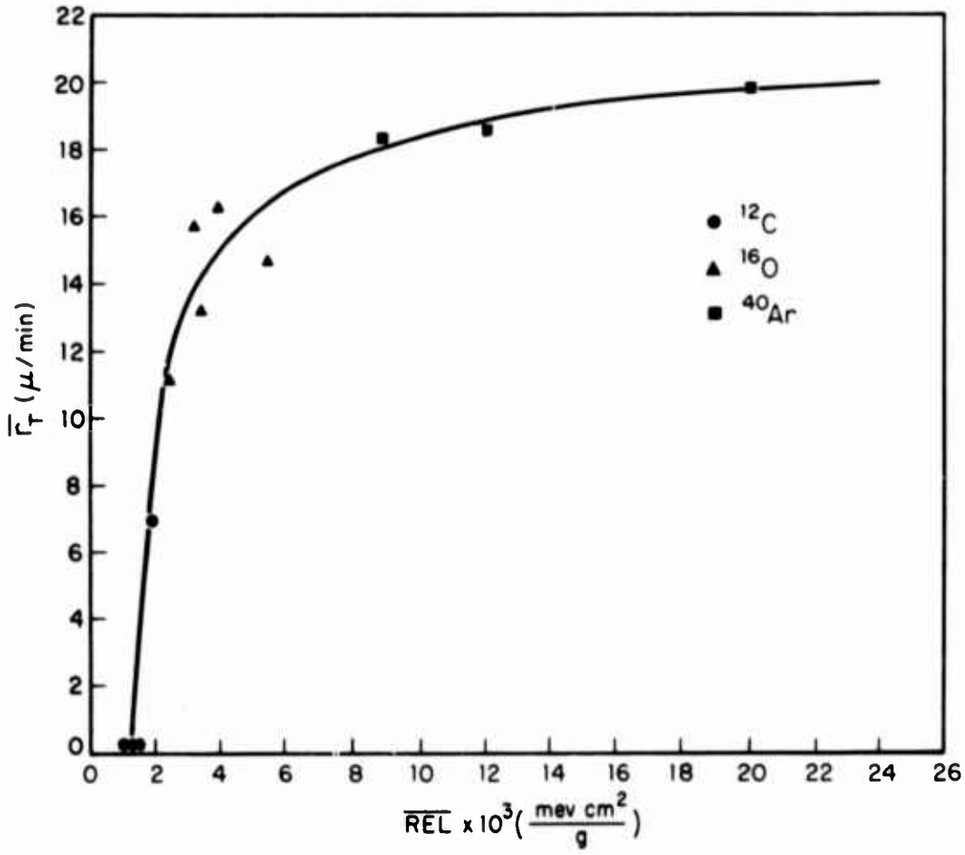

FIGURE VII-2. The average track etch rate, $\bar{r}_T$, as a function of particle average REL rate in NRDL-1 cellulose nitrate plastic.

can be treated as composed of two independent processes, namely, the etching along the particle's trajectory, r_T, and the etching of the bulk material, r_B. Here it is assumed that the entire information content of a track is contained in r_T and its variation over the length of the particle's trajectory in the solid.

In Table VII-1 the particle information content of tracks is summarized. The following relationships are observed:

a. The residual range, R, of the stopping particle in the detector is a function of the particle's kinetic energy, charge, and mass.

b. The track etch rate, r_T, is a measure of the particle's REL.

c. The rate of change of θ or L with range is a measure of the rate of change of REL with range, $d(REL)/dR$.

d. The registration range (the region where $r_T > r_B$) of the stopping particle in the detector is a function of the particle's charge, z, and mass, M.

TABLE VII-1 Particle Information Content of Etched Tracks

Measurable Track Parameter	Detector Variable	Particle Parameters
Residual range, R	I_{adj}, A/Z	E, z, M
θ	r_B/r_T	REL (z,β)
L	F_T	REL (z,β)
$\frac{d\theta}{dR}$	$\frac{dr_T}{d(REL)}$	$\frac{d(REL)}{dR}$
$\frac{dL}{dR}$	$\frac{dr_T}{d(REL)}$	$\frac{d(REL)}{dR}$
R_{reg}	REL_{crit}, I_{adj}, A/Z	z,M

We now seek how best to determine r_T from the measurable features of the track. Previously it was shown that there are two track parameters that are measures of r_T, namely the cone angle,

$$\theta = \sin^{-1} (r_B/r_T) \tag{7.1}$$

and the track length

$$L = \int_o^t r_T \, dt'. \tag{7.2}$$

Assuming ideal etching conditions, the cone angle is a measure of r_T at every point along the trajectory. On the other hand, the measurement of the track length yields an average value of r_T for that segment of the trajectory. Here,

$$\bar{r}_T = L/t, \tag{7.3}$$

where L is the true track length and includes the portion removed with the bulk etch of the surface. Knowledge of either θ or L is sufficient to determine r_T; however, there are some important practical considerations. It is observed that there is a sine relationship between θ and r_T. For many tracks, $r_T \gtrsim 10\ r_B$, and the corresponding $\theta \lesssim 6^\circ$. Here, the determination of r_T through θ involves the measurement of small cone angles, and measurement errors may become significant. In these situations L is probably a better measure of r_T. At the other extreme, for tracks where $r_T \simeq 2\ r_B$, the cone angles are large, $\theta \simeq 30^\circ$. The track lengths are correspondingly small and require large bulk etch corrections. Here less accuracy in the absolute value of θ is required. Also, the observation of a track segment with a large cone angle is an immediate visual indication that the REL of the particle is approaching the REL_{crit} of the material. However, the

observation of a short track may only mean that the range of the particle is small. The decision on whether θ, or L, or both should be measured must be made individually for every measuring situation encountered.

C. Particle Identification Techniques

The residual range, R, of a charged particle with a charge z, and a mass M is given by

$$R = \int_{E}^{o} \frac{dE'}{\left(\frac{dE'}{dx}\right)} \tag{7.4}$$

where E is the kinetic energy at that point corresponding to a velocity $v = \beta c$. The rate of energy loss, dE/dx, as well as the restricted rate of energy loss, REL, are functions of the particle charge and velocity. Inversely, the particle's charge may be determined by measuring two quantities such as E and dE/dx (or REL); the variation in dE/dx (or REL) over an interval of range may also be used. If the particle's velocity is known, z may be determined by a single measurement of dE/dx.

Here we are concerned with two categories of particles:

(a) Those that stop in the dielectric track detector stack (see Figure VII-3), where the range and REL can be used to determine z.

(b) Those that show appreciable slowing down, but do not stop in the stack. Here REL and its variation over the available portion of the trajectory can be used. Very fast particles whose velocity remains essentially constant during traversal of the stack, or particles that undergo nuclear interactions are not considered.

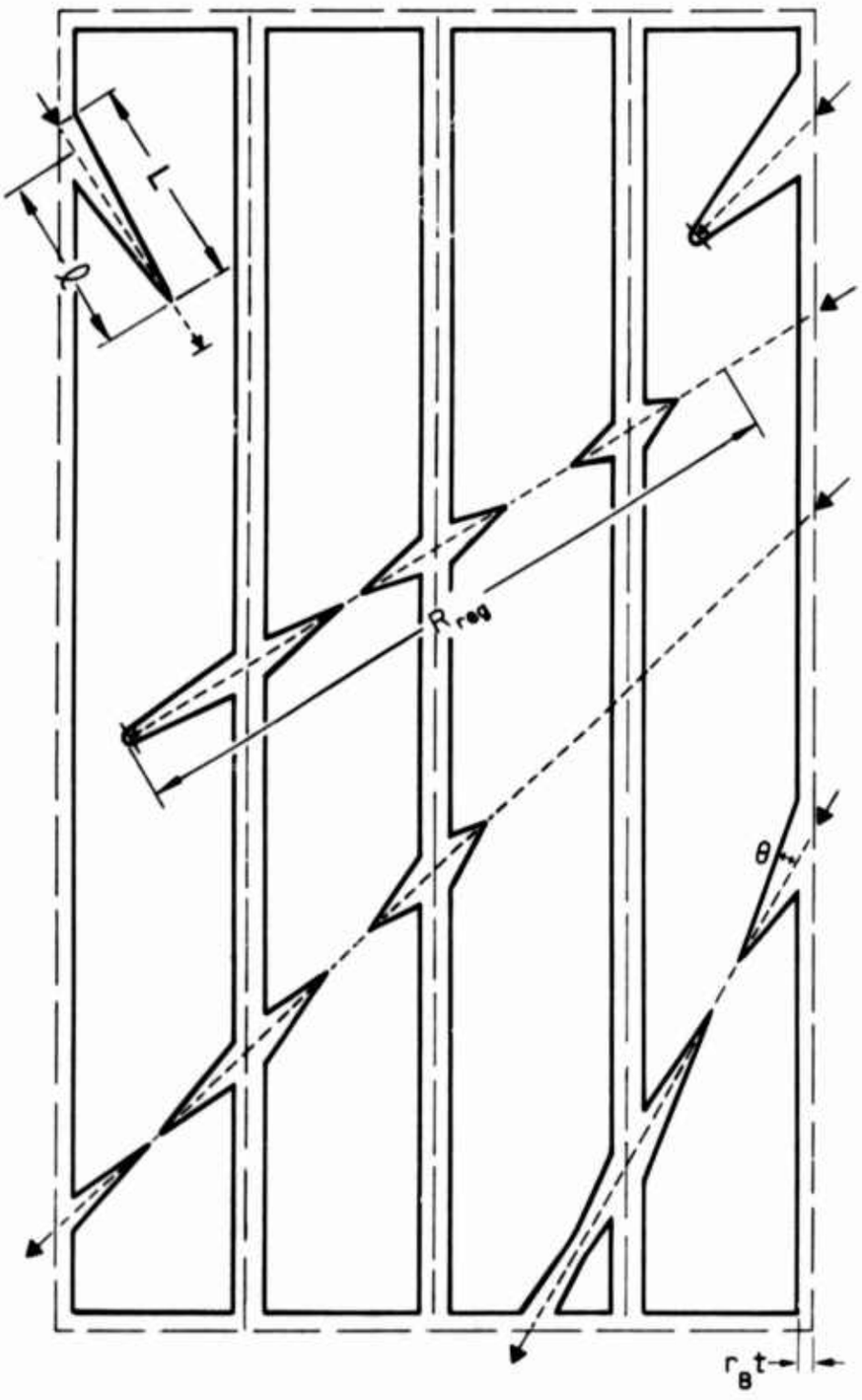

FIGURE VII-3. The various observed categories of etched tracks in a stack of cellulose nitrate plastic layers.

A charged particle penetrating a stack of dielectric track detectors produces a series of collinear, etchable track segments over the part of its range where REL of the particle is above the critical value required by the material. A subsequent partial etch treatment for a time t reveals a series of etched tracks, each of length L and having a cone angle θ (see Figure VII-3). The entire information content of such a track ensemble resides in the following track parameters: the length of each track segment, L, the variation of L as a function of R, the cone angle, θ, of each track segment, and the variation of θ as a function of R. The cone angle is a function of REL of the particle, decreasing with increasing REL, and quickly becoming large when REL approaches the critical value of the material. The track length of an individual segment of the entire track is defined for specific etch conditions. For an etch time, t, L is given by Equation (7.2). The quantity L will approach zero where β is sufficiently high such that REL drops below REL_{crit}.

Each stopping particle of sufficient initial energy traversing a stack of sufficient dimensions will produce etchable tracks at every plastic surface between the point where $REL = REL_{crit}$ and the point where the particle comes to rest. The length of this region of the particle trajectory is R_{reg}, the registration range. In Figure V-4 the predicted R_{reg} is given for NRDL-1 cellulose nitrate as a function of z for the most abundant isotope of each element.

1. Evaluation of z for Particles Whose Entire Registration Range is Contained Within the Stack

From Figure V-4 it is observed that the measurement of the particle's R_{reg} is a measure of its charge. The sensitivity of R_{reg} method is embodied in the fact that R_{reg} varies approximately as Mz^2 for carbon through $Mz^{3.8}$ for iron. Thus the accuracy of the R_{reg} determination need not be great in order to discriminate between the adjacent z's.

The precision of the z determination is governed by the ability to locate both ends of the registration range. In some cases the stopping end of the particle trajectory can be determined only to approximately $\pm$ one-half the distance from the point where the particle last registered to its expected, but undetected, registration point on the next plastic surface. However, if the track in the stopping layer of plastic is etched to the stopping end (indicated by rounding off of the track) this end of the registration range is quite precisely determined. The point where REL equals REL_{crit} can also be determined to within $\pm$ one-half of the distance between surfaces along the trajectory. This has been shown for 500 micron thick layers (see Section D of this Chapter). In stacks composed of much thinner layers, this point may not be as well defined. The uniqueness of the $REL = REL_{crit}$ point is the key to the accurate determination of z by the measurement of the registration range. If this point is unique, the very critical dependence of the registration range on z implies that z can be determined to $\pm$ 1 or possibly with complete confidence.

2. Evaluation of z for Particles Whose Entire Registration Range is Not Contained Within the Stack

If the entire registration range is not contained within the stack, z cannot be determined by the method designated above. However, if a sufficient fraction of the registration range can be observed, z identification can be achieved by determining the change in REL as a function of distance along the particle trajectory.

Assuming that the track etch rate, r_T, is only a function of REL, i.e.,

$$r_T = fn\ (REL)\ . \tag{7.5}$$

Then the rate of change of r_T with respect to the distance along the trajectory, R, is a constant times a function of z determined from the range energy relationship of the ion, i.e.,

$$\left(\frac{dr_T}{dR}\right)_{REL} = \left(\frac{dr_T}{d(REL)}\right)_{REL} \left(\frac{d(REL)}{dR}\right)_{REL}\ . \tag{7.6}$$

If dr_T/dR is measured at a particular value of r_T a specific value of REL is implied and $dr_T/d(REL)$ evaluated at this point is a constant for all of the particles measured. For a given value of REL, $d(REL)/dR$ is only a function of z. In NRDL-1 cellulose nitrate at $REL = 1.5 \times 10^3 \frac{MeV\ cm^2}{g}$, a value not far above the critical value, $d(REL)/dR$ can be represented approximately by,

$$\frac{d(REL)}{dR} = 2.54 \times 10^7\ z^{-3.6} \left(\frac{MeV\ cm^4}{g^2}\right) \qquad \text{for } 5 < z < 40. \tag{7.7}$$

Therefore,

$$\frac{dr_T}{dR} = C\ z^{-3.6} \qquad \text{for } 5 < z < 40, \tag{7.8}$$

where C is a function of the chemistry of the stopping material and of the etching conditions. The $z^{-3.6}$ dependence of d(REL)/dR is found to hold over the entire useful range of the particle's REL (see Figure VII-2), up to about REL = $12 \times 10^3 \frac{\text{MeV cm}^2}{\text{g}}$. From Equation (7.8) it is observed that as in the case of the registration range, R_{reg}, the rate of change of r_T with R is quite a sensitive function of z. Of course, a sufficient length of the particle's trajectory must be contained within the stack for an accurate determination of $\frac{dL}{dR}$ or $\frac{d\theta}{dR}$.

3. Isotopic Mass Separation of Particles

In the previous discussion it was stated that R_{reg} varies approximately as Mz^2 for carbon through or $z^{3.8}$ for iron. Since the quantity R_{reg} is proportional to the particle's mass, the heavy isotopes of a given element will have greater R_{reg} values than the light isotopes. Thus, if R_{reg} can be measured precisely, isotopic mass separation for individual particles may be possible. The measurement of R_{reg} for different mass particles within a given z group would yield discrete values of R_{reg}. The different z groups are well separated in R_{reg} so that overlapping of light isotopes of charge z and heavy isotopes of charge (z+1) is not expected to be a problem. It may also be possible to determine the mass by noting that dr_T/dR is proportional to $\frac{1}{M} z^{-3.6}$.

These measurements would require thin, homogeneous, and uniform plastics. The stack would have to be very carefully prepared. This would be required for an accurate determination of the REL = REL_{crit} points.

During the preparation of this dissertation, Price et al.[65] reported another method of mass separation. This method is in principle similar to the second method described. On a statistical basis, isotopic mass separation of particles differing in mass by 9% was shown to be possible. Using artificially accelerated ions of ^{10}B and ^{11}B they were able to show that for a given etch time the heavier isotope particles gave consistently longer track lengths.

D. Cosmic Ray Measurements

In order to investigate the various possible techniques for charge determination, a stack was assembled and exposed for approximately 11 hours at an altitude of 144,000 ft over Manitoba, Canada. The stack consisted of 12, 1 x 3 inch, 500 micron thick sheets of cellulose nitrate plastic and 18, Ilford K.5, 1 x 3 inch, 600 micron thick emulsion pellicles. Upon recovery, the nuclear emulsions were mounted on glass and processed in a standard manner. The cellulose nitrate sheets were etched together in a 10M NaOH solution for a period of 15 hours at 23°C. The etch time was short enough that for more than one-half of the particles that traverse the entire thickness of a single cellulose nitrate sheet and where etching proceeds from both sides (see Figure VII-3) the tracks did not etch completely through.

For each track the parameters measured in each layer of the stack included the position of the intersection of the trajectory with the surface, the azimuthal and dip angles of the trajectory, and the length and the cone angle of the etched tracks.

Sixty different cosmic ray particles were recorded. Thirty of these produced tracks in more than one plastic layer and were followed to find the locations of the stopping end and the points on the trajectory where REL dropped below REL_{crit}. For the particles registering at the exterior surface of the stack one or both of these points could not be observed. Only two particles produced tracks in all 12 layers of plastic, but 15 particles registered in more than 3 layers.

For 33 of the 60 particles found, both the $REL = REL_{crit}$ point and the stopping point were contained within the stack. For these z was determined according to Figure V-4. For the six layers of emulsion which were located between the layers of plastic, an approximate plastic equivalent thickness of 0.15 g/cm^2 was used.

The z distribution determined by using the R_{reg} criterion is shown as the gray area in Figure VII-4. Since the z determination has not been restricted to integral values, the peaks observed in the figure indicate that charge discrimination is being achieved. The precision in the z determination varied from approximately $\pm$ 0.3 for z = 18 to $\pm$ 3 for some of the particles measured as z = 7. The non-uniformity of the plastic layers and the presence of the nuclear emulsions between some of the layers significantly decreased the accuracy of the R_{reg} measurements, making mass separation impossible.

The evaluation of z for the particles whose entire registration range was not contained within the stack was accomplished by measurements of dL/dR. Of the particles with z's determined by the registration range, 10 had sufficient range to permit a determination of dL/dR, the slope of the plot of track length, L, vs. distance along the

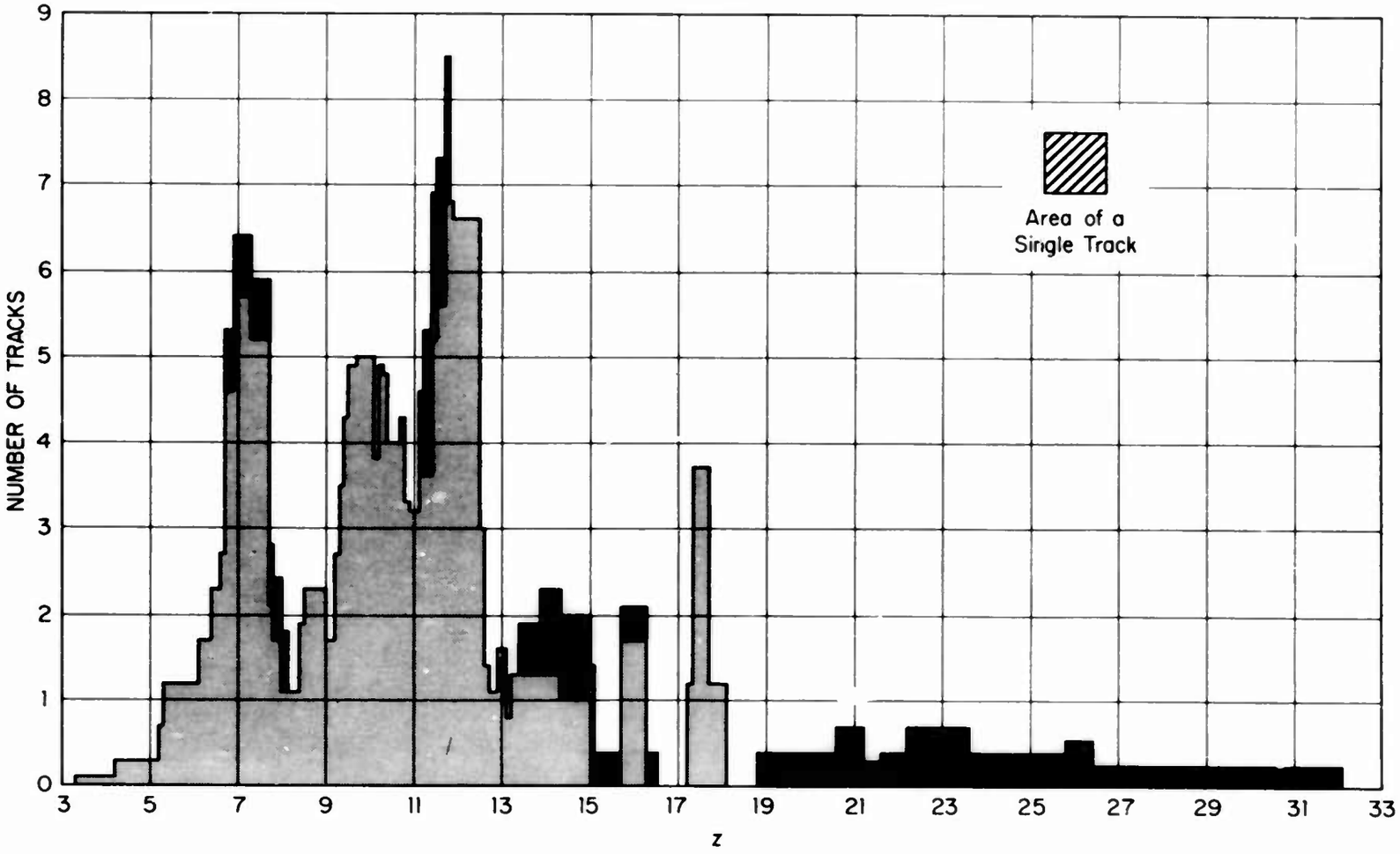

FIGURE VII-4. The measured charge distribution; gray area represents tracks measured by R_{reg} method; black area shows tracks measured by dL/dR method.

trajectory, R. The 10 values of dL/dR are plotted in Figure VII-5. The solid line is given by

$$\frac{dL}{dR} = (643 \pm 65)\, z^{-3.63} \qquad \text{for } 5 < z < 40, \tag{7.9}$$

or

$$z = 5.92 \pm 16 \left(\frac{dL}{dR}\right)^{-0.276}, \tag{7.10}$$

showing that the data are well represented by the $z^{-3.63}$ dependence as given by Equation (7.8).

It is found that the plot of L vs. R can, in most cases, be represented by a straight line, indicating that the quantity $(dL/dR)_{REL}$ is fairly insensitive to the value of REL at which it is evaluated. For some tracks, however, there is some curvature in the L vs. R plot. This is the reason for the choice of REL = 1.5×10^3 $\frac{\text{MeV cm}^2}{\text{g}}$, a value not far above the critical value. For this value of REL, the slopes of the L vs. R plots are measured in the region of the shortest track lengths which are usually less than 100 microns.

Nine values of z which could not be determined by using the registration range have been determined by measuring dL/dR. These are included in Figure VII-4 as black areas. For the remaining 18 particles z could not be determined; here the portion of R_{reg} within the stack was simply too short for an accurate determination of dL/dR.

The distribution given in Figure VII-4 is in general agreement with the measurement of cosmic ray abundances by others. In particular, the peaks at Z = 10, 12, 14, 16, and 18 are typical of other measurements.[67,68] The apparent peaks at Z = 21, 23, and 26 are not statistically significant. An anomalous feature of Figure VII-4 is the peak at Z = 7. There should be two well-defined peaks at Z = 6

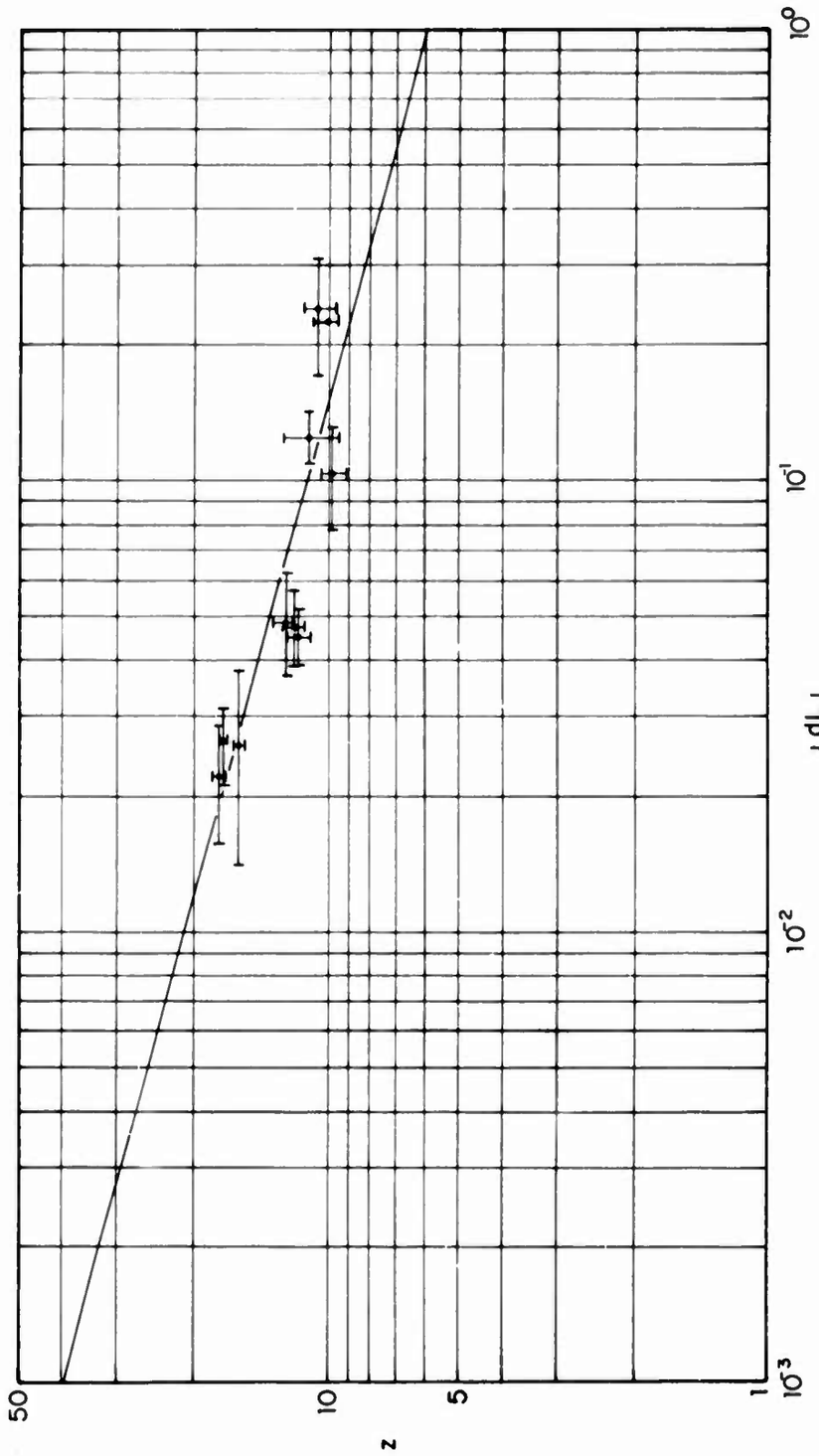

FIGURE VII-5. The rate of change of the etched track length with respect to the particle range vs. z (z determined by R_{reg} method).

and 8; however, these appear to be absent. Here, there is a strong possibility of systematic errors in the measurement of R_{reg} which arises as a result of the relatively thick plastic layers used (500 μ), which tends to combine the Z = 6 and 8 particles into Z = 7 group. This occurs because only about one plastic thickness is traversed by the R_{reg} for each of these particles, a situation which can be avoided by using thinner plastics.

In comparing the flux values of particles recorded here with those measured by others, the bias of the detector as well as that of the stack must be taken into account. The nature of this detector is such that the registration efficiency is much higher for the higher z particles as compared with the lighter ions (as seen from the relative abundances of Z = 7 and Z = 12 in Figure VII-4). Thus while the fluxes of alpha particles in cosmic radiation are fairly high, the number of tracks registered in the stack will be very low. This response can be altered by varying the thickness of individual plastic layers. Charge identification of very heavy particles such as iron was not satisfactorily achieved simply because of the small size of this stack. For charge identification of z = 26 ions using the R_{reg} method, a minimum stack thickness of 10 g/cm^2 is required. Even when using the dL/dR method a larger stack is desirable. It is likely that a sizable fraction of the unidentified 18 particles belongs to the iron group. Having taken the above biases into account (as well as the somewhat uncertain amount of shielding experienced during the balloon flight), the measurements of the differential energy spectrum (particles/m^2 sec (MeV/nuc) sterad.) at the top of the atmosphere compare favorably with

measurements of Anand, et al.[69] However, the small stack volume and the short exposure time result in rather poor statistics which severely limit the usefulness of this comparison.

CHAPTER VIII

SUMMARY AND CONCLUSIONS

In this dissertation several conclusions were made concerning dielectric charged particle track detectors. The significant features are summarized below.

In Chapter IV regarding the chemical etch development of tracks in cellulose nitrate plastics, the main conclusions were the following:

1. In many practical instances, the geometry of etched tracks can be well approximated by that of mathematical cones. This approximation gives the relationships between the various useful track parameters.

2. The track etch rate ratio, r_T/r_B, can be substantially increased through the reduction of the bulk etch rate, r_B.

3. The bulk etch rate, r_B, was found to vary inversely with the degree of polymerization of the nitrocellulose.

4. The inclusion of plasticizers (and to a lesser extent of low concentrations of residual solvents) in the nitrocellulose matrix greatly reduces the bulk etch rate. This probably occurs because of the reduced solubility of OH^- ions in the polymer. A decrease in r_B by a factor of 40 was achieved for the plasticized, 200,000 sec, as compared with 18-25 cps nitrocellulose.

5. A factor of 5 decrease in r_B was observed for the more highly nitrated, 11.8 - 12.2% N_2, as compared with 10.9 - 11.2% N_2, plasticized nitrocellulose.

6. The etch rate ratio, r_T/r_B, can be increased by etching at lower temperatures. Simple theoretical arguments were presented to explain this behavior.

7. When highly nitrated, plasticized nitrocellulose, having a high degree of polymerization was etched in 10M NaOH solution at 23°C, etch rates ratios in excess of 1000 were achieved for 8 MeV/nucleon ^{16}O ions. The resultant tracks, having cone angles of only several minutes, show a high degree of detail (such as recoiling particles) along the particle's trajectory.

8. Latent tracks have good thermal stability. The activation free energy for the annealing process is of the order of 1 eV, thus implying that the process involves atomic motion. Annealing of irradiated samples reduces the track etch rate r_T. For complete track irradication the softening temperature of the plastic must be approached. For the lightly ionizing particles track annealing proceeds at a higher rate than for the heavily ionizing particles.

In Chapter V a new track registration criterion was presented. The more important features follow:

1. The total rate of energy loss of a charged particle cannot be used to predict track registration.

2. The quantity called the restricted energy loss rate, REL, of charged particles was found to correctly predict track registration in

cellulose nitrate and the polycarbonate plastics. In order to produce a latent (etchable) track a charged particle must have REL above a critical value, REL_{crit}, that is characteristic of the recording material.

3. It is possible to assign a sensitivity to each of the polymer detectors. In order to produce latent tracks in NRDL-1 cellulose nitrate and Lexan polycarbonate plastics, REL of 1.1×10^3 and 3.3×10^3 MeV cm^2/g, respectively, is required.

In Chapter VI a general method for the calculation of range-energy and energy loss relations of multicharged particles in matter was described. The conclusions are listed below:

1. The method may be used to generate range-energy and energy loss relations for a wide variety of heavy charged particles and a broad energy spectrum in stopping materials of known composition.

2. The range calculations agree to better than 4% with experimental measurements using lithium drifted silicon detectors for 2 - 10 MeV/nucleon ^{12}C and ^{20}Ne ions.

3. The length of etched tracks, when etched until the tips of the tracks become round, agrees with the calculated range to better than 2%. This is for 1 - 10 MeV/nucleon ^{12}C, ^{16}O and ^{40}Ar ions.

4. Track lengths can be used for accurate determination of particle energy.

The results and conclusions of Chapter VII regarding the identification of charged particles using dielectric track detectors are listed below:

1. Based on the REL registration criterion, a stopping charged particle produces a latent track over the extent of its range where its REL > REL_{crit} for that material. The length of this region, R_{reg}, (the registration range) varies approximately as Mz^2 for carbon through $Mz^{3.8}$ for iron. Charge (and possibly mass) determination can be accomplished through the measurement of a particle's R_{reg}.

2. If the entire registration range is not contained within the boundaries of a stack of dielectric detector layers, charge and mass identification can be achieved through the measurement of the rate of change of the particle's REL with respect to its range. This may be accomplished by measurement of track lengths or, in some cases, the track cone angles.

During the course of these investigations, a number of new applications have become apparent; these are described in Appendix VII. It is clear that the unique properties of the dielectric track detectors make them well suitable for measurements involving heavily ionizing charged particles.

APPENDIX I

ENERGY PER NUCLEON AS A FUNCTION OF THE PARTICLE VELOCITY

In the following table the particle velocity $\beta = v/c$, $(1-\beta)$, β^2, and $(\gamma\beta)^2 = \beta^2/(1-\beta^2)$ are given as a function of the particle kinetic energy in MeV/nucleon.

ENERGY (MeV)/(NUCLEON)	β	$1-\beta$	β^2	$(\gamma\beta)^2$
0.01	0.463451E-02	9.95366E-01	2.14787E-05	2.14791E-05
0.02	0.655413E-02	9.93446E-01	4.29567E-05	4.29585E-05
0.03	0.802708E-02	9.91973E-01	6.44340E-05	6.44381E-05
0.04	0.926879E-02	9.90731E-01	8.59106E-05	8.59179E-05
0.05	0.103627E-01	9.89637E-01	1.07386E-04	1.07398E-04
0.06	0.113517E-01	9.88648E-01	1.28862E-04	1.28878E-04
0.08	0.131076E-01	9.86892E-01	1.71810E-04	1.71840E-04
0.10	0.146545E-01	9.85345E-01	2.14756E-04	2.14802E-04
0.12	0.160530E-01	9.83947E-01	2.57698E-04	2.57765E-04
0.15	0.179474E-01	9.82053E-01	3.22108E-04	3.22211E-04
0.20	0.207230E-01	9.79277E-01	4.29442E-04	4.29627E-04
0.25	0.231681E-01	9.76832E-01	5.36759E-04	5.37048E-04
0.30	0.253783E-01	9.74622E-01	6.44059E-04	6.44475E-04
0.40	0.293020E-01	9.70698E-01	8.58608E-04	8.59365E-04
0.50	0.327580E-01	9.67242E-01	1.07309E-03	1.07424E-03
0.60	0.358817E-01	9.64118E-01	1.28750E-03	1.28916E-03
0.80	0.414260E-01	9.58574E-01	1.71611E-03	1.71906E-03
1.00	0.463082E-01	9.53692E-01	2.14445E-03	2.14906E-03
1.20	0.507199E-01	9.49280E-01	2.57251E-03	2.57914E-03
1.50	0.566929E-01	9.43307E-01	3.21408E-03	3.22445E-03
2.00	0.654370E-01	9.34563E-01	4.28200E-03	4.30042E-03
2.50	0.731314E-01	9.26869E-01	5.34821E-03	5.37696E-03
3.00	0.800793E-01	9.19921E-01	6.41270E-03	6.45409E-03
4.00	0.923935E-01	9.07606E-01	8.53656E-03	8.61006E-03
5.00	0.103216E-00	8.96784E-01	1.06536E-02	1.07683E-02
6.00	0.112977E-00	8.87023E-01	1.27639E-02	1.29289E-02
8.00	0.130267E-00	8.69753E-01	1.69843E-02	1.72570E-02
10.00	0.145389E-00	8.54611E-01	2.11379E-02	2.15944E-02
12.00	0.159013E-00	8.40987E-01	2.52850E-02	2.59409E-02
15.00	0.177360E-00	8.22640E-01	3.14564E-02	3.24780E-02
20.00	0.203992E-00	7.96008E-01	4.16126E-02	4.34194E-02
25.00	0.227178E-00	7.72822E-01	5.16099E-02	5.44184E-02
30.00	0.247894E-00	7.52106E-01	6.14516E-02	6.54751E-02
40.00	0.284044E-00	7.15956E-01	8.06808E-02	8.77615E-02
50.00	0.315159E-00	6.84841E-01	9.93251E-02	1.10279E-01
60.00	0.342648E-00	6.57352E-01	1.17408E-01	1.33026E-01
80.00	0.389843E-00	6.10157E-01	1.51977E-01	1.79214E-01
100.00	0.429598E-00	5.70402E-01	1.84555E-01	2.26324E-01
120.00	0.463994E-00	5.36006E-01	2.15290E-01	2.74357E-01
150.00	0.508168E+00	4.91832E-01	2.58235E-01	3.48136E-01
200.00	0.567770E+00	4.32230E-01	3.22363E-01	4.75715E-01
250.00	0.615239E+00	3.84761E-01	3.78520E-01	6.09061E-01
300.00	0.654198E+00	3.45802E-01	4.27975E-01	7.48174E-01
400.00	0.714627E+00	2.85373E-01	5.10691E-01	1.04370E+00
500.00	0.759396E+00	2.40604E-01	5.76683E-01	1.36229E+00
600.00	0.793833E+00	2.06167E-01	6.30171E-01	1.70396E+00
800.00	0.843023E+00	1.56977E-01	7.10688E-01	2.45648E+00
1000.00	0.876077E+00	1.23923E-01	7.67511E-01	3.30127E+00
1200.00	0.899500E+00	1.00500E-01	8.09100E-01	4.23834E+00
1500.00	0.923746E+00	7.62540E-02	8.53307E-01	5.81694E+00
2000.00	0.948201E+00	5.17993E-02	8.99085E-01	8.90929E+00
2500.00	0.962472E+00	3.75275E-02	9.26353E-01	1.25783E+01
3000.00	0.971543E+00	2.84569E-02	9.43896E-01	1.68240E+01
4000.00	0.982010E+00	1.79900E-02	9.64344E-01	2.70455E+01
5000.00	0.987600E+00	1.24001E-02	9.75354E-01	3.95738E+01
6000.00	0.990935E+00	9.06493E-03	9.81952E-01	5.44088E+01
8000.00	0.994550E+00	5.44969E-03	9.89130E-01	9.09990E+01
10000.00	0.996365E+00	3.63463E-03	9.92744E-01	1.36816E+02

APPENDIX II

THE TIGHT BINDING SHELL CORRECTION, C/Z, FOR CELLULOSE NITRATE

The tight binding shell correction, C/Z, for cellulose nitrate is calculated using the following relation:

$$\langle C/Z \rangle = \langle A/Z \rangle \sum_i \frac{f_i C_i}{A_i} ,$$

where

A_i = atomic weight of the i^{th} material component,

f_i = fraction by weight of the i^{th} component,

$$C_i = \sum_{m=2}^{3} \sum_{n=1}^{3} a_{mn} (\beta\gamma)^{-2n} \left(I_{adj}\right)_i^m$$ (Equation (16) of Reference 60).

CELLULOSE NITRATE A/Z = 1.939

E (MeV/nuc)	Shell Correction*	E (MeV/nuc)	Shell Correction
1.00	-1.313E+02	120.00	2.010E-02
1.20	-7.289E+01	150.00	1.565E-02
1.50	-3.485E+01	200.00	1.131E-02
2.00	-1.285E+01	250.00	8.763E-03
2.50	-5.552E+00	300.00	7.096E-03
3.00	-2.575E+00	350.00	5.922E-03
3.50	-1.192E+00	400.00	5.053E-03
4.00	-4.925E-01	500.00	3.856E-03
5.00	8.991E-02	600.00	3.074E-03
6.00	2.719E-01	700.00	2.527E-03
7.00	3.235E-01	800.00	2.125E-03
8.00	3.280E-01	1000.00	1.579E-03
10.00	2.960E-01	1200.00	1.228E-03
12.00	2.563E-01	1500.00	8.937E-04
15.00	2.069E-01	2000.00	5.828E-04
20.00	1.522E-01	2500.00	4.126E-04
25.00	1.185E-01	3000.00	3.083E-04
30.00	9.636E-02	3500.00	2.396E-04
35.00	8.082E-02	4000.00	1.917E-04
40.00	6.940E-02	5000.00	1.310E-04
50.00	5.384E-02	6000.00	9.527E-05
60.00	4.380E-02	7000.00	7.244E-05
70.00	3.681E-02	8000.00	5.696E-05
80.00	3.168E-02	10000.00	3.788E-05
100.00	2.466E-02	12000.00	2.701E-05
		15000.00	1.776E-05

*The shell correction was calculated according to procedures described in Reference 60. The calculations are not accurate below about 8 MeV/nucleon.

APPENDIX III

THE EFFECTIVE CHARGE, z*, FOR VARIOUS IONS AS A FUNCTION OF THE PARTICLE VELOCITY, β

This is a numerical listing of Equation (5.6),

$$z^* = z\left[1-\exp\left(-125\ \beta/z^{2/3}\right)\right] .$$

Although strictly true <u>only</u> for nuclear emulsions, Equation (5.6) can be used for other solids, except for very heavy ions at low incident velocities.[56,61]

Z^*

β	Z = 1	Z = 2	Z = 3	Z = 4	Z = 5	Z = 6	Z = 7	Z = 8	Z = 9	Z = 10	Z = 11
0.0010	0.117503	0.151449	0.174971	0.193584	0.209243	0.222894	0.235078	0.246134	0.256290	0.265710	0.274514
0.0011	0.128466	0.165948	0.191897	0.212419	0.229679	0.244723	0.258148	0.270327	0.281515	0.291890	0.301586
0.0012	0.139292	0.180334	0.208721	0.231162	0.250028	0.266470	0.281138	0.294445	0.306665	0.317999	0.328589
0.0014	0.160543	0.208767	0.242068	0.268368	0.290467	0.309716	0.326884	0.342454	0.356751	0.370007	0.382392
0.0016	0.181269	0.236756	0.275017	0.305208	0.330561	0.352637	0.372319	0.390164	0.406548	0.421736	0.435923
0.0018	0.201484	0.264308	0.307572	0.341684	0.370314	0.395233	0.417444	0.437578	0.456058	0.473186	0.489184
0.0020	0.221199	0.291429	0.339737	0.377799	0.409729	0.437509	0.462262	0.484695	0.505283	0.524361	0.542177
0.0025	0.268384	0.357393	0.418481	0.466536	0.506803	0.541807	0.572977	0.601209	0.627107	0.651097	0.673494
0.0030	0.312711	0.420810	0.494894	0.553099	0.601825	0.644150	0.681817	0.715917	0.747184	0.776138	0.803161
0.0035	0.354351	0.481779	0.569045	0.637542	0.694837	0.744574	0.788813	0.828846	0.865540	0.899507	0.931200
0.0040	0.393469	0.540393	0.641001	0.719915	0.785882	0.843115	0.893998	0.940025	0.982196	1.021226	1.057631
0.0045	0.430217	0.596745	0.710827	0.800271	0.875002	0.939808	0.997401	1.049479	1.097182	1.141317	1.182475
0.0050	0.464739	0.650921	0.778587	0.878658	0.962237	1.034688	1.099054	1.157237	1.210518	1.259801	1.305751
0.0055	0.497168	0.703006	0.844340	0.955125	1.047627	1.127789	1.198984	1.263324	1.322229	1.376701	1.427480
0.0060	0.527633	0.753080	0.908148	1.029719	1.131211	1.219145	1.297223	1.367767	1.432337	1.492037	1.547679
0.0070	0.583138	0.847502	1.030152	1.173468	1.293114	1.396749	1.488737	1.571819	1.647840	1.718103	1.783570
0.0080	0.632121	0.934774	1.145041	1.310261	1.448242	1.567756	1.673820	1.769594	1.857205	1.938162	2.013573
0.0090	0.675948	1.015438	1.253229	1.440434	1.596878	1.732410	1.852687	1.961283	2.060606	2.152373	2.237837
0.0100	0.713495	1.089993	1.355108	1.564306	1.739293	1.890947	2.025548	2.147075	2.258219	2.360893	2.456504
0.0110	0.747160	1.158903	1.451044	1.682184	1.875749	2.043594	2.192603	2.327150	2.450203	2.563872	2.669714
0.0120	0.776870	1.222595	1.541385	1.794357	2.006494	2.190571	2.354048	2.501686	2.636720	2.761457	2.877603
0.0140	0.826226	1.335874	1.706567	2.002680	2.251800	2.468347	2.660855	2.834812	2.993971	3.141018	3.277947
0.0160	0.864665	1.432647	1.853043	2.191326	2.477003	2.725869	2.947401	3.147755	3.331164	3.500676	3.658558
0.0180	0.894601	1.515319	1.982931	2.362155	2.683752	2.964612	3.215025	3.441737	3.649427	3.841475	4.020409
0.0200	0.917915	1.585944	2.098110	2.516849	2.873558	3.185947	3.464975	3.717909	3.949822	4.164404	4.364426
0.0250	0.956063	1.720703	2.332176	2.842645	3.282786	3.671225	4.020001	4.337332	4.629081	4.899573	5.152099
0.0300	0.976482	1.811603	2.505496	3.096875	3.613260	4.072817	4.487884	4.867155	5.216979	5.542126	5.846273
0.0350	0.987412	1.872919	2.633834	3.295259	3.880134	4.405156	4.882305	5.320336	5.725803	6.103729	6.458044
0.0400	0.993262	1.914279	2.728565	3.450066	4.095649	4.680184	5.214800	5.707962	6.166189	6.584562	6.997196
0.0450	0.996393	1.942178	2.799232	3.570867	4.269689	4.907784	5.495090	6.039516	6.547342	7.023597	7.472347
0.0500	0.998070	1.960997	2.851337	3.665132	4.410236	5.096134	5.731372	6.323109	6.877230	7.398565	7.891096
0.0550	0.998967	1.973691	2.889919	3.738691	4.523734	5.252004	5.930557	6.565679	7.162747	7.726294	8.260138
0.0600	0.999447	1.982253	2.918489	3.796091	4.615390	5.380995	6.098467	6.773160	7.409861	8.012735	8.585372
0.0700	0.999842	1.991925	2.955307	3.875835	4.749180	5.576079	6.359338	7.102425	7.808848	8.481907	9.124603
0.0800	0.999955	1.996326	2.975495	3.924393	4.836430	5.709681	6.544723	7.313320	8.107724	8.840313	9.543414
0.0900	0.999987	1.998328	2.986564	3.953961	4.893329	5.801177	6.676464	7.519563	8.331602	9.114102	9.868697
0.1000	0.999996	1.999239	2.992633	3.971966	4.930436	5.863838	6.770083	7.648505	8.499316	9.323253	10.121336
0.1100	0.999999	1.999654	2.995961	3.982929	4.954634	5.906750	6.836613	7.742840	8.624945	9.483026	10.317559
0.1200	1.000000	1.999843	2.997785	3.989605	4.970415	5.936139	6.883891	7.811858	8.719041	9.605078	10.469961
0.1400	1.000000	1.999967	2.999334	3.996146	4.987418	5.970048	6.941365	7.899295	8.842351	9.769539	10.680263
0.1600	1.000000	1.999993	2.999800	3.998571	4.994649	5.985952	6.970389	7.946096	8.911538	9.865512	10.807123
0.1800	1.000000	1.999999	2.999940	3.999470	4.997724	5.993412	6.985046	7.971148	8.950361	9.921519	10.883650
0.2000	1.000000	2.000000	2.999982	3.999804	4.999032	5.996910	6.992448	7.984556	8.972148	9.954201	10.929814
0.2500	1.000000	2.000000	2.999999	3.999984	4.999886	5.999535	6.998631	7.996763	8.992430	9.988086	10.980163
0.3000	1.000000	2.000000	3.000000	3.999999	4.999987	5.999930	6.999752	7.999321	8.998480	9.998901	10.994394
0.3500	1.000000	2.000000	3.000000	4.000000	4.999998	5.999989	6.999955	7.999858	8.999635	9.999194	10.998415
0.4000	1.000000	2.000000	3.000000	4.000000	5.000000	5.999998	6.999992	7.999970	8.999914	9.999790	10.999552
0.4500	1.000000	2.000000	3.000000	4.000000	5.000000	6.000000	6.999999	7.999994	8.999980	9.999945	10.999873
0.5000	1.000000	2.000000	3.000000	4.000000	5.000000	6.000000	7.000000	7.999999	8.999995	9.999986	10.999964
0.5500	1.000000	2.000000	3.000000	4.000000	5.000000	6.000000	7.000000	8.000000	8.999999	9.999996	10.999990
0.6000	1.000000	2.000000	3.000000	4.000000	5.000000	6.000000	7.000000	8.000000	9.000000	9.999999	10.999997
0.7000	1.000000	2.000000	3.000000	4.000000	5.000000	6.000000	7.000000	8.000000	9.000000	10.000000	11.000000
0.8000	1.000000	2.000000	3.000000	4.000000	5.000000	6.000000	7.000000	8.000000	9.000000	10.000000	11.000000
0.9000	1.000000	2.000000	3.000000	4.000000	5.000000	6.000000	7.000000	8.000000	9.000000	10.000000	11.000000
1.0000	1.000000	2.000000	3.000000	4.000000	5.000000	6.000000	7.000000	8.000000	9.000000	10.000000	11.000000

Z^*

β	Z=12	Z=13	Z=14	Z=15	Z=16	Z=17	Z=18	Z=26	Z=35	Z=36	Z=54
0.0010	0.282793	0.290619	0.298049	0.305130	0.311900	0.318391	0.324630	0.367687	0.406504	0.410384	0.470409
0.0011	0.310703	0.319321	0.327503	0.335300	0.342754	0.349900	0.356769	0.404169	0.446894	0.451164	0.517224
0.0012	0.338547	0.347959	0.356893	0.365407	0.373547	0.381350	0.388849	0.440598	0.487236	0.491897	0.563998
0.0014	0.394035	0.405039	0.415485	0.425437	0.434951	0.444071	0.452836	0.513302	0.567780	0.573224	0.657423
0.0016	0.449260	0.461863	0.473824	0.485221	0.496114	0.506556	0.516590	0.585799	0.648137	0.654365	0.750685
0.0018	0.504222	0.518430	0.531914	0.544759	0.557037	0.568805	0.580113	0.658090	0.728303	0.735320	0.843785
0.0020	0.558922	0.574741	0.589754	0.604054	0.617720	0.630819	0.643405	0.730175	0.808287	0.816089	0.936721
0.0025	0.694536	0.714412	0.733268	0.751227	0.768387	0.784831	0.800629	0.909492	1.007425	1.017205	1.168351
0.0030	0.828543	0.852512	0.875247	0.896896	0.917578	0.937395	0.956430	1.087536	1.205404	1.217170	1.398970
0.0035	0.960962	0.989060	1.015707	1.041076	1.065309	1.088523	1.110820	1.264317	1.402229	1.415993	1.628583
0.0040	1.091811	1.124073	1.154663	1.183782	1.211591	1.238229	1.263811	1.439844	1.597907	1.613679	1.857193
0.0045	1.221109	1.257568	1.292133	1.325029	1.356442	1.386527	1.415416	1.614125	1.792447	1.810235	2.084805
0.0050	1.348874	1.389563	1.428131	1.464831	1.499873	1.533430	1.565648	1.787169	1.985853	2.005667	2.311424
0.0055	1.475125	1.520074	1.562674	1.603205	1.641900	1.678950	1.714518	1.958985	2.178133	2.199983	2.537053
0.0060	1.599880	1.649118	1.695777	1.740164	1.782535	1.823101	1.862041	2.129582	2.369292	2.393188	2.761698
0.0070	1.844970	1.902871	1.957724	2.009896	2.059687	2.107347	2.153089	2.467154	2.748279	2.776290	3.208049
0.0080	2.084284	2.150951	2.214095	2.274141	2.331436	2.386270	2.438887	2.799951	3.122863	3.155026	3.650512
0.0090	2.317959	2.393485	2.465008	2.533011	2.597888	2.659969	2.719532	3.128042	3.493097	3.529444	4.089121
0.0100	2.546127	2.630597	2.710579	2.786614	2.859145	2.928542	2.995115	3.451493	3.859031	3.899593	4.523909
0.0110	2.768918	2.862408	2.950923	3.035059	3.115310	3.192084	3.265728	3.770370	4.220715	4.265523	4.954910
0.0120	2.986458	3.089037	3.186149	3.278450	3.366481	3.450691	3.531460	4.084738	4.578198	4.627283	5.382155
0.0140	3.406280	3.527210	3.641685	3.750480	3.854229	3.953465	4.048634	4.700198	5.280757	5.338476	6.225514
0.0160	3.806548	3.946010	4.078032	4.203501	4.323147	4.437582	4.547321	5.298374	5.967090	6.033547	7.054244
0.0180	4.188173	4.346295	4.495997	4.638279	4.773962	4.903736	5.028183	5.879752	6.637574	6.712861	7.868597
0.0200	4.552024	4.728883	4.896356	5.055548	5.207371	5.352592	5.491856	6.444802	7.292573	7.376775	8.668824
0.0250	5.389222	5.612978	5.825013	6.026678	6.219094	6.403208	6.579820	7.788973	8.864656	8.971461	10.609186
0.0300	6.132315	6.402573	6.658938	6.902971	7.135977	7.359057	7.573152	9.040749	10.347540	10.477302	12.466494
0.0350	6.791879	7.107769	7.407795	7.693690	7.966909	8.228687	8.480084	10.206482	11.746288	11.899247	14.244300
0.0400	7.377304	7.737586	8.080262	8.407191	8.719947	9.019875	9.308131	11.292086	13.065672	13.241973	15.946009
0.0450	7.896924	8.300083	8.684131	9.051015	9.402395	9.739697	10.064153	12.303067	14.310196	14.509890	17.574878
0.0500	8.358135	8.802454	9.226399	9.631966	10.020868	10.394589	10.754416	13.244557	15.484108	15.707168	19.134024
0.0550	8.767503	9.251128	9.713351	10.156183	10.581364	10.990408	11.384640	14.121332	16.591414	16.837743	20.626432
0.0600	9.130856	9.651843	10.150630	10.629208	11.089318	11.532484	11.960047	14.937839	17.635893	17.905330	22.054960
0.0700	9.739623	10.329355	10.895917	11.441189	11.966840	12.474357	12.965067	16.406339	19.550425	19.865381	24.731191
0.0800	10.219223	10.869769	11.496907	12.102325	12.687552	13.253977	13.802856	17.679894	21.253865	21.613116	27.183218
0.0900	10.597064	11.300829	11.981538	12.640638	13.279475	13.899294	14.501241	18.784386	22.769487	23.171533	29.429824
0.1000	10.894735	11.644662	12.372338	13.078947	13.765624	14.433444	15.083418	19.742257	24.117999	24.561139	31.488218
0.1100	11.129247	11.918920	12.687474	13.435829	14.164899	14.875577	15.568723	20.572971	25.317827	25.800220	33.374167
0.1200	11.314001	12.137680	12.941596	13.726412	14.492826	15.241545	15.973276	21.293408	26.385365	26.905081	35.102119
0.1400	11.574225	12.451358	13.311762	14.155658	14.983351	15.795210	16.591636	22.460064	28.180304	28.768724	38.135867
0.1600	11.735736	12.650932	13.552466	14.440232	15.314231	16.174548	17.021332	23.337532	29.601251	30.250488	40.682597
0.1800	11.835981	12.777909	13.708987	14.628894	15.537422	16.434448	17.319927	23.997497	30.726130	31.428623	42.820490
0.2000	11.898199	12.858697	13.810766	14.753970	15.687973	16.612517	17.527419	24.493871	31.616630	32.365346	44.615179
0.2500	11.969105	12.954375	13.935476	14.911954	15.883397	16.849442	17.809771	25.261102	33.113443	33.951183	47.940538
0.3000	11.990624	12.985268	13.977999	14.968491	15.956426	16.941500	17.923427	25.637501	33.948062	34.845102	50.087610
0.3500	11.997154	12.995243	13.992498	14.988724	15.983717	16.977270	17.969177	25.822160	34.413443	35.348996	51.473902
0.4000	11.999136	12.998464	13.997442	14.995965	15.993915	16.991168	17.987593	25.912753	34.672937	35.633036	52.368984
0.4500	11.999738	12.999504	13.999128	14.998556	15.997726	16.996568	17.995006	25.957197	34.817631	35.793146	52.946908
0.5000	11.999920	12.999840	13.999703	14.999483	15.999150	16.998667	17.997990	25.979001	34.893312	35.883399	53.320054
0.5500	11.999976	12.999948	13.999899	14.999815	15.999683	16.999482	17.999191	25.989698	34.943299	35.934273	53.560982
0.6000	11.999993	12.999983	13.999965	14.999934	15.999881	16.999799	17.999674	25.994946	34.968383	35.962950	53.716541
0.7000	11.999999	12.999998	13.999996	14.999992	15.999983	16.999970	17.999947	25.998784	34.990170	35.988227	53.881830
0.8000	12.000000	13.000000	14.000000	14.999999	15.999998	16.999995	17.999991	25.999707	34.996943	35.996259	53.950737
0.9000	12.000000	13.000000	14.000000	15.000000	16.000000	16.999999	17.999999	25.999930	34.999050	35.998811	53.979463
1.0000	12.000000	13.000000	14.000000	15.000000	16.000000	17.000000	18.000000	25.999983	34.999704	35.999622	53.991438

APPENDIX IV

RESTRICTED ENERGY LOSS RATE TABLES

In the following tables the restricted energy loss rate, $\left(\frac{dE}{dx}\right)_{\omega < 10^3 \text{ eV}}$ in MeV cm^2/g is listed for nine representative ions in NRDL-1 cellulose nitrate and polycarbonate resin plastics.

RESTRICTED ENERGY LOSS RATE IN NRDL-1 CELLULOSE NITRATE (MEV CM2/GM)

I = 77.2 A/Z = 1.918 W = 1000.

ENRG./NUC. (MEV/AMU)	1 H	4 HE	12 C	16 O	20 NE	28 SI	40 AR	56 FE	84 KR
3.00	9.800+01	3.906+02	3.196+03	5.287+03	7.664+03	1.296+04	1.869+04	3.867+04	6.584+04
3.50	8.086+01	3.228+02	2.695+03	4.504+03	6.587+03	1.130+04	1.646+04	2.741+04	4.185+04
4.00	6.991+01	2.793+02	2.367+03	3.930+03	5.878+03	1.021+04	1.501+04	2.531+04	3.867+04
4.50	6.215+01	2.484+02	2.129+03	3.614+03	5.358+03	9.402+03	1.393+04	2.377+04	3.667+04
5.00	5.626+01	2.249+02	1.945+03	3.320+03	4.949+03	8.764+03	1.308+04	2.255+04	3.509+04
5.50	5.157+01	2.062+02	1.795+03	3.080+03	4.612+03	8.234+03	1.237+04	2.153+04	3.377+04
6.00	4.772+01	1.908+02	1.670+03	2.878+03	4.327+03	7.780+03	1.176+04	2.064+04	3.261+04
7.00	4.170+01	1.668+02	1.471+03	2.552+03	3.863+03	7.030+03	1.073+04	1.913+04	3.063+04
8.00	3.716+01	1.486+02	1.318+03	2.298+03	3.496+03	6.426+03	9.894+03	1.787+04	2.895+04
9.00	3.359+01	1.343+02	1.196+03	2.092+03	3.198+03	5.925+03	9.189+03	1.679+04	2.748+04
10.00	3.069+01	1.228+02	1.096+03	1.923+03	2.948+03	5.501+03	8.584+03	1.585+04	2.617+04
12.00	2.627+01	1.051+02	9.410+02	1.658+03	2.555+03	4.818+03	7.594+03	1.426+04	2.393+04
14.00	2.303+01	9.211+01	8.265+02	1.460+03	2.258+03	4.291+03	6.817+03	1.298+04	2.207+04
16.00	2.055+01	8.219+01	7.382+02	1.306+03	2.025+03	3.872+03	6.190+03	1.192+04	2.050+04
18.00	1.858+01	7.433+01	6.681+02	1.184+03	1.838+03	3.530+03	5.672+03	1.102+04	1.915+04
20.00	1.698+01	6.794+01	6.109+02	1.083+03	1.685+03	3.247+03	5.238+03	1.026+04	1.797+04
22.00	1.566+01	6.264+01	5.634+02	9.997+02	1.556+03	3.008+03	4.868+03	9.600+03	1.694+04
24.00	1.454+01	5.817+01	5.233+02	9.289+02	1.447+03	2.803+03	4.550+03	9.024+03	1.603+04
26.00	1.359+01	5.434+01	4.889+02	8.682+02	1.353+03	2.626+03	4.272+03	8.517+03	1.522+04
28.00	1.276+01	5.103+01	4.592+02	8.156+02	1.272+03	2.472+03	4.029+03	8.067+03	1.449+04
30.00	1.203+01	4.814+01	4.331+02	7.695+02	1.200+03	2.336+03	3.814+03	7.665+03	1.383+04
35.00	1.057+01	4.226+01	3.803+02	6.759+02	1.055+03	2.058+03	3.370+03	6.826+03	1.244+04
40.00	9.446+00	3.778+01	3.400+02	6.044+02	9.437+02	1.843+03	3.026+03	6.164+03	1.132+04
45.00	8.562+00	3.425+01	3.082+02	5.479+02	8.557+02	1.673+03	2.751+03	5.629+03	1.040+04
50.00	7.846+00	3.138+01	2.824+02	5.021+02	7.843+02	1.534+03	2.526+03	5.185+03	9.627+03
55.00	7.254+00	2.901+01	2.611+02	4.642+02	7.252+02	1.419+03	2.339+03	4.814+03	8.974+03
60.00	6.755+00	2.702+01	2.432+02	4.323+02	6.754+02	1.322+03	2.180+03	4.497+03	8.414+03
70.00	5.962+00	2.385+01	2.146+02	3.816+02	5.962+02	1.166+03	1.927+03	3.988+03	7.500+03
80.00	5.359+00	2.144+01	1.929+02	3.430+02	5.359+02	1.050+03	1.734+03	3.595+03	6.788+03
90.00	4.885+00	1.954+01	1.759+02	3.126+02	4.885+02	9.572+02	1.581+03	3.283+03	6.217+03
100.00	4.501+00	1.801+01	1.621+02	2.881+02	4.501+02	8.821+02	1.457+03	3.030+03	5.750+03
120.00	3.920+00	1.568+01	1.411+02	2.508+02	3.920+02	7.682+02	1.269+03	2.642+03	5.030+03
140.00	3.498+00	1.399+01	1.259+02	2.239+02	3.498+02	6.857+02	1.133+03	2.361+03	4.503+03
160.00	3.180+00	1.272+01	1.145+02	2.035+02	3.180+02	6.232+02	1.030+03	2.147+03	4.100+03
180.00	2.930+00	1.172+01	1.055+02	1.875+02	2.930+02	5.742+02	9.491+02	1.979+03	3.782+03
200.00	2.728+00	1.091+01	9.823+01	1.746+02	2.728+02	5.348+02	8.840+02	1.843+03	3.526+03
220.00	2.563+00	1.025+01	9.228+01	1.640+02	2.563+02	5.024+02	8.305+02	1.732+03	3.314+03
240.00	2.425+00	9.700+00	8.730+01	1.552+02	2.425+02	4.753+02	7.857+02	1.639+03	3.137+03
260.00	2.308+00	9.232+00	8.309+01	1.477+02	2.308+02	4.524+02	7.478+02	1.560+03	2.986+03
280.00	2.208+00	8.830+00	7.947+01	1.413+02	2.208+02	4.327+02	7.152+02	1.492+03	2.857+03
300.00	2.120+00	8.482+00	7.633+01	1.357+02	2.120+02	4.156+02	6.870+02	1.433+03	2.745+03
350.00	1.946+00	7.785+00	7.007+01	1.246+02	1.946+02	3.815+02	6.306+02	1.316+03	2.520+03
400.00	1.816+00	7.265+00	6.539+01	1.162+02	1.816+02	3.560+02	5.885+02	1.229+03	2.353+03
450.00	1.716+00	6.863+00	6.177+01	1.098+02	1.716+02	3.363+02	5.559+02	1.160+03	2.223+03
500.00	1.636+00	6.545+00	5.891+01	1.047+02	1.636+02	3.207+02	5.302+02	1.106+03	2.120+03
550.00	1.572+00	6.288+00	5.659+01	1.006+02	1.572+02	3.081+02	5.093+02	1.063+03	2.037+03
600.00	1.519+00	6.076+00	5.469+01	9.722+01	1.519+02	2.977+02	4.922+02	1.027+03	1.968+03
700.00	1.438+00	5.752+00	5.176+01	9.202+01	1.438+02	2.818+02	4.659+02	9.720+02	1.863+03
800.00	1.379+00	5.517+00	4.965+01	8.827+01	1.379+02	2.703+02	4.469+02	9.323+02	1.787+03
900.00	1.335+00	5.342+00	4.807+01	8.547+01	1.335+02	2.617+02	4.327+02	9.027+02	1.730+03
1000.00	1.302+00	5.208+00	4.687+01	8.333+01	1.302+02	2.552+02	4.218+02	8.801+02	1.687+03

RESTRICTED ENERGY LOSS RATE IN LEXAN (MEV CM2/GM)

I = 69.5 A/Z = 1.896 W = 1000.

ENRG./NUC. (MEV/AMU)	1 H	4 HE	12 C	16 O	20 NE	28 SI	40 AR	56 FE	84 KR
3.00	1.016+02	4.048+02	3.312+03	5.480+03	7.943+03	1.344+04	1.937+04	3.179+04	4.751+04
3.50	8.401+01	3.353+02	2.800+03	4.680+03	6.844+03	1.174+04	1.710+04	2.803+04	4.306+04
4.00	7.271+01	2.904+02	2.462+03	4.149+03	6.113+03	1.062+04	1.561+04	2.632+04	4.022+04
4.50	6.466+01	2.584+02	2.215+03	3.760+03	5.575+03	9.782+03	1.450+04	2.473+04	3.815+04
5.00	5.854+01	2.340+02	2.023+03	3.455+03	5.150+03	9.119+03	1.361+04	2.347+04	3.651+04
5.50	5.365+01	2.145+02	1.868+03	3.204+03	4.799+03	8.567+03	1.287+04	2.240+04	3.513+04
6.00	4.964+01	1.985+02	1.738+03	2.993+03	4.501+03	8.093+03	1.223+04	2.147+04	3.392+04
7.00	4.336+01	1.734+02	1.530+03	2.653+03	4.017+03	7.310+03	1.116+04	1.989+04	3.185+04
8.00	3.862+01	1.545+02	1.370+03	2.388+03	3.634+03	6.679+03	1.028+04	1.858+04	3.009+04
9.00	3.489+01	1.396+02	1.243+03	2.174+03	3.322+03	6.156+03	9.586+03	1.765+04	2.855+04
10.00	3.187+01	1.275+02	1.138+03	1.997+03	3.062+03	5.712+03	8.914+03	1.686+04	2.718+04
12.00	2.726+01	1.090+02	9.766+02	1.720+03	2.651+03	5.000+03	7.881+03	1.560+04	2.498+04
14.00	2.388+01	9.554+01	8.572+02	1.514+03	2.342+03	4.450+03	7.071+03	1.396+04	2.289+04
16.00	2.130+01	8.520+01	7.653+02	1.354+03	2.099+03	4.014+03	6.417+03	1.235+04	2.125+04
18.00	1.926+01	7.703+01	6.923+02	1.227+03	1.905+03	3.659+03	5.878+03	1.142+04	1.984+04
20.00	1.760+01	7.038+01	6.329+02	1.122+03	1.745+03	3.364+03	5.426+03	1.063+04	1.862+04
22.00	1.622+01	6.487+01	5.835+02	1.035+03	1.612+03	3.115+03	5.042+03	9.942+03	1.755+04
24.00	1.506+01	6.023+01	5.418+02	9.618+02	1.498+03	2.903+03	4.711+03	9.344+03	1.660+04
26.00	1.406+01	5.626+01	5.061+02	8.988+02	1.401+03	2.719+03	4.423+03	8.817+03	1.575+04
28.00	1.320+01	5.282+01	4.752+02	8.441+02	1.316+03	2.558+03	4.170+03	8.349+03	1.499+04
30.00	1.245+01	4.981+01	4.482+02	7.963+02	1.242+03	2.417+03	3.946+03	7.932+03	1.431+04
35.00	1.093+01	4.372+01	3.934+02	6.991+02	1.091+03	2.128+03	3.486+03	7.061+03	1.286+04
40.00	9.767+00	3.907+01	3.516+02	6.249+02	9.758+02	1.906+03	3.129+03	6.374+03	1.170+04
45.00	8.851+00	3.540+01	3.186+02	5.664+02	8.845+02	1.729+03	2.843+03	5.819+03	1.075+04
50.00	8.109+00	3.243+01	2.919+02	5.189+02	8.105+02	1.586+03	2.610+03	5.356+03	9.950+03
55.00	7.495+00	2.998+01	2.698+02	4.796+02	7.493+02	1.467+03	2.416+03	4.974+03	9.273+03
60.00	6.979+00	2.791+01	2.512+02	4.466+02	6.977+02	1.366+03	2.252+03	4.646+03	8.692+03
70.00	6.158+00	2.463+01	2.217+02	3.941+02	6.157+02	1.206+03	1.990+03	4.118+03	7.746+03
80.00	5.534+00	2.213+01	1.992+02	3.541+02	5.533+02	1.084+03	1.790+03	3.712+03	7.008+03
90.00	5.042+00	2.017+01	1.815+02	3.227+02	5.042+02	9.880+02	1.632+03	3.389+03	6.417+03
100.00	4.646+00	1.858+01	1.672+02	2.973+02	4.646+02	9.104+02	1.504+03	3.127+03	5.934+03
120.00	4.044+00	1.618+01	1.456+02	2.588+02	4.044+02	7.925+02	1.310+03	2.726+03	5.190+03
140.00	3.608+00	1.443+01	1.299+02	2.309+02	3.608+02	7.072+02	1.169+03	2.435+03	4.644+03
160.00	3.279+00	1.312+01	1.180+02	2.098+02	3.279+02	6.426+02	1.062+03	2.214+03	4.228+03
180.00	3.021+00	1.208+01	1.087+02	1.933+02	3.021+02	5.920+02	9.786+02	2.040+03	3.900+03
200.00	2.813+00	1.125+01	1.013+02	1.800+02	2.813+02	5.513+02	9.113+02	1.900+03	3.634+03
220.00	2.642+00	1.057+01	9.511+01	1.691+02	2.642+02	5.178+02	8.560+02	1.785+03	3.416+03
240.00	2.499+00	9.997+00	8.998+01	1.600+02	2.499+02	4.899+02	8.098+02	1.689+03	3.233+03
260.00	2.378+00	9.513+00	8.562+01	1.522+02	2.378+02	4.662+02	7.706+02	1.607+03	3.078+03
280.00	2.275+00	9.098+00	8.188+01	1.456+02	2.275+02	4.458+02	7.369+02	1.537+03	2.944+03
300.00	2.185+00	8.738+00	7.864+01	1.398+02	2.185+02	4.282+02	7.078+02	1.476+03	2.828+03
350.00	2.005+00	8.019+00	7.217+01	1.283+02	2.005+02	3.929+02	6.495+02	1.355+03	2.596+03
400.00	1.870+00	7.482+00	6.734+01	1.197+02	1.870+02	3.666+02	6.060+02	1.264+03	2.423+03
450.00	1.767+00	7.067+00	6.360+01	1.131+02	1.767+02	3.463+02	5.724+02	1.194+03	2.289+03
500.00	1.685+00	6.739+00	6.065+01	1.078+02	1.685+02	3.302+02	5.458+02	1.139+03	2.183+03
550.00	1.618+00	6.473+00	5.825+01	1.036+02	1.618+02	3.172+02	5.243+02	1.094+03	2.097+03
600.00	1.564+00	6.254+00	5.629+01	1.001+02	1.564+02	3.065+02	5.066+02	1.057+03	2.026+03
700.00	1.480+00	5.919+00	5.327+01	9.470+01	1.480+02	2.900+02	4.794+02	1.000+03	1.917+03
800.00	1.419+00	5.676+00	5.108+01	9.081+01	1.419+02	2.781+02	4.597+02	9.592+02	1.839+03
900.00	1.374+00	5.495+00	4.945+01	8.792+01	1.374+02	2.692+02	4.451+02	9.286+02	1.780+03
1000.00	1.339+00	5.356+00	4.821+01	8.570+01	1.339+02	2.625+02	4.339+02	9.052+02	1.735+03

APPENDIX V

RANGE-ENERGY AND ENERGY LOSS RATE TABLES

In the following tables the ranges in g/cm^2 and the (dE/dx) values in MeV cm^2/g are listed for nine representative ions in each stopping material. The materials are arranged in the order of increasing I_{adj}. The intervals between the forty-eight energy points have been chosen such that a linear interpolation contributes less than 1% error. The values of I_{adj} are labeled by a non-subscripted I for typographical reasons. More places of precision are given than are significant to eliminate rounding errors and for the sake of differential measurements.

RANGE IN LEXAN (GM/CM2) I = 69.5 A/Z = 1.896

ENRG./NUC. (MEV/AMU)	1 H	4 HE	12 C	16 O	20 NE	28 SI	40 AR	56 FE	84 KR
0.10	1.263E-04	2.120E-04	2.227E-04	2.382E-04	2.536E-04	2.807E-04	3.419E-04	3.883E-04	4.930E-04
0.12	1.503E-04	2.487E-04	2.536E-04	2.704E-04	2.872E-04	3.170E-04	3.840E-04	4.334E-04	5.480E-04
0.15	1.890E-04	3.045E-04	2.989E-04	3.166E-04	3.351E-04	3.692E-04	4.440E-04	4.969E-04	6.248E-04
0.20	2.610E-04	4.000E-04	3.723E-04	3.901E-04	4.102E-04	4.497E-04	5.382E-04	5.949E-04	7.418E-04
0.25	3.429E-04	4.994E-04	4.444E-04	4.609E-04	4.818E-04	5.250E-04	6.276E-04	6.863E-04	8.496E-04
0.30	4.328E-04	6.032E-04	5.161E-04	5.304E-04	5.511E-04	5.968E-04	7.139E-04	7.733E-04	9.510E-04
0.40	6.388E-04	8.243E-04	6.605E-04	6.678E-04	6.863E-04	7.340E-04	8.704E-04	9.383E-04	1.141E-03
0.50	8.770E-04	1.066E-03	8.081E-04	8.054E-04	8.196E-04	8.660E-04	1.021E-03	1.096E-03	1.318E-03
0.60	1.148E-03	1.336E-03	9.601E-04	9.448E-04	9.527E-04	9.954E-04	1.166E-03	1.248E-03	1.498E-03
0.70	1.444E-03	1.635E-03	1.117E-03	1.087E-03	1.087E-03	1.124E-03	1.308E-03	1.396E-03	1.653E-03
0.80	1.771E-03	1.962E-03	1.280E-03	1.232E-03	1.223E-03	1.251E-03	1.448E-03	1.529E-03	1.813E-03
1.00	2.508E-03	2.699E-03	1.623E-03	1.534E-03	1.502E-03	1.508E-03	1.726E-03	1.801E-03	2.125E-03
1.20	3.352E-03	3.543E-03	1.990E-03	1.852E-03	1.792E-03	1.770E-03	2.003E-03	2.066E-03	2.429E-03
1.50	4.810E-03	5.002E-03	2.587E-03	2.362E-03	2.250E-03	2.173E-03	2.424E-03	2.457E-03	2.853E-03
2.00	7.738E-03	7.929E-03	3.710E-03	3.303E-03	3.082E-03	2.886E-03	3.149E-03	3.109E-03	3.551E-03
2.50	1.118E-02	1.137E-02	4.967E-03	4.341E-03	3.988E-03	3.644E-03	3.906E-03	3.768E-03	4.235E-03
3.00	1.519E-02	1.538E-02	6.378E-03	5.492E-03	4.981E-03	4.459E-03	4.706E-03	4.445E-03	4.922E-03
3.50	1.974E-02	1.993E-02	7.944E-03	6.758E-03	6.065E-03	5.334E-03	5.554E-03	5.147E-03	5.618E-03
4.00	2.484E-02	2.503E-02	9.662E-03	8.140E-03	7.240E-03	6.273E-03	6.453E-03	5.877E-03	6.328E-03
5.00	3.667E-02	3.686E-02	1.362E-02	1.126E-02	9.871E-03	8.342E-03	8.409E-03	7.430E-03	7.804E-03
6.00	5.064E-02	5.084E-02	1.828E-02	1.486E-02	1.288E-02	1.068E-02	1.059E-02	9.117E-03	9.367E-03
7.00	6.677E-02	6.696E-02	2.366E-02	1.893E-02	1.628E-02	1.328E-02	1.299E-02	1.095E-02	1.103E-02
8.00	8.505E-02	8.524E-02	2.976E-02	2.352E-02	2.007E-02	1.617E-02	1.563E-02	1.293E-02	1.280E-02
10.00	1.277E-01	1.279E-01	4.397E-02	3.419E-02	2.876E-02	2.272E-02	2.159E-02	1.732E-02	1.654E-02
12.00	1.766E-01	1.768E-01	6.029E-02	4.643E-02	3.860E-02	3.009E-02	2.823E-02	2.215E-02	2.091E-02
15.00	2.636E-01	2.638E-01	8.926E-02	6.817E-02	5.601E-02	4.292E-02	3.974E-02	3.041E-02	2.732E-02
20.00	4.432E-01	4.433E-01	1.491E-01	1.131E-01	9.194E-02	6.897E-02	6.290E-02	4.680E-02	4.149E-02
25.00	6.644E-01	6.645E-01	2.229E-01	1.684E-01	1.362E-01	1.007E-01	9.090E-02	6.642E-02	5.782E-02
30.00	9.254E-01	9.256E-01	3.099E-01	2.336E-01	1.884E-01	1.380E-01	1.236E-01	8.912E-02	7.614E-02
35.00	1.225E+00	1.225E+00	4.097E-01	3.085E-01	2.483E-01	1.808E-01	1.608E-01	1.149E-01	9.700E-02
40.00	1.561E+00	1.562E+00	5.219E-01	3.926E-01	3.156E-01	2.289E-01	2.025E-01	1.435E-01	1.201E-01
50.00	2.341E+00	2.341E+00	7.817E-01	5.875E-01	4.715E-01	3.402E-01	2.988E-01	2.094E-01	1.729E-01
60.00	3.255E+00	3.255E+00	1.086E+00	8.160E-01	6.543E-01	4.708E-01	4.116E-01	2.860E-01	2.341E-01
70.00	4.297E+00	4.297E+00	1.434E+00	1.076E+00	8.626E-01	6.196E-01	5.403E-01	3.729E-01	3.033E-01
80.00	5.459E+00	5.460E+00	1.821E+00	1.367E+00	1.095E+00	7.857E-01	6.838E-01	4.695E-01	3.801E-01
100.00	8.125E+00	8.125E+00	2.710E+00	2.034E+00	1.628E+00	1.167E+00	1.013E+00	6.905E-01	5.551E-01
120.00	1.121E+01	1.121E+01	3.739E+00	2.805E+00	2.246E+00	1.608E+00	1.394E+00	9.463E-01	7.568E-01
150.00	1.656E+01	1.656E+01	5.522E+00	4.142E+00	3.315E+00	2.372E+00	2.054E+00	1.389E+00	1.105E+00
200.00	2.717E+01	2.717E+01	9.057E+00	6.794E+00	5.437E+00	3.887E+00	3.364E+00	2.268E+00	1.793E+00
250.00	3.960E+01	3.960E+01	1.320E+01	9.903E+00	7.924E+00	5.663E+00	4.899E+00	3.298E+00	2.599E+00
300.00	5.361E+01	5.361E+01	1.787E+01	1.340E+01	1.072E+01	7.664E+00	6.628E+00	4.458E+00	3.507E+00
400.00	8.554E+01	8.554E+01	2.851E+01	2.139E+01	1.711E+01	1.223E+01	1.057E+01	7.104E+00	5.577E+00
500.00	1.217E+02	1.217E+02	4.058E+01	3.043E+01	2.435E+01	1.739E+01	1.504E+01	1.010E+01	7.922E+00
600.00	1.613E+02	1.613E+02	5.376E+01	4.032E+01	3.226E+01	2.305E+01	1.992E+01	1.338E+01	1.049E+01
700.00	2.035E+02	2.035E+02	6.785E+01	5.089E+01	4.071E+01	2.908E+01	2.514E+01	1.688E+01	1.322E+01
800.00	2.480E+02	2.480E+02	8.267E+01	6.200E+01	4.960E+01	3.543E+01	3.063E+01	2.056E+01	1.611E+01
1000.00	3.420E+02	3.420E+02	1.140E+02	8.550E+01	6.840E+01	4.886E+01	4.223E+01	2.835E+01	2.220E+01
1200.00	4.409E+02	4.409E+02	1.470E+02	1.102E+02	8.818E+01	6.299E+01	5.444E+01	3.654E+01	2.861E+01

DE/DX IN LEXAN (MEV CM2/GM) I = 69.5 A/Z = 1.896

ENRG./NUC. (MEV/AMU)	1 H	4 HE	12 C	16 O	20 NE	28 SI	40 AR	56 FE	84 KR
0.10	8.582E+02	2.145E+03	7.555E+03	9.721E+03	1.158E+04	1.908E+04	1.850E+04	2.407E+04	2.948E+04
0.12	8.109E+02	2.170E+03	7.799E+03	1.014E+04	1.218E+04	1.571E+04	1.943E+04	2.554E+04	3.152E+04
0.15	7.437E+02	2.133E+03	8.049E+03	1.062E+04	1.288E+04	1.644E+04	2.053E+04	2.736E+04	3.411E+04
0.20	6.506E+02	2.054E+03	8.275E+03	1.113E+04	1.369E+04	1.806E+04	2.188E+04	2.971E+04	3.756E+04
0.25	5.820E+02	1.969E+03	8.360E+03	1.142E+04	1.423E+04	1.909E+04	2.281E+04	3.148E+04	4.028E+04
0.30	5.283E+02	1.887E+03	8.363E+03	1.159E+04	1.458E+04	1.986E+04	2.349E+04	3.286E+04	4.231E+04
0.40	4.496E+02	1.754E+03	8.234E+03	1.167E+04	1.495E+04	2.088E+04	2.601E+04	3.487E+04	4.594E+04
0.50	3.941E+02	1.563E+03	8.018E+03	1.157E+04	1.504E+04	2.147E+04	2.714E+04	3.623E+04	4.846E+04
0.60	3.524E+02	1.407E+03	7.769E+03	1.138E+04	1.497E+04	2.178E+04	2.790E+04	3.715E+04	5.037E+04
0.70	3.197E+02	1.278E+03	7.510E+03	1.114E+04	1.481E+04	2.190E+04	2.839E+04	3.952E+04	5.135E+04
0.80	2.933E+02	1.172E+03	7.253E+03	1.088E+04	1.460E+04	2.190E+04	2.869E+04	4.052E+04	5.301E+04
1.00	2.529E+02	1.011E+03	6.766E+03	1.033E+04	1.408E+04	2.164E+04	2.890E+04	4.188E+04	5.462E+04
1.20	2.249E+02	8.995E+02	6.362E+03	9.846E+03	1.358E+04	2.128E+04	2.885E+04	4.273E+04	5.566E+04
1.50	1.935E+02	7.742E+02	5.821E+03	9.153E+03	1.280E+04	2.055E+04	2.839E+04	4.326E+04	5.953E+04
2.00	1.581E+02	6.323E+02	5.081E+03	8.145E+03	1.159E+04	1.917E+04	2.716E+04	4.300E+04	6.117E+04
2.50	1.342E+02	5.366E+02	4.499E+03	7.312E+03	1.054E+04	1.782E+04	2.573E+04	4.199E+04	6.141E+04
3.00	1.168E+02	4.672E+02	4.032E+03	6.621E+03	9.631E+03	1.657E+04	2.429E+04	4.064E+04	6.094E+04
3.50	1.036E+02	4.142E+02	3.649E+03	6.042E+03	8.855E+03	1.544E+04	2.291E+04	3.914E+04	5.979E+04
4.00	9.308E+01	3.723E+02	3.326E+03	5.551E+03	8.185E+03	1.443E+04	2.163E+04	3.760E+04	5.845E+04
5.00	7.751E+01	3.100E+02	2.785E+03	4.767E+03	7.093E+03	1.272E+04	1.936E+04	3.461E+04	5.537E+04
6.00	6.664E+01	2.666E+02	2.398E+03	4.181E+03	6.263E+03	1.137E+04	1.750E+04	3.194E+04	5.226E+04
7.00	5.895E+01	2.358E+02	2.122E+03	3.750E+03	5.643E+03	1.033E+04	1.604E+04	2.972E+04	4.948E+04
8.00	5.295E+01	2.118E+02	1.905E+03	3.378E+03	5.138E+03	9.474E+03	1.480E+04	2.777E+04	4.688E+04
10.00	4.416E+01	1.766E+02	1.590E+03	2.825E+03	4.366E+03	8.133E+03	1.283E+04	2.452E+04	4.229E+04
12.00	3.802E+01	1.521E+02	1.369E+03	2.433E+03	3.790E+03	7.136E+03	1.134E+04	2.194E+04	3.844E+04
15.00	3.162E+01	1.265E+02	1.138E+03	2.024E+03	3.160E+03	6.045E+03	9.670E+03	1.898E+04	3.330E+04
20.00	2.491E+01	9.965E+01	8.969E+02	1.594E+03	2.491E+03	4.846E+03	7.809E+03	1.554E+04	2.817E+04
25.00	2.071E+01	8.285E+01	7.456E+02	1.326E+03	2.071E+03	4.053E+03	6.584E+03	1.322E+04	2.423E+04
30.00	1.793E+01	7.130E+01	6.417E+02	1.141E+03	1.783E+03	3.492E+03	5.716E+03	1.155E+04	2.132E+04
35.00	1.571E+01	6.286E+01	5.657E+02	1.006E+03	1.571E+03	3.080E+03	5.075E+03	1.029E+04	1.909E+04
40.00	1.410E+01	5.640E+01	5.076E+02	9.024E+02	1.410E+03	2.763E+03	4.561E+03	9.298E+03	1.733E+04
50.00	1.179E+01	4.716E+01	4.245E+02	7.546E+02	1.179E+03	2.311E+03	3.819E+03	7.852E+03	1.472E+04
60.00	1.021E+01	4.085E+01	3.677E+02	6.537E+02	1.021E+03	2.002E+03	3.309E+03	6.843E+03	1.287E+04
70.00	9.064E+00	3.626E+01	3.263E+02	5.801E+02	9.064E+02	1.777E+03	2.937E+03	6.096E+03	1.150E+04
80.00	8.189E+00	3.275E+01	2.948E+02	5.241E+02	8.189E+02	1.605E+03	2.653E+03	5.526E+03	1.044E+04
100.00	6.938E+00	2.775E+01	2.498E+02	4.441E+02	6.938E+02	1.360E+03	2.248E+03	4.688E+03	8.903E+03
120.00	6.086E+00	2.435E+01	2.191E+02	3.895E+02	6.086E+02	1.193E+03	1.972E+03	4.114E+03	7.839E+03
150.00	5.216E+00	2.086E+01	1.878E+02	3.338E+02	5.216E+02	1.022E+03	1.690E+03	3.526E+03	6.741E+03
200.00	4.322E+00	1.729E+01	1.556E+02	2.766E+02	4.322E+02	8.471E+02	1.400E+03	2.921E+03	5.598E+03
250.00	3.771E+00	1.509E+01	1.358E+02	2.414E+02	3.771E+02	7.392E+02	1.222E+03	2.549E+03	4.887E+03
300.00	3.397E+00	1.359E+01	1.223E+02	2.174E+02	3.397E+02	6.659E+02	1.101E+03	2.297E+03	4.403E+03
400.00	2.921E+00	1.169E+01	1.052E+02	1.870E+02	2.921E+02	5.726E+02	9.466E+02	1.975E+03	3.786E+03
500.00	2.632E+00	1.053E+01	9.476E+01	1.685E+02	2.632E+02	5.159E+02	8.528E+02	1.779E+03	3.411E+03
600.00	2.439E+00	9.756E+00	8.780E+01	1.561E+02	2.439E+02	4.780E+02	7.902E+02	1.649E+03	3.161E+03
700.00	2.302E+00	9.209E+00	8.288E+01	1.473E+02	2.302E+02	4.512E+02	7.459E+02	1.556E+03	2.984E+03
800.00	2.202E+00	8.806E+00	7.926E+01	1.409E+02	2.202E+02	4.315E+02	7.133E+02	1.488E+03	2.853E+03
1000.00	2.067E+00	8.267E+00	7.441E+01	1.323E+02	2.067E+02	4.051E+02	6.696E+02	1.397E+03	2.679E+03
1200.00	1.985E+00	7.941E+00	7.147E+01	1.271E+02	1.985E+02	3.891E+02	6.432E+02	1.342E+03	2.573E+03

RANGE IN MYLAR (GM/CM2) I = 73.2 A/Z = 1.915

ENRG./NUC. (MEV/AMU)	1 H	4 HE	12 C	16 O	20 NE	28 SI	40 AR	56 FE	84 KR
0.10	1.310E-04	2.193E-04	2.295E-04	2.458E-04	2.616E-04	2.895E-04	3.525E-04	4.004E-04	5.083E-04
0.12	1.560E-04	2.575E-04	2.618E-04	2.791E-04	2.963E-04	3.270E-04	3.960E-04	4.469E-04	5.651E-04
0.15	1.964E-04	3.155E-04	3.087E-04	3.268E-04	3.452E-04	3.809E-04	4.580E-04	5.124E-04	6.442E-04
0.20	2.714E-04	4.147E-04	3.846E-04	4.027E-04	4.234E-04	4.640E-04	5.551E-04	6.135E-04	7.650E-04
0.25	3.560E-04	5.178E-04	4.591E-04	4.760E-04	4.973E-04	5.417E-04	6.474E-04	7.078E-04	8.762E-04
0.30	4.496E-04	6.253E-04	5.332E-04	5.477E-04	5.689E-04	6.158E-04	7.365E-04	7.975E-04	9.808E-04
0.40	6.626E-04	8.538E-04	6.823E-04	6.895E-04	7.084E-04	7.573E-04	8.979E-04	9.678E-04	1.176E-03
0.50	9.082E-04	1.103E-03	8.345E-04	8.314E-04	8.458E-04	8.935E-04	1.053E-03	1.130E-03	1.360E-03
0.60	1.185E-03	1.381E-03	9.911E-04	9.750E-04	9.830E-04	1.027E-03	1.203E-03	1.287E-03	1.535E-03
0.70	1.492E-03	1.688E-03	1.153E-03	1.121E-03	1.121E-03	1.159E-03	1.349E-03	1.433E-03	1.704E-03
0.80	1.827E-03	2.024E-03	1.320E-03	1.271E-03	1.261E-03	1.290E-03	1.493E-03	1.577E-03	1.869E-03
1.00	2.583E-03	2.780E-03	1.672E-03	1.581E-03	1.548E-03	1.555E-03	1.779E-03	1.856E-03	2.190E-03
1.20	3.447E-03	3.645E-03	2.048E-03	1.907E-03	1.846E-03	1.823E-03	2.064E-03	2.129E-03	2.504E-03
1.50	4.941E-03	5.138E-03	2.661E-03	2.430E-03	2.316E-03	2.238E-03	2.496E-03	2.532E-03	2.941E-03
2.00	7.948E-03	8.146E-03	3.815E-03	3.398E-03	3.172E-03	2.971E-03	3.244E-03	3.203E-03	3.659E-03
2.50	1.147E-02	1.167E-02	5.103E-03	4.461E-03	4.100E-03	3.749E-03	4.020E-03	3.880E-03	4.363E-03
3.00	1.557E-02	1.577E-02	6.546E-03	5.640E-03	5.118E-03	4.584E-03	4.841E-03	4.575E-03	5.069E-03
3.50	2.023E-02	2.042E-02	8.147E-03	6.935E-03	6.227E-03	5.481E-03	5.710E-03	5.296E-03	5.784E-03
4.00	2.544E-02	2.563E-02	9.903E-03	8.348E-03	7.430E-03	6.442E-03	6.631E-03	6.044E-03	6.513E-03
5.00	3.752E-02	3.771E-02	1.395E-02	1.154E-02	1.012E-02	8.560E-03	8.635E-03	7.636E-03	8.027E-03
6.00	5.179E-02	5.199E-02	1.871E-02	1.521E-02	1.320E-02	1.095E-02	1.086E-02	9.365E-03	9.630E-03
7.00	6.826E-02	6.846E-02	2.420E-02	1.937E-02	1.667E-02	1.361E-02	1.333E-02	1.124E-02	1.133E-02
8.00	8.694E-02	8.713E-02	3.043E-02	2.406E-02	2.054E-02	1.656E-02	1.603E-02	1.326E-02	1.314E-02
10.00	1.304E-01	1.305E-01	4.490E-02	3.493E-02	2.939E-02	2.324E-02	2.210E-02	1.775E-02	1.707E-02
12.00	1.802E-01	1.804E-01	6.153E-02	4.741E-02	3.942E-02	3.075E-02	2.888E-02	2.268E-02	2.134E-02
15.00	2.698E-01	2.690E-01	9.104E-02	6.955E-02	5.716E-02	4.383E-02	4.060E-02	3.111E-02	2.849E-02
20.00	4.516E-01	4.518E-01	1.520E-01	1.153E-01	9.373E-02	7.035E-02	6.419E-02	4.781E-02	4.243E-02
25.00	6.767E-01	6.769E-01	2.270E-01	1.715E-01	1.388E-01	1.026E-01	9.271E-02	6.778E-02	5.887E-02
30.00	9.423E-01	9.425E-01	3.156E-01	2.379E-01	1.919E-01	1.406E-01	1.260E-01	9.091E-02	7.774E-02
35.00	1.247E+00	1.247E+00	4.171E-01	3.141E-01	2.528E-01	1.841E-01	1.638E-01	1.171E-01	9.897E-02
40.00	1.589E+00	1.589E+00	5.312E-01	3.996E-01	3.212E-01	2.330E-01	2.062E-01	1.463E-01	1.225E-01
50.00	2.382E+00	2.382E+00	7.953E-01	5.978E-01	4.797E-01	3.462E-01	3.041E-01	2.132E-01	1.763E-01
60.00	3.311E+00	3.311E+00	1.105E+00	8.301E-01	6.656E-01	4.790E-01	4.189E-01	2.911E-01	2.385E-01
70.00	4.370E+00	4.370E+00	1.458E+00	1.095E+00	8.774E-01	6.303E-01	5.496E-01	3.795E-01	3.088E-01
80.00	5.552E+00	5.552E+00	1.852E+00	1.390E+00	1.114E+00	7.991E-01	6.955E-01	4.776E-01	3.869E-01
100.00	8.261E+00	8.261E+00	2.755E+00	2.068E+00	1.656E+00	1.186E+00	1.030E+00	7.023E-01	5.648E-01
120.00	1.140E+01	1.140E+01	3.801E+00	2.852E+00	2.283E+00	1.634E+00	1.417E+00	9.623E-01	7.697E-01
150.00	1.683E+01	1.683E+01	5.612E+00	4.210E+00	3.370E+00	2.411E+00	2.088E+00	1.412E+00	1.123E+00
200.00	2.761E+01	2.761E+01	9.204E+00	6.904E+00	5.525E+00	3.950E+00	3.419E+00	2.305E+00	1.823E+00
250.00	4.024E+01	4.024E+01	1.341E+01	1.006E+01	8.052E+00	5.755E+00	4.978E+00	3.352E+00	2.642E+00
300.00	5.447E+01	5.447E+01	1.813E+01	1.362E+01	1.090E+01	7.787E+00	6.734E+00	4.530E+00	3.564E+00
400.00	8.690E+01	8.690E+01	2.897E+01	2.173E+01	1.738E+01	1.242E+01	1.074E+01	7.217E+00	5.666E+00
500.00	1.236E+02	1.236E+02	4.122E+01	3.091E+01	2.473E+01	1.767E+01	1.527E+01	1.026E+01	8.048E+00
600.00	1.638E+02	1.638E+02	5.440E+01	4.095E+01	3.276E+01	2.341E+01	2.023E+01	1.359E+01	1.065E+01
700.00	2.067E+02	2.067E+02	6.891E+01	5.168E+01	4.135E+01	2.954E+01	2.553E+01	1.714E+01	1.343E+01
800.00	2.518E+02	2.518E+02	8.395E+01	6.296E+01	5.037E+01	3.598E+01	3.110E+01	2.088E+01	1.636E+01
1000.00	3.473E+02	3.473E+02	1.158E+02	8.682E+01	6.946E+01	4.961E+01	4.288E+01	2.879E+01	2.254E+01
1200.00	4.476E+02	4.476E+02	1.492E+02	1.119E+02	8.953E+01	6.395E+01	5.527E+01	3.710E+01	2.905E+01

DE/DX IN MYLAR (MEV CM2/GM) I = 73.2 A/Z = 1.915

ENRG./NUC. (MEV/AMU)	1 H	4 HE	12 C	16 O	20 NE	28 SI	40 AR	56 FE	84 KR
0.10	8.209E+02	2.100E+03	7.302E+03	9.409E+03	1.121E+04	1.461E+04	1.793E+04	2.333E+04	2.858E+04
0.12	7.758E+02	2.086E+03	7.237E+03	9.812E+03	1.179E+04	1.522E+04	1.882E+04	2.476E+04	3.056E+04
0.15	7.131E+02	2.052E+03	7.780E+03	1.027E+04	1.246E+04	1.592E+04	1.990E+04	2.652E+04	3.307E+04
0.20	6.256E+02	1.978E+03	8.002E+03	1.077E+04	1.326E+04	1.750E+04	2.129E+04	2.880E+04	3.642E+04
0.25	5.609E+02	1.900E+03	8.088E+03	1.106E+04	1.378E+04	1.849E+04	2.211E+04	3.051E+04	3.906E+04
0.30	5.101E+02	1.823E+03	8.095E+03	1.122E+04	1.413E+04	1.924E+04	2.277E+04	3.186E+04	4.122E+04
0.40	4.355E+02	1.699E+03	7.980E+03	1.131E+04	1.449E+04	2.025E+04	2.522E+04	3.382E+04	4.455E+04
0.50	3.826E+02	1.517E+03	7.780E+03	1.123E+04	1.459E+04	2.083E+04	2.633E+04	3.514E+04	4.701E+04
0.60	3.427E+02	1.368E+03	7.546E+03	1.105E+04	1.454E+04	2.114E+04	2.708E+04	3.605E+04	4.887E+04
0.70	3.113E+02	1.245E+03	7.301E+03	1.083E+04	1.439E+04	2.127E+04	2.757E+04	3.835E+04	5.032E+04
0.80	2.858E+02	1.142E+03	7.057E+03	1.058E+04	1.419E+04	2.127E+04	2.787E+04	3.933E+04	5.145E+04
1.00	2.467E+02	9.869E+02	6.591E+03	1.006E+04	1.370E+04	2.105E+04	2.809E+04	4.068E+04	5.303E+04
1.20	2.192E+02	8.768E+02	6.195E+03	9.593E+03	1.321E+04	2.069E+04	2.804E+04	4.150E+04	5.403E+04
1.50	1.889E+02	7.554E+02	5.674E+03	8.917E+03	1.247E+04	1.999E+04	2.762E+04	4.205E+04	5.783E+04
2.00	1.544E+02	6.177E+02	4.960E+03	7.946E+03	1.130E+04	1.868E+04	2.644E+04	4.183E+04	5.946E+04
2.50	1.312E+02	5.246E+02	4.396E+03	7.140E+03	1.028E+04	1.737E+04	2.507E+04	4.088E+04	5.973E+04
3.00	1.142E+02	4.570E+02	3.942E+03	6.470E+03	9.406E+03	1.617E+04	2.368E+04	3.959E+04	5.921E+04
3.50	1.013E+02	4.053E+02	3.570E+03	5.907E+03	8.653E+03	1.508E+04	2.235E+04	3.815E+04	5.821E+04
4.00	9.110E+01	3.644E+02	3.255E+03	5.430E+03	8.002E+03	1.410E+04	2.111E+04	3.666E+04	5.694E+04
5.00	7.588E+01	3.035E+02	2.726E+03	4.665E+03	6.938E+03	1.243E+04	1.892E+04	3.377E+04	5.398E+04
6.00	6.531E+01	2.612E+02	2.350E+03	4.097E+03	6.133E+03	1.113E+04	1.712E+04	3.120E+04	5.100E+04
7.00	5.779E+01	2.312E+02	2.080E+03	3.676E+03	5.529E+03	1.012E+04	1.570E+04	2.906E+04	4.833E+04
8.00	5.193E+01	2.077E+02	1.868E+03	3.313E+03	5.037E+03	9.283E+03	1.450E+04	2.717E+04	4.582E+04
10.00	4.333E+01	1.733E+02	1.560E+03	2.772E+03	4.283E+03	7.975E+03	1.258E+04	2.401E+04	4.137E+04
12.00	3.732E+01	1.493E+02	1.344E+03	2.388E+03	3.720E+03	7.001E+03	1.112E+04	2.150E+04	3.763E+04
15.00	3.105E+01	1.242E+02	1.118E+03	1.987E+03	3.103E+03	5.934E+03	9.489E+03	1.851E+04	3.312E+04
20.00	2.448E+01	9.790E+01	8.811E+02	1.566E+03	2.447E+03	4.760E+03	7.669E+03	1.526E+04	2.763E+04
25.00	2.036E+01	8.142E+01	7.329E+02	1.303E+03	2.036E+03	3.983E+03	6.469E+03	1.299E+04	2.378E+04
30.00	1.752E+01	7.009E+01	6.308E+02	1.121E+03	1.752E+03	3.433E+03	5.619E+03	1.135E+04	2.094E+04
35.00	1.545E+01	6.180E+01	5.562E+02	9.888E+02	1.545E+03	3.028E+03	4.990E+03	1.011E+04	1.875E+04
40.00	1.387E+01	5.546E+01	4.992E+02	8.874E+02	1.387E+03	2.717E+03	4.485E+03	9.140E+03	1.703E+04
50.00	1.160E+01	4.639E+01	4.175E+02	7.422E+02	1.160E+03	2.273E+03	3.756E+03	7.721E+03	1.447E+04
60.00	1.005E+01	4.019E+01	3.617E+02	6.430E+02	1.005E+03	1.969E+03	3.255E+03	6.731E+03	1.266E+04
70.00	8.917E+00	3.567E+01	3.210E+02	5.707E+02	8.917E+02	1.748E+03	2.889E+03	5.998E+03	1.131E+04
80.00	8.057E+00	3.223E+01	2.900E+02	5.156E+02	8.057E+02	1.579E+03	2.610E+03	5.437E+03	1.027E+04
100.00	6.827E+00	2.731E+01	2.458E+02	4.370E+02	6.827E+02	1.338E+03	2.212E+03	4.613E+03	8.759E+03
120.00	5.990E+00	2.396E+01	2.156E+02	3.833E+02	5.990E+02	1.174E+03	1.941E+03	4.048E+03	7.714E+03
150.00	5.133E+00	2.053E+01	1.848E+02	3.285E+02	5.133E+02	1.006E+03	1.663E+03	3.470E+03	6.634E+03
200.00	4.254E+00	1.702E+01	1.531E+02	2.723E+02	4.254E+02	8.338E+02	1.378E+03	2.875E+03	5.510E+03
250.00	3.713E+00	1.485E+01	1.337E+02	2.376E+02	3.713E+02	7.277E+02	1.203E+03	2.510E+03	4.811E+03
300.00	3.345E+00	1.338E+01	1.204E+02	2.141E+02	3.345E+02	6.556E+02	1.084E+03	2.261E+03	4.335E+03
400.00	2.877E+00	1.151E+01	1.036E+02	1.841E+02	2.877E+02	5.638E+02	9.320E+02	1.945E+03	3.728E+03
500.00	2.592E+00	1.037E+01	9.331E+01	1.659E+02	2.592E+02	5.080E+02	8.398E+02	1.752E+03	3.359E+03
600.00	2.402E+00	9.608E+00	8.648E+01	1.537E+02	2.402E+02	4.708E+02	7.783E+02	1.624E+03	3.113E+03
700.00	2.268E+00	9.071E+00	8.164E+01	1.451E+02	2.268E+02	4.445E+02	7.347E+02	1.533E+03	2.939E+03
800.00	2.169E+00	8.675E+00	7.808E+01	1.388E+02	2.169E+02	4.251E+02	7.027E+02	1.466E+03	2.811E+03
1000.00	2.036E+00	8.146E+00	7.331E+01	1.303E+02	2.036E+02	3.991E+02	6.598E+02	1.377E+03	2.639E+03
1200.00	1.956E+00	7.826E+00	7.043E+01	1.252E+02	1.956E+02	3.835E+02	6.339E+02	1.323E+03	2.536E+03

RANGE IN NROL-1 CELLULOSE NITRATE (GM/CM2) I = 77.2 A/Z = 1.918

ENRG./NUC. (MEV/AMU)	1 H	4 HE	12 C	16 O	20 NE	28 SI	40 AR	56 FE	84 KR
0.01	1.995E-05	3.883E-05	4.998E-05	5.612E-05	6.210E-05	7.339E-05	9.310E-05	1.103E-04	1.430E-04
0.02	3.366E-05	6.312E-05	7.797E-05	8.589E-05	9.390E-05	1.094E-04	1.378E-04	1.622E-04	2.102E-04
0.03	4.658E-05	8.509E-05	1.025E-04	1.114E-04	1.207E-04	1.391E-04	1.741E-04	2.038E-04	2.633E-04
0.04	5.921E-05	1.060E-04	1.244E-04	1.348E-04	1.449E-04	1.655E-04	2.061E-04	2.399E-04	3.091E-04
0.06	8.421E-05	1.463E-04	1.641E-04	1.780E-04	1.892E-04	2.130E-04	2.629E-04	3.031E-04	3.884E-04
0.08	1.093E-04	1.858E-04	2.006E-04	2.159E-04	2.302E-04	2.560E-04	3.137E-04	3.588E-04	4.575E-04
0.10	1.347E-04	2.251E-04	2.351E-04	2.517E-04	2.678E-04	2.963E-04	3.609E-04	4.098E-04	5.202E-04
0.12	1.607E-04	2.646E-04	2.682E-04	2.859E-04	3.035E-04	3.348E-04	4.054E-04	4.575E-04	5.784E-04
0.15	2.025E-04	3.244E-04	3.165E-04	3.349E-04	3.542E-04	3.900E-04	4.689E-04	5.245E-04	6.594E-04
0.20	2.801E-04	4.267E-04	3.944E-04	4.127E-04	4.338E-04	4.752E-04	5.684E-04	6.280E-04	7.830E-04
0.25	3.673E-04	5.329E-04	4.709E-04	4.878E-04	5.095E-04	5.548E-04	6.629E-04	7.246E-04	8.969E-04
0.30	4.636E-04	6.435E-04	5.469E-04	5.614E-04	5.829E-04	6.307E-04	7.541E-04	8.165E-04	1.004E-03
0.35	5.687E-04	7.585E-04	6.230E-04	6.342E-04	6.548E-04	7.041E-04	8.371E-04	9.049E-04	1.106E-03
0.40	6.822E-04	8.779E-04	6.997E-04	7.067E-04	7.258E-04	7.756E-04	9.194E-04	9.907E-04	1.204E-03
0.50	9.336E-04	1.133E-03	8.554E-04	8.519E-04	8.664E-04	9.150E-04	1.078E-03	1.157E-03	1.392E-03
0.60	1.216E-03	1.417E-03	1.015E-03	9.987E-04	1.007E-03	1.051E-03	1.231E-03	1.318E-03	1.571E-03
0.70	1.529E-03	1.730E-03	1.181E-03	1.148E-03	1.148E-03	1.186E-03	1.381E-03	1.467E-03	1.744E-03
0.80	1.871E-03	2.072E-03	1.351E-03	1.301E-03	1.291E-03	1.321E-03	1.528E-03	1.614E-03	1.913E-03
1.00	2.640E-03	2.842E-03	1.710E-03	1.617E-03	1.583E-03	1.591E-03	1.820E-03	1.900E-03	2.241E-03
1.20	3.519E-03	3.721E-03	2.093E-03	1.950E-03	1.887E-03	1.865E-03	2.111E-03	2.178E-03	2.562E-03
1.50	5.037E-03	5.239E-03	2.717E-03	2.482E-03	2.366E-03	2.288E-03	2.552E-03	2.589E-03	3.008E-03
2.00	8.082E-03	8.284E-03	3.887E-03	3.464E-03	3.235E-03	3.033E-03	3.313E-03	3.274E-03	3.741E-03
2.50	1.169E-02	1.189E-02	5.203E-03	4.551E-03	4.185E-03	3.828E-03	4.107E-03	3.966E-03	4.461E-03
3.00	1.584E-02	1.604E-02	6.669E-03	5.748E-03	5.219E-03	4.678E-03	4.943E-03	4.675E-03	5.181E-03
3.50	2.056E-02	2.077E-02	8.293E-03	7.064E-03	6.346E-03	5.590E-03	5.827E-03	5.409E-03	5.910E-03
4.00	2.585E-02	2.605E-02	1.007E-02	8.498E-03	7.567E-03	6.567E-03	6.764E-03	6.171E-03	6.654E-03
5.00	3.810E-02	3.830E-02	1.417E-02	1.173E-02	1.030E-02	8.719E-03	8.800E-03	7.790E-03	8.196E-03
6.00	5.257E-02	5.277E-02	1.900E-02	1.546E-02	1.342E-02	1.114E-02	1.106E-02	9.548E-03	9.827E-03
7.00	6.927E-02	6.947E-02	2.457E-02	1.968E-02	1.694E-02	1.385E-02	1.356E-02	1.145E-02	1.156E-02
8.00	8.819E-02	8.839E-02	3.088E-02	2.443E-02	2.086E-02	1.684E-02	1.631E-02	1.351E-02	1.340E-02
10.00	1.321E-01	1.323E-01	4.550E-02	3.541E-02	2.981E-02	2.359E-02	2.245E-02	1.805E-02	1.739E-02
12.00	1.825E-01	1.827E-01	6.232E-02	4.803E-02	3.995E-02	3.119E-02	2.931E-02	2.305E-02	2.171E-02
15.00	2.720E-01	2.722E-01	9.215E-02	7.040E-02	5.788E-02	4.442E-02	4.117E-02	3.158E-02	2.896E-02
20.00	4.567E-01	4.569E-01	1.537E-01	1.166E-01	9.482E-02	7.121E-02	6.502E-02	4.848E-02	4.307E-02
25.00	6.840E-01	6.842E-01	2.295E-01	1.734E-01	1.403E-01	1.038E-01	9.382E-02	6.866E-02	5.969E-02
30.00	9.521E-01	9.523E-01	3.189E-01	2.404E-01	1.939E-01	1.421E-01	1.274E-01	9.202E-02	7.876E-02
35.00	1.260E+00	1.260E+00	4.213E-01	3.173E-01	2.554E-01	1.861E-01	1.656E-01	1.185E-01	1.002E-01
40.00	1.605E+00	1.605E+00	5.364E-01	4.036E-01	3.249E-01	2.354E-01	2.084E-01	1.479E-01	1.240E-01
50.00	2.404E+00	2.405E+00	8.030E-01	6.035E-01	4.844E-01	3.496E-01	3.072E-01	2.155E-01	1.782E-01
60.00	3.342E+00	3.342E+00	1.115E+00	8.379E-01	6.719E-01	4.836E-01	4.229E-01	2.941E-01	2.411E-01
70.00	4.410E+00	4.410E+00	1.471E+00	1.105E+00	8.855E-01	6.361E-01	5.548E-01	3.832E-01	3.120E-01
80.00	5.602E+00	5.602E+00	1.869E+00	1.403E+00	1.124E+00	8.064E-01	7.020E-01	4.822E-01	3.908E-01
100.00	8.334E+00	8.334E+00	2.779E+00	2.086E+00	1.670E+00	1.197E+00	1.039E+00	7.088E-01	5.702E-01
120.00	1.150E+01	1.150E+01	3.834E+00	2.877E+00	2.303E+00	1.649E+00	1.430E+00	9.709E-01	7.769E-01
150.00	1.698E+01	1.698E+01	5.660E+00	4.246E+00	3.399E+00	2.431E+00	2.106E+00	1.425E+00	1.134E+00
200.00	2.784E+01	2.784E+01	9.281E+00	6.962E+00	5.571E+00	3.983E+00	3.447E+00	2.325E+00	1.838E+00
250.00	4.057E+01	4.057E+01	1.352E+01	1.014E+01	8.118E+00	5.802E+00	5.019E+00	3.379E+00	2.664E+00
300.00	5.491E+01	5.491E+01	1.830E+01	1.373E+01	1.098E+01	7.850E+00	6.789E+00	4.567E+00	3.593E+00
350.00	7.064E+01	7.064E+01	2.355E+01	1.766E+01	1.413E+01	1.010E+01	8.731E+00	5.870E+00	4.613E+00
400.00	8.759E+01	8.759E+01	2.920E+01	2.190E+01	1.752E+01	1.252E+01	1.082E+01	7.275E+00	5.712E+00
500.00	1.246E+02	1.246E+02	4.154E+01	3.116E+01	2.493E+01	1.781E+01	1.539E+01	1.034E+01	8.111E+00
600.00	1.651E+02	1.651E+02	5.503E+01	4.127E+01	3.302E+01	2.359E+01	2.039E+01	1.369E+01	1.073E+01
700.00	2.083E+02	2.083E+02	6.943E+01	5.208E+01	4.166E+01	2.976E+01	2.573E+01	1.727E+01	1.354E+01
800.00	2.538E+02	2.538E+02	8.459E+01	6.344E+01	5.076E+01	3.628E+01	3.134E+01	2.104E+01	1.648E+01
1000.00	3.499E+02	3.499E+02	1.166E+02	8.747E+01	6.997E+01	4.998E+01	4.320E+01	2.900E+01	2.271E+01
1200.00	4.509E+02	4.509E+02	1.503E+02	1.127E+02	9.018E+01	6.442E+01	5.568E+01	3.737E+01	2.926E+01

DE/DX IN NRDL-1 CELLULOSE NITRATE (MEV CM2/GM) I = 77.2 A/I = 1.918

ENRG./NUC. (MEV/AMU)	1 H	4 HE	12 C	16 O	20 NE	28 SI	40 AR	56 FE	84 KR
0.01	6.908E+02	1.511E+03	3.856E+03	4.760E+03	5.511E+03	6.718E+03	7.672E+03	9.159E+03	1.059E+04
0.02	7.585E+02	1.756E+03	4.653E+03	5.913E+03	6.988E+03	8.765E+03	1.015E+04	1.234E+04	1.441E+04
0.03	7.854E+02	1.876E+03	5.096E+03	6.599E+03	7.905E+03	1.007E+04	1.183E+04	1.458E+04	1.719E+04
0.04	7.969E+02	1.945E+03	5.690E+03	7.071E+03	8.559E+03	1.106E+04	1.311E+04	1.634E+04	1.941E+04
0.06	8.003E+02	2.013E+03	6.354E+03	7.691E+03	9.455E+03	1.249E+04	1.502E+04	1.905E+04	2.291E+04
0.08	7.922E+02	2.034E+03	6.796E+03	8.654E+03	1.005E+04	1.350E+04	1.641E+04	2.112E+04	2.565E+04
0.10	7.903E+02	2.033E+03	7.110E+03	9.166E+03	1.093E+04	1.426E+04	1.750E+04	2.278E+04	2.792E+04
0.12	7.481E+02	2.020E+03	7.338E+03	9.563E+03	1.149E+04	1.485E+04	1.838E+04	2.418E+04	2.985E+04
0.15	6.388E+02	1.988E+03	7.576E+03	1.001E+04	1.215E+04	1.554E+04	1.942E+04	2.590E+04	3.230E+04
0.20	6.060E+02	1.920E+03	7.794E+03	1.050E+04	1.293E+04	1.707E+04	2.069E+04	2.812E+04	3.557E+04
0.25	5.446E+02	1.847E+03	7.883E+03	1.078E+04	1.344E+04	1.805E+04	2.159E+04	2.980E+04	3.815E+04
0.30	4.963E+02	1.774E+03	7.895E+03	1.095E+04	1.379E+04	1.879E+04	2.224E+04	3.112E+04	4.026E+04
0.35	4.573E+02	1.704E+03	7.859E+03	1.103E+04	1.401E+04	1.935E+04	2.391E+04	3.218E+04	4.203E+04
0.40	4.250E+02	1.658E+03	7.793E+03	1.105E+04	1.415E+04	1.978E+04	2.464E+04	3.304E+04	4.353E+04
0.50	3.742E+02	1.484E+03	7.607E+03	1.097E+04	1.426E+04	2.036E+04	2.574E+04	3.434E+04	4.594E+04
0.60	3.357E+02	1.340E+03	7.386E+03	1.081E+04	1.422E+04	2.067E+04	2.648E+04	3.524E+04	4.777E+04
0.70	3.053E+02	1.221E+03	7.153E+03	1.060E+04	1.409E+04	2.081E+04	2.697E+04	3.750E+04	4.919E+04
0.80	2.806E+02	1.122E+03	6.919E+03	1.037E+04	1.390E+04	2.083E+04	2.727E+04	3.847E+04	5.030E+04
1.00	2.426E+02	9.703E+02	6.470E+03	9.866E+03	1.343E+04	2.062E+04	2.750E+04	3.981E+04	5.187E+04
1.20	2.153E+02	8.611E+02	6.078E+03	9.396E+03	1.295E+04	2.027E+04	2.745E+04	4.061E+04	5.285E+04
1.50	1.957E+02	7.427E+02	5.573E+03	8.753E+03	1.223E+04	1.960E+04	2.706E+04	4.117E+04	5.359E+04
2.00	1.520E+02	6.080E+02	4.878E+03	7.810E+03	1.110E+04	1.833E+04	2.594E+04	4.099E+04	5.822E+04
2.50	1.292E+02	5.168E+02	4.328E+03	7.025E+03	1.011E+04	1.707E+04	2.461E+04	4.009E+04	5.853E+04
3.00	1.126E+02	4.504E+02	3.884E+03	6.370E+03	9.256E+03	1.590E+04	2.327E+04	3.885E+04	5.805E+04
3.50	9.989E+01	3.996E+02	3.519E+03	5.819E+03	8.520E+03	1.483E+04	2.198E+04	3.746E+04	5.711E+04
4.00	8.983E+01	3.593E+02	3.210E+03	5.351E+03	7.882E+03	1.388E+04	2.077E+04	3.602E+04	5.588E+04
5.00	7.485E+01	2.994E+02	2.689E+03	4.600E+03	6.838E+03	1.225E+04	1.862E+04	3.320E+04	5.302E+04
6.00	6.449E+01	2.580E+02	2.321E+03	4.045E+03	6.053E+03	1.097E+04	1.687E+04	3.072E+04	5.015E+04
7.00	5.710E+01	2.284E+02	2.055E+03	3.631E+03	5.460E+03	9.986E+03	1.548E+04	2.863E+04	4.756E+04
8.00	5.132E+01	2.053E+02	1.846E+03	3.274E+03	4.976E+03	9.165E+03	1.430E+04	2.678E+04	4.512E+04
10.00	4.285E+01	1.714E+02	1.543E+03	2.741E+03	4.235E+03	7.880E+03	1.242E+04	2.369E+04	4.078E+04
12.00	3.692E+01	1.477E+02	1.329E+03	2.362E+03	3.680E+03	6.922E+03	1.099E+04	2.123E+04	3.713E+04
15.00	3.073E+01	1.229E+02	1.106E+03	1.967E+03	3.071E+03	5.871E+03	9.384E+03	1.839E+04	3.270E+04
20.00	2.423E+01	9.694E+01	8.724E+02	1.551E+03	2.423E+03	4.713E+03	7.590E+03	1.509E+04	2.731E+04
25.00	2.016E+01	8.065E+01	7.258E+02	1.290E+03	2.016E+03	3.945E+03	6.406E+03	1.285E+04	2.352E+04
30.00	1.736E+01	6.944E+01	6.250E+02	1.111E+03	1.736E+03	3.401E+03	5.566E+03	1.123E+04	2.072E+04
35.00	1.531E+01	6.124E+01	5.511E+02	9.798E+02	1.531E+03	3.000E+03	4.944E+03	1.001E+04	1.856E+04
40.00	1.374E+01	5.496E+01	4.947E+02	8.794E+02	1.374E+03	2.693E+03	4.444E+03	9.055E+03	1.686E+04
50.00	1.150E+01	4.598E+01	4.138E+02	7.357E+02	1.150E+03	2.253E+03	3.723E+03	7.652E+03	1.433E+04
60.00	9.960E+00	3.984E+01	3.586E+02	6.375E+02	9.960E+02	1.952E+03	3.227E+03	6.672E+03	1.254E+04
70.00	8.842E+00	3.537E+01	3.183E+02	5.659E+02	8.842E+02	1.733E+03	2.865E+03	5.947E+03	1.121E+04
80.00	7.989E+00	3.196E+01	2.876E+02	5.113E+02	7.989E+02	1.566E+03	2.588E+03	5.391E+03	1.018E+04
100.00	6.771E+00	2.708E+01	2.438E+02	4.334E+02	6.771E+02	1.327E+03	2.194E+03	4.575E+03	8.686E+03
120.00	5.941E+00	2.376E+01	2.139E+02	3.802E+02	5.941E+02	1.164E+03	1.925E+03	4.015E+03	7.651E+03
150.00	5.092E+00	2.037E+01	1.833E+02	3.259E+02	5.092E+02	9.980E+02	1.650E+03	3.442E+03	6.580E+03
200.00	4.220E+00	1.688E+01	1.519E+02	2.701E+02	4.220E+02	8.272E+02	1.367E+03	2.853E+03	5.467E+03
250.00	3.684E+00	1.473E+01	1.326E+02	2.357E+02	3.684E+02	7.220E+02	1.193E+03	2.490E+03	4.773E+03
300.00	3.319E+00	1.328E+01	1.195E+02	2.124E+02	3.319E+02	6.505E+02	1.075E+03	2.244E+03	4.301E+03
350.00	3.055E+00	1.222E+01	1.100E+02	1.955E+02	3.055E+02	5.987E+02	9.897E+02	2.065E+03	3.959E+03
400.00	2.855E+00	1.142E+01	1.028E+02	1.827E+02	2.855E+02	5.595E+02	9.249E+02	1.930E+03	3.700E+03
500.00	2.573E+00	1.029E+01	9.262E+01	1.647E+02	2.573E+02	5.042E+02	8.335E+02	1.739E+03	3.334E+03
600.00	2.384E+00	9.538E+00	8.584E+01	1.526E+02	2.384E+02	4.673E+02	7.726E+02	1.612E+03	3.090E+03
700.00	2.251E+00	9.005E+00	8.105E+01	1.441E+02	2.251E+02	4.412E+02	7.294E+02	1.522E+03	2.918E+03
800.00	2.153E+00	8.613E+00	7.752E+01	1.378E+02	2.153E+02	4.220E+02	6.977E+02	1.456E+03	2.791E+03
1000.00	2.022E+00	8.089E+00	7.280E+01	1.294E+02	2.022E+02	3.964E+02	6.552E+02	1.367E+03	2.621E+03
1200.00	1.943E+00	7.773E+00	6.996E+01	1.244E+02	1.943E+02	3.809E+02	6.296E+02	1.314E+03	2.519E+03

RANGE IN CELLULOSE NITRATE UNPLASTICIZED (GM/CM2) I = 81.1 A/Z = 1.939

ENRG./NUC. (MEV/AMU)	1 H	4 HE	12 C	16 O	20 NE	28 SI	40 AR	56 FE	84 KR
0.10	1.396E-04	2.328E-04	2.427E-04	2.598E-04	2.764E-04	3.058E-04	3.723E-04	4.228E-04	5.367E-04
0.12	1.667E-04	2.739E-04	2.770E-04	2.951E-04	3.132E-04	3.455E-04	4.183E-04	4.720E-04	5.967E-04
0.15	2.104E-04	3.361E-04	3.269E-04	3.458E-04	3.656E-04	4.025E-04	4.838E-04	5.412E-04	6.803E-04
0.20	2.911E-04	4.424E-04	4.075E-04	4.263E-04	4.479E-04	4.905E-04	5.866E-04	6.480E-04	8.079E-04
0.25	3.817E-04	5.526E-04	4.867E-04	5.039E-04	5.262E-04	5.727E-04	6.842E-04	7.477E-04	9.254E-04
0.30	4.816E-04	6.671E-04	5.653E-04	5.800E-04	6.020E-04	6.511E-04	7.783E-04	8.425E-04	1.036E-03
0.40	7.076E-04	9.095E-04	7.231E-04	7.299E-04	7.495E-04	8.007E-04	9.489E-04	1.022E-03	1.242E-03
0.50	9.670E-04	1.173E-03	8.837E-04	8.797E-04	8.945E-04	9.444E-04	1.113E-03	1.194E-03	1.436E-03
0.60	1.258E-03	1.465E-03	1.049E-03	1.031E-03	1.039E-03	1.085E-03	1.270E-03	1.359E-03	1.621E-03
0.70	1.580E-03	1.787E-03	1.219E-03	1.185E-03	1.185E-03	1.224E-03	1.425E-03	1.513E-03	1.799E-03
0.80	1.931E-03	2.139E-03	1.394E-03	1.342E-03	1.332E-03	1.362E-03	1.577E-03	1.665E-03	1.973E-03
1.00	2.720E-03	2.928E-03	1.763E-03	1.667E-03	1.633E-03	1.640E-03	1.877E-03	1.959E-03	2.312E-03
1.20	3.621E-03	3.830E-03	2.157E-03	2.009E-03	1.945E-03	1.922E-03	2.177E-03	2.246E-03	2.642E-03
1.50	5.177E-03	5.385E-03	2.796E-03	2.556E-03	2.437E-03	2.357E-03	2.631E-03	2.670E-03	3.102E-03
2.00	8.299E-03	8.507E-03	3.997E-03	3.564E-03	3.330E-03	3.124E-03	3.413E-03	3.374E-03	3.857E-03
2.50	1.200E-02	1.221E-02	5.349E-03	4.681E-03	4.306E-03	3.941E-03	4.220E-03	4.086E-03	4.599E-03
3.00	1.625E-02	1.646E-02	6.850E-03	5.908E-03	5.366E-03	4.813E-03	5.088E-03	4.815E-03	5.339E-03
3.50	2.109E-02	2.130E-02	8.513E-03	7.255E-03	6.521E-03	5.749E-03	5.996E-03	5.569E-03	6.089E-03
4.00	2.650E-02	2.670E-02	1.034E-02	8.724E-03	7.772E-03	6.749E-03	6.956E-03	6.351E-03	6.853E-03
5.00	3.902E-02	3.923E-02	1.453E-02	1.203E-02	1.057E-02	8.953E-03	9.043E-03	8.013E-03	8.436E-03
6.00	5.382E-02	5.403E-02	1.946E-02	1.584E-02	1.376E-02	1.144E-02	1.136E-02	9.815E-03	1.011E-02
7.00	7.089E-02	7.109E-02	2.516E-02	2.016E-02	1.736E-02	1.420E-02	1.392E-02	1.177E-02	1.189E-02
8.00	9.023E-02	9.044E-02	3.161E-02	2.502E-02	2.138E-02	1.726E-02	1.673E-02	1.388E-02	1.377E-02
10.00	1.350E-01	1.352E-01	4.652E-02	3.621E-02	3.050E-02	2.416E-02	2.300E-02	1.851E-02	1.785E-02
12.00	1.864E-01	1.866E-01	6.366E-02	4.908E-02	4.084E-02	3.191E-02	3.001E-02	2.363E-02	2.227E-02
15.00	2.776E-01	2.778E-01	9.408E-02	7.189E-02	5.912E-02	4.540E-02	4.211E-02	3.233E-02	2.968E-02
20.00	4.659E-01	4.661E-01	1.568E-01	1.189E-01	9.677E-02	7.271E-02	6.642E-02	4.957E-02	4.409E-02
25.00	6.974E-01	6.976E-01	2.340E-01	1.768E-01	1.431E-01	1.059E-01	9.577E-02	7.015E-02	6.105E-02
30.00	9.705E-01	9.707E-01	3.250E-01	2.451E-01	1.977E-01	1.449E-01	1.300E-01	9.396E-02	8.049E-02
35.00	1.284E+00	1.284E+00	4.294E-01	3.234E-01	2.603E-01	1.897E-01	1.689E-01	1.209E-01	1.024E-01
40.00	1.635E+00	1.635E+00	5.466E-01	4.113E-01	3.306E-01	2.399E-01	2.124E-01	1.509E-01	1.266E-01
50.00	2.449E+00	2.449E+00	8.179E-01	6.147E-01	4.934E-01	3.562E-01	3.130E-01	2.197E-01	1.818E-01
60.00	3.403E+00	3.403E+00	1.136E+00	8.533E-01	6.842E-01	4.925E-01	4.308E-01	2.997E-01	2.458E-01
70.00	4.490E+00	4.490E+00	1.498E+00	1.125E+00	9.016E-01	6.478E-01	5.650E-01	3.904E-01	3.181E-01
80.00	5.703E+00	5.703E+00	1.902E+00	1.428E+00	1.144E+00	8.210E-01	7.147E-01	4.911E-01	3.982E-01
100.00	8.482E+00	8.482E+00	2.829E+00	2.123E+00	1.700E+00	1.218E+00	1.058E+00	7.216E-01	5.808E-01
120.00	1.170E+01	1.170E+01	3.901E+00	2.927E+00	2.344E+00	1.678E+00	1.455E+00	9.883E-01	7.910E-01
150.00	1.727E+01	1.727E+01	5.759E+00	4.321E+00	3.458E+00	2.474E+00	2.143E+00	1.445E+00	1.154E+00
200.00	2.832E+01	2.832E+01	9.441E+00	7.082E+00	5.668E+00	4.052E+00	3.507E+00	2.365E+00	1.871E+00
250.00	4.127E+01	4.127E+01	1.376E+01	1.032E+01	8.257E+00	5.902E+00	5.105E+00	3.438E+00	2.710E+00
300.00	5.585E+01	5.585E+01	1.862E+01	1.396E+01	1.117E+01	7.984E+00	6.905E+00	4.645E+00	3.655E+00
400.00	8.908E+01	8.908E+01	2.969E+01	2.227E+01	1.782E+01	1.273E+01	1.101E+01	7.398E+00	5.809E+00
500.00	1.267E+02	1.267E+02	4.224E+01	3.168E+01	2.535E+01	1.811E+01	1.565E+01	1.052E+01	8.249E+00
600.00	1.678E+02	1.678E+02	5.595E+01	4.196E+01	3.357E+01	2.398E+01	2.073E+01	1.392E+01	1.091E+01
700.00	2.118E+02	2.118E+02	7.059E+01	5.295E+01	4.236E+01	3.026E+01	2.616E+01	1.756E+01	1.376E+01
800.00	2.580E+02	2.580E+02	8.599E+01	6.450E+01	5.160E+01	3.686E+01	3.186E+01	2.139E+01	1.676E+01
1000.00	3.556E+02	3.556E+02	1.185E+02	8.891E+01	7.113E+01	5.081E+01	4.391E+01	2.948E+01	2.309E+01
1200.00	4.583E+02	4.583E+02	1.528E+02	1.146E+02	9.166E+01	6.548E+01	5.659E+01	3.798E+01	2.974E+01

DE/DX IN CELLULOSE NITRATE UNPLASTICIZED (MEV CM2/GM) I = 81.1 A/Z = 1.939

ENRG./NUC. (MEV/AMU)	1 H	4 HE	12 C	16 O	20 NE	28 SI	40 AR	56 FE	84 KR
0.10	7.560E+02	1.954E+03	6.869E+03	8.864E+03	1.058E+04	1.380E+04	1.695E+04	2.207E+04	2.705E+04
0.12	7.163E+02	1.942E+03	7.090E+03	9.247E+03	1.112E+04	1.438E+04	1.780E+04	2.342E+04	2.892E+04
0.15	6.607E+02	1.912E+03	7.320E+03	9.680E+03	1.176E+04	1.504E+04	1.881E+04	2.509E+04	3.130E+04
0.20	5.827E+02	1.849E+03	7.534E+03	1.015E+04	1.251E+04	1.653E+04	2.004E+04	2.725E+04	3.447E+04
0.25	5.248E+02	1.781E+03	7.624E+03	1.044E+04	1.301E+04	1.748E+04	2.091E+04	2.888E+04	3.697E+04
0.30	4.791E+02	1.713E+03	7.640E+03	1.060E+04	1.335E+04	1.820E+04	2.155E+04	3.014E+04	3.902E+04
0.40	4.115E+02	1.605E+03	7.550E+03	1.070E+04	1.372E+04	1.917E+04	2.388E+04	3.203E+04	4.219E+04
0.50	3.631E+02	1.440E+03	7.378E+03	1.064E+04	1.383E+04	1.974E+04	2.495E+04	3.329E+04	4.453E+04
0.60	3.263E+02	1.302E+03	7.171E+03	1.049E+04	1.380E+04	2.006E+04	2.568E+04	3.418E+04	4.632E+04
0.70	2.971E+02	1.188E+03	6.950E+03	1.030E+04	1.368E+04	2.020E+04	2.617E+04	3.488E+04	4.771E+04
0.80	2.733E+02	1.092E+03	6.728E+03	1.008E+04	1.351E+04	2.022E+04	2.647E+04	3.733E+04	4.880E+04
1.00	2.365E+02	9.460E+02	6.299E+03	9.599E+03	1.306E+04	2.004E+04	2.672E+04	3.864E+04	5.033E+04
1.20	2.097E+02	8.387E+02	5.913E+03	9.138E+03	1.259E+04	1.969E+04	2.666E+04	3.942E+04	5.128E+04
1.50	1.810E+02	7.241E+02	5.428E+03	8.520E+03	1.190E+04	1.906E+04	2.630E+04	3.998E+04	5.493E+04
2.00	1.483E+02	5.934E+02	4.757E+03	7.612E+03	1.081E+04	1.784E+04	2.523E+04	3.985E+04	5.655E+04
2.50	1.262E+02	5.047E+02	4.224E+03	6.853E+03	9.858E+03	1.663E+04	2.396E+04	3.900E+04	5.688E+04
3.00	1.100E+02	4.400E+02	3.793E+03	6.218E+03	9.031E+03	1.550E+04	2.267E+04	3.781E+04	5.645E+04
3.50	9.764E+01	3.905E+02	3.439E+03	5.684E+03	8.317E+03	1.447E+04	2.142E+04	3.648E+04	5.556E+04
4.00	8.783E+01	3.513E+02	3.138E+03	5.228E+03	7.698E+03	1.354E+04	2.025E+04	3.509E+04	5.439E+04
5.00	7.320E+01	2.928E+02	2.630E+03	4.497E+03	6.682E+03	1.196E+04	1.817E+04	3.237E+04	5.165E+04
6.00	6.314E+01	2.526E+02	2.272E+03	3.959E+03	5.922E+03	1.073E+04	1.649E+04	2.998E+04	4.891E+04
7.00	5.592E+01	2.237E+02	2.013E+03	3.556E+03	5.345E+03	9.769E+03	1.514E+04	2.797E+04	4.641E+04
8.00	5.028E+01	2.011E+02	1.809E+03	3.208E+03	4.874E+03	8.970E+03	1.399E+04	2.617E+04	4.405E+04
10.00	4.200E+01	1.680E+02	1.512E+03	2.687E+03	4.151E+03	7.719E+03	1.216E+04	2.317E+04	3.985E+04
12.00	3.620E+01	1.448E+02	1.303E+03	2.317E+03	3.608E+03	6.784E+03	1.076E+04	2.078E+04	3.631E+04
15.00	3.015E+01	1.206E+02	1.085E+03	1.929E+03	3.013E+03	5.758E+03	9.200E+03	1.802E+04	3.201E+04
20.00	2.379E+01	9.514E+01	8.563E+02	1.522E+03	2.378E+03	4.625E+03	7.446E+03	1.480E+04	2.676E+04
25.00	1.979E+01	7.918E+01	7.126E+02	1.267E+03	1.979E+03	3.873E+03	6.287E+03	1.261E+04	2.306E+04
30.00	1.705E+01	6.819E+01	6.137E+02	1.091E+03	1.705E+03	3.340E+03	5.465E+03	1.103E+04	2.032E+04
35.00	1.504E+01	6.014E+01	5.413E+02	9.623E+02	1.504E+03	2.947E+03	4.856E+03	9.829E+03	1.822E+04
40.00	1.350E+01	5.399E+01	4.859E+02	8.639E+02	1.350E+03	2.645E+03	4.366E+03	8.892E+03	1.655E+04
50.00	1.129E+01	4.518E+01	4.066E+02	7.228E+02	1.129E+03	2.214E+03	3.658E+03	7.517E+03	1.407E+04
60.00	9.787E+00	3.915E+01	3.523E+02	6.264E+02	9.787E+02	1.918E+03	3.171E+03	6.555E+03	1.232E+04
70.00	8.689E+00	3.476E+01	3.128E+02	5.561E+02	8.689E+02	1.703E+03	2.815E+03	5.844E+03	1.102E+04
80.00	7.852E+00	3.141E+01	2.827E+02	5.025E+02	7.852E+02	1.539E+03	2.543E+03	5.298E+03	1.000E+04
100.00	6.656E+00	2.662E+01	2.396E+02	4.260E+02	6.656E+02	1.305E+03	2.156E+03	4.497E+03	8.537E+03
120.00	5.840E+00	2.336E+01	2.102E+02	3.738E+02	5.840E+02	1.145E+03	1.892E+03	3.947E+03	7.520E+03
150.00	5.006E+00	2.003E+01	1.802E+02	3.204E+02	5.006E+02	9.812E+02	1.622E+03	3.384E+03	6.469E+03
200.00	4.150E+00	1.660E+01	1.494E+02	2.656E+02	4.150E+02	8.134E+02	1.345E+03	2.805E+03	5.375E+03
250.00	3.622E+00	1.449E+01	1.304E+02	2.318E+02	3.622E+02	7.100E+02	1.174E+03	2.449E+03	4.694E+03
300.00	3.264E+00	1.306E+01	1.175E+02	2.089E+02	3.264E+02	6.397E+02	1.058E+03	2.206E+03	4.230E+03
400.00	2.808E+00	1.123E+01	1.011E+02	1.797E+02	2.808E+02	5.504E+02	9.098E+02	1.898E+03	3.639E+03
500.00	2.531E+00	1.012E+01	9.111E+01	1.620E+02	2.531E+02	4.960E+02	8.200E+02	1.711E+03	3.280E+03
600.00	2.346E+00	9.383E+00	8.445E+01	1.501E+02	2.346E+02	4.598E+02	7.601E+02	1.586E+03	3.040E+03
700.00	2.215E+00	8.860E+00	7.974E+01	1.418E+02	2.215E+02	4.341E+02	7.177E+02	1.497E+03	2.871E+03
800.00	2.119E+00	8.475E+00	7.628E+01	1.356E+02	2.119E+02	4.153E+02	6.865E+02	1.432E+03	2.746E+03
1000.00	1.990E+00	7.961E+00	7.165E+01	1.274E+02	1.990E+02	3.901E+02	6.449E+02	1.345E+03	2.579E+03
1200.00	1.913E+00	7.652E+00	6.886E+01	1.224E+02	1.913E+02	3.749E+02	6.198E+02	1.293E+03	2.479E+03

RANGE IN ALUMINUM (GM/CM2) I = 163.0 A/Z = 2.075

ENRG./NUC. (MEV/AMU)	1 H	4 HE	12 C	16 O	20 NE	28 SI	40 AR	56 FE	84 KR
0.10	2.129E-04	3.484E-04	3.559E-04	3.800E-04	4.036E-04	4.456E-04	5.421E-04	6.150E-04	7.803E-04
0.12	2.596E-04	4.152E-04	4.082E-04	4.330E-04	4.585E-04	5.043E-04	6.098E-04	6.871E-04	8.679E-04
0.15	3.333E-04	5.159E-04	4.842E-04	5.092E-04	5.367E-04	5.887E-04	7.063E-04	7.585E-04	9.900E-04
0.20	4.661E-04	6.859E-04	6.065E-04	6.301E-04	6.593E-04	7.186E-04	8.575E-04	9.449E-04	1.176E-03
0.25	6.104E-04	8.586E-04	7.256E-04	7.460E-04	7.755E-04	8.399E-04	1.001E-03	1.091E-03	1.348E-03
0.30	7.652E-04	1.035E-03	8.430E-04	8.589E-04	8.876E-04	9.552E-04	1.139E-03	1.229E-03	1.509E-03
0.40	1.104E-03	1.397E-03	1.076E-03	1.079E-03	1.104E-03	1.174E-03	1.388E-03	1.491E-03	1.810E-03
0.50	1.480E-03	1.779E-03	1.309E-03	1.297E-03	1.314E-03	1.383E-03	1.625E-03	1.745E-03	2.091E-03
0.60	1.891E-03	2.192E-03	1.545E-03	1.514E-03	1.522E-03	1.585E-03	1.853E-03	1.980E-03	2.358E-03
0.70	2.337E-03	2.639E-03	1.784E-03	1.732E-03	1.729E-03	1.784E-03	2.075E-03	2.201E-03	2.616E-03
0.80	2.818E-03	3.120E-03	2.029E-03	1.953E-03	1.937E-03	1.981E-03	2.292E-03	2.420E-03	2.867E-03
1.00	3.883E-03	4.185E-03	2.538E-03	2.405E-03	2.358E-03	2.373E-03	2.718E-03	2.841E-03	3.354E-03
1.20	5.085E-03	5.388E-03	3.074E-03	2.875E-03	2.790E-03	2.767E-03	3.140E-03	3.248E-03	3.827E-03
1.50	7.152E-03	7.455E-03	3.939E-03	3.621E-03	3.467E-03	3.372E-03	3.776E-03	3.847E-03	4.482E-03
2.00	1.132E-02	1.162E-02	5.561E-03	4.993E-03	4.690E-03	4.432E-03	4.867E-03	4.841E-03	5.535E-03
2.50	1.644E-02	1.674E-02	7.438E-03	6.551E-03	6.056E-03	5.583E-03	6.021E-03	5.854E-03	6.616E-03
3.00	2.197E-02	2.228E-02	9.404E-03	8.172E-03	7.467E-03	6.758E-03	7.188E-03	6.859E-03	7.650E-03
3.50	2.825E-02	2.855E-02	1.157E-02	9.942E-03	8.995E-03	8.010E-03	8.415E-03	7.892E-03	8.690E-03
4.00	3.523E-02	3.553E-02	1.393E-02	1.186E-02	1.064E-02	9.338E-03	9.702E-03	8.956E-03	9.743E-03
5.00	5.130E-02	5.160E-02	1.931E-02	1.613E-02	1.427E-02	1.224E-02	1.247E-02	1.119E-02	1.191E-02
6.00	7.018E-02	7.048E-02	2.561E-02	2.102E-02	1.839E-02	1.547E-02	1.552E-02	1.359E-02	1.417E-02
7.00	9.188E-02	9.218E-02	3.284E-02	2.651E-02	2.300E-02	1.905E-02	1.885E-02	1.617E-02	1.655E-02
8.00	1.164E-01	1.167E-01	4.102E-02	3.267E-02	2.812E-02	2.298E-02	2.249E-02	1.894E-02	1.906E-02
10.00	1.705E-01	1.708E-01	5.906E-02	4.622E-02	3.920E-02	3.144E-02	3.026E-02	2.478E-02	2.429E-02
12.00	2.337E-01	2.340E-01	8.011E-02	6.202E-02	5.191E-02	4.106E-02	3.901E-02	3.125E-02	2.995E-02
15.00	3.450E-01	3.453E-01	1.172E-01	8.985E-02	7.422E-02	5.762E-02	5.397E-02	4.213E-02	3.932E-02
20.00	5.730E-01	5.733E-01	1.932E-01	1.469E-01	1.198E-01	9.081E-02	8.368E-02	6.342E-02	5.732E-02
25.00	8.518E-01	8.521E-01	2.862E-01	2.166E-01	1.756E-01	1.308E-01	1.192E-01	8.854E-02	7.822E-02
30.00	1.179E+00	1.179E+00	3.953E-01	2.984E-01	2.411E-01	1.776E-01	1.604E-01	1.174E-01	1.020E-01
35.00	1.553E+00	1.553E+00	5.199E-01	3.919E-01	3.159E-01	2.310E-01	2.069E-01	1.498E-01	1.285E-01
40.00	1.972E+00	1.972E+00	6.596E-01	4.966E-01	3.997E-01	2.909E-01	2.588E-01	1.858E-01	1.577E-01
50.00	2.939E+00	2.939E+00	9.818E-01	7.383E-01	5.930E-01	4.290E-01	3.783E-01	2.679E-01	2.240E-01
60.00	4.069E+00	4.069E+00	1.358E+00	1.021E+00	8.190E-01	5.904E-01	5.178E-01	3.629E-01	3.004E-01
70.00	5.353E+00	5.353E+00	1.786E+00	1.342E+00	1.076E+00	7.739E-01	6.763E-01	4.702E-01	3.862E-01
80.00	6.783E+00	6.783E+00	2.263E+00	1.699E+00	1.362E+00	9.782E-01	8.529E-01	5.891E-01	4.811E-01
100.00	1.005E+01	1.005E+01	3.353E+00	2.517E+00	2.016E+00	1.445E+00	1.257E+00	8.604E-01	6.966E-01
120.00	1.383E+01	1.383E+01	4.613E+00	3.461E+00	2.772E+00	1.985E+00	1.723E+00	1.173E+00	9.440E-01
150.00	2.036E+01	2.036E+01	6.789E+00	5.094E+00	4.078E+00	2.918E+00	2.529E+00	1.714E+00	1.370E+00
200.00	3.328E+01	3.328E+01	1.109E+01	8.323E+00	6.661E+00	4.763E+00	4.124E+00	2.784E+00	2.208E+00
250.00	4.838E+01	4.838E+01	1.613E+01	1.210E+01	9.682E+00	6.921E+00	5.989E+00	4.036E+00	3.197E+00
300.00	6.537E+01	6.537E+01	2.179E+01	1.634E+01	1.308E+01	9.347E+00	8.085E+00	5.443E+00	4.286E+00
400.00	1.040E+02	1.040E+02	3.467E+01	2.600E+01	2.081E+01	1.487E+01	1.286E+01	8.643E+00	6.793E+00
500.00	1.477E+02	1.477E+02	4.923E+01	3.692E+01	2.954E+01	2.111E+01	1.825E+01	1.226E+01	9.624E+00
600.00	1.953E+02	1.953E+02	6.511E+01	4.884E+01	3.907E+01	2.791E+01	2.413E+01	1.621E+01	1.271E+01
700.00	2.461E+02	2.461E+02	8.205E+01	6.154E+01	4.924E+01	3.517E+01	3.040E+01	2.042E+01	1.601E+01
800.00	2.995E+02	2.995E+02	9.985E+01	7.489E+01	5.991E+01	4.280E+01	3.699E+01	2.484E+01	1.947E+01
1000.00	4.121E+02	4.121E+02	1.374E+02	1.030E+02	8.243E+01	5.888E+01	5.089E+01	3.417E+01	2.676E+01
1200.00	5.302E+02	5.302E+02	1.767E+02	1.326E+02	1.061E+02	7.576E+01	6.548E+01	4.395E+01	3.442E+01

DE/DX IN ALUMINUM (MEV CM2/GM) I = 163.0 A/Z = 2.075

ENRG./NUC. (MEV/AMU)	1 H	4 HE	12 C	16 O	20 NE	28 SI	40 AR	56 FE	84 KR
0.10	4.387E+02	1.201E+03	4.517E+03	5.901E+03	7.097E+03	9.341E+03	1.192E+04	1.507E+04	1.853E+04
0.12	4.198E+02	1.195E+03	4.657E+03	6.149E+03	7.454E+03	9.725E+03	1.209E+04	1.599E+04	1.980E+04
0.15	3.947E+02	1.186E+03	4.814E+03	6.439E+03	7.882E+03	1.018E+04	1.278E+04	1.713E+04	2.143E+04
0.20	3.602E+02	1.168E+03	4.983E+03	6.780E+03	8.408E+03	1.120E+04	1.363E+04	1.861E+04	2.361E+04
0.25	3.342E+02	1.147E+03	5.082E+03	7.007E+03	8.781E+03	1.187E+04	1.425E+04	1.975E+04	2.534E+04
0.30	3.129E+02	1.125E+03	5.136E+03	7.161E+03	9.054E+03	1.240E+04	1.472E+04	2.066E+04	2.677E+04
0.40	2.797E+02	1.091E+03	5.163E+03	7.329E+03	9.401E+03	1.316E+04	1.540E+04	2.201E+04	2.902E+04
0.50	2.540E+02	1.007E+03	5.125E+03	7.380E+03	9.580E+03	1.365E+04	1.724E+04	2.297E+04	3.070E+04
0.60	2.332E+02	9.306E+02	5.050E+03	7.361E+03	9.651E+03	1.397E+04	1.784E+04	2.366E+04	3.202E+04
0.70	2.158E+02	8.627E+02	4.952E+03	7.295E+03	9.650E+03	1.416E+04	1.827E+04	2.528E+04	3.306E+04
0.80	2.008E+02	8.026E+02	4.841E+03	7.198E+03	9.598E+03	1.426E+04	1.858E+04	2.603E+04	3.389E+04
1.00	1.764E+02	7.058E+02	4.599E+03	6.949E+03	9.394E+03	1.427E+04	1.890E+04	2.711E+04	3.509E+04
1.20	1.572E+02	6.288E+02	4.349E+03	6.661E+03	9.111E+03	1.411E+04	1.896E+04	2.777E+04	3.585E+04
1.50	1.344E+02	5.375E+02	3.977E+03	6.196E+03	8.602E+03	1.365E+04	1.871E+04	2.819E+04	3.647E+04
2.00	1.118E+02	4.474E+02	3.550E+03	5.633E+03	7.949E+03	1.298E+04	1.820E+04	2.841E+04	3.995E+04
2.50	9.616E+01	3.846E+02	3.195E+03	5.139E+03	7.341E+03	1.224E+04	1.749E+04	2.809E+04	4.052E+04
3.00	8.450E+01	3.380E+02	2.900E+03	4.719E+03	6.796E+03	1.153E+04	1.671E+04	2.748E+04	4.053E+04
3.50	7.544E+01	3.018E+02	2.650E+03	4.344E+03	6.312E+03	1.086E+04	1.592E+04	2.672E+04	4.017E+04
4.00	6.818E+01	2.727E+02	2.433E+03	4.023E+03	5.883E+03	1.023E+04	1.517E+04	2.589E+04	3.959E+04
5.00	5.754E+01	2.301E+02	2.067E+03	3.515E+03	5.189E+03	9.183E+03	1.382E+04	2.426E+04	3.813E+04
6.00	5.033E+01	2.013E+02	1.811E+03	3.146E+03	4.675E+03	8.375E+03	1.275E+04	2.283E+04	3.665E+04
7.00	4.484E+01	1.794E+02	1.614E+03	2.849E+03	4.255E+03	7.696E+03	1.182E+04	2.150E+04	3.513E+04
8.00	4.052E+01	1.621E+02	1.457E+03	2.583E+03	3.907E+03	7.120E+03	1.101E+04	2.030E+04	3.364E+04
10.00	3.411E+01	1.364E+02	1.228E+03	2.181E+03	3.363E+03	6.198E+03	9.689E+03	1.821E+04	3.038E+04
12.00	2.957E+01	1.183E+02	1.064E+03	1.892E+03	2.945E+03	5.496E+03	8.656E+03	1.651E+04	2.846E+04
15.00	2.478E+01	9.913E+01	8.922E+02	1.586E+03	2.476E+03	4.710E+03	7.478E+03	1.448E+04	2.542E+04
20.00	1.970E+01	7.880E+01	7.092E+02	1.261E+03	1.970E+03	3.825E+03	6.125E+03	1.206E+04	2.159E+04
25.00	1.648E+01	6.592E+01	5.932E+02	1.055E+03	1.648E+03	3.223E+03	5.213E+03	1.037E+04	1.880E+04
30.00	1.425E+01	5.699E+01	5.129E+02	9.118E+02	1.425E+03	2.791E+03	4.556E+03	9.130E+03	1.670E+04
35.00	1.260E+01	5.041E+01	4.537E+02	8.066E+02	1.260E+03	2.470E+03	4.067E+03	8.180E+03	1.506E+04
40.00	1.134E+01	4.536E+01	4.083E+02	7.258E+02	1.134E+03	2.223E+03	3.666E+03	7.429E+03	1.374E+04
50.00	9.524E+00	3.810E+01	3.429E+02	6.095E+02	9.524E+02	1.867E+03	3.084E+03	6.316E+03	1.177E+04
60.00	8.276E+00	3.310E+01	2.979E+02	5.296E+02	8.276E+02	1.622E+03	2.681E+03	5.531E+03	1.035E+04
70.00	7.362E+00	2.949E+01	2.650E+02	4.712E+02	7.362E+02	1.443E+03	2.385E+03	4.946E+03	9.287E+03
80.00	6.664E+00	2.666E+01	2.399E+02	4.265E+02	6.664E+02	1.306E+03	2.159E+03	4.495E+03	8.458E+03
100.00	5.663E+00	2.265E+01	2.039E+02	3.624E+02	5.663E+02	1.110E+03	1.835E+03	3.825E+03	7.246E+03
120.00	4.978E+00	1.991E+01	1.792E+02	3.186E+02	4.978E+02	9.758E+02	1.613E+03	3.365E+03	6.401E+03
150.00	4.277E+00	1.711E+01	1.540E+02	2.737E+02	4.277E+02	8.382E+02	1.386E+03	2.891E+03	5.522E+03
200.00	3.554E+00	1.421E+01	1.279E+02	2.274E+02	3.554E+02	6.965E+02	1.151E+03	2.402E+03	4.602E+03
250.00	3.107E+00	1.243E+01	1.119E+02	1.989E+02	3.107E+02	6.091E+02	1.007E+03	2.101E+03	4.026E+03
300.00	2.804E+00	1.122E+01	1.009E+02	1.794E+02	2.804E+02	5.496E+02	9.085E+02	1.895E+03	3.634E+03
400.00	2.417E+00	9.670E+00	8.703E+01	1.547E+02	2.417E+02	4.738E+02	7.833E+02	1.634E+03	3.133E+03
500.00	2.183E+00	8.731E+00	7.858E+01	1.397E+02	2.183E+02	4.278E+02	7.072E+02	1.476E+03	2.829E+03
600.00	2.026E+00	8.106E+00	7.295E+01	1.297E+02	2.026E+02	3.972E+02	6.565E+02	1.370E+03	2.626E+03
700.00	1.916E+00	7.664E+00	6.898E+01	1.226E+02	1.916E+02	3.755E+02	6.208E+02	1.295E+03	2.483E+03
800.00	1.835E+00	7.341E+00	6.607E+01	1.175E+02	1.835E+02	3.597E+02	5.946E+02	1.241E+03	2.378E+03
1000.00	1.728E+00	6.912E+00	6.221E+01	1.106E+02	1.728E+02	3.387E+02	5.599E+02	1.168E+03	2.240E+03
1200.00	1.664E+00	6.658E+00	5.992E+01	1.065E+02	1.664E+02	3.262E+02	5.393E+02	1.125E+03	2.157E+03

RANGE IN SILICON (GM/CM2) I = 172.3 A/Z = 2.004

ENRG./NUC. (MEV/AMU)	1 H	4 HE	12 C	16 O	20 NE	28 SI	40 AR	56 FE	84 KR
0.10	2.120E-04	3.469E-04	3.532E-04	3.770E-04	4.003E-04	4.419E-04	5.376E-04	6.098E-04	7.736E-04
0.12	2.588E-04	4.131E-04	4.052E-04	4.297E-04	4.548E-04	5.002E-04	6.048E-04	6.813E-04	8.605E-04
0.15	3.327E-04	5.138E-04	4.808E-04	5.054E-04	5.325E-04	5.839E-04	7.005E-04	7.819E-04	9.816E-04
0.20	4.656E-04	6.835E-04	6.024E-04	6.255E-04	6.543E-04	7.130E-04	8.505E-04	9.371E-04	1.166E-03
0.25	6.096E-04	8.557E-04	7.208E-04	7.407E-04	7.697E-04	8.333E-04	9.927E-04	1.082E-03	1.336E-03
0.30	7.638E-04	1.031E-03	8.375E-04	8.528E-04	8.810E-04	9.477E-04	1.130E-03	1.219E-03	1.496E-03
0.40	1.100E-03	1.391E-03	1.068E-03	1.072E-03	1.096E-03	1.165E-03	1.377E-03	1.479E-03	1.794E-03
0.50	1.473E-03	1.770E-03	1.299E-03	1.287E-03	1.304E-03	1.372E-03	1.612E-03	1.726E-03	2.073E-03
0.60	1.880E-03	2.179E-03	1.533E-03	1.502E-03	1.510E-03	1.572E-03	1.838E-03	1.963E-03	2.338E-03
0.70	2.321E-03	2.620E-03	1.770E-03	1.718E-03	1.715E-03	1.769E-03	2.057E-03	2.183E-03	2.594E-03
0.80	2.796E-03	3.095E-03	2.013E-03	1.936E-03	1.921E-03	1.964E-03	2.272E-03	2.399E-03	2.843E-03
1.00	3.846E-03	4.146E-03	2.515E-03	2.383E-03	2.337E-03	2.392E-03	2.694E-03	2.816E-03	3.325E-03
1.20	5.031E-03	5.331E-03	3.044E-03	2.847E-03	2.764E-03	2.742E-03	3.112E-03	3.219E-03	3.793E-03
1.50	7.067E-03	7.367E-03	3.897E-03	3.584E-03	3.432E-03	3.399E-03	3.741E-03	3.812E-03	4.442E-03
2.00	1.117E-02	1.147E-02	5.497E-03	4.938E-03	4.640E-03	4.587E-03	4.819E-03	4.795E-03	5.504E-03
2.50	1.622E-02	1.652E-02	7.348E-03	6.476E-03	5.988E-03	5.924E-03	5.960E-03	5.797E-03	6.554E-03
3.00	2.167E-02	2.197E-02	9.284E-03	8.073E-03	7.380E-03	6.883E-03	7.112E-03	6.790E-03	7.576E-03
3.50	2.783E-02	2.813E-02	1.141E-02	9.814E-03	8.884E-03	7.917E-03	8.321E-03	7.810E-03	8.604E-03
4.00	3.469E-02	3.499E-02	1.373E-02	1.170E-02	1.050E-02	9.225E-03	9.589E-03	8.860E-03	9.644E-03
5.00	5.047E-02	5.077E-02	1.901E-02	1.590E-02	1.407E-02	1.208E-02	1.232E-02	1.107E-02	1.178E-02
6.00	6.899E-02	6.929E-02	2.519E-02	2.069E-02	1.811E-02	1.525E-02	1.531E-02	1.343E-02	1.401E-02
7.00	9.027E-02	9.057E-02	3.229E-02	2.607E-02	2.264E-02	1.877E-02	1.859E-02	1.597E-02	1.635E-02
8.00	1.143E-01	1.146E-01	4.030E-02	3.211E-02	2.765E-02	2.262E-02	2.216E-02	1.869E-02	1.882E-02
10.00	1.672E-01	1.675E-01	5.792E-02	4.535E-02	3.848E-02	3.090E-02	2.977E-02	2.441E-02	2.395E-02
12.00	2.289E-01	2.292E-01	7.851E-02	6.080E-02	5.091E-02	4.031E-02	3.834E-02	3.075E-02	2.952E-02
15.00	3.377E-01	3.380E-01	1.148E-01	8.800E-02	7.272E-02	5.651E-02	5.297E-02	4.142E-02	3.872E-02
20.00	5.604E-01	5.607E-01	1.890E-01	1.437E-01	1.173E-01	8.893E-02	8.202E-02	6.224E-02	5.633E-02
25.00	8.376E-01	8.329E-01	2.797E-01	2.117E-01	1.717E-01	1.280E-01	1.167E-01	8.679E-02	7.678E-02
30.00	1.152E+00	1.152E+00	3.862E-01	2.916E-01	2.356E-01	1.736E-01	1.569E-01	1.150E-01	10.000E-02
35.00	1.517E+00	1.517E+00	5.078E-01	3.829E-01	3.086E-01	2.258E-01	2.023E-01	1.466E-01	1.259E-01
40.00	1.925E+00	1.926E+00	6.440E-01	4.849E-01	3.903E-01	2.841E-01	2.529E-01	1.817E-01	1.545E-01
50.00	2.868E+00	2.868E+00	9.582E-01	7.206E-01	5.788E-01	4.188E-01	3.694E-01	2.618E-01	2.192E-01
60.00	3.969E+00	3.969E+00	1.325E+00	9.959E-01	7.990E-01	5.761E-01	5.054E-01	3.544E-01	2.936E-01
70.00	5.220E+00	5.221E+00	1.742E+00	1.309E+00	1.049E+00	7.549E-01	6.599E-01	4.590E-01	3.773E-01
80.00	6.614E+00	6.614E+00	2.207E+00	1.657E+00	1.328E+00	9.539E-01	8.319E-01	5.748E-01	4.698E-01
100.00	9.799E+00	9.799E+00	3.269E+00	2.453E+00	1.965E+00	1.409E+00	1.225E+00	8.391E-01	6.797E-01
120.00	1.348E+01	1.348E+01	4.495E+00	3.373E+00	2.701E+00	1.935E+00	1.679E+00	1.144E+00	9.207E-01
150.00	1.984E+01	1.984E+01	6.614E+00	4.962E+00	3.972E+00	2.843E+00	2.464E+00	1.671E+00	1.335E+00
200.00	3.241E+01	3.241E+01	1.080E+01	8.109E+00	6.486E+00	4.639E+00	4.016E+00	2.712E+00	2.151E+00
250.00	4.711E+01	4.711E+01	1.570E+01	1.178E+01	9.427E+00	6.739E+00	5.831E+00	3.930E+00	3.104E+00
300.00	6.363E+01	6.363E+01	2.121E+01	1.591E+01	1.273E+01	9.099E+00	7.871E+00	5.299E+00	4.175E+00
400.00	1.012E+02	1.012E+02	3.374E+01	2.531E+01	2.025E+01	1.447E+01	1.251E+01	8.412E+00	6.612E+00
500.00	1.437E+02	1.437E+02	4.790E+01	3.593E+01	2.874E+01	2.054E+01	1.776E+01	1.193E+01	9.365E+00
600.00	1.900E+02	1.900E+02	6.335E+01	4.751E+01	3.801E+01	2.716E+01	2.348E+01	1.577E+01	1.237E+01
700.00	2.394E+02	2.394E+02	7.982E+01	5.987E+01	4.789E+01	3.422E+01	2.958E+01	1.986E+01	1.997E+01
800.00	2.913E+02	2.913E+02	9.712E+01	7.284E+01	5.827E+01	4.163E+01	3.598E+01	2.416E+01	1.893E+01
1000.00	4.008E+02	4.008E+02	1.336E+02	1.002E+02	8.016E+01	5.727E+01	4.950E+01	3.323E+01	2.609E+01
1200.00	5.156E+02	5.156E+02	1.719E+02	1.289E+02	1.031E+02	7.366E+01	6.367E+01	4.274E+01	3.347E+01

DE/DX IN SILICON (MEV CM2/GM) I = 172.3 A/Z = 2.004

ENRG./NUC. (MEV/AMU)	1 H	4 HE	12 C	16 O	20 NE	28 SI	40 AR	56 FE	84 KR
0.10	4.372E+02	1.201E+03	4.940E+03	5.937E+03	7.145E+03	9.410E+03	1.161E+04	1.520E+04	1.868E+04
0.12	4.186E+02	1.196E+03	4.881E+03	6.186E+03	7.503E+03	9.796E+03	1.218E+04	1.612E+04	1.997E+04
0.15	3.941E+02	1.187E+03	4.839E+03	6.478E+03	7.934E+03	1.029E+04	1.288E+04	1.727E+04	2.160E+04
0.20	3.605E+02	1.170E+03	5.011E+03	6.823E+03	8.465E+03	1.128E+04	1.374E+04	1.87[illegible]E+04	2.380E+04
0.25	3.351E+02	1.151E+03	5.113E+03	7.055E+03	8.844E+03	1.196E+04	1.437E+04	1.991E+04	2.555E+04
0.30	3.144E+02	1.131E+03	5.172E+03	7.219E+03	9.122E+03	1.250E+04	1.484E+04	2.089E+04	2.700E+04
0.40	2.818E+02	1.100E+03	5.205E+03	7.390E+03	9.479E+03	1.327E+04	1.654E+04	2.220E+04	2.927E+04
0.50	2.565E+02	1.017E+03	5.173E+03	7.448E+03	9.667E+03	1.377E+04	1.739E+04	2.317E+04	3.097E+04
0.60	2.358E+02	9.411E+02	5.101E+03	7.434E+03	9.745E+03	1.410E+04	1.800E+04	2.388E+04	3.230E+04
0.70	2.184E+02	8.734E+02	5.007E+03	7.372E+03	9.750E+03	1.430E+04	1.845E+04	2.442E+04	3.336E+04
0.80	2.035E+02	8.133E+02	4.898E+03	7.279E+03	9.702E+03	1.441E+04	1.876E+04	2.628E+04	3.420E+04
1.00	1.790E+02	7.159E+02	4.658E+03	7.034E+03	9.504E+03	1.443E+04	1.910E+04	2.738E+04	3.569E+04
1.20	1.595E+02	6.382E+02	4.408E+03	6.747E+03	9.229E+03	1.427E+04	1.917E+04	2.806E+04	3.620E+04
1.50	1.363E+02	5.491E+02	4.030E+03	6.275E+03	8.707E+03	1.381E+04	1.892E+04	2.849E+04	3.885E+04
2.00	1.136E+02	4.544E+02	3.602E+03	5.712E+03	8.057E+03	1.314E+04	1.842E+04	2.873E+04	4.038E+04
2.50	9.775E+01	3.910E+02	3.246E+03	5.217E+03	7.449E+03	1.241E+04	1.772E+04	2.843E+04	4.098E+04
3.00	8.595E+01	3.438E+02	2.948E+03	4.789E+03	6.902E+03	1.170E+04	1.694E+04	2.783E+04	4.101E+04
3.50	7.679E+01	3.071E+02	2.697E+03	4.417E+03	6.419E+03	1.102E+04	1.616E+04	2.708E+04	4.067E+04
4.00	6.943E+01	2.777E+02	2.478E+03	4.094E+03	5.983E+03	1.040E+04	1.540E+04	2.626E+04	4.010E+04
5.00	5.869E+01	2.348E+02	2.108E+03	3.583E+03	5.287E+03	9.348E+03	1.406E+04	2.464E+04	3.868E+04
6.00	5.137E+01	2.055E+02	1.849E+03	3.210E+03	4.767E+03	8.533E+03	1.298E+04	2.321E+04	3.722E+04
7.00	4.579E+01	1.832E+02	1.648E+03	2.909E+03	4.349E+03	7.847E+03	1.204[illegible]+04	2.188E+04	3.570E+04
8.00	4.139E+01	1.656E+02	1.489E+03	2.639E+03	3.990E+03	7.264E+03	1.123E+04	2.067E+04	3.421E+04
10.00	3.487E+01	1.395E+02	1.255E+03	2.230E+03	3.438E+03	6.330E+03	9.889E+03	1.857E+04	3.144E+04
12.00	3.024E+01	1.210E+02	1.089E+03	1.935E+03	3.012E+03	5.618E+03	8.842E+03	1.685E+04	2.900E+04
15.00	2.536E+01	1.015E+02	9.131E+02	1.623E+03	2.534E+03	4.818E+03	7.646E+03	1.479E+04	2.594E+04
20.00	2.018E+01	8.070E+01	7.269E+02	1.291E+03	2.017E+03	3.916E+03	6.269E+03	1.233E+04	2.206E+04
25.00	1.688E+01	6.754E+01	6.078E+02	1.081E+03	1.688E+03	3.302E+03	5.339E+03	1.061E+04	1.923E+04
30.00	1.460E+01	5.841E+01	5.257E+02	9.345E+02	1.460E+03	2.860E+03	4.669E+03	9.350E+03	1.709E+04
35.00	1.292E+01	5.169E+01	4.652E+02	8.270E+02	1.292E+03	2.532E+03	4.170E+03	8.381E+03	1.542E+04
40.00	1.163E+01	4.652E+01	4.187E+02	7.443E+02	1.163E+03	2.279E+03	3.760E+03	7.614E+03	1.408E+04
50.00	9.770E+00	3.908E+01	3.517E+02	6.253E+02	9.770E+02	1.915E+03	3.164E+03	6.478E+03	1.206E+04
60.00	8.492E+00	3.397E+01	3.057E+02	5.435E+02	8.492E+02	1.664E+03	2.751E+03	5.674E+03	1.061E+04
70.00	7.556E+00	3.023E+01	2.720E+02	4.836E+02	7.556E+02	1.481E+03	2.448E+03	5.076E+03	9.527E+03
80.00	6.841E+00	2.736E+01	2.463E+02	4.378E+02	6.841E+02	1.341E+03	2.216E+03	4.614E+03	8.679E+03
100.00	5.815E+00	2.326E+01	2.093E+02	3.721E+02	5.815E+02	1.140E+03	1.884E+03	3.928E+03	7.438E+03
120.00	5.113E+00	2.049E+01	1.841E+02	3.272E+02	5.113E+02	1.002E+03	1.657E+03	3.456E+03	6.573E+03
150.00	4.393E+00	1.757E+01	1.581E+02	2.812E+02	4.393E+02	8.610E+02	1.423E+03	2.970E+03	5.672E+03
200.00	3.651E+00	1.461E+01	1.314E+02	2.337E+02	3.651E+02	7.157E+02	1.183E+03	2.468E+03	4.729E+03
250.00	3.193E+00	1.277E+01	1.150E+02	2.044E+02	3.193E+02	6.259E+02	1.035E+03	2.159E+03	4.138E+03
300.00	2.882E+00	1.153E+01	1.038E+02	1.844E+02	2.882E+02	5.649E+02	9.338E+02	1.948E+03	3.735E+03
400.00	2.485E+00	9.941E+00	8.947E+01	1.591E+02	2.485E+02	4.871E+02	8.053E+02	1.680E+03	3.221E+03
500.00	2.244E+00	8.978E+00	8.080E+01	1.436E+02	2.244E+02	4.399E+02	7.272E+02	1.517E+03	2.909E+03
600.00	2.084E+00	8.336E+00	7.502E+01	1.334E+02	2.084E+02	4.084E+02	6.752E+02	1.409E+03	2.701E+03
700.00	1.971E+00	7.883E+00	7.095E+01	1.261E+02	1.971E+02	3.863E+02	6.385E+02	1.332E+03	2.554E+03
800.00	1.888E+00	7.551E+00	6.796E+01	1.208E+02	1.888E+02	3.700E+02	6.116E+02	1.276E+03	2.447E+03
1000.00	1.778E+00	7.111E+00	6.400E+01	1.138E+02	1.778E+02	3.485E+02	5.760E+02	1.202E+03	2.304E+03
1200.00	1.713E+00	6.851E+00	6.166E+01	1.096E+02	1.713E+02	3.357E+02	5.549E+02	1.158E+03	2.220E+03

RANGE IN EMULSION (GM/CM2) I = 303.4 A/Z = 2.204

ENRG./NUC. (MEV/AMU)	1 H	4 HE	12 C	16 O	20 NE	28 SI	40 AR	56 FE	84 KR
0.10	3.316E-04	5.264E-04	5.203E-04	5.528E-04	5.854E-04	6.445E-04	7.828E-04	8.866E-04	1.124E-03
0.12	4.073E-04	6.311E-04	5.984E-04	6.313E-04	6.662E-04	7.301E-04	8.812E-04	9.909E-04	1.250E-03
0.15	5.259E-04	7.885E-04	7.118E-04	7.440E-04	7.811E-04	8.532E-04	1.021E-03	1.138E-03	1.427E-03
0.20	7.353E-04	1.051E-03	8.938E-04	9.224E-04	9.611E-04	1.043E-03	1.241E-03	1.364E-03	1.696E-03
0.25	9.581E-04	1.315E-03	1.070E-03	1.093E-03	1.131E-03	1.219E-03	1.449E-03	1.575E-03	1.943E-03
0.30	1.193E-03	1.580E-03	1.243E-03	1.258E-03	1.295E-03	1.387E-03	1.649E-03	1.776E-03	2.176E-03
0.40	1.695E-03	2.116E-03	1.583E-03	1.579E-03	1.609E-03	1.704E-03	2.009E-03	2.154E-03	2.609E-03
0.50	2.239E-03	2.669E-03	1.919E-03	1.893E-03	1.912E-03	2.004E-03	2.351E-03	2.512E-03	3.014E-03
0.60	2.825E-03	3.259E-03	2.256E-03	2.203E-03	2.210E-03	2.295E-03	2.678E-03	2.856E-03	3.399E-03
0.70	3.453E-03	3.887E-03	2.597E-03	2.514E-03	2.505E-03	2.579E-03	2.995E-03	3.173E-03	3.769E-03
0.80	4.123E-03	4.557E-03	2.942E-03	2.826E-03	2.800E-03	2.859E-03	3.304E-03	3.485E-03	4.128E-03
1.00	5.590E-03	6.026E-03	3.652E-03	3.460E-03	3.392E-03	3.414E-03	3.910E-03	4.085E-03	4.823E-03
1.20	7.232E-03	7.667E-03	4.394E-03	4.114E-03	3.996E-03	3.968E-03	4.506E-03	4.665E-03	5.498E-03
1.50	1.003E-02	1.047E-02	5.581E-03	5.144E-03	4.935E-03	4.813E-03	5.399E-03	5.512E-03	6.429E-03
2.00	1.566E-02	1.609E-02	7.790E-03	7.025E-03	6.620E-03	6.285E-03	6.922E-03	6.909E-03	7.949E-03
2.50	2.256E-02	2.300E-02	1.034E-02	9.153E-03	8.493E-03	7.875E-03	8.527E-03	8.329E-03	9.444E-03
3.00	2.992E-02	3.036E-02	1.297E-02	1.133E-02	1.040E-02	9.479E-03	1.013E-02	9.725E-03	1.089E-02
3.50	3.813E-02	3.856E-02	1.581E-02	1.367E-02	1.244E-02	1.116E-02	1.179E-02	1.114E-02	1.234E-02
4.00	4.720E-02	4.763E-02	1.887E-02	1.619E-02	1.460E-02	1.294E-02	1.352E-02	1.259E-02	1.379E-02
5.00	6.791E-02	6.835E-02	2.581E-02	2.173E-02	1.935E-02	1.676E-02	1.721E-02	1.561E-02	1.674E-02
6.00	9.202E-02	9.246E-02	3.386E-02	2.800E-02	2.467E-02	2.097E-02	2.122E-02	1.881E-02	1.980E-02
7.00	1.195E-01	1.200E-01	4.304E-02	3.497E-02	3.056E-02	2.559E-02	2.558E-02	2.222E-02	2.298E-02
8.00	1.495E-01	1.499E-01	5.302E-02	4.250E-02	3.685E-02	3.049E-02	3.013E-02	2.575E-02	2.625E-02
10.00	2.166E-01	2.170E-01	7.539E-02	5.931E-02	5.065E-02	4.113E-02	3.998E-02	3.326E-02	3.306E-02
12.00	2.945E-01	2.949E-01	1.014E-01	7.880E-02	6.634E-02	5.311E-02	5.097E-02	4.149E-02	4.038E-02
15.00	4.309E-01	4.314E-01	1.468E-01	1.129E-01	9.369E-02	7.395E-02	6.956E-02	5.519E-02	5.234E-02
20.00	7.081E-01	7.086E-01	2.392E-01	1.822E-01	1.491E-01	1.140E-01	1.060E-01	8.160E-02	7.493E-02
25.00	1.045E+00	1.045E+00	3.514E-01	2.664E-01	2.165E-01	1.623E-01	1.492E-01	1.124E-01	1.008E-01
30.00	1.438E+00	1.438E+00	4.825E-01	3.647E-01	2.951E-01	2.186E-01	1.988E-01	1.474E-01	1.299E-01
35.00	1.885E+00	1.886E+00	6.316E-01	4.765E-01	3.846E-01	2.825E-01	2.546E-01	1.856E-01	1.622E-01
40.00	2.385E+00	2.385E+00	7.981E-01	6.014E-01	4.845E-01	3.539E-01	3.164E-01	2.298E-01	1.976E-01
50.00	3.533E+00	3.533E+00	1.181E+00	8.884E-01	7.141E-01	5.179E-01	4.584E-01	3.278E-01	2.772E-01
60.00	4.859E+00	4.870E+00	1.626E+00	1.222E+00	9.814E-01	7.088E-01	6.234E-01	4.405E-01	3.683E-01
70.00	6.393E+00	6.383E+00	2.131E+00	1.601E+00	1.284E+00	9.250E-01	8.103E-01	5.672E-01	4.702E-01
80.00	8.064E+00	8.069E+00	2.691E+00	2.021E+00	1.620E+00	1.165E+00	1.018E+00	7.072E-01	5.824E-01
100.00	1.190E+01	1.190E+01	3.969E+00	2.980E+00	2.387E+00	1.713E+00	1.491E+00	1.025E+00	8.359E-01
120.00	1.631E+01	1.631E+01	5.441E+00	4.083E+00	3.270E+00	2.344E+00	2.036E+00	1.391E+00	1.126E+00
150.00	2.392E+01	2.392E+01	7.976E+00	5.985E+00	4.791E+00	3.430E+00	2.975E+00	2.021E+00	1.622E+00
200.00	3.891E+01	3.891E+01	1.297E+01	9.733E+00	7.790E+00	5.572E+00	4.826E+00	3.263E+00	2.596E+00
250.00	5.639E+01	5.639E+01	1.880E+01	1.410E+01	1.129E+01	8.069E+00	6.984E+00	4.712E+00	3.729E+00
300.00	7.600E+01	7.600E+01	2.534E+01	1.901E+01	1.521E+01	1.087E+01	9.405E+00	6.336E+00	5.000E+00
400.00	1.209E+02	1.209E+02	4.017E+01	3.013E+01	2.411E+01	1.723E+01	1.490E+01	1.002E+01	7.894E+00
500.00	1.707E+02	1.707E+02	5.689E+01	4.267E+01	3.414E+01	2.439E+01	2.109E+01	1.418E+01	1.114E+01
600.00	2.253E+02	2.253E+02	7.509E+01	5.632E+01	4.506E+01	3.219E+01	2.783E+01	1.870E+01	1.467E+01
700.00	2.834E+02	2.834E+02	9.448E+01	7.086E+01	5.669E+01	4.050E+01	3.501E+01	2.352E+01	1.844E+01
800.00	3.444E+02	3.444E+02	1.148E+02	8.611E+01	6.889E+01	4.922E+01	4.254E+01	2.857E+01	2.240E+01
1000.00	4.729E+02	4.729E+02	1.576E+02	1.182E+02	9.458E+01	6.756E+01	5.840E+01	3.921E+01	3.072E+01
1200.00	6.073E+02	6.073E+02	2.024E+02	1.518E+02	1.215E+02	8.677E+01	7.500E+01	5.039E+01	3.944E+01

DE/DX IN EMULSION (MEV CM2/GM) I = 303.4 A/Z = 2.204

ENRG./NUC. (MEV/AMU)	1 H	4 HE	12 C	16 O	20 NE	28 SI	40 AR	56 FE	84 KR
0.10	2.690E+02	7.647E+02	3.025E+03	3.991E+03	4.830E+03	6.402E+03	7.923E+03	1.041E+04	1.283E+04
0.12	2.593E+02	7.630E+02	3.118E+03	4.156E+03	5.070E+03	6.664E+03	8.314E+03	1.104E+04	1.371E+04
0.15	2.473E+02	7.618E+02	3.227E+03	4.356E+03	5.363E+03	6.975E+03	8.790E+03	1.183E+04	1.483E+04
0.20	2.310E+02	7.600E+02	3.356E+03	4.600E+03	5.733E+03	7.483E+03	9.388E+03	1.286E+04	1.634E+04
0.25	2.186E+02	7.568E+02	3.442E+03	4.774E+03	6.007E+03	8.161E+03	9.831E+03	1.366E+04	1.756E+04
0.30	2.082E+02	7.518E+02	3.499E+03	4.901E+03	6.214E+03	8.543E+03	1.017E+04	1.430E+04	1.856E+04
0.40	1.910E+02	7.458E+02	3.557E+03	5.059E+03	6.498E+03	9.109E+03	1.137E+04	1.528E+04	2.015E+04
0.50	1.769E+02	7.012E+02	3.567E+03	5.135E+03	6.665E+03	9.495E+03	1.199E+04	1.598E+04	2.135E+04
0.60	1.647E+02	6.574E+02	3.545E+03	5.158E+03	6.755E+03	9.760E+03	1.245E+04	1.649E+04	2.230E+04
0.70	1.541E+02	6.163E+02	3.503E+03	5.145E+03	6.791E+03	9.936E+03	1.279E+04	1.686E+04	2.306E+04
0.80	1.447E+02	5.784E+02	3.447E+03	5.106E+03	6.788E+03	1.005E+04	1.305E+04	1.822E+04	2.367E+04
1.00	1.287E+02	5.149E+02	3.310E+03	4.976E+03	6.700E+03	1.012E+04	1.335E+04	1.905E+04	2.498E+04
1.20	1.156E+02	4.623E+02	3.156E+03	4.805E+03	6.541E+03	1.006E+04	1.346E+04	1.959E+04	2.517E+04
1.50	9.968E+01	3.987E+02	2.916E+03	4.512E+03	6.231E+03	9.813E+03	1.337E+04	1.999E+04	2.712E+04
2.00	8.350E+01	3.340E+02	2.627E+03	4.140E+03	5.810E+03	9.405E+03	1.311E+04	2.028E+04	2.832E+04
2.50	7.259E+01	2.904E+02	2.396E+03	3.826E+03	5.432E+03	8.974E+03	1.272E+04	2.022E+04	2.892E+04
3.00	6.435E+01	2.574E+02	2.198E+03	3.546E+03	5.081E+03	8.533E+03	1.227E+04	1.994E+04	2.912E+04
3.50	5.788E+01	2.315E+02	2.028E+03	3.298E+03	4.762E+03	8.105E+03	1.179E+04	1.954E+04	2.905E+04
4.00	5.261E+01	2.105E+02	1.876E+03	3.078E+03	4.473E+03	7.699E+03	1.131E+04	1.906E+04	2.880E+04
5.00	4.529E+01	1.812E+02	1.626E+03	2.750E+03	4.032E+03	7.055E+03	1.052E+04	1.819E+04	2.820E+04
6.00	3.991E+01	1.596E+02	1.436E+03	2.486E+03	3.670E+03	6.503E+03	9.809E+03	1.730E+04	2.738E+04
7.00	3.577E+01	1.431E+02	1.287E+03	2.270E+03	3.369E+03	6.028E+03	9.176E+03	1.645E+04	2.648E+04
8.00	3.248E+01	1.299E+02	1.168E+03	2.070E+03	3.115E+03	5.619E+03	8.615E+03	1.565E+04	2.556E+04
10.00	2.756E+01	1.102E+02	9.921E+02	1.762E+03	2.712E+03	4.950E+03	7.675E+03	1.423E+04	2.379E+04
12.00	2.404E+01	9.615E+01	8.654E+02	1.538E+03	2.393E+03	4.429E+03	6.924E+03	1.304E+04	2.217E+04
15.00	2.029E+01	8.116E+01	7.304E+02	1.299E+03	2.027E+03	3.835E+03	6.049E+03	1.158E+04	2.007E+04
20.00	1.626E+01	6.506E+01	5.855E+02	1.041E+03	1.626E+03	3.152E+03	5.019E+03	9.783E+03	1.732E+04
25.00	1.369E+01	5.475E+01	4.927E+02	8.760E+02	1.369E+03	2.[illegible]E+03	4.310E+03	8.500E+03	1.526E+04
30.00	1.189E+01	4.755E+01	4.279E+02	7.608E+02	1.189E+03	2.[illegible]E+03	3.792E+03	7.539E+03	1.367E+04
35.00	1.055E+01	4.222E+01	3.800E+02	6.755E+02	1.055E+03	2.068E+03	3.403E+03	6.795E+03	1.241E+04
40.00	9.526E+00	3.810E+01	3.429E+02	6.097E+02	9.526E+02	1.867E+03	3.078E+03	6.200E+03	1.139E+04
50.00	8.038E+00	3.215E+01	2.894E+02	5.144E+02	8.038E+02	1.575E+03	2.603E+03	5.309E+03	9.831E+03
60.00	7.009E+00	2.804E+01	2.523E+02	4.486E+02	7.009E+02	1.374E+03	2.271E+03	4.673E+03	8.700E+03
70.00	6.254E+00	2.501E+01	2.251E+02	4.002E+02	6.254E+02	1.226E+03	2.026E+03	4.195E+03	7.842E+03
80.00	5.674E+00	2.269E+01	2.042E+02	3.631E+02	5.674E+02	1.112E+03	1.838E+03	3.825E+03	7.168E+03
100.00	4.839E+00	1.936E+01	1.742E+02	3.097E+02	4.839E+02	9.485E+02	1.568E+03	3.268E+03	6.174E+03
120.00	4.266E+00	1.706E+01	1.536E+02	2.730E+02	4.266E+02	8.362E+02	1.382E+03	2.883E+03	5.475E+03
150.00	3.676E+00	1.471E+01	1.324E+02	2.353E+02	3.676E+02	7.206E+02	1.191E+03	2.485E+03	4.743E+03
200.00	3.066E+00	1.227E+01	1.104E+02	1.963E+02	3.066E+02	6.010E+02	9.935E+02	2.073E+03	3.971E+03
250.00	2.689E+00	1.075E+01	9.679E+01	1.721E+02	2.689E+02	5.270E+02	8.711E+02	1.817E+03	3.483E+03
300.00	2.431E+00	9.724E+00	8.752E+01	1.556E+02	2.431E+02	4.765E+02	7.877E+02	1.643E+03	3.150E+03
400.00	2.102E+00	8.410E+00	7.569E+01	1.346E+02	2.102E+02	4.121E+02	6.812E+02	1.421E+03	2.725E+03
500.00	1.903E+00	7.610E+00	6.849E+01	1.218E+02	1.903E+02	3.729E+02	6.164E+02	1.286E+03	2.466E+03
600.00	1.769E+00	7.078E+00	6.370E+01	1.132E+02	1.769E+02	3.468E+02	5.733E+02	1.196E+03	2.293E+03
700.00	1.676E+00	6.703E+00	6.032E+01	1.072E+02	1.676E+02	3.284E+02	5.429E+02	1.133E+03	2.172E+03
800.00	1.607E+00	6.428E+00	5.785E+01	1.029E+02	1.607E+02	3.150E+02	5.207E+02	1.086E+03	2.083E+03
1000.00	1.516E+00	6.066E+00	5.459E+01	9.705E+01	1.516E+02	2.972E+02	4.913E+02	1.025E+03	1.965E+03
1200.00	1.463E+00	5.853E+00	5.268E+01	9.365E+01	1.463E+02	2.868E+02	4.741E+02	9.892E+02	1.896E+03

APPENDIX VI

MICROSCOPE EQUIPMENT FOR TRACK ANALYSIS

In the analysis of cosmic ray stacks composed of many layers of plastic a serious problem lies in the numerous measurements which are required. For each of the three dimensional etched particle tracks, measurement of track parameters such as the length and the cone angle must be made. The retrival of information such as the charge, mass, and velocity requires tracing of tracks through all of the stack layers in which an etchable track was produced. Thus, the operator is required to make several sets of x, y, and z coordinate measurements for each track in each of the layers along the particle trajectory.

The assemblage of track coordinate data is easily computer programmed. The computer program can be designed to yield the dip and the azimuthal angle of a track as well as the other quantities required. However, the tedious sequence of reading, recording, and then transferring to a computer tape or card format some 14 digits required to locate each of the points along the track seriously limits the rate of data reduction. These considerations led to the search for semi-automatic data recording equipment.

A. The Digitized Measuring Microscope

A number of semi-automatic readout systems were investigated. Most of these were wholly unsuitable for mounting on microscope stages. One, however, utilizing light-weight shaft-position encoders and translating circuitry providing digital output to an IBM card punch, had been successfully used in conjunction with nuclear emulsion measurements. This unit, which is manufactured by the Datex Corporation of Monrovia, California, was adopted.

1. Description

The digitized measuring microscope consists of two major assemblies: the basic measuring microscope assembly, including the three shaft-position encoders mechanically coupled to the stage of the microscope, and the electronic gear, including translator and storage modules for the encoders, fixed-data keyboard, and the IBM card punch.

2. The Microscope Assembly (Figure AVI-1)

Each assembly consists of a Bausch and Lomb (B&L) "Dynaptic" microscope, an American Optical Company "Ortho-Illuminator", and a Lawrence Radiation Laboratory (LRL) measuring stage, which is attached directly to the microscope stand. The microscope and the illuminator are mounted firmly on a common baseboard.

The "Dynaptic" stand is tilted approximately 14 degrees about its inclination joint and held rigidly in this position by two support legs bolted between the microscope foot and the attached LRL stage. The tilt serves a dual purpose; first, to provide clearance for the enclosed mirror housing of the Ortho-Illuminator; second, to increase

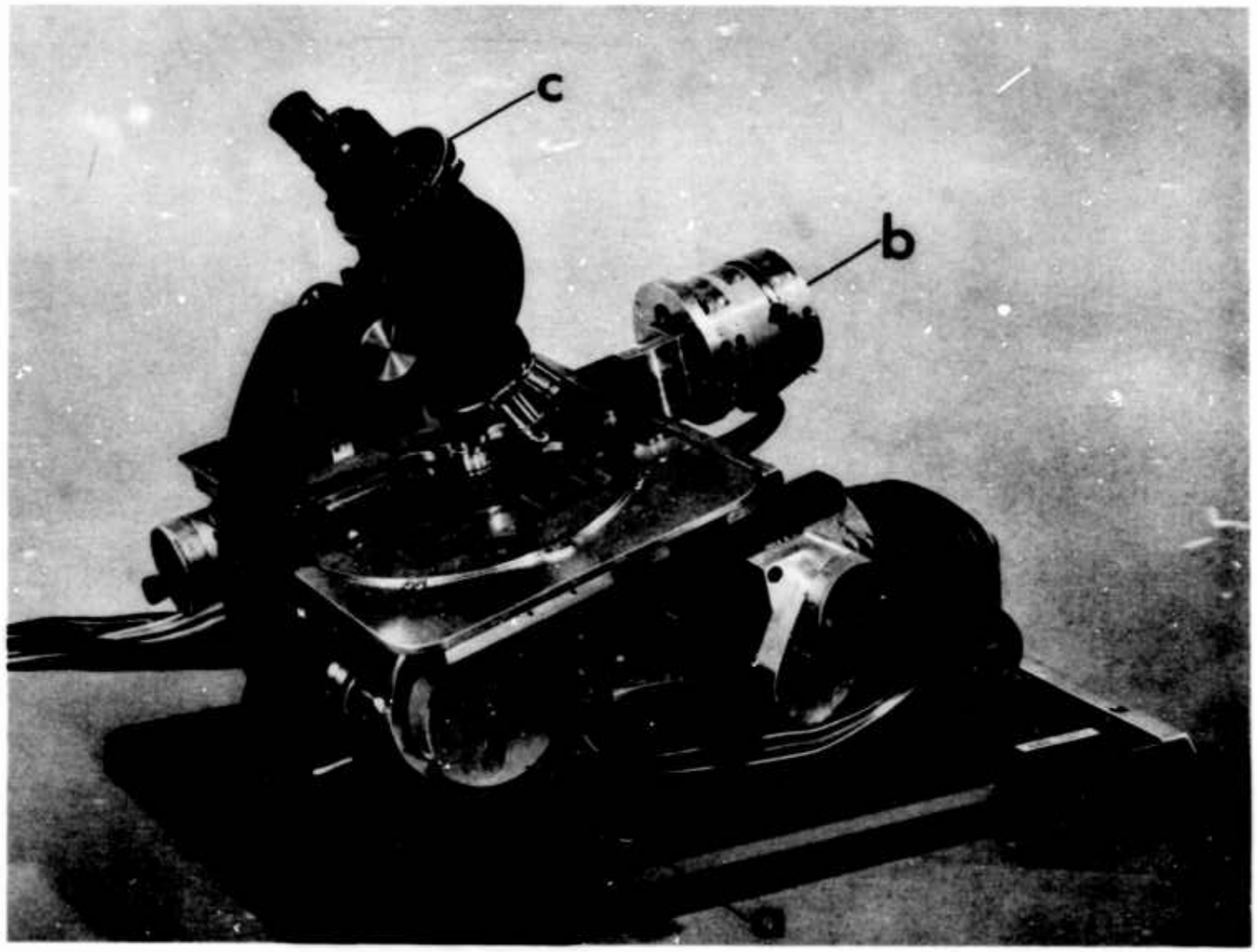

FIGURE AVI-1. The range measuring microscope, (a) fine focus z-axis encoder, (b) y-axis encoder, (c) gonicmeter device. Note: the x-axis encoder cannot be seen in this view.

the projection angle of the microscope's binocular eyetube to the more convenient 45 degrees now universal on late model microscopes. A further modification on the microscope stand is a set of 1-inch thick spacer blocks inserted behind both overhead and substage optical assemblies to increase the working capacity of the microscope for larger plate sizes and permit larger y-axis motion of the mechanical stage.

Scanning routines call for an extremely versatile illuminator. The wide range of magnifications used and the considerable variation in optical specimen density, require readily adjusted light levels. A two position intensity switch and an assortment of filters of different colors and densities allow the required control of contrast and resolution and aids in reducing eye fatigue. Most important, the collimated light beam from the illuminator's field lens can be delicately realigned as the operator switches from one high-power objective to another.

The LRL large plate measuring stage which is attached to a laboratory microscope stand appears massive and cumbersome. The design, however, is highly sophisticated and is the result of some ten years of continual development and improvement. Most of the 17 pound weight of the stage is concentrated in thick dove-tail way guides of precision-ground toolsteel. The entire stage assembly is hung beneath a supporting plate attached directly to the microscope stage bracket. Precision lead screws were custom-fabricated for these stages by Hanson-Whitney Company, Hartford, Conn.

An aid to track-length measurements was the construction of a superplate with built-in turntable. Plate sizes of 4 in. x 4 in. and smaller are firmly held and rotated until a particle track is aligned with one axis of travel. Thus, long straight tracks can be rapidly followed and measured by turning only one lead screw knob.

3. Three-Axes Encoding System

Considerable thought was given to the mounting of the Datex encoders so that: (1) their 3 inch diameter would not interfere with moving components or with the overhang of a large specimen plate, (2) their 44-oz. combined weight would not upset the dynamic stability of the stage, and (3) their shafts could be connected to turn in a precise 1 to 1 ratio with the lead screw rotation. Mounting the encoders to be independent of the stage would have involved unusual aligning problems and loss of precision through sets of right-angle gears and telescoping shafts.

To maximize stability, both the x and the y encoders were mounted near the junction of the x-y way units. The z-axis encoder was attached to the microscope's fine-focus knob. Since the B&L microscope's fine focusing mechanism provides 100 microns of travel per dial revolution over a total range of approximately 18 turns, the maximum count required is 1800. Here, an encoder less bulky and much less expensive than the 100,000 count stage-axes encoders could be used. A 1000-count single-turn Datex unit was geared one-to-ten with the fine-focus knob. This arrangement provides 1-micron least-interval readout over a 10-turn range, somewhat limiting the full travel of the fine-focus unit but proving to be more than adequate for all standard plastic thicknesses.

4. The Electronic System (Figure AVI-2)

Solid state electronics translate the 99,999 discrete positional readouts for the x and the y stage-axis encoders and the 999 readouts for the z axis encoder into a decimal representation suitable for IBM card punch ingestion. A memory hold permits the operator to continue to his next measuring position during the relatively slow punchout time for each coordinate data set. In addition to the translator module, a fixed-information module permits the operator to select up to 20 decades of indicative information which is punched simultaneously with the encoder data. Inch-high, illuminated numerals display the x, y or z coordinate reading as demanded by the operator's selector switch. A second window on this panel displays the number of measurements taken since the start of the run. An IBM 526 printing summary punch completes the electronic readout system.

5. Evaluation

This instrument is particularly well suited for the accurate and rapid measurement of cosmic ray stacks. While it is not essential to have a visual display of coordinate data during measuring sessions, this accessory has proved valuable as a checking device. Before actual measurements are begun, one may readily verify if encoders and translator are functioning properly. Routine stage calibrations also are greatly facilitated.

The slight friction of the encoder brushes adds some 2 oz.-in. of torque to the stage positioning knobs. Other than this, neither the performance nor the stability of the stage shows any adverse effects from the encoder installations.

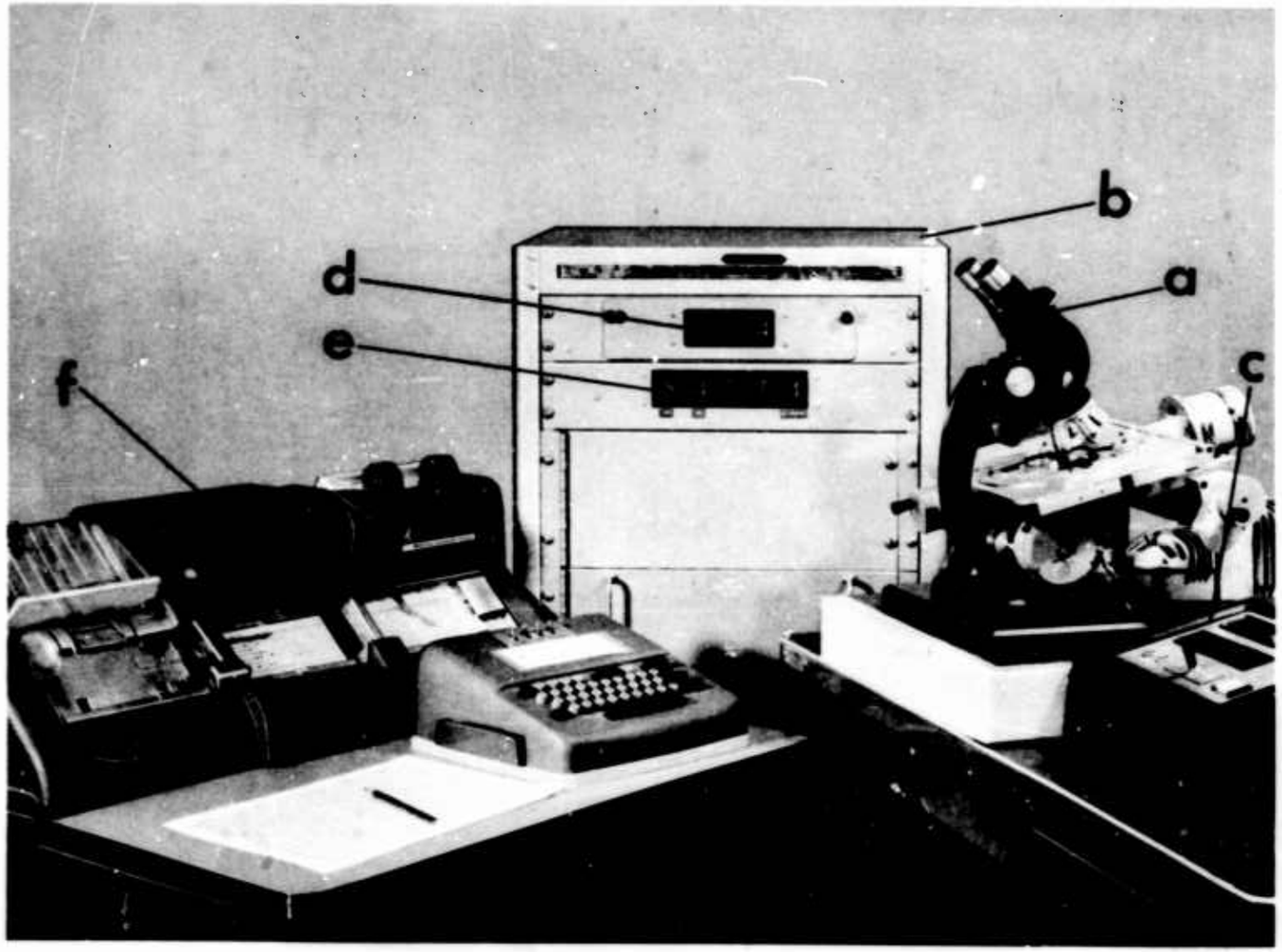

FIGURE AVI-2. The range measuring microscope system, (a) microscope assembly, (b) Datex translator and storage modules, (c) Datex control module, (d) card counter, (e) x,y,z-axis coordinate visual display unit, and (f) IBM 526 printing summary card punch.

With the automatic readout system in operation, track measurements can be performed with remarkable efficiency. Equally important, random errors associated with dial-reading, recording of data, and transcribing these data to IBM cards, are completely eliminated.

The one remaining error involved in track measurements, that incurred by the operator when inaccurately, or incorrectly setting the measuring point to his eyepiece cross hairs, is not corrected through this conversion to digitized readout. Such errors are reduced, however, because the measuring procedure is much more routine, requiring less thought. Such errors as the failure to take up for backlash will occur less often.

B. Microscope Equipped for Photomicrography and Precise Measurement of Short Tracks

1. Microscope

The English Cooke M-4005 Universal Microscope was found to be well suited for this purpose. The microscope, in addition to its normal photomicrographic capability was modified to include auxiliary instrumentation to obtain ultra-precise measurements in the y and z directions. The fixed binocular body and exceptionally stable overarm of the M-4005 was ideally suited for the installation of a filar micrometer with both remote control and automatic readout features. The following auxiliary equipment was installed on the Cooke microscope.

2. Photomicrographic Equipment (Figure AVI-3)

A Leitz Makam camera and Leitz Micro-Ibso photomicrographic attachment are held rigidly over the third eyetube by a truss arm clamped to the camera pillar accessory supplied with the microscope.

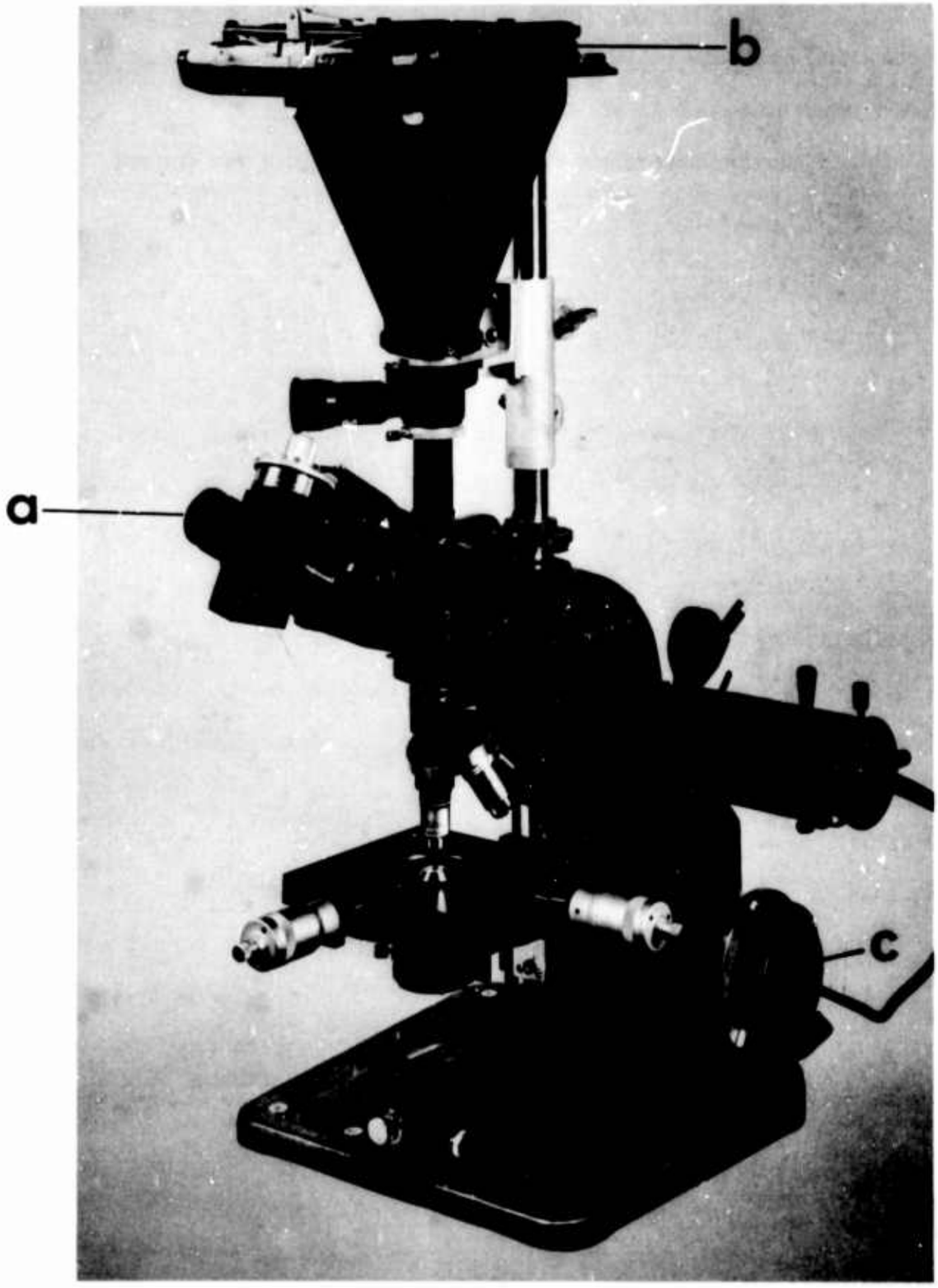

FIGURE AVI-3. Modified Cooke, Troughton and Simms microscope, (a) Koristka filar micrometer, (b) adaptor for Polaroid 4 x 5 inch film packets, and (c) z-axis encoder.

An auxiliary eyetube built into the Micro-Ibso unit permits monitoring exact image placement in the film plane.

A tilting superplate for 1 in. x 3 in. plates was devised for attaching to the Cooke's mechanical stage. Fine adjustments of the tilt with a worm gear enabled segments of dipping tracks to be brought into sharp focal-plane registration across the entire field of view (see Figure AVI-4).

3. Filar Micrometer Attachment with Digitized Remote Control (Figure AVI-3)

A filar micrometer functions as a modified eyepiece and is fitted to the microscope eyetube. An enlarged section houses a miniature way system. The moving component of this is a glass plate inscribed with a sharp line or filar. A fine pitch screw, actuated by a graduated knob, moves the filar across the plane of the image formed by the microscope objective. The precision of measurements is about 100 times that of a stage-axis measuring screw. However, filar eyepiece devices are poorly engineered for operator efficiency. The delicate setting adjustments must be made with one's hand suspended at forehead level. After adjusting the filar the operator must move his head some 10 in. away from the eyepiece for adequate viewing of the graduated dial. Before recording each reading, it may be necessary to look into the eyepiece again to note the number of full turns of advance on an internal linear scale.

A customized installation was devised to eliminate much of this tedium. A high precision Koristka filar eyepiece was modified for positive clamping to one of the Cooke's binocular eyetubes. It

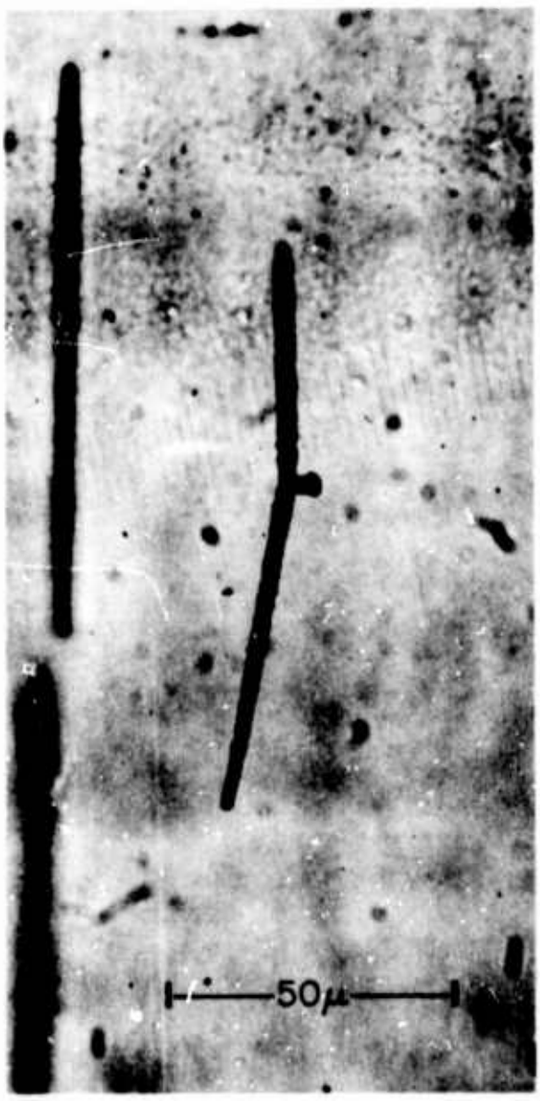

FIGURE AVI-4. Photomicrograph of a somewhat overetched track of a 5 MeV/nucleon ^{12}C ion. Note the track of the recoil ion. The ^{12}C ion entered the specimen with a dip angle of 20^{o}.

is easily adjusted by a fine pitch spur gear fitted on its lead screw shaft that mates precisely with a companion gear driven by a remote control mechanism. This mechanism consists of a no-backlash pulley and a winding drum system, using a fine, multi-strand steel cable. All components are mounted on a detachable auxiliary arm, which follows the general contour of the microscope's overarm back and down to the instrument base. Idler pulleys lead and return the cable along this arm.

A remote control knob, geared to the winding drum, is positioned adjacent to the microscope's fine-focus knob. One of the operator's hands can rest conveniently on the microscope base and manipulate both the filar and the fine-focus travel. Also geared to the winding drum is a Datex encoder identical to the 100,000 count units used on the digitized measuring microscope described above. It is wired to share the same translator and card punch circuitry. Geared to turn one-to-one with the filar micrometer's screw, the encoder provides 1000 discrete readouts per revolution as compared with the 50 graduations around the original filar micrometer dial.

A spare fine-focus knob, located on the opposite side of the Cooke microscope's overarm, enables a straightforward digitization of the fine-focus, z-axis, to be made. An arrangement of change gears was provided so that either a 1000 count, or a 100,000 count, Datex encoder can be driven at various least-count ratios. Even when geared one-to-one with the fine-focus knob, the encoder readout is 1/10-micron least-interval as compared with the 1-micron least-interval reading obtainable from the graduated focusing knob.

4. Evaluation

The photomicrographic equipment has served as an important part of the instrumentation for the measurement of particle tracks. The laborious tasks of measurement are sometimes more efficiently carried out on photomicrographs of track segments rather than through the direct observation of the microscope image at the high magnifications required. At the same time photomicrographs provide a permanent record of the track phenomena studied.

The filar micrometer is indispensable where very small incremental measurements must be made. Tests performed using the Cooke filar eyepiece attachment show that a trained operator, given a sharp, high contrast image point, can approach and reset on this point to an accuracy of better than 0.1 micron. Such excellent results are attributable not only to the ultra-fine encoder readout and the precision of the Koristka filar eyepiece, but also to the manual remote control mechanism.

APPENDIX VII

NEW APPLICATIONS OF DIELECTRIC TRACK DETECTORS

During the course of this research, a number of new applications have become apparent.

A. The Bulk Etch Rate Dosimeter

Measurements of the bulk etch rate of cellulose nitrate exposed to gamma radiation show little change in r_B for absorbed doses below 10^6 rad (see Table V-1). Above 10^6 rad, r_B varies in an approximately linear fashion with dose. In the dose range from 10^6 to about 10^9 rad this phenomenon can be used to measure the radiation dose.

A bulk etch rate dosimeter has a number of advantages over other dosimeters in this dose region. It can be made as compact as desirable. The exposed dosimeters are easily read by a simple measurement of r_B. The "latent image" stability is very high. Most dielectric detecting materials are chemically resistant and physically tough. The detectors may be placed in direct contact with the radiation environment and, therefore, register the total, unattenuated dose. The dosimeter may be utilized for the measurement of high doses of soft x or gamma rays (such as occur during weapons tests) that have very small penetration depths in matter. By successively etching each

time removing only a few microns of the specimen surface, a depth-dose profile may be measured.

B. Measurement of Radioactive Species in Solutions

The high chemical stability of some of the dielectric track detectors makes them suitable for the measurement of alpha particle and fission fragment emitters in solution. Some of the many possible applications include: monitoring the concentrations of alpha emitters in deep-ocean environments, measurements of alpha emitters released during undersea accidents, measurement of very low concentrations of fissionable isotopes through utilization of neutron bombardment, and measurement of alpha and fission fragment emitters in the presence of high backgrounds of gamma and beta radiation.

C. Radioautography of Fallout Particles

The capability of recording heavily ionizing charged particles while at the same time being insensitive to high backgrounds of beta and gamma radiations, suggest this application. Individual fallout particles may be analyzed for their content of alpha emitters and, with neutron irradiation, for heavy fissionable isotopes. The alpha particle energies may be determined by accurate measurement of etched track lengths.

D. Measurement of "Thin-Down" Flux of Primary Cosmic Rays at High Altitudes

In several years military combat planes as well as the civilian supersonic transport planes will be flying at 60,000 - 65,000 foot

altitudes. At the present time, the radiation environment at these altitudes is imperfectly known. This is particularly true in the case of the highly ionizing, heavy, stopping primaries. The low flux of the heavy particle component does not easily lend itself to conventional methods of measurement. The sensitive detectors are completely saturated by the light component before a statistically meaningful number of heavy particles has been recorded. The less sensitive detectors, such as the insensitive nuclear emulsions, must be flown in large quantities to achieve a sufficiently large number of tracks during the approximately one day balloon exposures. Also, for these detectors there is a tremendous scanning procedure necessary to find the particle tracks of interest.

Measurements of the heavy particle, low flux component of the cosmic radiation at 60,000 - 65,000 foot altitudes can be solved through the use of dielectric track detectors. Because of their characteristic sensitivity threshold, the correct dielectric track detecting material can be chosen, which will register only the heavy component. Charge identification of particles can also be achieved. Three layer stacks of dielectric track detectors would be flown, suspended below a balloon. These would be of large area (several square meters). The stack would consist of a central layer of cellulose nitrate sandwiched between two layers of Lexan polycarbonate plastic. Since the thickness of the sandwich need not exceed 2mm, the stack would be of modest weight. The central cellulose nitrate layer would be etched for an extended period in order to develop tracks to a size visible to the unaided eye. Thus the number and the position of

tracks would be readily established. The two layers of Lexan, etched for a shorter time, would give indication of the particle charge through the use of R_{reg} and the dr_T/dR methods.

E. Heavy Particle Dosimeter

Conventional passive dosimeters presently in use for the proton component of dose are inadequate for the measurement of the multi-charged component of galactic and solar radiation. The contribution of such radiation to the total dose received during the extended space flights (such as the 30 day missions of the Manned Orbiting Laboratory and the 18 month missions of manned Mars vehicles) will be considerable.

A heavy particle dosimetry system capable of discriminating between different linear energy transfer (LET) multicharged particles can be achieved through the utilization of threshold type dielectric track detectors. The small size of the system would permit its inclusion into the radiation badge of the astronaut. The system should also be useful in measurements of the high fluxes of alpha particles emitted during solar flares.

F. Cosmic Ray Measurements

It now appears feasible to measure the fluxes of the ultra-high z particles ($z > 26$) whose knowledge is currently of great interest to cosmic ray physicists. Since R_{reg} for these particles in cellulose nitrate is prohibitively large, a lower sensitivity material (such as the polycarbonate resin) could be utilized. It is possible that the

detectors could be refined, in the future, to the point where the measurement of the isotopic abundance of all of the elements present in cosmic rays could be achieved. The unique properties of these detectors make them also well suited to the measurement of the cosmic ray spectra outside of the earth's magnetosphere.

G. Penetration of High Velocity Microparticles

The nature and extent of the cosmic dust in the vicinity of the earth, as well as the phenomenon of high velocity impact is currently of great interest to investigators in several fields of science and technology. Numerous observations and measurements have been reported on cratering by projectiles of various sizes, velocities, and compositions in a variety of target materials.(70) Experiments involving the bombardment of cellulose nitrate with high velocity microparticles revealed that cellulose nitrate plastic, and the chemical etch principle can be effectively utilized in these studies.

Utilizing an electrothermal gun, a series of firings with 50 micron diameter spherical borosilicate glass projectiles were performed on 500 micron thick specimens of NRDL-1 cellulose nitrate and Lexan plastics.* Targets were oriented such that the projectiles entered the surface with dip angles of 90, 45 and 30 degrees (see Figure AVII-1). The velocity of impact varied from about 7.5 to 15.0 km/sec. Analysis of the data indicated that the impact behavior of the cellulose nitrate

*The firings were obtained through the courtesy of C. N. Scully, North American Aviation, Inc., Downey, California (1967).

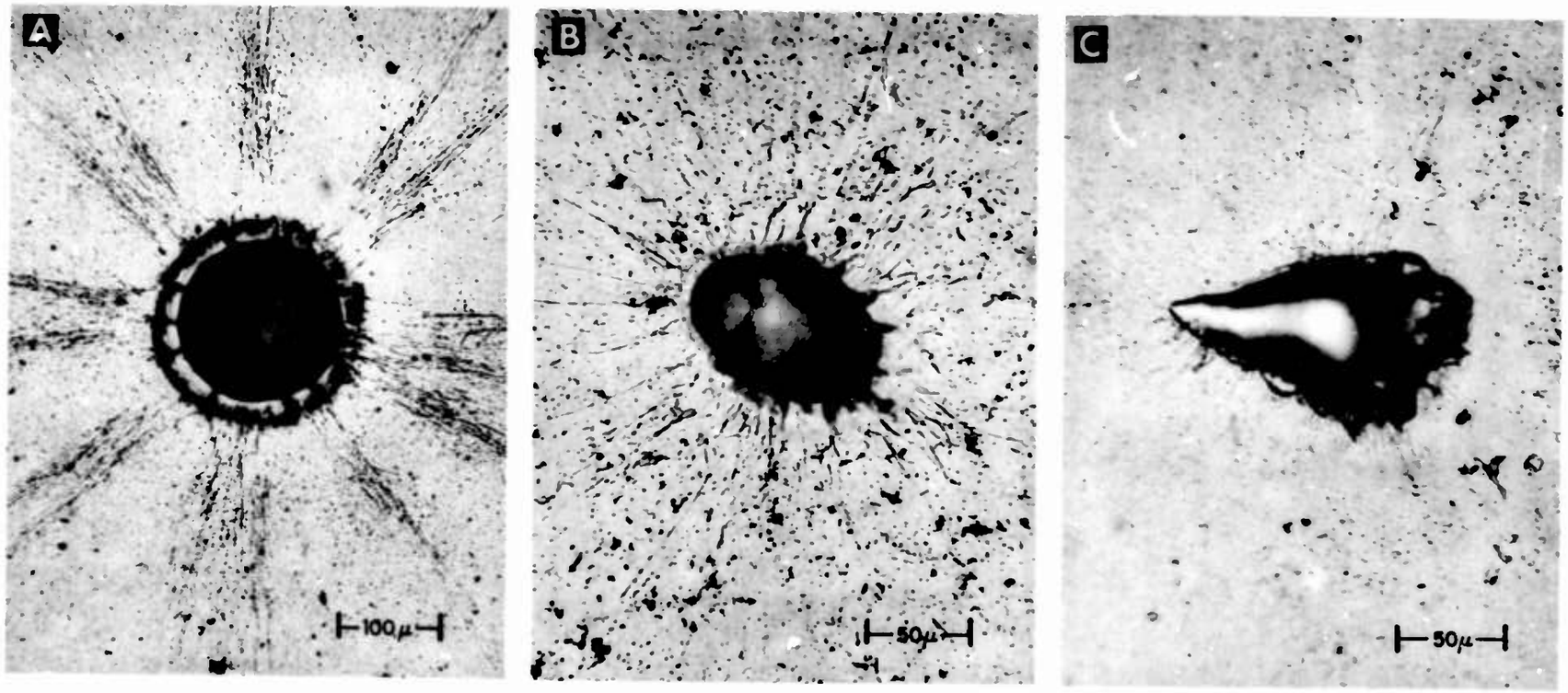

FIGURE AVII-1. Craters in NRDL-1 cellulose nitrate resulting from impacts of high velocity, 50 micron diameter glass spheres; (A) v = 15.1 km/sec, δ = 90°, d = 132 μ; (B) v = 15.1 km/sec, δ = 45°, d = 112 μ; (C) v = 6.6 km/sec, δ = 30°, d = 56 μ.

targets was highly regular and that the dimensionless depth of penetration (depth of penetration divided by the projectile diameter) is given by a constant multiplied by the logarithm of the ratio of the impact velocity to a second constant, $[(d/D) = c_1 \log(v/c_2)]$. This implies a high degree of microscopic homogeneity of the plastic. In contrast, the data for the Lexan target impacts are much more irregular. It is well known that certain plastic materials appear to lack microscopic homogeneity and that the crater dimensions do not scale smoothly with velocity. For example, penetration in Lucite targets is usually quite irregular.

In a separate set of experiments 500 micron thick specimens of NRDL-1 cellulose nitrate plastic were bombarded with spherical iron particles with velocities of 1.7 - 45 km/sec and masses of 10^{-10} - 10^{-15} g.* Targets were oriented such that projectiles entered the surface with dip angles of 90 or 45 degrees. Again, a uniform behavior of the plastic was observed. For the lowest velocity, largest particles, the experiment revealed an unusual behavior by the bombarding particles and the polymer target matrix. Most of the iron projectiles survived the impact. The larger particles (10^{-10}g, 1.7 km/sec) penetrated the polymer to a depth of about 20 microns. Only about one-third of the initial path of the projectile showed any signs of mechanical damage, the remainder of the path was not visible through an optical microscope. Figure AVII-2 shows this effect. Here a particle of about 2.5 micron diameter, incident at an angle of 45° to the plane of the target, entered the polymer at (a), producing an

*Courtesy of J. F. Friichtenicht, TRW, Inc., Redondo Beach, California (1967).

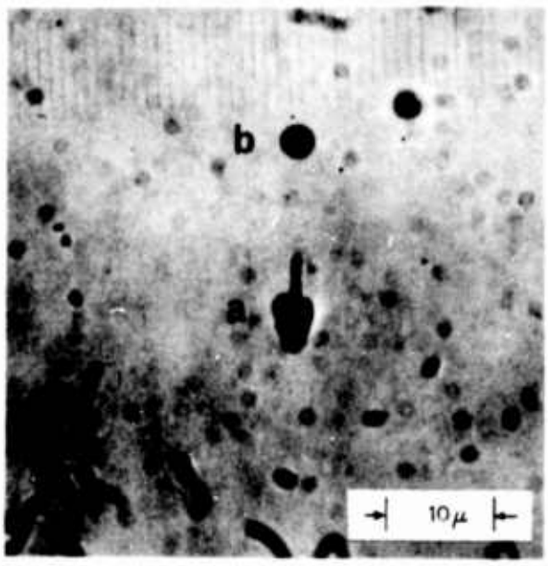

FIGURE AVII-2. Iron particle of 2.5 micron diameter and a velocity of about 2.0 km/sec enters the specimen at (a) with a 45° angle of incidence. The particle comes to rest at (b).

elliptical crater. The crater is followed by a narrow neck region of visible damage and a terminal region that shows no visible mechanical damage. The intact particle is visible at (b). It was possible to reveal the healed track region by chemical etching. A solution of 10M NaOH was found to preferentially attack this portion of the path. In Figure AVII-3 are shown photomicrographs of two tracks that were subjected to repeated etching: (a) unetched tracks, (b) etched for 2 minutes at 60°C, (c) etched for 5 minutes, and (d) etched for 20 minutes. Although the neck of the path is a partially hollow region, as shown by its immediate accessability to fluids, the etching behavior of the path beyond the neck region gives indication that mechanical healing of the matrix is complete. The sharp terminus of the etched track indicated that the preferentially attacked region is much smaller than the particle diameter.

Some of the possible applications of cellulose nitrate and of the chemical etching technique are listed below:

1. In space exposures, simultaneous flux measurements of the heavy particle cosmic ray component and of micrometeorites are feasible.

2. The microscopic craters resulting from small, hypervelocity particles can be enlarged, using the chemical etching technique, to a size convenient for counting.

3. The etching technique can be used to study the ionization and the healing phenomena in certain solids after passage of high velocity microparticles.

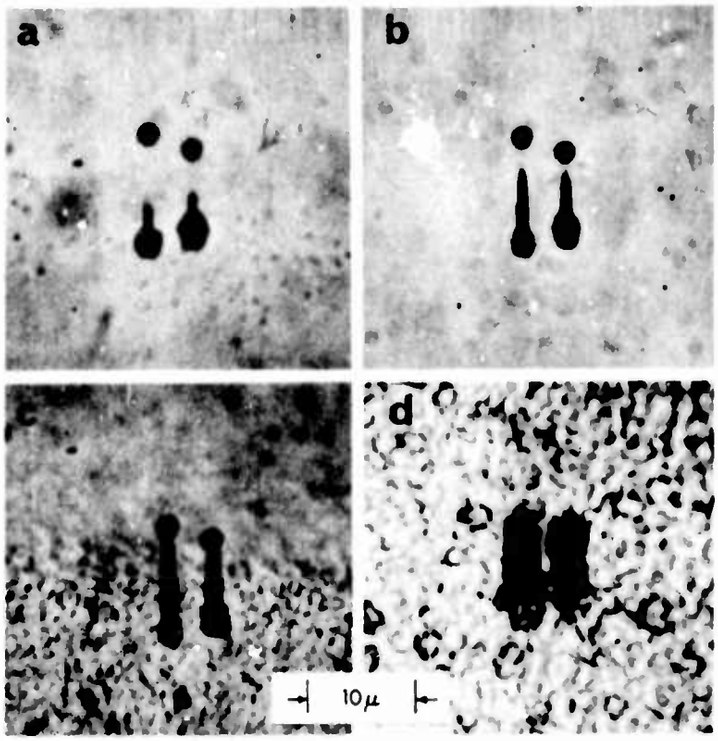

FIGURE AVII-3. a. Unetched tracks of two iron particles.
b. Same two tracks after a 2 minute, 60°C etch in a 10M NaOH solution.
c. Tracks as seen after 5 minute etch.
d. Tracks after 20 minutes of etch. The heavily etch-pitted surface results from irradiation by positive iron ions which accompany the bombardments. Tracks as seen after 20 minutes of etch appear very similar to that produced by nuclear particles after a similar etch time.

REFERENCES

1. R. L. Fleischer, P. B. Price, and R. M. Walker, Ann. Rev. Nucl. Sci. 15, 1 (1965).

2. E. Cieslak, J. Piekarz, and J. Zakrzewski, Nucl. Inst. Methods, 39, 224 (1965).

3. R. L. Fleischer and P. B. Price, Phys. Rev. 133, B63 (1964).

4. G. N. Flerov, Yu. Ts. Oganesyan, Yu. Lobanov, V. I. Kuznetsov, V. A. Druin, V. P. Perelygin, K. A. Gavrilov, S. P. Tretiakova, and V. M. Plotko, Phys. Letters 13, 73 (1964).

5. A. F. Linev, B. N. Markov, A. A. Pleve, and S. M. Polikanov, Nucl. Phys. (in press).

6. P. B. Price and R. M. Walker, Proc. Intern. Congr. Electron Microscopy, 5th, Paper G4 (1962).

7. R. L. Fleischer, P. B. Price and R. M. Walker, Proc. Conf. Registration Particle Tracks in Crystals, (Nucl. Res. Center, Strasbough, 1963).

8. P. B. Price, R. L. Fleischer, R. M. Walker and E. L. Hubbard, Proc. Conf. Reactions Complex Nuclei, 3rd, 332 (Univ. Calif. Press, Berkeley, Calif. 1963).

9. A. S. Soldatov, G. N. Smirenkin, S. P. Kapitza and Y. M. Tsipeniuk, Phys. Letters 14, 217 (1965).

10. R. L. Fleischer, P. B. Price and R. M. Walker, Appl. Phys. Letters 3, 28 (1963).

11. J. Mory and R. M. Walker, Fifth Intern. Conf. Nucl. Phot. (CERN, 1964).

12. P. Prevo, R. E. Dahl and H. H. Yoshikawa, J. Appl. Phys. 35, 2636 (1964).

13. R. L. Fleischer, P. B. Price and R. M. Walker, J. Nucl. Sci. Eng., 22, 153 (1965).

14. S. Pretre, E. Tochilin and N. Goldstein, "A Standardized Method for Making Neutron Fluence Measurements by Fission Fragment Tracks in Plastics," USNRDL-TR-1089 (1966). U.S.Naval Radiological Defense Laboratory, San Francisco, Calif.

15. M. Maurette, "Études des Traces D'ions Lourds Dans les Minéraux Naturels D'origine Terrestre Et Extra-Terrestre," Bull. Soc. franc. Miner. Crist., LXXXIX, (1966).

16. R. H. Brill, R. L. Fleischer, P. B. Price and R. M. Walker, J. Glass Studies, 6, 151 (1964).

17. R. L. Fleischer and P. B. Price, Geochim. Cosmochim. Acta, 28, 755 (1964).

18. R. L. Fleischer and P. B. Price, J. Geophys. Res. 69, 331 (1964).

19. R. L. Fleischer, P. B. Price and R. M. Walker, Geochim. Cosmochim. Acta, 29, 161 (1965).

20. R. L. Fleischer, P. B. Price, R. M. Walker and L. S. B. Leakey, Science, 148, 72 (1965).

21. R. L. Fleischer, P. B. Price, E. M. Symes and D. S. Miller, Science, 143, 349 (1964).

22. R. L. Fleischer, P. B. Price, R. M. Walker and M. Maurette, J. Geophys. Res., 72, 331 (1967).

23. R. L. Fleischer, P. B. Price, R. M. Walker, M. Maurette and G. Morgan, J. Geophys. Res., 72, 335 (1967).

24. S. H. Seal, Cancer, 17, 637 (1964).

25. E. V. Benton and M. M. Collver, Health Physics, 13, 495 (1967).

26. D. A. Young, Nature, 182, 375 (1958).

27. P. B. Price and R. M. Walker, J. Appl. Phys. 33, 3400 (1962).

28. R. L. Fleischer and P. B. Price, J. Appl. Phys. 34, 2903 (1963).

29. R. L. Fleischer and P. B. Price, Science 140, 1221 (1963).

30. R. L. Fleischer and P. B. Price, Geochim. Cosmochim. Acta, 28, 1705 (1964).

31. S. Amelinckx, The Direct Observation of Dislocations, Academic Press, New York and London (1964), p. 15.

32. R. L. Fleischer, P. B. Price, R. M. Walker and E. L. Hubbard, Phys. Rev. 133, A1443 (1964).

33. R. L. Fleischer, P. B. Price, R. M. Walker, R. C. Filz, K. Fukui, M. W. Friedlander, E. Holeman, R. S. Rajan and A. S. Tomhane, Science, 155, 187 (1967).

34. R. L. Fleischer, P. B. Price and R. M. Walker, J. Appl. Phys. 36, 3645 (1965).

35. R. L. Fleischer, P. B. Price and R. M. Walker, Phys. Rev. 156, 353 (1967).

36. R. Pfohl, M. Monnin and M. Debeauvais, C. R. Acad. Sci. Paris, 261, 2216 (1965).

37. R. Rossi, High-Energy Particles, Prentice Hall, New York (1961).

38. F. A. Bovey, The Effects of Ionizing Radiations on Natural and Synthetic High Polymers, Interscience Publishers, Inc., New York, (1958), p. 16.

39. W. H. Barkas, M. J. Berger in National Academy of Sciences - National Research Council Publication 1133, 103 (1964).

40. F. D. Miles, Cellulose Nitrate, Oliver and Boyd, London (1955).

41. Nitrocellulose - Chemical and Physical Properties, Hercules Powder Company, Wilmington, Del. (1963).

42. R. L. Wakeman, The Chemistry of Commercial Plastics, Reinhold Pub. Co., New York (1947).

43. E. Heuser, Cellulose Chemistry, J. Wiley and Sons, Inc., London (1944).

44. Handbook of Chemistry and Physics, Chemical Rubber Co., (1965).

45. R. S. Alger, Radiation Effects in Polymers, in Physics and Chemistry of the Organic Solid State, D. Fox, Editor, Interscience Pub. New York and London (1965).

46. A. Charlesby, Atomic Radiation and Polymers, Pergamon Press, Oxford, London, New York, Paris (1960).

47. M. Burton, Experimental Techniques and Current Concepts - Organic Substances, in The Effects of Radiation on Materials, J. J. Harwood, H. H. Hausner, J. G. Morse and W. G. Rauch, Editors, Reinhold Pub. Co., New York (1958).

48. J. G. Carrol and R. O. Bolt, Radiation Effects on Organic Materials, Academic Press, New York and London (1963).

49. W. E. Gloor, E. D. Klug, Cellulose Data, Interscience Pub. New York and London (1955).

50. S. L. Whetstone and T. D. Thomas, Phys. Rev. 154, 1174 (1967).

51. S. W. Cosper, J. Cerny and R. G. Gatti, Phys. Rev. 154, 1193 (1967).

52. J. S. Fraser, J. C. D. Milton, H. R. Bowman and S. G. Thompson, Can. J. Phys. 41, 2080 (1963).

53. E. L. Hubbard, W. R. Baker, K. W. Ehlers, H. S. Gordon, R. M. Main, N. J. Norris, R. Peters, L. Smith, C. M. VanAtta, F. Voelker, C. E. Anderson, R. Beringer, R. L. Gluckstern, W. J. Knox, M. S. Malkin, A. R. Quinton, L. Schwartcz and G. W. Wheeler, Rev. Sci. Instr. 32, 621 (1961).

54. B. Rossi, High-Energy Particles, Prentice Hall, New York (1961).

55. S. V. Starodubtsev and A. M. Romanov, The Passage of Charged Particles Through Matter, Atomic Energy Commission-tR-6468 (1965).

56. W. H. Barkas, Nuclear Research Emulsions, Academic Press, New York and London (1963).

57. L. C. Yuan and C. S. Wu, Eds., Methods of Experimental Phys. 5, Pt. A., 1, Academic Press, New York and London (1955).

58. H. A. Bethe, Ann. Physik (7) 5, 325 (1930).

59. F. Bloch, Physik 81, 363 (1933).

60. National Academy of Sciences - National Research Council Publication-1133 (1964).

61. H. H. Heckman, B. L. Perkins, W. B. Simon, F. M. Smith and W. H. Barkas, Phys. Rev. 117, 544 (1960).

62. J. F. Janni, Calculations of Energy Loss, Range, Path Length, Straggling, Multiple Scattering and the Probability of Inelastic Nuclear Collisons for 0.1 to 1000 MeV Protons, Air Force Weapons Laboratory, Albuquerque, New Mexico, AFWL-TR-65-150 (1966).

63. W. Whaling, Encyclopedia of Physics, 34, 193, S. Fluegge, Editor, Springer-Verlag, Berlin (1958).

64. R. P. Henke and E. V. Benton, Phys. Rev. 139, A2017 (1965).

65. P. B. Price, R. L. Fleischer, D. D. Peterson, C. O'Ceallaigh, D. O'Sullivan, A. Thompson, Identification of Isotopes of Energetic Particles with Dielectric Track Detectors, General Electric Research and Development Center, Schenectady, New York, G.E. Report No. 67-C-279 (1967).

66. R. P. Henke and E. V. Benton, Charged Particle Tracks in Polymers No. 5: A Computer Code for the Computation of Heavy-Ion Range-Energy Relationships in any Stopping Material, USNRDL-TR-67-122 (1967), U.S. Naval Radiological Defense Laboratory, San Francisco, California.

67. K. A. Neelakantan and P. G. Shukla, Phys. Rev. 130, 362 (1963).

68. O. Mathiesen, C. E. Long, P. S. Freier and C. J. Waddington, The Charge Distribution of the Energetic Very Heavy Nuclei in the Primary Cosmic Radiation, University of Minnesota School of Physics and Astronomy, Technical Report CR-100 (1967).

69. K. C. Anand, S. Biswas, P. J. Lavakare, S. Ramadurai, N. Sreenivasan, V. S. Bhatia, V. S. Chokan and S. D. Pabbi, J. Geophys. Res., 71, 4687 (1966).

70. Seventh Hypervelocity Impact Symposium, Martin Company, Orlando, Florida (1965).

UNCLASSIFIED

Security Classification

DOCUMENT CONTROL DATA - R & D

(Security classification of title, body of abstract and indexing annotation must be entered when the overall report is classified)

1. ORIGINATING ACTIVITY (Corporate author) U. S. Naval Radiological Defense Laboratory San Francisco, California 94135	2a. REPORT SECURITY CLASSIFICATION UNCLASSIFIED 2b. GROUP

3. REPORT TITLE

A STUDY OF CHARGED PARTICLE TRACKS IN CELLULOSE NITRATE

4. DESCRIPTIVE NOTES (Type of report and inclusive dates)

5. AUTHOR(S) (First name, middle initial, last name)

Eugene V. Benton

6. REPORT DATE	7a. TOTAL NO. OF PAGES	7b. NO. OF REFS
11 March 1968	257	70

8a. CONTRACT OR GRANT NO.	9a. ORIGINATOR'S REPORT NUMBER(S)
b. PROJECT NO. DLP, CNM, Subproject ZF 011 01 01 c. NASA-Defense Purchase Request Number A-65315 d. MSC, Request Number T-68092-G	USNRDL-TR-68-14 9b. OTHER REPORT NO(S) (Any other numbers that may be assigned this report)

10. DISTRIBUTION STATEMENT

This document has been approved for public release and sale; its distribution is unlimited.

11. SUPPLEMENTARY NOTES	12. SPONSORING MILITARY ACTIVITY
	Office of Naval Material, Washington, D. C. 20360, National Aeronautics and Space Adm., Moffett Field, Calif. 94035, & Manned Spcft. Ctr., Houston

13. ABSTRACT

Both experimental and theoretical contributions are presented on the topic of dielectric charged particle track detectors. Cellulose nitrate was the principal track recording material. The study covers four areas:

1. The Chemical Etch Development of Tracks.

There have been no previous systematic studies of the chemical etch development of particle tracks in dielectric track detectors. Part of the research reported here is an investigation of the effects of the different constituents of cellulose nitrate plastic on the chemical etch development of tracks. The dependence of track etching on certain etching solution parameters is discussed.

It has been found that the degree of preferential etching of the particle damage trails can be significantly increased by reducing the chemical attack rate, r_B, of the undamaged bulk material. The quantity r_B is lower for the more highly nitrated (12.4% vs. 10.9% N_2) and higher degree of polymerization (1000 vs. 50) nitrocellulose. The presence of plasticizers greatly reduces r_B, and the presence of residual solvents in concentrations of a few percent also has a similar, but smaller effect. Preferential etching can also be increased by etching at lower temperatures. The thermal stability of tracks is discussed. The geometry of tracks is examined. Useful relationships between track parameters are derived. Experimental observations of etched tracks in several types of cellulose nitrate plastic are reported.

2. Track Registration Criteria.

The knowledge of which particles produce latent (etchable) tracks in a given polymer is basic to the understanding of the track etch phenomena. It is also

(Abstract continued on another page)

14. KEY WORDS	LINK A		LINK B		LINK C	
	ROLE	WT	ROLE	WT	ROLE	WT
Charged particle tracks Cellulose nitrate Dielectric track detector Dosimetry						

UNCLASSIFIED
Security Classification

DOCUMENT CONTROL DATA - R & D

(Security classification of title, body of abstract and indexing annotation must be entered when the overall report is classified)

1. ORIGINATING ACTIVITY *(Corporate author)*	2a. REPORT SECURITY CLASSIFICATION: UNCLASSIFIED 2b. GROUP

3. REPORT TITLE

A STUDY OF CHARGED PARTICLE TRACKS IN CELLULOSE NITRATE

4. DESCRIPTIVE NOTES *(Type of report and inclusive dates)*

5. AUTHOR(S) *(First name, middle initial, last name)*

Eugene V. Benton

6. REPORT DATE	7a. TOTAL NO. OF PAGES	7b. NO. OF REFS
8a. CONTRACT OR GRANT NO. b. PROJECT NO. c. d.	9a. ORIGINATOR'S REPORT NUMBER(S): USNRDL-TR-68-14 9b. OTHER REPORT NO(S) *(Any other numbers that may be assigned this report)*	

10. DISTRIBUTION STATEMENT

11. SUPPLEMENTARY NOTES	12. SPONSORING MILITARY ACTIVITY

13. ABSTRACT

(Abstract continued from another page)

essential to the practical utilization of these detectors in quantitative measurements.

A new track registration criterion is presented. The criterion is based upon the restricted energy loss rate of charged particles. In order to produce an etchable track, a charged particle must possess a restricted energy loss rate above some critical value that is characteristic of the material. This criterion, as well as the two previously proposed criteria, are critically examined.

3. Range-Energy Calculations and Comparisons with the Etched Tracks Lengths.

The knowledge of range-energy relations is essential in the study and use of any charged particle detector. Most of the dielectric track detector materials require comprehensive range-energy data. The relationship between the ranges of particles, and the etched track lengths also needed to be established.

The calculations were carried out using the basic method of Barkas and Berger which has been modified and extended to include lower energies. Range-energy and energy loss data are given in the form of tables for a wide variety of particles and a broad energy spectrum in a wide variety of stopping materials. The range calculations have been checked experimentally with the use of lithium drifted solid state detectors. It is shown that the length of the etched tracks, when etched until the tips of the tracks become round, agrees closely with the calculated range and, therefore, is a good measure of the particle energy.

(Abstract continued on another page)

UNCLASSIFIED
Security Classification

DOCUMENT CONTROL DATA - R & D

(Security classification of title, body of abstract and indexing annotation must be entered when the overall report is classified)

1. ORIGINATING ACTIVITY (Corporate author)	2a. REPORT SECURITY CLASSIFICATION: UNCLASSIFIED 2b. GROUP

3. REPORT TITLE

A STUDY OF CHARGED PARTICLE TRACKS IN CELLULOSE NITRATE

4. DESCRIPTIVE NOTES (Type of report and inclusive dates)

5. AUTHOR(S) (First name, middle initial, last name)

Eugene V. Benton

6. REPORT DATE	7a. TOTAL NO. OF PAGES	7b. NO. OF REFS
8a. CONTRACT OR GRANT NO. b. PROJECT NO. c. d.	9a. ORIGINATOR'S REPORT NUMBER(S): USNRDL-TR-68-14 9b. OTHER REPORT NO(S) (Any other numbers that may be assigned this report)	

10. DISTRIBUTION STATEMENT

11. SUPPLEMENTARY NOTES	12. SPONSORING MILITARY ACTIVITY

13. ABSTRACT

(Abstract continued from another page)

4. Charged Particle Detection.

The use of the dielectric track detectors for quantitative measurements of multicharged particles is examined. Measurements of the dependence of the track etch rate on the restricted energy loss rate of charged particles are presented. The information content of tracks is examined. A simple, direct and accurate method for charge determination of multicharged cosmic ray particles is presented. The method is based on the measurement of the portion of the particle range over which a latent track is produced by a charged particle penetrating layers of plastic.

DD FORM 1 NOV 68 1473 (PAGE 1)

S/N 0101-807-6801

UNCLASSIFIED
Security Classification